Imperial College London
Department of Aeronautics and Department of Surgery and Cancer

The Effect of Compressive Thyroid Goitres on the Airway

Charlotte McIntyre

This thesis is submitted for the degree of Doctor of Philosophy, Imperial College London

Abstract

This work comprises an assessment of the use of computational fluid dynamics (CFD) to investigate the airflow through the tracheas of subjects with symptomatic, compressive, retrosternal thyroid goitres. In order to do this, 3D volume meshes were created to accurately represent patients' airways from individual CT scans. CFD was used to assess airflow through the tracheas of study subjects undergoing thyroid surgery in a prospective, observational study. The CFD employed an SST (Menter) K-omega steady RANS turbulence model that was validated using an experimental model; this RANS-based model was then used to estimate pressure loss across the pathological tracheas.

Twenty-one subjects were included in the study, and they underwent pre-and post-operative lung function tests and quality of life questionnaires. A geometric analysis was performed on the subjects' tracheas and the results were correlated with the pressure loss, as estimated by CFD. The results showed that both the minimum cross-sectional area of the trachea (A_{min}) and the hydraulic diameter of the trachea are very strongly correlated with the pressure loss across the trachea, as estimated using CFD, at flow rates of 15L/min and 30L/min (representing breathing at rest and light exercise respectively).

Using the A_{min} and a loss co-efficient equation, the pressure loss across the trachea can be estimated and when comparing the results with the pressure loss estimations using CFD, there is no significant difference. This presents an opportunity to estimate pressure loss across the trachea in a patient using the A_{min}, without the need to perform CFD. In a healthy trachea, the estimated pressure loss is thought to be around 5 Pa at 15L/min. Comparing the estimated pressure loss across the trachea in a patient with a compressive goitre with a normal pressure loss of 5 Pa, could add more useful information when deciding whether to operate.

Declaration of Originality

I declare that the work presented in this thesis is my own, and any work done by others is explicitly attributed.

Charlotte McIntyre

Copyright Statement

The copyright of this thesis rests with the author. Unless otherwise indicated, its contents are licensed under a Creative Commons Attribution-Non Commercial 4.0 International Licence (CC BY-NC). Under this licence, you may copy and redistribute the material in any medium or format. You may also create and distribute modified versions of the work. This is on the condition that: you credit the author and do not use it, or any derivative works, for a commercial purpose. When reusing or sharing this work, ensure you make the licence terms clear to others by naming the licence and linking to the licence text. Where a work has been adapted, you should indicate that the work has been changed and describe those changes. Please seek permission from the copyright holder for uses of this work that are not included in this licence or permitted under UK Copyright Law.

Acknowledgements

Firstly, I would like to acknowledge my supervisors, Prof. Denis J. Doorly and Prof. Neil S. Tolley, who have been a constant source of guidance and expertise throughout my research. I will remain forever grateful for their patience and generosity with their time.

Furthermore, I would like to thank Qiwei Xiao, Jan Rose, Louisa Ritchie, Alastair Bates, Raul Cetto and Catherine Rennie, whom have all contributed through their research to this field and have also supported the work of this thesis. I also extend my appreciation to Prof. Robert C. Schroter, and Dr Peter Vincent, and Dr Gita Madani for their invaluable input.

I am thankful to the Royal College of Surgeons for the research fellowship award which funded part of this research.

Finally, I am indebted to my family and friends for their support throughout this period of time.

Contents

ABSTRACT **2**

DECLARATION OF ORIGINALITY **3**

COPYRIGHT STATEMENT **4**

ACKNOWLEDGEMENTS **5**

CONTENTS **6**

LIST OF FIGURES **9**

LIST OF TABLES **13**

CHAPTER 1 INTRODUCTION **16**

1.1 THYROID GOITRE AND THE IMPACT ON THE AIRWAY 16
1.2 MECHANICS OF BREATHING 21
1.3 COMPUTATIONAL FLUID DYNAMICS (CFD) 27
1.3.1 Modelling flow in the large airways 27
1.3.2 Potential use of CFD as a tool for assessing patients with large airway pathology 29
1.4 AIMS AND THESIS OUTLINE 31

CHAPTER 2 STUDY COHORTS **34**

2.1 DESCRIPTION OF THE STUDY COHORT 34
2.2 ETHICAL APPROVAL 34
2.3 INCLUSION CRITERIA AND DATA GATHERED 34

CHAPTER 3 GEOMETRIC ANALYSIS OF THE AIRWAY **39**

3.1 INTRODUCTION 40
3.2 TRANSLATING CT SCAN DATA TO A VIRTUAL AIRWAY GEOMETRY 47
3.3 CHOICE OF LANDMARKS 54
3.3.1 Effect of the upper airway 55
3.3.2 Effect of glottic closure angle 56
3.3.3 Effect on the main bronchi 57
3.3.4 Surface Mesh modifications 57
3.4 METHODS 63
3.4.1 Measuring the minimum diameter of the trachea and the % constriction 63
3.4.2 Measuring the minimum cross-sectional area and % area constriction 64
3.4.3 Ellipticity 64
3.4.4 Measuring the length of constriction 64
3.4.5 PACS (Picture Archiving and Communications System) measurements 64
3.4.6 Intra-user repeatability 65
3.5 RESULTS AND DISCUSSION 66
3.6 CONCLUSIONS 71

CHAPTER 4 CFD ANALYSIS OF AIRWAY FLOWS: METHODS **73**

4.1 INTRODUCTION 73
4.2 GENERATING A VOLUME MESH 74
4.3 DEFINING BOUNDARY CONDITIONS 77
4.4 CHOICE OF CFD METHODOLOGY 79
4.5 MESH INDEPENDENCE TESTS 83
4.6 EFFECT OF TIME STEP FOR UNSTEADY SIMULATIONS 85
4.7 EXPERIMENTAL MODEL AND CFD VALIDATION STUDY 86
4.7 VALIDATING A STEADY RANS MODEL IN THE TRUNCATED AIRWAY 91
4.9 INFLOW DOMAIN TRUNCATION EFFECTS 94
4.10 CONCLUDING REMARKS 98

CHAPTER 5 CFD ASSESSMENT OF COMPRESSIVE GOITRE **100**

5.1 INTRODUCTION 100

5.2 RANS model of pressure loss at 15 and 30 L/min ... 106
5.2.1 Overview of geometries and pressure losses ... 107
5.3 Patterns of flow ... 117
5.4 Correlating geometric analysis with pressure loss ... 128
5.5 Loss predictions using A_{MIN} ... 134
5.6 Hydraulic diameter ... 143
5.7 Area of the glottis ... 146
5.7 Discussion and conclusions ... 146

CHAPTER 6 POTENTIAL APPLICATION OF CFD FOR SURGICAL PLANNING AND PATHOPHYSIOLOGICAL UNDERSTANDING OF THE AIRWAY ... 151

6.1 Introduction ... 151
6.2 Simulating post-operative improvement in tracheal flow ... 152
6.3 Comparison of a sudden expansion and a gradual expansion ... 160
6.4 Simplifying the tracheal geometry ... 169
6.5 Concluding remarks ... 175

CHAPTER 7 LUNG FUNCTION TESTS ... 177

7.1 Introduction ... 178
7.1.1 What is spirometry and how is it performed? ... 178
7.1.2 Issues with spirometry ... 180
7.1.3 Flow Volume Loop Curve appearance ... 181
7.2 Studies using spirometry to assess subjects with upper airway obstruction ... 181
7.2.1 Positional Spirometry ... 185
7.2.2 Work of breathing and pressure loss across the trachea ... 185
7.3 Aims ... 187
7.4 Methods ... 188
7.4.1 Spirometry ... 188
7.4.2 Difference in pre- and post-operative lung function tests ... 188
7.4.3 Visual inspection of flow volume loops ... 188
7.4.4 FEV_1/PEF ratio ... 191
7.4.5 Upright and Supine Lung function tests ... 191
7.4.6 Correlation between tracheal measurements and lung function tests ... 192
7.4.7 Calculating an estimate of the pressure loss using the flow volume loop ... 192
7.5 Results ... 194
7.5.1 Pre- and post-operative lung function tests ... 194
7.5.2 Visual inspection of the flow volume loops ... 198
7.5.3 FEV_1/PEF ratio ... 200
7.5.4 Correlation between tracheal measurements and lung function tests ... 200
7.5.5 Upright and Supine Lung function tests ... 203
7.5.6 Calculating an estimate of the pressure loss using the flow volume loop ... 204
7.6 Conclusions ... 209

CHAPTER 8 QUALITY OF LIFE QUESTIONNAIRES ... 210

8.1 ThyPro questionnaire and MRC dyspnoea scale ... 210
8.1.1 ThyPro Questionnaire ... 210
8.1.2 Validity and Reliability of ThyPro ... 211
8.1.3 MRC Dyspnoea Scale ... 212
8.2 Aims ... 213
8.3 Methods ... 214
8.4 Results ... 215
8.4.1 ThyPro ... 215
8.4.2 MRC Dyspnoea Results ... 222
8.5 Conclusions ... 224

CHAPTER 9 CONCLUSIONS AND FURTHER WORK ... 226

9.1 Geometric analysis of the airway ... 227
9.2 Validation of the tracheal volume mesh ... 229
9.3 Validation of the steady RANS model ... 230
9.4 CFD assessment of the compressed airway ... 231

9.5 USE OF CFD FOR SURGICAL PLANNING 233
9.6 LUNG FUNCTION TESTS 234
9.7 QUALITY OF LIFE QUESTIONNAIRES 235
9.8 MAIN ACHIEVEMENTS AND LIMITATIONS 236
9.9 FUTURE WORK 238
9.10 CONCLUDING REMARKS 238
BIBLIOGRAPHY 239
LIST OF PUBLICATIONS AND CONTRIBUTIONS 247
APPENDICES 249

List of Figures

Figure 1.1. Schematic of the thyroid gland and its relation to the trachea (2) 16
Figure 1.2 Schematic of the thoracic inlet (4) 17
Figure 1.3. Schematic of the upper and lower airways (15) 22
Figure 1.4. Schematic of the trachea and the major bronchi (17) 23
Figure 1.5. Standard lung volumes and capacities from a spirometry trace (18) 24
Figure 1.6. schematic of the afferent "input" signals and efferent "output" signals that contribute to the sensation of dyspnoea (20) 27
Figure 2.1. A patient performing a spirometry manoeuvre (33) 36
Figure 3.1. The 3 planes visible on Mimics 22.0 (coronal, axial and sagittal – clockwise from the upper left) 50
Figure 3.2. Threshold selection for selecting the airway structures in Mimics 22.0 50
Figure 3.3. 'leakage' from the trachea into the lung parenchyma 51
Figure 3.4. 3D reconstruction from the pre-selected threshold after region growing 52
Figure 3.5. A surface mesh pre and post smoothing (left to right) 53
Figure 3.6. Pre and post using the subdivision scheme 'Butterfly' to increase the number of surface triangles (left to right) 53
Figure 3.7. Voronoi diagram to demonstrate how a centerline is calculated (53) 54
Figure 3.8. Standardized glottis 59
Figure 3.9. Imported and appended glottis and trachea 59
Figure 3.10. Standardized glottis re-sized to the trachea 60
Figure 3.11. Boolean union of the glottis and trachea 60
Figure 3.12. View from above the glottis to visualize the glottic opening 61
Figure 3.13. Image of subject 1's tracheal surface mesh from above showing the glottis and glottic angle 61
Figure 3.14. Image of subject 13's tracheal surface mesh from above showing the glottis and glottic angle 62
Figure 3.15. Image of subject 18's tracheal surface mesh from above showing the glottis and glottic angle 62
Figure 3.16. Subject 12 tracheal surface mesh pre-modifications (left) and post modifications (right) 63
Figure 3.17. CT scan of the neck and chest in the axial plane, as it would be viewed on PACS, with a single 2D measurement being taken of the trachea 65
Figure 3.18. Planes of the trachea, perpendicular to the centerline, used to measure the diameter and calculate the cross-sectional area along the length of the trachea 65
Figure 3.19. Diameter of the trachea 2cm above the carina taken from VMTK and the diameters taken from PACS 69
Figure 3.20. Minimum diameter taken from VMTK, and the minimum diameter taken from PACS 69
Figure 3.21. Intra-user variability of the selected upper threshold (HU) when segmenting the airway 71
Figure 3.22. Intra-user variability of the minimum cross-sectional area (mm2) when the original thresholding was used to create the tracheal model and when the re-test thresholding was used to create the tracheal model 71
Figure 4.1. Plane through the volume mesh to demonstrate the prism layer 75

Figure 4.2. A volume mesh demonstrating the wall y+ values are all lower than 0.4. 76
Figure 4.3. Volume mesh with both inlet and outlet extrusions (left), volume mesh with face and half sphere (right) 79
Figure 4.4. Sagittal slice of the volume mesh to demonstrate the density of cells in mesh 1,2 and 3 83
Figure 4.5. Sagittal plane of vorticity for the three volume meshes 84
Figure 4.6. A schematic of the 3D printed airway model demonstrating the position of the 37 pressure recording taps 87
Figure 4.7. Static pressure along the length of the trachea from tap 1-37 comparing the experimental, LES and steady RANS results 88
Figure 4.8. Sagittal section of the airway model and the static pressure 89
Figure 4.10. Static pressure loss along the length of the trachea for the experimental model and the steady RANS model at a flow rate of 50L/min 90
Figure 4.11. Static pressure loss along the length of the trachea for the experimental model and the steady RANS model at a flow rate of 60L/min 91
Figure 4.12. Static pressure loss along the length of the trachea for the experimental model and the steady RANS model at a flow rate of 80L/min 91
Figure 4.13. Minimum cross-sectional area (Amin) of the subjects' tracheas 93
Figure 4.14. Full airway model with outlet extensions with the plane of peak turbulence highlighted 95
Figure 4.15. Truncated airway model with inlet and outlet extensions with the plane of peak turbulence highlighted 95
Figure 4.16. The mean of total pressure along the length of the airway comparing the full airway model with the truncated airway model at 30L/min using a steady RANS model 96
Figure 4.19. The velocity along the length of the airway comparing the full airway model with the truncated airway model 97
Figure 4.18. The turbulent kinetic energy along the length of the trachea comparing the full airway model with the truncated model 98
Figure 4.19. Sagittal plane demonstrating the change in turbulent kinetic energy along the length of the airway comparing the full airway model with the truncated model at 30L/min using a steady RANS model 98
Figure 5.1. Streamlines to demonstrate the disturbance in flow and the velocity of flow through three tracheas at a flow rate of 30L/min 120
Figure 5.2 Magnitude of Wall Shear Stress (Pa) for subjects 6, 18 and 21 at a flow rate of 30L/min 122
Figure 5.3. Turbulent kinetic energy (J/Kg) for subjects 6 and 18 at a flow rate of 30L/min 124
Figure 5.4. Magnitude of Vorticity (/s) for subjects 6, 18 and 21 at a flow rate of 30L/min 126
Figure 5.5. Static pressure (Pa) for subjects 6, 18 and 21 at a flow rate of 30L/min 128
Figure 5.6. Pressure loss across the trachea against the % constriction of the trachea at flow rates 30L/min and 15l/min (outliers removed: subjects 9, 17 and 21) 129
Figure 5.7. Pressure loss across the trachea against the minimum cross-sectional area of the trachea at flow rates 30L/min and 15l/min (outliers removed: cases 9 and 21) 130
Figure 5.8. %constriction of the trachea against the minimum cross-sectional area of the trachea 131
Figure 5.9. Loss co-efficient 'K' at a flow rate of 15L/min and 30L/min against the % constriction of the trachea 133
Figure 5.10. Loss co-efficient 'K' at a flow rate of 15 L/min and 30 L/min against the minimum cross-sectional area of the trachea 134

Figure 5.11. Estimated pressure loss using CFD and using a loss co-efficient of 1.2 against the minimum cross-sectional area at a flow rate of 15L/min.....135
Figure 5.12. Estimated pressure loss using CFD and using a loss co-efficient of 1.2 against the minimum cross-sectional area at a flow rate of 30L/min.....136
Figure 5.13. Pressure loss across the trachea as estimated by CFD (red) and as estimated using a loss co-efficient of 1.6 (blue) at a flow rate of 15L/min against the minimum cross-sectional area of the trachea.....137
Figure 5.14. Pressure loss across the trachea as estimated by CFD (red) and as estimated using a loss co-efficient of 1.30 (blue) at a flow rate of 30L/min against the minimum cross-sectional area of the trachea.....137
Figure 5.15. Pressure loss (Pa) against 1/Amin2 (mm2) for flow rates of 15 L/min and 30 L/min (outliers removed: subject 9 and 21).....139
Figure 5.16. Pressure loss (Pa) against 1/Amin2 (mm2) for subjects with a constriction >35% 141
Figure 5.17 Pressure loss (Pa) against 1/Amin2 (mm2) for subjects with a constriction <35% (outlier removed: subject 3).....141
Figure 6.1. Anterior view of subject 21's trachea i) pre-operative ii) simulated post-operative 153
Figure 6.2. Lateral view of subject 21's trachea i) pre-operative ii) simulated post-operative 153
Figure 6.3. Cross-sectional area of the trachea along the distance of the trachea in i) subject 21 pre-operatively ii) subject 21 simulated post-operative trachea 154
Figure 6.4. Streamlines demonstrating the magnitude of velocity (m/s) in subject 21 i) pre-operative trachea ii) simulated post-operative trachea.....155
Figure 6.5. Tracheal surface mesh demonstrating the wall shear stress (Pa) in subject 21 i) pre-operative trachea ii) simulated post-operative trachea 156
Figure 6.6. Volume render of the trachea demonstrating the vorticity in subject 21 i) pre-operative trachea ii) simulated post-operative trachea.....157
Figure 6.7. Volume render of the trachea demonstrating the static pressure (Pa) in subject 21 i) pre-operative trachea ii) simulated post-operative trachea.....157
Figure 6.8. Three tracheal geometries placed in a sagittal orientation with centrelines i) pre-operative ii) pre-operative 11 months later iii) post-operative 158
Figure 6.9. Graphical representation of the velocity profile in the boundary layer. The last profile represents reverse flow which shows separated flow (92).....161
Figure 6.10. i) surface mesh representation of the tracheal constriction followed by a sudden expansion and ii) a magnified view of the mesh demonstrating the constriction.....162
Figure 6.11. i) surface mesh representation of the tracheal constriction followed by a gradual expansion and ii) a magnified view of the mesh demonstrating the constriction.....163
Figure 6.12. Cross-sectional area of the trachea along the length of the trachea (first ring to the carina) for the sudden expansion (blue) and the gradual expansion (red) 163
Figure 6.13. Total pressure (Pa) along the length of the trachea (glottis to the carina) for the sudden expansion (blue) and the gradual expansion (red).....164
Figure 6.14. Static pressure (Pa) along the length of the trachea (glottis to the carina) for the sudden expansion (blue) and the gradual expansion (red).....165
Figure 6.15. Isoplane of the magnitude of velocity (m/s) in i) gradual expansion and ii) sudden expansion.....166
Figure 6.16. Isoplane of the static pressure (Pa) in i) gradual expansion and ii) sudden expansion 166
Figure 6.17. Surface mesh representation of the magnitude of wall shear stress (Pa) in i) gradual expansion and ii) sudden expansion 167

Figure 6.18. Isoplane of the vorticity in i) gradual expansion and ii) sudden expansion 168
Figure 6.19. From left to right tracheal geometry of subject 5 compared with the simplified geometry, reconstructed using the normal diameter and the tracheal geometry of subject 19 compared with the simplified geometry, reconstructed using the normal diameter 170
Figure 6.20. From left to right: the un-modified tracheal geometry of subject 21 and the modified tracheal geometry, compared with the simplified geometry, reconstructed using the normal diameter and the tracheal geometry. 171
Figure 6.21. Volume renders of static pressure (Pa) for subject 21 a) reference geometry b) tracheal geometry rebuilt using the hydraulic diameter and c) tracheal geometry using the normal diameter 173
Figure 6.22. Volume renders of total pressure (Pa) for subject 21 a) reference geometry b) tracheal geometry rebuilt using the hydraulic diameter and c) tracheal geometry using the normal diameter 174
Figure 6.23. Volume renders of velocity (m/s) for subject 21 a) reference geometry b) tracheal geometry rebuilt using the hydraulic diameter and c) tracheal geometry using the normal diameter 174
Figure 7.1. Schematic of a subject undergoing spirometry (97).....179
Figure 7.2. Schematic of a flow volume loop demonstrating a successful FVC manoeuvre. PEF = peak expiratory flow, MEF = maximal expiratory flow, FEF = forced expiratory flow, FVC = forced vital capacity, FIF = forced inspiratory flow (99) 180
Figure 7.3. Schematic of flow-volume loops demonstrating the different types of airway obstruction (101).....181
Figure 7.4. Example pre-operative flow volume loop (left) and post-operative flow volume (right) from subject 7 190
Figure 7.5. Re-plotted inspiratory data from the original flow volume loops of one subject both pre- and post-operatively for subject 7 191
Figure 7.6. Pre- and post-operative FEV1 results for the main subjects 196
Figure 7.7 Pre- and post-operative PEF results for the main subjects 197
Figure 7.8. Pre- and post-operative FEV1/PEF results for the main subjects 197
Figure 7.9. a) Pre and b) post-operative flow volume loop classification 199
Figure 7.10. Pre-operative FEV1/PEF plotted against the minimum cross-sectional area of the trachea 203
Figure 7.12 A graph taken from Cross et al (114) to show the minute volume (VE) plotted against the estimated work of breathing (Wb).....207
Figure 8.1. Pre-operative goitre symptoms vs pre-operative FEV1/PEF 221

List of Tables

Table 2.1. Patient demographics and details of surgery 38
Table 2.2. Co-morbidities and the number of subjects with the co-morbidity 39
Table 2.3. Symptoms described in the pre-operative clinic letter and the frequency of the symptom being documented 39
Table 3.1. The geometric analysis of the tracheal models using the centerline data derived from planes perpendicular to the centerline where: Dmin = minimum diameter, Amin = Minimum cross-sectional area 67
Table 3.2. The median, range, and IQ range of the length of constriction (when the constriction is >35%) of the 21 tracheal models 67
Table 3.3 The paired sample statistics of measurements taken from PACS and those taken from planes perpendicular to the plane (VMTK) 68
Table 3.4. Paired differences of measurements taken from PACS with those taken from planes perpendicular to the plane (VMTK) 68
Table 3.5. Comparison of % reduction in the minimum diameter (minimum diameter / diameter of the trachea 2cm above the carina) between measurements taken from PACS and measurements taken from VMTK 68
Table 4.1. Volume mesh validity checks and the values required for a valid volume mesh ... 77
Table 4.2. Physics model for LES simulations 80
Table 4.3. Physics model used for steady RANS 81
Table 4.4. The number of elements in each mesh 83
Table 4.5. Pressure loss across the trachea for volume meshes 1,2 and 3 84
Table 4.6. Results of the pressure loss with differing timesteps 86
Table 4.7. Pressure loss as estimated using LES model and a steady RANS model in the truncated airway model with a moderate and a severe constriction at a flow rate of 15L/min 93
Table 4.8. Pressure loss as estimated using LES model and a steady RANS model in subject 9 at 30L/min 94
Table 5.1 The anterior-posterior view of the trachea (pre-processing on the left and post-processing on the right) for the 21 subjects and the results of the pressure loss as estimated by a steady RANS model of turbulence (and using an LES model for subject 21) at steady flow rates of 15L/min and 30L/min 112
Table 5.2 The estimated pressure loss across the trachea for each subject as calculated using CFD (steady RANS model) for the flow rates 15 L/min and 30 L/min in order of the minimum cross-sectional area of the trachea (ascending order). The most constricted case (subject 21) shows the estimated pressure loss calculated using an LES model for the flow rates 15 L/min and 30 L/min. 117
Table 5.3. Key geometric and flow measures obtained for the three subjects representing a mild constriction, a moderate constriction, and a severe constriction 118
Table 5.4 Correlation between the % constriction of the trachea and the pressure loss (outliers removed: cases 9, 17 and 21) 129
Table 5.5. Correlation between the Amin of the trachea and the pressure loss 130
Table 5.6. Correlation between the % constriction of the trachea and the minimum cross-sectional area 131
Table 5.7. Correlation between the length of constriction of the trachea (for those tracheas where the degree of constriction was >35%) and the pressure loss 132
Table 5.8 Loss co-efficient between the % constriction and the loss co-efficient at 15L/min and at 30L/min 133

Table 5.9 Correlation between the minimum cross-sectional area of the trachea and the loss coefficient at 15L/min and at 30L/min 134
Table 5.10. Wilcoxon signed rank test of differences between the pressure loss as estimated using CFD and the pressure loss as estimated using a loss co-efficient of 1.2 136
Table 5.11. Wilcoxon signed rank test between the pressure loss as estimated using CFD and the pressure loss as estimated using a loss co-efficient of 1.6 and 1.3 138
Table 5.12. Correlation between 1/Amin2 and the pressure loss as estimated by CFD at flow rates of 15 L/min and 30 L/min. *denotes significant results 139
Table 5.13. Correlation between pressure loss (Pa) against 1/Amin2 (mm2) for subjects with a constriction >35% 140
Table 5.14. Correlation between pressure loss (Pa) against 1/Amin2 (mm2) for subjects with a constriction <35% (outlier removed: subject 3) 140
Table 5.15. ΔP /Q2 using the pressure loss estimation from CFD (steady RANS) simulations for each geometry. Q1 is the flow rate 15 L/min and Q2 is the flow rate 30 L/min 143
Table 5.16 The minimum diameter, maximum diameter, hydraulic diameter and ellipticity of the trachea at the minimum cross-sectional area 145
Table 5.17 Correlation between the hydraulic diameter at the minimum cross-sectional area of the trachea and the pressure loss across the trachea 145
Table 5.18. Correlation between the pressure loss as estimated by CFD and the minimum cross-sectional area of the trachea (either the glottis or the constriction - the smaller of the two measurements) 146
Table 6.1. Total pressure loss (Pa) across the trachea for subjects 5, 19 and 21 and the total pressure loss (Pa) across the simplified tracheal models for subjects 5, 19 and 21, and the relative difference 172
Table 7.1. Pre-operative lung function tests 194
Table 7.2.Post-operative lung function tests 195
Table 7.3. Wilcoxon Signed Rank Test to test for a significant difference between the pre- and post-operative median lung function tests FEV_1 and FEV_1/PEF 195
Table 7.4. t-test to assess for a significant difference between the pre- and post-operative mean lung function tests FEV_1 and FEV_1/PEF 195
Table 7.5. Correlation co-efficient and p values for tracheal measurements and lung function tests for the study subjects 202
Table 7.6. Table to show the mean +/- standard deviation of upright and supine pre-operative lung function tests 204
Table 7.7. Paired samples t-test to assess for significant differences between the upright and supine pre-operative lung function tests 204
Table 7.8. Pre- and post-operative measures of average flow rates, estimates of power of inspiration across the trachea and estimates of pressure loss across the trachea 205
Table 7.9. Paired samples test between pre- and post-operative measures of flow rate 205
Table 7.10. Wilcoxon signed rank test between pre- and post-operative estimates of the power of breathing and pressure loss 205
Table 7.11 Estimated inspiratory tracheal resistive work of breathing for the main subjects 208
Table 8.1 Pre-operative and post-operative median scores (inter quartile range) for the ThyPro items as reported by the subjects 216
Table 8.2. Wilcoxon signed rank test for pre- and post-operative ThyPro scores *significant result at the $p<0.05$ 217
Table 8.3. % of subjects who experienced no change, an improvement in symptoms or worsened symptoms for each item of the ThyPro questionnaire when reported pre and post operatively 218

Table 8.4. Cohen's D effect size 219
Table 8.5. Mean scores for ThyPro scales for a normal population and the pre- and post-operative goitre group (where the data is not normally distributed and therefore a mean value cannot be given, the data is not presented) 220
Table 8.6. Pearson's correlation between pre-operative goitre symptoms and pre-operative lung function test parameters. ** denotes statistical significance when $p<0.05$ 221
Table 8.7. Pearson's or Spearman's correlation between pre-operative goitre symptoms 222
Table 8.8 Pre- and post-operative median scores (interquartile range) of the MRC dyspnoea scale score as reported by the subjects 222
Table 8.9. Correlation co-efficient for pre-operative MRC score and: pre-operative lung function tests (PEF, FEV_1, FEV_1/PEF), weight of the excised thyroid gland, smallest cross-sectional area of the trachea, % reduction in the cross-sectional area of the trachea, pressure loss as calculated using CFD at a flow rate of 15L/min and 30L/min, and ThyPro pre-operative Goitre symptoms. **denotes statistical significance when $p<0.05$ 223

Chapter 1 Introduction

1.1 Thyroid goitre and the impact on the airway
1.2 Mechanics of breathing
1.3 Computational fluid dynamics (CFD)
1.3.1 Modelling flow in the large airways
1.3.2 Potential use of CFD as a tool for assessing patients with large airway pathology
1.4 Aims and Thesis outline

1.1 Thyroid goitre and the impact on the airway

The thyroid gland is a butterfly-shaped gland that is positioned in the neck immediately in front of the trachea (see figure 1.1). The gland produces thyroid hormones and is involved the regulation of many important functions in the body. A thyroid goitre refers to the abnormal, excessive growth of the thyroid gland. In a healthy adult without iodine deficiency the mean weight of the thyroid gland is 10-20g. (1)

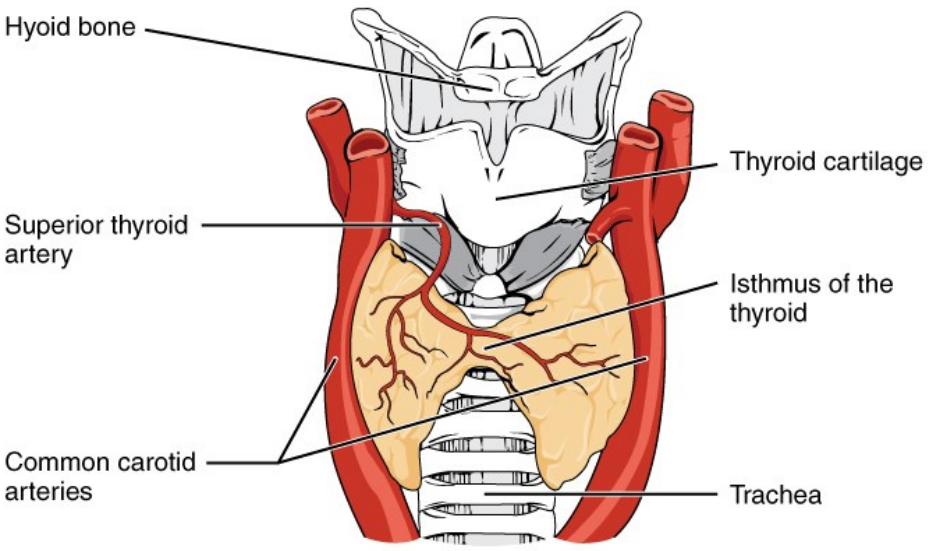


Figure 1.1. Schematic of the thyroid gland and its relation to the trachea (2)

Understanding the anatomical position of the thyroid gland is important when considering the effects an enlarged thyroid gland can have on surrounding structures. The

thyroid gland sits immediately anterior to the trachea and wraps itself around the trachea in a posterior-lateral fashion. Closely related structures include: the oesophagus which sits posterior to the trachea, the great vessels of the neck (the carotid artery and the internal jugular vein) which sit lateral to the thyroid on either side, the parathyroid glands which are most commonly found closely related to the superior and posterior poles of the thyroid on either side, and the recurrent laryngeal nerves, which run close to the trachea on either side. As the thyroid gland increases in size, initially it tends to extend laterally in the neck. As the gland continues to increase in size it can begin to extend inferiorly towards the mediastinum. Below the thyroid gland sits the thoracic inlet (see figure 1.2). This is an anatomical space connecting the neck to the mediastinum. It is bounded anteriorly by the sternum and clavicles, laterally by the first ribs and posteriorly by the spine. If the thyroid gland extends down through the thoracic inlet, it becomes a 'retrosternal' thyroid goitre or a 'substernal' thyroid goitre, this is the most commonly accepted definition of a retrosternal goitre. Around 90% of retrosternal thyroid goitres sit in the anterior mediastinum, with around 10% extending into the posterior mediastinum. (3)

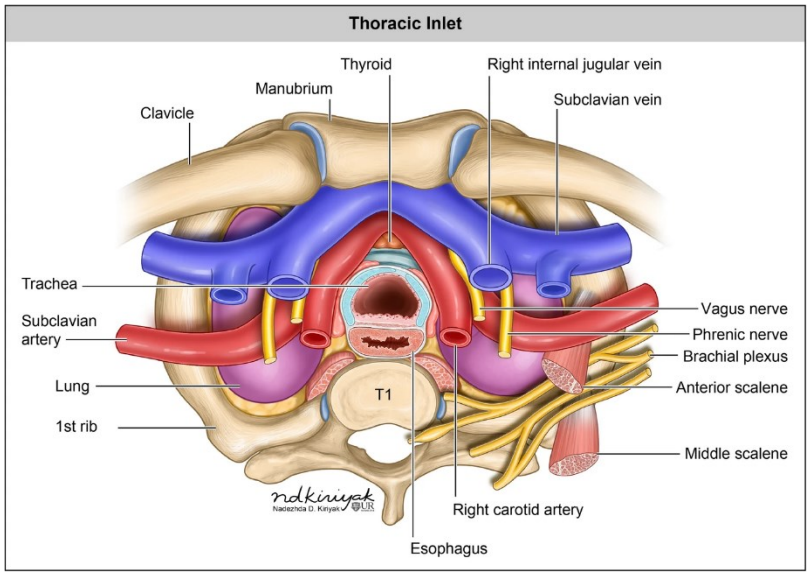


Figure 1.2 Schematic of the thoracic inlet (4)

There are two subgroups of goitre; the first being non-toxic goitres where the gland produces the correct amount of thyroid hormone (euthyroid), or an insufficient amount of thyroid hormone (hypothyroid), and the second subgroup being toxic goitres where the gland produces an excess of thyroid hormone (hyperthyroid). This thesis will be considering the first type of goitre – non-toxic goitres. Worldwide the most common cause of a non-toxic goitre is

iodine insufficiency, which leads to endemic goitre, accounting for 90% of goitres. (5) In iodine sufficient regions of the world the most common type of non-toxic goitre is the multinodular goitre.

The natural history of multinodular goitres is variable amongst patients however, in most patients there is slow growth of the goitre over many years. It is estimated that in some patients there can be up to 20% annual increase in growth. In a small number of patients, the growth may plateau or even regress. (6) Due to the slow growing nature of most multinodular goitres, these patients tend to present with symptoms later in life. Retrosternal goitres tend to be diagnosed in the 5th and 6th decade of life and are more common in women than in men. (3) There is an estimated 4% malignancy rate in multinodular goitres, and this should be kept in mind when planning the management. An increased area of functioning within the multinodular goitre can progress to overt hyperthyroidism or a toxic nodule within the gland (Plummer's nodule), and this occurs in around 5% over a 5 year period. (7)

A large number of multinodular goitres are asymptomatic and may only be picked up incidentally on cross-sectional imaging performed for other reasons. Larger cervical goitres (those that haven't extended retrosternally) may be visible and palpable in the neck and diagnosed on routine examination of the neck. Once growth has been substantial enough for the goitre to become retrosternal the patient tends to be symptomatic, with one series quoting symptoms present in up to 90% of patients with a retrosternal goitre. (8) The most common symptom is exertional dyspnoea (breathlessness on exercise) which is present in up to 60% of patients with a retrosternal goitre. (9) Due to the compression of the trachea from the thyroid gland a number of other airway symptoms can be present: cough, positional dyspnoea (breathlessness when lying flat), contribution to symptoms caused by obstructive sleep apnoea and in extreme cases, where the trachea has become severely compressed, the patient may present with stridor. Due to the proximity of the oesophagus some patients have dysphagia (difficulty swallowing). Patients often complain of a pressure type feeling in their neck. Cosmetic concerns are fairly common amongst patients with a visible goitre. Other, rarer, symptoms include a hoarse voice due to compression of the recurrent laryngeal nerve, Horner's syndrome, and superior vena cava syndrome.

When these patients present to the outpatient clinic, they are normally investigated with an ultrasound scan to look at the nature of the nodules in the thyroid gland and any suspicious nodules undergo fine needle aspiration to determine if there is a cancerous or indeterminate nodule. The patient will undergo a set of blood tests including thyroid function tests to assess the function of the thyroid gland, looking for under-activity (hypothyroidism), normal function

(euthyroid) or over-activity (hyperthyroidism). During the physical examination of the patient the neck will be examined and if the thyroid gland is large and the doctor is unable to palpate below the thyroid gland (i.e. the thyroid gland extends below the level of the sternal notch) then a retrosternal goitre is suspected and cross-sectional imaging, normally a non-contrast CT scan of the patient's neck and chest, is requested. The CT scan provides important information including: the size, shape, and extension of the thyroid gland into the patient's mediastinum, compression, and degree of compression of surrounding structures e.g., the trachea. If surgery is planned, the CT scan will also help decide the likelihood of a sternotomy being required. This is required in around 2% of patients with a retrosternal goitre. (10) A thorough patient history will assess for any compressive symptoms or cosmetic concerns that the patient may be experiencing. Some units may perform lung function tests including flow volume loops to assess for upper airway obstruction if the patient has suggestive symptoms.

A literature review by White et al (10) highlighted the lack of high-level evidence on the management of retrosternal goitres. The management options for patients with non-toxic, retrosternal multinodular goitres in areas of iodine sufficiency are either a conservative approach with interval imaging to assess for changes in size of the goitre, or surgery. In large goitres there is no role for radioactive iodine or thyroid hormone suppression. Total thyroidectomy is preferred over subtotal thyroidectomy due to the higher recurrence rate with subtotal thyroidectomy (0.2% vs 8.4%). (11) In select patients a lobectomy or hemithyroidectomy (when half of the thyroid gland is excised) is more appropriate and this may be for a number of reasons; an asymmetrical goitre where only one half of the goitre is enlarged leading to unilateral compressive symptoms, a pre-operative vocal cord palsy or an intra-operative vocal cord palsy.

The decision to operate takes into account a number of different factors and is not a straight-forward decision. In asymptomatic patients there is a good argument for a more conservative approach with interval imaging. In younger, medically fit patients with symptomatic goitres an operation provides them relief of symptoms and prevents any further growth or complications associated with the goitre. However, a large number of patients fall outside of these two groups and are symptomatic but also elderly with comorbidities. The surgical risk in this group is greater and careful consideration needs to take place prior to operating. A large observational study assessing the risks of cervical thyroidectomy versus retrosternal thyroidectomy found that the risk of damage to the recurrent laryngeal nerve increases from 0.6% to 2.1%, the risk of hypoparathyroidism increases from 3.5% to 5.5%, the risk of post-operative bleeding increases from 0.9% to 2.2% and the risk of mortality is

increased fourteen-fold (from 0.1% to 1.4%). (12) The complications of surgery have the potential to dramatically affect the quality of life of the patient and may outweigh the benefits of surgery. In a study carried out by the author of the thesis, looking at the quality of life in patients with post-thyroidectomy hypoparathyroidism, this patient group had a significantly lower scores across all domains of the SF-36 than the control population (refer to the full study by McIntyre et al in the appendix).

In 2014 the American Thyroid Association published a statement on the 'Optimal Surgical Management of Goitre'. This statement is the current gold standard used for assessing and managing patients presenting with benign goitres. This statement includes a recommendation that thyroidectomy should be considered in patients with a 35% or greater reduction in the AP diameter of their trachea. This recommendation was based on a retrospective study by Stang et al. (13) The study looked at all patients who underwent thyroid surgery at one hospital over a six-year period and identified 197 patients who underwent thyroid surgery with symptoms of positional dyspnoea or tracheal compression found on a CT scan, or both. 54 of the patients had a thyroid lobectomy and 143 patients had a total thyroidectomy. 151 of the patients had a retrosternal goitre. The 151 patients with a retrosternal goitre were all managed surgically with a standard cervical incision and there was no requirement for sternotomy.

Positional dyspnoea was defined as the patient reporting any symptoms related to difficulty breathing when lying flat or leaning forward. Tracheal compression was measured on CT imaging by the surgeon and defined as the greatest percent reduction in transverse tracheal diameter. The authors didn't define which part of the trachea they used as a standard for the tracheal diameter i.e., which part of the trachea was used to compare the compressed part of the trachea.

They found that in the group of patients who had tracheal compression of 15-34% there was 67% rate of reporting an improvement in their symptoms post operatively. In the group of patients who had tracheal compression of 35% or greater there was a 95-98% reported rate of improvement in symptoms post operatively. The authors concluded that this inflexion point at 35% indicated that patients with 35% or greater tracheal compression should be considered for surgery. These results were statistically significant with p values of <0.01 and <0.001 respectively.

The main limitation with this study is the retrospective nature and the reliance on previous medical records. Patients reporting an "Improvement in their symptoms" is a

subjective measure of post-operative outcomes and may be subject to clinician bias. The patient may have reported an improvement in their symptoms however this may not necessarily indicate an improvement in their positional dyspnoea symptoms and may have referred to an improvement in other symptoms which could have been relieved by undergoing thyroidectomy i.e., dysphagia, hoarse voice, cosmetic concerns.

The issues that arise from the current guideline is that there is an over-simplification of the problem. A 2-dimensional measurement taken from a CT scan doesn't take into account the length or shape of the compression, both which are factors known to affect the airflow through the trachea. (14) At present, the clinical dilemma thyroid surgeons are left with in clinic is deciding which patients to operate on and which patients to take a more conservative approach.

1.2 Mechanics of breathing

The upper airway conducts air to the lungs. Other functions of the upper airway include phonation, olfaction, air warming and humidification. The upper airway comprises the nasal cavity, the nasopharynx, the oropharynx, the hypopharynx, the larynx, and the extra-thoracic segment of the trachea. The lower airway comprises the intrathoracic segment of the trachea, the bronchi, the bronchioles, which lead down to the alveoli where gas exchange takes place (see figure 1.3).

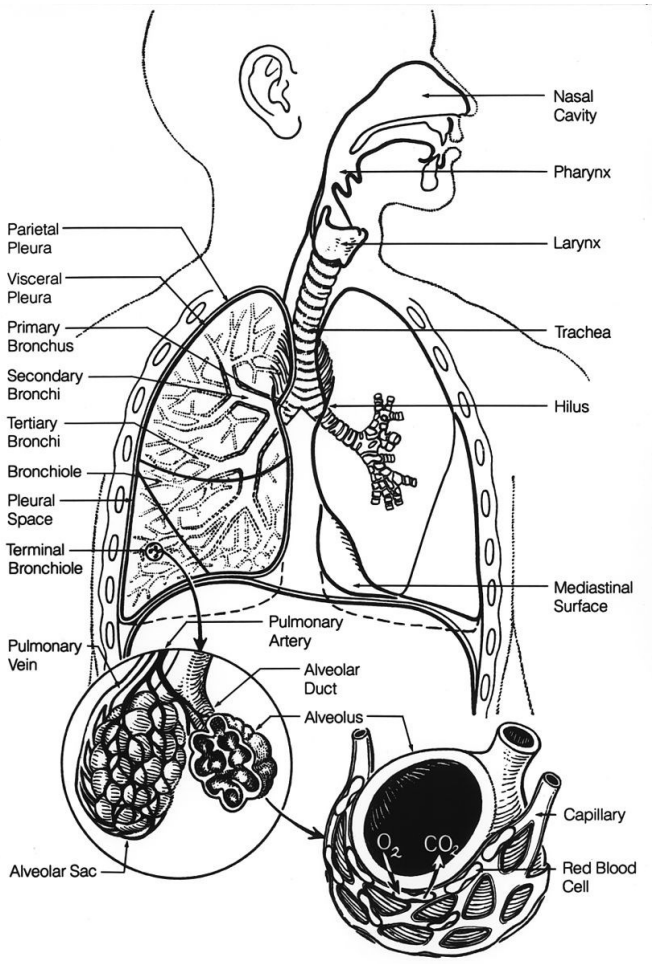


Figure 1.3. Schematic of the upper and lower airways (15)

Of particular interest to this thesis is the anatomy of the trachea (see figure 1.4). The trachea has two main sections; the extra-thoracic segment and the intrathoracic segment which are anatomically divided at the level of sternum. On average the length of the trachea is between 100-120 mm in the healthy adult. It extends from the lower border of the larynx down to the carina (where the trachea divides into the left and right bronchi). The trachea is made up of five distinct tissue layers: the inner mucosal layer, the submucosal layer, cartilaginous rings and muscle and an outer adventitia. Posteriorly the wall of the trachea consists of the trachealis muscle, which can collapse inwards into the lumen of the trachea during expiration as the intrathoracic pressure increases. Anteriorly the trachea is supported by 18-22 cartilaginous incomplete rings. The wall of the trachea is between 1-3mm thick and on a CT scan is defined by the contrast between intraluminal gas and mediastinal fatty tissue. The average transverse internal diameter of the trachea in a healthy male adult is 15-25 mm and in a healthy female adult is 10-21 mm. (16)

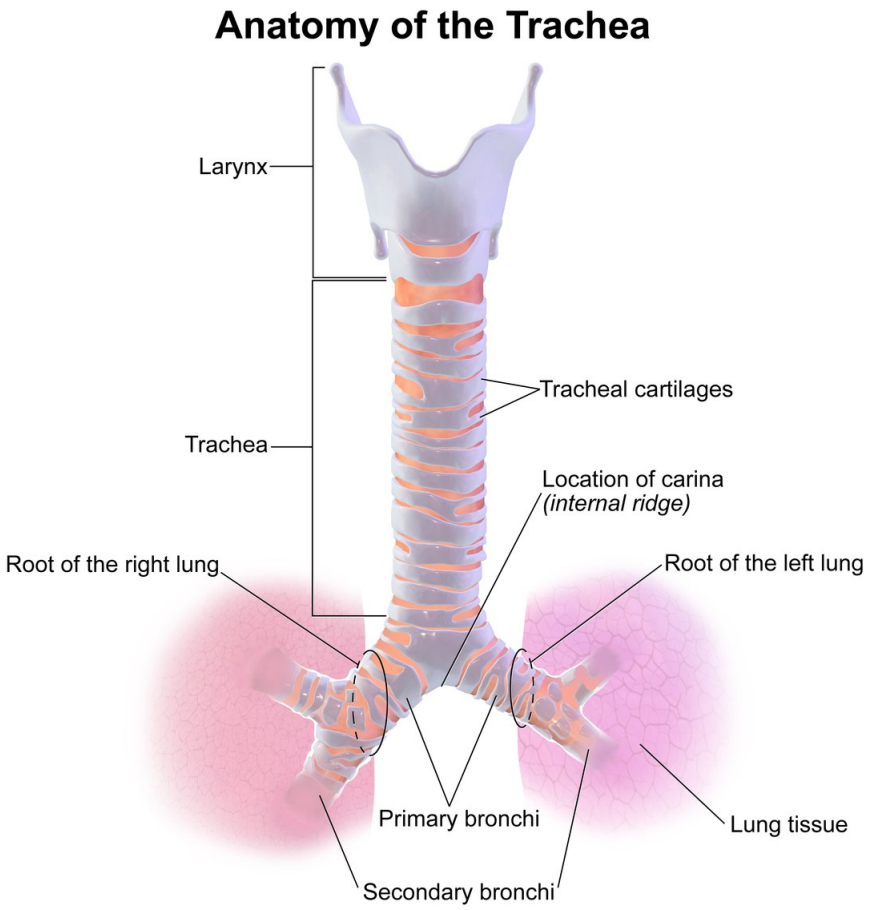


Figure 1.4. Schematic of the trachea and the major bronchi (17)

Air enters the body through the mouth or nostrils. In the nasal cavity, air is warmed and humidified as it passes over and around the turbinates (large outpouchings within the nasal cavity). The airflow is then forced around an almost 90-degree bend as it enters into the nasopharynx and passes into the oropharynx. The soft palate, tongue base, tonsils and other surrounding soft tissues can all collapse inwards during sleep which creates an obstruction within the upper airway and leads to the apnoeas and hypopneas that occur in patients with obstructive sleep apnoea. Air continues to flow through the hypopharynx and here it encounters the glottis and surrounding supraglottic structures. Due to the natural narrowing of the airway at this point, the glottis behaves like an orifice and produces a flow jet which contributes significantly to energy losses at this point in the airway.

When considering air flow through the trachea we think in terms of volumetric flow rates. Throughout the literature, studies of airflow through the large airways tends to refer to quiet breathing (15L/min), light exercise (30L/min) or moderate exercise (60L/min). In the

large airways the Reynolds number is often greater than 2300 and the flow is considered to be turbulent or at least transitional. Lower down the respiratory tract in the lower airways flow becomes more laminar and pipe friction and entrance effects are the main source of energy loss. In the large airways, due to the large Reynolds number, flow cannot be considered to be Poiseuille flow. Poiseuille flow doesn't take into account disturbances to the flow caused by entrance effects, flow separation due to sudden expansion following a narrowing in the airway, or curvature of the airway.

Airflow into the lungs is driven by the difference in pressure *(*D*P)* between the pressure at the airway opening, the barometric pressure (*PB*) and the alveolar pressure (*PA).*

$$\dot{V} \propto \Delta P = PB - PA \qquad \text{Equation 1.1}$$

A healthy adult patient has a tidal volume of around 500mls, this is the volume of air that is breathed in and out during quiet (resting) breathing. The total lung capacity is around 6L. There is a large inspiratory and expiratory reserve for when the individual has an increased respiratory drive i.e., during exercise (see figure 1.5).

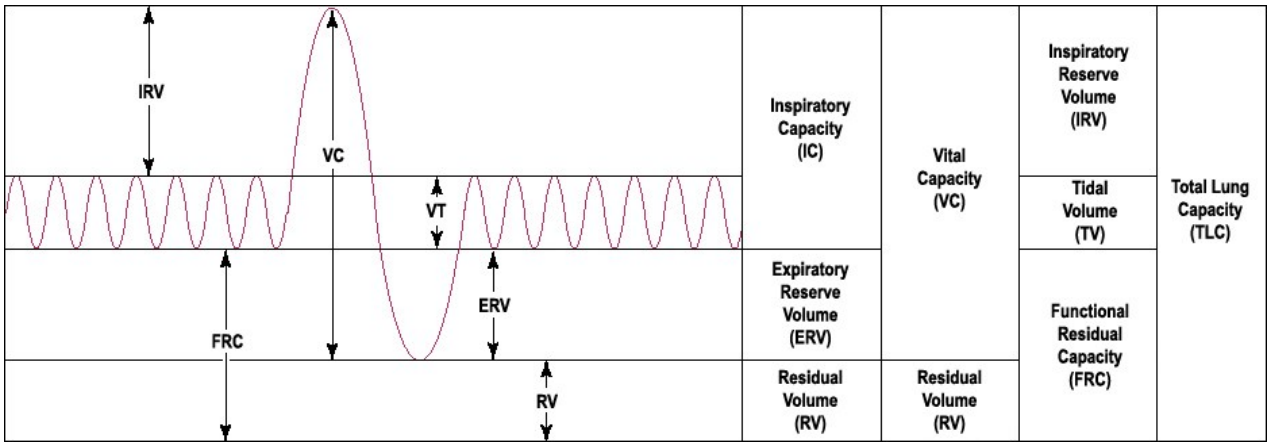


Figure 1.5. Standard lung volumes and capacities from a spirometry trace (18)

The work of breathing is made up of two main components; the work required to expand the lungs and the work required to overcome the resistance to filling and emptying the lungs. The work required to expand the lungs can be described as "elastic work", as this is the work performed to overcome the elastance of the chest wall and lungs. The work required to

overcome the resistance to filling and emptying the lungs can be described as “resistance work” and is largely made up of the airway resistance to air passing in and out of the airways. During the course of this thesis, we will be considering the “resistance work” of breathing due to the increased airway resistance encountered if the airway is compressed by a retrosternal goitre.

Resistance to airflow can be divided into major and minor losses. Major losses can be described by the Darcy-Weisbach pipe friction equation:

$$h_L = f.\frac{L}{D}\frac{U^2}{2g} \qquad \text{(Equation 1.2)}$$

Where:

h_L = head loss

f = friction loss

L = length of the pipe

D = diameter

U = mean flow velocity

Expressing the loss directly in terms of pressure:

$$\Delta P_L = f.\frac{L}{D}\frac{\rho U^2}{2} \qquad \text{(Equation 1.3)}$$

Where:

P_L = Pressure loss across the length of the pipe

ρ = density of air at body temperature

In the large airways minor losses dominate. These minor losses are a result of changes in the airway e.g., constrictions, sudden expansions, curvature, branching leading to entrance effects. Minor losses are normally expressed in terms of the loss coefficient:

$$\Delta P = K_L.\frac{\rho U^2}{2} \qquad \text{(Equation 1.4)}$$

Where:

K_L= loss coefficient

Dyspnoea is the medical term for describing the subjective sensation of breathing discomfort. There are many causes of dyspnoea, and the pathophysiology is complex and varied. There is a distinction between a breathing "sensation", which is a brought about by the stimulation of a receptor leading to neural activation, and a breathing "perception" which is the patient's reaction to the sensation. There are multiple types of receptors throughout the cardiopulmonary system involved in the sensation of dyspnoea, and these are divided into the two main types: chemoreceptors and mechanoreceptors. We will consider here the stimulation of mechanoreceptors with relation to the sensation of dyspnoea. If there is an increased mechanical load on the ventilation system of the body e.g., increased airway resistance, this is detected by stimulation of a number of different mechanoreceptors throughout the upper airway, the lungs (pulmonary receptors) and the chest wall. The system is designed to recognise if there is a mismatch in the effort or work of breathing and the expected airflow into the lungs. Therefore, an increase in the work of breathing secondary to, for example, a compressed trachea, and the resultant reduced airflow leads to the sensation of dyspnoea. Figure 1.6 demonstrates a simplified schematic of the afferent "input" signals and efferent "output" signals that contribute to the sensation of dyspnoea. (19)

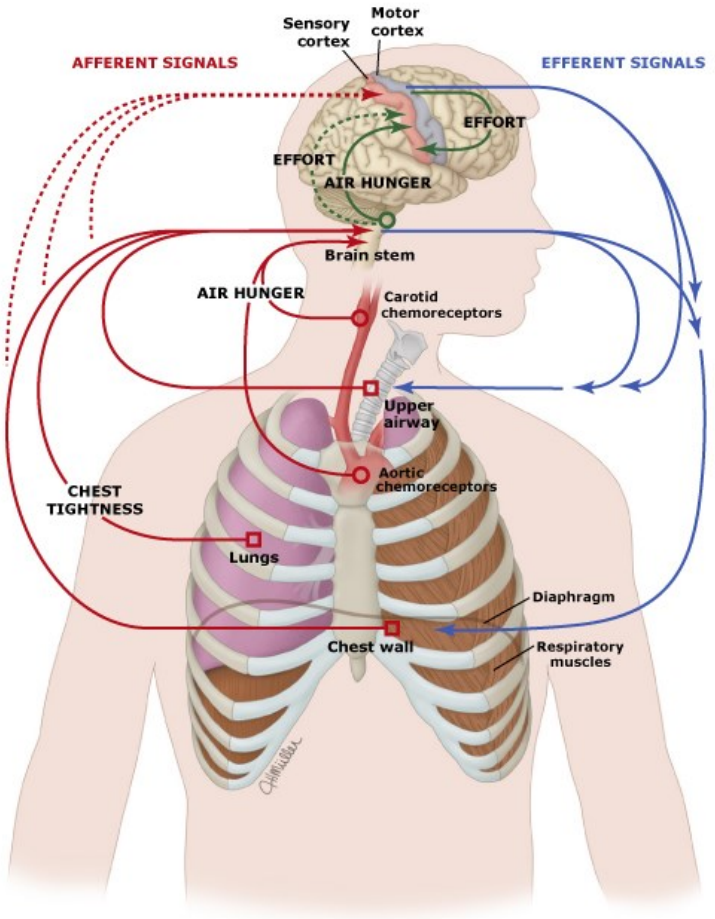


Figure 1.6. schematic of the afferent "input" signals and efferent "output" signals that contribute to the sensation of dyspnoea (20)

1.3 Computational fluid dynamics (CFD)

1.3.1 Modelling flow in the large airways

The use of computational fluid dynamics (CFD) to analyse the human airway has become an increasing area of interest over recent years. A review published by Faizal et al (21) summarises the extensive use of CFD for studying the airway across different medical specialities and different airway diseases ranging from asthma to obstructive sleep apnoea. Medical imaging can be used to create models of a patient's airway and, using CFD, the flow through the patient's airway can be modelled, providing a wealth of data such as flow properties and flow patterns. CFD can be used to assess the impact of airway disease e.g., tracheal stenosis, bronchial tumours, vocal cord palsy, on the flow of air through the human respiratory tract. It

can be used to aid surgical planning by manipulation of the 3D model of the patient's airway to represent post-operative changes and then using CFD to predict how surgery would affect the airflow.

There are some key steps involved in using CFD to accurately estimate flow through the airways. The first step is providing an accurate representation of the patient's airway. This is most commonly performed using computer tomography (CT) scans. A surface mesh is created to represent the desired area of interest. This is then translated into a volume mesh which can be exported to simulation software such as STAR-CCM+. It is not uncommon for studies to use simplified models of the airway due to the reduced computational time; however simplified models reduce the accuracy of the results.

Next, an appropriate simulation model needs to be selected to reflect both the clinical problem and the type of flow that will be modelled. In the upper airway the flow can be laminar, transitional, or turbulent, due to the complexity of the upper airway anatomy, by the time flow has reached the adult trachea the flow is turbulent. Direct numerical stimulation (DNS) solves Navier stokes equations directly without using a turbulence model. However, solving Navier stokes equations directly for complicated problems is computationally very expensive. Instead, a turbulence model can be used. The two main types of turbulence models used are: large eddy simulation (LES) and Reynold's averaged Navier-Stokes (RANS). LES is a turbulence model whereby the large-scale eddies are directly resolved, and the small-scale turbulence is modelled. The transport equations are solved by using a spatial filter, with the solution variables being divided into a filtered, a sub-filtered and a sub-grid value. RANS equations are based on the observation that the flow field contains many small eddies and oscillations which can be treated in a time-averaged sense. RANS is thought to be less accurate than LES however it is computationally much less expensive. There are eight different RANS models available and all of them calculate both Navier-Stokes equations with the addition of a turbulence eddy viscosity term. The models differ in the way in which the equations are computed, and they also differ in how they model the flow close to the walls. The SST k-omega turbulence model has been favoured in some large airway studies due to its superior accuracy of flow modelling in the near wall region and its treatment of adverse pressure gradients. (22)

A mesh independence study is normally required to ensure that the volume mesh is of sufficient quality to generate accurate and repeatable results. The simulation results need a validation study to ensure that the simulation accurately reflects real life results. Bates et al (23) published a CFD benchmark dataset of airflow in tracheas. This detailed paper used a reference solution of a computationally expensive near DNS (quasi-DNS) simulation model.

This was then used to validate LES as a turbulence model in the same pathological trachea. The quasi-DNS simulation was highly resolved with a mesh of 9.2 million elements and a timestep of 0.01ms. A mesh validation study with LES showed that a mesh with 2.2 million elements, 5 prism layers and a time step of 0.1ms offered accurate results without being computationally expensive. The pressure loss across the pathological trachea was calculated to be 53.8 Pa with both simulation models (quasi-DNS and LES). Although computationally less expensive than quasi-DNS, each LES simulation took around 2800-4000 core hours to run and therefore is still an expensive computation.

A number of studies have used RANS to model air flow through the large airways and have generally found good agreement with experimental data (24-27). There isn't a universally agreed turbulence model for modelling flow through the large airways and the literature would suggest that the turbulence model that correlates well with experimental data varies from case to case and is dependent on both the airway model and clinical problem.

Bates et al (28) used an LES model to explore the power loss mechanisms within the pathological trachea. Four pathological airway geometries and one healthy airway geometry were analysed. They found that in the healthy trachea had two areas of energy loss: flow losses associated with the glottic jet and distal to the jet there is an area of frictional losses at the wall of the trachea. In the pathological tracheas (which were compressed by thyroid goitres) the areas of energy loss were more complex. Downstream of areas of constriction there were additional areas of flow separation and flow disturbance leading to internal flow losses. Typically, in a healthy adult, the trachea contributes around 5% of the total airway resistance. This increases to several times of the flow resistance in compressed tracheas.

Xiao et al (29) analysed airflow through the trachea in a patient who had a progressively enlarging thyroid goitre over a number of years. Using energy flux analysis, it was found that the large airway regions that contribute most to airway resistance are downstream of the tracheal constriction (where there is flow separation and flow disturbance), the glottis and the tongue base. A further study by Bates et al (14) found that with an increasing degree of compression and curvature of the trachea there are increased energy losses.

1.3.2 Potential use of CFD as a tool for assessing patients with large airway pathology

In clinical practice we have a limited number of ways of assessing patients with large airway pathology, namely the patient's reported symptoms, medical imaging e.g., CT scans, direct

visualisation i.e., airway endoscopy and lung function tests. The information provided by these tools is limited. CFD provides a way of acquiring a much greater level of detail of the effect of the airway pathology on the flow through the airways. CFD can accurately predict changes in airway pressure, wall sheer stress, flow disturbances and changes to the velocity of air flow. Acquiring detailed information about the flow of air through the pathological airway has the potential to aid surgical planning. It may be able to help predict which patients may benefit from surgery. In a retrospective study by De Backer et al (30) they showed that CFD was able to accurately predict which OSA patients would benefit from mandibular advancement surgery. Furthermore, CFD can be used to help model post-operative changes to the airway prior to surgery taking place.

There have been a number of recent studies that have assessed the use of CFD for surgical planning in the large airways. Mylavarapu et al (22) used a RANS k-W model to simulate air flow through the large airways of a patient suffering with a glottic and tracheal stenosis. They manipulated the surface geometry to simulate post-operative changes and simulated airflow through a number of different manipulated "post-operative" geometries in order to assess the affect that surgery would have on airflow. They concluded that CFD was particularly helpful in understanding how post-surgical changes would improve the airflow through the stenotic areas and that CFD has the potential to be used for patient-individualised surgical planning. Zhao et al (31) made a similar conclusion in their study detailing the simulation of a middle turbinate reduction surgery. They simulated airflow through the pre-operative nasal airway and the "post-operative" nasal airway (after manipulating the surface mesh to represent the post-operative changes). The team commented that using CFD provides a quantitative evaluation of surgical effectiveness pre-operatively by modelling the potential outcome of a surgical intervention.

Many of the studies in the literature are limited by assessing only one or two patients and the studies are retrospective. Studies are also limited in that the real-life post-operative outcomes and measures are not reported.

The work presented in this thesis will explore the use of CFD to investigate the airflow through the tracheas of subjects with compressive thyroid goitres.

1.4 Aims and Thesis outline

This section details aims and the structure of the thesis and provides a brief summary of contents of each chapter.

The aims and objectives of this thesis:

i) Assess the use of computational fluid dynamics (CFD) to investigate the airflow through the tracheas of subjects with symptomatic, compressive, retrosternal thyroid goitres.

ii) Create and validate a tracheal volume mesh in order to standardize the approach for performing CFD on a 3D model of a patient's trachea. Validate a steady RANS model of CFD for simulating airflow through the trachea.

iii) Estimate the pressure loss across the trachea in a series of patients with symptomatic, compressive retrosternal thyroid goitres by employing a steady RANS CFD model.

iv) Consider the use of CFD for surgical planning in patients with a symptomatic, compressive, retrosternal thyroid goitre.

v) Assess the pre- and post-operative lung function tests of a series of patients with symptomatic, compressive retrosternal thyroid goitres.

vi) Study the pre- and post-operative quality of life series of patients with symptomatic, compressive retrosternal thyroid goitres.

The structure of the thesis:

Chapter two describes the cohort of patients recruited for the main thyroid goitre study and details the inclusion and exclusion criteria. The ethical approval for the study is documented.

Chapter three presents a brief literature review of the methods involved in translating CT scan data into a virtual airway geometry. This chapter includes a description of the methods used in this thesis to create realistic 3D surface meshes of the subjects' airway and the rationale behind the methods utilised. The 3D surface meshes of subjects in the main goitre study undergo geometric analysis and the results are presented.

Chapter four is the main methods chapter for the CFD analysis of the airway flows. Firstly, there is a description of the methods used to generate volume meshes from the 3D surface meshes. The turbulence models used in the thesis are detailed followed by a series of validation tests to ensure accuracy and repeatability of the methods used. A steady RANS turbulence model is validated against an experimental model.

The main results of the thesis are presented in Chapter five**.** A steady RANS turbulence model is used to simulate airflow through the tracheas of subjects undergoing thyroidectomy for compressive thyroid goitres and the results are presented. Pressure loss across the pathological trachea is estimated using CFD. The patterns of flow are studied in three of the geometries: a mildly compressed trachea, a moderately compressed trachea, and a severely compressed trachea. The pressure loss across the pathological trachea is correlated with the geometric analysis. A loss co-efficient is used to estimate pressure loss using the minimum cross-sectional area of the trachea and this is compared with the CFD prediction of pressure loss.

Chapter six explores the potential applications of CFD for surgical planning and pathophysiological understanding of the airway. A subject's tracheal surface mesh is modified to create a surface mesh that would represent the post-operative changes to the trachea. CFD is then used to simulate airflow through the 'post-operative' trachea and the results of the pre- and post-op pressure loss are compared.

Chapter seven analyses the results of the pre- and post-operative lung function tests that the main subjects underwent as part of the study. Pre- and post-operative spirometry results are compared to look for any significant changes. A small number of subjects had both upright and supine testing, the results of these tests are compared. An average flow rate was calculated for each subject using the flow-volume loop and the power loss for a breath at this flow rate was calculated. The estimated pre- and post-operative power losses across the subjects' tracheas are compared to look for significant differences.

Chapter eight examines the outcomes of the quality-of-life questionnaires completed by the main study subjects: the ThyPro and the MRC dyspnoea scale, which were completed both before and after surgery. The results are correlated with the geometric analysis of the tracheal surface meshes, the lung function tests, and the pre-operative pressure loss as estimated by CFD.

Finally, Chapter nine makes concluding remarks about the work carried out in the thesis and discusses potential for future work.

Chapter 2 Study Cohorts

2.1 Description of the study cohort
2.2 Ethical approval
2.3 Inclusion criteria and data gathered

2.1 Description of the study cohort

To investigate the effect of compressive thyroid goitres on the airway, competent, adult patients undergoing thyroid surgery for retrosternal goitres with compressive symptoms at a tertiary referral centre were invited to be included in the study. Patients were excluded from the study if: they were undergoing surgery for a thyroid malignancy or suspected thyroid malignancy, they were diagnosed with a pre-operative vocal cord palsy, they lacked capacity to consent to take part in the study, they had any other significant airway pathology (e.g., tracheal stenosis), or if the patient was not biochemically euthyroid.

2.2 Ethical approval

Ethical approval was granted by the London Research Ethical Committee (REC number: 17/LO/1464). Sponsorship approval was granted by Imperial College JRCO.

2.3 Inclusion criteria and data gathered

Study subjects were initially assessed in the outpatient clinic and, as part of their normal pre-operative investigations, they underwent a CT scan of the neck and chest, and a pre-operative set of lung function tests including a flow-volume loop.

In addition, the subjects completed a set of pre-operative, validated questionnaires including the Medical Research Council (MRC) breathlessness scale and the Thyroid-related Quality of life measure (ThyPro).

The following pre-operative data was collected: demographic data, thyroid status, medical co-morbidities, history of respiratory disease, smoking status, number of flights of stairs subjects reported they were able to climb prior to becoming breathless, history of OSA, ability to lie flat, symptoms related to the goitre recorded in the clinic letter, and pre-operative vocal cord assessment on flexible nasolaryngoscopy.

Pre-operative CT neck and chest scans were performed on all subjects. These were performed using a Philips Ingenuity Flex[32] CT scanner with the following acquisition protocol; 120kV, slice thickness 2mm, iDose. The subject was in the head-first supine (HFS) position for the CT scan and the scan was taken during quiet breathing, specifically during inspiration.

Pre-operative lung function tests were performed prior to surgery in the spirometry laboratory using the Carefusion Vyntus spirometer. The protocol published by the European Respiratory Society (32) was followed by qualified technicians. Prior to each set of tests the equipment was calibrated. The subject's height, weight, race, sex, and age were recorded, and any inhaler/drug therapy use was noted.

The standard position for spirometry is with the subject sat upright with their feet flat on the ground, legs uncrossed without any tight fitted/restrictive clothing. A nose clip is applied, and the patient is asked to form a tight seal around the spirometer mouthpiece (see figure 2.1). In order to measure the forced vital capacity (FVC) and forced expiratory volume in 1 second (FEV_1) the subject is asked to take in a deep breath, as large as possible and then to blow out as fast as they possibly can and to keep blowing out until they have no more air left to blow out. Peak expiratory flow (PEF) is obtained from the same manoeuvre. The inspiratory vital capacity (IVC) manoeuvre follows on from the FVC FEV_1 manoeuvre and is performed by asking the subject to take a fast, deep breath back in after breathing all of the way out. The manoeuvres are repeated to ensure that there is reproducibility and that the repeated results meet the minimum accepted criteria. Three of the best test results need to be within 5% of each other. The following results were recorded:

- Forced expiratory volume in 1 second (FEV_1)
- Forced vital capacity (FVC) which is the maximum volume of air exhaled by a subject when exhaling out as fast as possible
- FEV_1/FVC ratio
- Peak expiratory flow (PEF) this is the maximal flow that can be blown out when exhaling at a steady rate
- Forced expiratory flow (FEF)
- Forced inspiratory flow (FIF)
- Inspiratory vital capacity (IVC), the maximum amount of air which can be inhaled after a full expiration.

In addition, three, repeatable flow volume loops were recorded in order to assess the subjects for evidence of upper airway obstruction. Where possible, the lung function tests were recorded in both the upright and supine position.



Figure 2.1. A patient performing a spirometry manoeuvre (33)

A consultant thyroid surgeon performed or supervised a trainee surgeon performing the thyroidectomy. The procedure was performed using the same standardized technique in all patients, under general anaesthetic. All patients had intra-operative intermittent recurrent laryngeal nerve monitoring using the NIM EMG tube and handheld stimulator (Medtronic, USA). All patients had one overnight stay in hospital and were discharged home the next day, in the absence of complications. Post-operative parathyroid hormone (PTH) levels and serum calcium levels were measured at 9pm on the evening of the surgery and then again at 6am the morning after surgery. Calcium supplements were prescribed, following the departmental guidelines, and adjusted for the PTH and serum calcium results. Female patients were commenced on 100 μg of Levothyroxine, and male patients on 125 μg on the first post-operative day. The initial post-surgical follow up was at two weeks post-operatively and then, in the absence of complications once more at >6months post-operatively for completion of post-operative lung function testing and quality of life questionnaires.

More than 6 months post-operatively subjects underwent lung function testing (as

described above) and completed the MRC breathlessness and the ThyPro questionnaires. If patients were lost to follow up, they were initially contacted by letter to attend a follow up clinic appointment. Failing this they were contacted via the telephone and invited back to clinic. If the patient once again failed to attend the follow up clinic appointment the questionnaires were sent in the post with a return envelope and an outpatient clinic appointment sent for the lung function tests.

The following post-operative data was collected: thyroid status (TSH, T3 and T4), ongoing requirement of calcium supplements (hypoparathyroidism), post-operative vocal cord assessment on flexible nasolaryngoscopy, post-operative complications, weight of the thyroid gland excised.

Twenty-one patients with compressive thyroid goitres had a full set of the pre- and post-operative data (aside from the lung function tests which were not completed for all of the patients). The demographics are shown in the table 2.1. The mean age (+/-SD) in years at the time of surgery was 57 +/-14. 15 of the patients were female and 6 were male, reflecting the predilection of thyroid disorders for the female population. Most patients (76.2%) underwent a total thyroidectomy, with 23.8% undergoing a hemithyroidectomy (one of which was a revision, having previously undergone sub-total thyroidectomy twenty years prior). Of the patients who underwent a hemithyroidectomy, none required thyroid hormone supplements at 6 months post-operatively. All patients had both pre-operative and post-operative flexible nasoendoscopy to assess for vocal cord dysfunction. 3 of the patients had a temporary vocal cord paresis following surgery, however they all recovered normal vocal cord function by 6 months. All patients were clinically and biochemically euthyroid at 6 months following surgery and for those who had a total thyroidectomy, were on a stable dose of Levothyroxine. Parathyroid hormone levels and serum calcium levels were normalised at 6 month post-operatively in all patients without the requirement of calcium or vitamin D supplements. The median (+/- IQ range) weight of the goitre excised was 80.0 g (+/-116.5). Three subjects were found to have incidental papillary microcarcinomas on histology. All of these three cases were discussed in the thyroid multi-disciplinary team meeting and no further treatment was recommended.

Age (years)	57 +/- 14 (mean +/- SD)
Sex	Female - 15 (71.4%) Male – 6 (28.5%)
Surgery	Total thyroidectomy – 16 (76.2%) Hemithyroidectomy – 5 (23.8%)
Weight of the goitre excised (g)	80.0 +/- 116.5 (median +/- IQ)
Pre-operative vocal cord palsy	0
Temporary vocal cord paresis	3
Post-operative vocal cord palsy at 6 months	0
Requiring calcium/vitamin D supplements at 6 months	0
Other surgical complications	0

Table 2.1. Patient demographics and details of surgery

A list of the co-morbidities and the number of subjects with the co-morbidity can be seen in table 2.2. Hypertension was the most common co-morbidity (5 subjects). The median (+/- IQ range) number of flights of stairs that the subjects can climb before being restricted by shortness of breath is 2 +/- 1 flight. 18 of the patients reported that they could lie flat, whilst 3 reported they couldn't lie flat, due to compression from the goitre.

The most common description of the subjects' symptoms in the pre-operative clinic letter was "shortness of breath", followed by "compressive symptoms" and "difficulty swallowing" (see table 2.3). Post operatively it was found that 17 of the clinic letters made a note that the symptoms had improved, whilst 4 of the letters did not mention the symptoms.

Co-morbidity	Number of subjects
Hypertension	5
Renal impairment	3
Diabetes type II	2
Obstructive sleep apnoea	1
Previous stroke	1
Chronic obstructive pulmonary disease	1
Angina	1
Asthma	1
Acromegaly	1

Table 2.2. Co-morbidities and the number of subjects with the co-morbidity

Symptoms in pre-operative clinic letter	Number of subjects with symptom documented
Shortness of breath	5
Compressive symptoms	4
Difficulty swallowing	4
Exertional breathlessness	3
Positional dyspnoea	2
Difficulty breathing	2
Noisy breathing when lying flat	1
Progressive breathlessness	1
Neck tightness	1
Discomfort around neck	1

Table 2.3. Symptoms described in the pre-operative clinic letter and the frequency of the symptom being documented

Chapter 3 Geometric analysis of the airway

3.1 Introduction
3.2 Translating CT scan data to a virtual airway geometry
3.3 Choice of landmarks
3.3.1 Effect of the upper airway
3.3.2 Effect of glottic closure angle
3.3.3 Effect on the main bronchi
3.3.4 Surface Mesh modifications
3.4 Methods
3.4.1 Measuring the minimum diameter of the trachea and the % constriction
3.4.2 Measuring the minimum cross-sectional area and % area constriction
3.4.3 Ellipticity
3.4.4 Measuring the length of constriction
3.4.5 PACS (Picture Archiving and Communications System) measurements
3.4.6 Intra-user repeatability
3.5 Results and discussion
3.6 Conclusions

3.1 Introduction

This chapter describes the geometric analysis of 21 tracheal geometries of patients undergoing a thyroidectomy for a compressive thyroid goitre. Firstly, there is a description of the method of converting a CT scan of the airway into a 3D tracheal model. These tracheal models are later used to create volume meshes which in turn can be used to run computational fluid dynamics (CFD) and thus providing us with information about the flow of air through the trachea (refer to Chapter 5). Next, we consider which parts of the airway are important to include in the

tracheal model, with regards to the extent of the upper airway included. The main considerations being the computational cost and time spent making the tracheal model versus the accuracy of the model. Following this there is a description of the tracheal modifications including the addition of a standardized glottic opening. The results of the geometrical analysis of the 21 tracheal models are presented and includes the:

- Minimum diameter of the trachea and the % diameter constriction
- Minimum cross-sectional area of the trachea and the % area constriction
- Ellipticity of the trachea at the minimum cross-sectional area
- Length of constriction

Finally, the results of an intra-user repeatability study of the thresholds used to create the 3D tracheal model from the CT scan are presented.

Patients with retrosternal goitres typically undergo CT scans as part of their initial investigation. Clinical assessment of a patient presenting with an enlarged thyroid gland will identify patients with a retrosternal goitre. If the clinician cannot palpate below the goitre, then the goitre is thought to extend below the level of the sternal notch. Goitres extending below the sternal notch can no longer be clearly visualized with an ultrasound scan. The CT scan provides important information about the size and extent of the intra-thoracic goitre which is important for surgical planning. The majority of retrosternal goitres can be removed through a standard cervical incision however this should be determined by the surgeon pre-operatively with the aid of a CT scan. If there is a suspicion that the thyroidectomy may require a sternotomy then the procedure will need to be performed by a surgeon who can perform sternotomies or have a cardiothoracic surgeon on standby intra-operatively. (34) Planning this in advance also ensures that the patient is adequately informed and consented for the procedure. The CT scan also provides crucial information about the extent of tracheal compression.

In 2014 the American Thyroid Association published a statement on the ‘Optimal Surgical Management of Goitre’. (35) This statement is the current gold standard used for assessing and managing patients presenting with benign goitres. This statement includes a recommendation that thyroidectomy should be considered in patients with a 35% or greater reduction in the AP diameter of their trachea on CT scan. There are a number of limitations regarding using the greatest reduction in diameter of the trachea as a predictor of post-operative outcomes. The greatest reduction in diameter is a 2-dimensional measurement which does not

take into account the shape of the trachea at the level of the compression, the length of tracheal compression or the amount of tracheal deviation away from the midline. A unilaterally enlarged thyroid lobe or an asymmetrically enlarged thyroid lobe may result in tracheal deviation rather than tracheal compression. The deviation of the trachea away from the midline results in disruption in the flow of air through the trachea as demonstrated by Bates et al. (28) The study used computational fluid dynamic simulations to demonstrate how curvature affects the airflow energy dissipation in the tracheas affected by goitres. They found that an increased loss was associated with curvature and length of constriction.

A further limitation of using the greatest reduction in the diameter of the trachea is that on a CT scan the diameter of the trachea will not be measured in a plane perpendicular to the centreline of the trachea and therefore does not represent the true diameter of the trachea.

The trachea is typically 10-12cm in total length in an adult subject and can be divided into an extra-thoracic segment (2-4cm in length) and an intra-thoracic segment (6-9cm in length) when the trachea descends behind the sternal notch. The trachea begins at the cricoid cartilage and ends at the level of the carina where it divides into the two main bronchi. It is made up of C-shaped cartilaginous rings and a posterior membranous wall which is collapsible with expiration. During inspiration the trachea can typically be seen on CT scan as a circular structure, however during expiration it becomes concave in shape due to the collapse of the posterior wall of the trachea into the tracheal lumen. (36)

Between individuals there is a variability in what is considered normal parameters for non-pathological tracheal measurements. Vock et al (37) studied the CT scans of 25 healthy men and 25 healthy women. They measured the cross-sectional area at three different points along the intra-thoracic trachea. CT scans were performed with the individuals in the supine position and during quiet breathing. The three points measured were the thoracic inlet, the supra-carinal level, and a level halfway between these two points. The mean cross-sectional area across all three levels was 194mm^2 (S.D. 35) in women and 272mm^2 (S.D. 33) in men. The study concluded that absolute tracheal cross sections of less than 120mm^2 in women and 190mm^2 in men or relative values of less than 2/3 compared with other levels should suggest an abnormality.

The trachea is made up of cartilaginous incomplete tracheal rings connected by soft tissue. Posteriorly is the trachealis muscle. The trachea can be divided into the extra-thoracic and the intra-thoracic component as described above. These two components behave differently during the breath cycle. During expiration, there is an increase in intrathoracic

pressure which results in prolapse of the trachealis muscle anteriorly into the airway leading to a physiological narrowing of the intrathoracic trachea. The extra-thoracic part of the trachea is not subject to the same rise in intra-thoracic pressure. If there is an intrathoracic large airway obstruction e.g., a retrosternal thyroid goitre with an intra-thoracic compressive component, this narrowing of the airway is more pronounced and there is a greater reduction in the airflow through the obstructed airway.

In patients with a fixed extra-thoracic obstruction, e.g. vocal cord paralysis, airflow will be reduced symmetrically in both inspiration and expiration, this is because the extra-thoracic part of the trachea is not subject to the rise in intra-thoracic pressure during expiration. (38)

The degree of change of the internal diameter of the trachea during inspiration and expiration is variable between patients. Stern et al (39) carried out a study using ten healthy volunteers who had dynamic CT in the supine position. The purpose of the study was to define the range of normal intra-thoracic tracheal diameters seen in CT imaging, during forced respiration. The dynamic scans were performed at 500-ms intervals for a 6s period whilst the patient was directed to perform forced inspiration and forced expiration manoeuvres. They found that the mean cross-sectional area decreased from 280mm^2 (S.D. 50.5mm^2, range 221-388mm^2) at the end of forced inspiration to 178mm^2 (S.D. 40.2mm^2, range 115-236mm^2). This gives a mean reduction of 35% (S.D. 18%, range 11-61%) in the tracheal cross-sectional area between the end of forced inspiration and the end of forced expiration.

Another study by Boiselle et al (40) studied 51 healthy volunteers who underwent CT scanning during forced exhalation with spirometric monitoring. The cross-sectional area of the trachea was calculated at 1cm above the aortic arch and 1cm above the carina. The mean percentage reduction, of the tracheal cross-sectional area, during forced expiration was 54.34% (S.D. 18.6%) in the upper trachea, and 56.4% (S.D. 19.3%) in the lower trachea.

To look at the effect of inspiration on airway dimensions Petersen et al (41) analysed CT scans of 961 healthy patients lying supine during maximal inspiration. They showed that airway lumen diameter increases with the level of inspiration, however this effect was more pronounced in higher generation airways (more peripheral airways).

To look at the difference in cross-sectional area of the trachea during inspiration and expiration Ederle et al (42) looked at 156 patients who had undergone HRCT during inspiration and expiration. The group pf 156 patients were divided into three groups: healthy, restrictive airways disease and obstructive airways disease, according to their pulmonary function tests. They found that the cross-sectional area of the trachea during inspiration was significantly greater than during expiration in all three groups ($p<0.0001$). The mean area of the trachea in

inspiration was 2.41cm^2 compared to a mean of 1.96cm^2 during expiration (a decrease of 17.3%). No significant differences were seen between the change in tracheal cross-sectional area between the three groups. (42)

The minimum cross-sectional area (A_{min}, also sometimes referred to as CSA_{min}) can be used an indicator of the severity of tracheal pathology. There are a number of pathologies which can lead to tracheal narrowing including tracheal stenosis, tracheobronchomalacia, excessive dynamic collapse of the airways (EDAC), inflammatory diseases of the trachea e.g., giant cell arteritis with polyangiitis, external compression e.g., mediastinal tumours, compressive thyroid goitres. It is generally accepted that during the dynamic changes that take place during breathing that collapse of the airway during maximal expiration of up to 50% is thought to be physiological. The gold standard for assessing the airway is with direct visualization. This is not always practical, and clinicians are increasingly relying on imaging modalities to make assessments of patients' airways.

Poiseuille's law states that for laminar flow in a pipe of constant, circular cross-section, the flow rate is proportional to the radius to the fourth power. Considering such a flow as an idealised model for flow in a single section of airway, it can be seen that a small reduction in the diameter of the airway leads to a significant reduction in the flow rate of air through the airway.

Poiseuille's law:

$$Q = \frac{\pi \Delta P r^4}{8 \eta L} \qquad \text{Equation 3.1}$$

Where: Q = flow rate

L = length of the pipe

ΔP = Pressure difference of the length L of the pipe

r = radius of the pipe

h = fluid dynamic viscosity

Measuring the A_{min} on a CT scan will not produce the same value as when measuring the A_{min} on a 3D-reconstruction of the trachea. When measuring the A_{min} on a 3D-reconstruction of the trachea, the centerline can be calculated and slices along the trachea perpendicular to the center

line are measured to find the A_{min}. On a CT scan the orientation of the trachea is not always perpendicular to the plane of the image and therefore the slices measured will not represent the true A_{min}.

A further limitation of using the A_{min} as an indicator of tracheal pathology is that it doesn't take into account the shape of the trachea. A compressed area of trachea that has become elliptical in shape will have a greater impact on the power loss than a circular trachea which has the same cross-sectional area. An area of severe constriction can produce a downstream jet similar to the jet produced by the larynx.

Due the large variability in individual patient's tracheal dimensions it is useful to measure an area of constricted trachea relative to another tracheal measurement within the same patient. The cross-sectional area of the trachea at 2cm above the carina is considered to be constant in the human trachea. (43)

$$\%\ \text{reduction in the tracheal cross} - \text{sectional area} = \left(\frac{A_{min}}{A_{trachea}}\right) \text{x}100$$

Where A_{min} =minimum cross-sectional area of the trachea

$A_{trachea}$ = cross-sectional area of the trachea 2cm above the carina

If the minimum cross-sectional area of the trachea has the same cross-sectional area as 2cm above the carina, then the constriction ratio will be 1. If the smallest cross-sectional area of the trachea is 50% of the area 2 cm above the carina, then the constriction ratio will be 0.5.

Another important variable to consider, when assessing the impact of compressive goiters on the trachea, is the length of trachea affected. This has been studied in subglottic stenosis (SGS). SGS is a disease resulting in a narrowing of the trachea. The pathophysiology is not well understood, and disease progression varies dramatically between patients. The stenotic (or narrowed) area can vary in both the severity of the stricture (cross sectional area) and the length of trachea affected.

To look at the effect of the varying severity of stricture and the varying length of stricture in subglottic stenosis Lin et al (44) used CT scans of six healthy subjects and of five subjects with a diagnosis of SGS. CFD simulations were performed, and the airway resistance was estimated. The team hypothesized that the upper airway resistance could be described using the Bernoulli obstruction theory. This would mean that a four-fold reduction in the cross-sectional area of the airway would result in a four-fold increase in the resistance. Most studies assume that Poiseuille's law governs airway resistance changes in the upper airway, whereby

four-fold decrease in the cross-sectional area results in a sixteen-fold increase in resistance. However, the authors point out the Poiseuille's law is only valid for laminar flow in straight, circular tubes. Airflow in the human airway can be both laminar and turbulent and the airway is not a straight tube.

In addition to analyzing the healthy and SGS subjects, Lin et al (22) also created models of SGS using a healthy adult model with a digitally manipulated subglottic region to simulate an airway constriction. This cylindrical segment was manipulated to represent cross sectional areas corresponding to 40%, 50%, 60%, 70%, 80% and 90% obstruction. The cylindrical segment was also varied in length and included the following lengths: 10mm, 15mm and 20mm. Following steady-state airflow CFD simulations at a flow rate representing quiet breathing they found that the obstruction length had a greater impact in models with more severe constrictions. In models with 50% obstruction the airway resistance increased by 6.4% when they length of constriction changed from 5mm to 20mm. In models with 70% and 90% obstruction the airway resistance increased by 8.8% and 17.3% respectively, when the length of constriction changed from 5mm to 20mm. They found that overall obstruction diameter had a greater impact on the airway resistance than the obstruction length when compared as independent variables.

Using the digitally manipulated models of SGS, Lin et al (22) demonstrated that the change in airway resistance relative to the reduction in airspace cross-sectional area can be described using the Bernoulli obstruction theory. They concluded that the degree of airflow limitation may be estimated based on anatomical measurements taken from CT scans alone. They propose using a relative reduction in airspace cross-sectional area ($A^{obstructed}/A^{healthy}$) as an estimate of the relative reduction in airflow ($Q^{obstructed}/Q^{healthy}$). The main limitation of this study is the use of digitally manipulated models of SGS and the authors conclude that further work needs to be done using CT scans of real patients.

Bates et al (14) investigated the effects of curvature on energy losses in the human trachea. Using a large eddy simulation (LES) they modelled flow through 4 curved tracheas and found that curvature and alignment of the laryngeal jet can be equally important as the degree of constriction. The study concludes that curvature can change the location of the glottal jet dominated region by moving the location of impingement, and thereby altering the redistribution of high velocity flow. Furthermore, curvature increases loss by forcing flow away from the center of the curvature (which is opposite to the Frenet normal), and therefore reducing the area within the trachea which is utilized by flow.

3.2 Translating CT scan data to a virtual airway geometry

Airway segmentation is the identification of the airway tree from CT scans or from MRI scans. Here we will consider segmentation using CT scans. Segmentation utilises the contrast between the airway lumen and the airway wall. Airway segmentation produces a 3-D representation of the airway which can then be used for computer-based airway analyses such as computational fluid dynamics (CFD). Airway segmentation is used widely in the field of biomedical imaging and there are a number of software packages which specialise in the segmentation of images for use in medical research. The literature in the field of airway segmentation reports a wide number of different techniques and these can be broadly split into manual, semi-automatic and automatic. (45)

Manual segmentation requires the user to completely define the boundary of the airway over the entire scan data; for 3D datasets this is highly time and labour intensive and is therefore impractical for routine use. Semi-automatic techniques allow the process of airway delineation to be wholly or partly automated but allow the expert user freedom to input explicit guidance, such as manual region selection; semi-automatic techniques are thus widely used in the literature. The disadvantage of semi-automatic segmentations is that it introduces inter- and intra-user variability. Fully automatic processing removes this variability (46), but requires the images to show sufficient contrast between the airway lumen and non-airway lumen.

The simplest means to distinguish between the airway and the surrounding tissue in an image is by comparison of intensity or greyscale values. CT displays the effective linear attenuation coefficient, expressed in Hounsfield units (HuS). Hounsfield units are used because they are relatively stable across systems, however, differ across tissues and, also within tissues if there is an abnormality. In CT the effective linear attenuation coefficient is determined for each spatial co-ordinate and its relative deviation from water is displayed as HU. A value of -1000 HU represents air, and 0 HU represents water (47).

The most frequently used method for airway segmentation is ‘region growing’. This is a semi-automatic technique which uses a seed location and a threshold. The user selects a defined upper and lower threshold in Hounsfield Units (HU) and places a seed, or a number of seeds inside the airway lumen on the CT scan along different 2-D slices. These seeds then undergo ‘region growing’ and all voxels within the region and within the defined threshold limits are included in the 3-D representation of the airway. This region growing technique is designed to develop a region within a lumen. One problem with region growing is leakage,

which is when parts extraneous to the region of interest are incorporated as part of the selection. Leakage can occur where there are partial volume effects or image noise. Leakage tends to happen in the lower airway where the definition between the airway lumen and the surrounding lung parenchyma is not as clear and can take place if the upper threshold is improperly selected. (48)

There is not a defined threshold in the literature for airway segmentation; this is because CT scans vary in quality and intensity and the precise threshold for each airway will be slightly different. There is also the issue of partial volume effect. If the airway is orientated in such a way that there is tilt of the airway towards the image plane the density values of the air inside the lumen increases due to the partial volume averaging of air and the lumen wall. This can lead to a reduced contrast between the air within the lumen and the lumen wall, thereby making wall detection difficult. (49)

As part of semi-automatic segmentation two thresholds need to be selected. If voxels adjacent to seed areas fall within these threshold limits, they are then included in the segmentation as part of the region growing. The lower threshold for segmenting the airway is normally set at the lowest possible value (-1024 HU), with a value of -1000 HU corresponding to air. There are two different ways of choosing an upper threshold. One would be to select a fixed upper threshold, the alternative method is the method described by Nakano et al. (50). Whilst reviewing the CT image, the lower threshold should be set to the lowest setting (normally around -1000 HU) the upper threshold can be increased gradually by the user until it includes all of the airway tree. The threshold should continue to be increased until there is leakage outside of the airway and then the threshold just prior to this leakage should then be used as the set threshold. The problem with this method is the inter and intra-user variability.

A further limitation of this technique is the non-standardization between studies and therefore this introduces variability in the segmentation, and this makes cross-study comparisons difficult.

In the literature, there isn't an agreed threshold for segmenting the airway. Groups have used different upper thresholding values for segmenting the airway ranging from -300 Hu to -600 Hu (6, 11, 12).

Weisshiemer et al (51) set out to answer the question 'should we be using a fixed threshold or an interactive threshold?'. An interactive threshold would be the same as the technique previously described by Nakano et al. (50) Weisshiemer at al (7) designed an experiment using a phantom oropharynx made from acrylic. This phantom oropharynx had a known volume and was filled with air. The acrylic outer box was then placed in water. A CT

scan of the phantom oropharynx was presented to expert users who used an interactive threshold for a region growing technique of segmentation. The phantom oropharynx was also segmented with a fixed threshold. The results of the segmentations were compared against the gold standard 'known volume' and the relative volume error was calculated. The results showed that with the fixed threshold there were volume errors of between -11.1% - 11.7%. The interactive threshold had smaller volume errors ranging from 0.2% - 6.4%. They also found that between different segmenting software there were differences in segmentation volumes, despite using a fixed threshold. This would indicate that although there is inter-user variability when using interactive threshold, the volume errors are smaller and therefore interactive thresholds, when performed by an expert are more accurate than using a fixed threshold. The work included in this thesis used an interactive upper threshold, decided by an expert user, to segment the airway from CT scans.

For the main thyroid goiter study anonymized DICOM CT scans were imported from PACS (picture archive and communication system) into Mimics 22.0 (segmentation software). The CT scan of the neck and chest can be viewed in 3 different planes; coronal, sagittal and axial (see figure 3.1). Airway thresholding was performed whereby the lowest threshold is selected, -1024 HU, and then the upper threshold is selected using the 'Nakano' method (see figure 3.2) (6). This involves starting with low threshold (around -600 HU) and slowly increasing the threshold until the region of interest, in this case the large airways, is included. The threshold is increased further until there is 'leak' outside of the airway and then reduced again until there is no longer any leak. The process is repeated as the scan is scrolled through in all three planes to ensure there is no leakage at different points along the length of the large airways. It was found that the most common area of leakage was at the two main bronchi when there was leakage to the surrounding lung parenchyma which in turn produces a connection with the lungs (see figure 3.3). The threshold was reduced until the point where there was no longer a connection at this anatomical location.

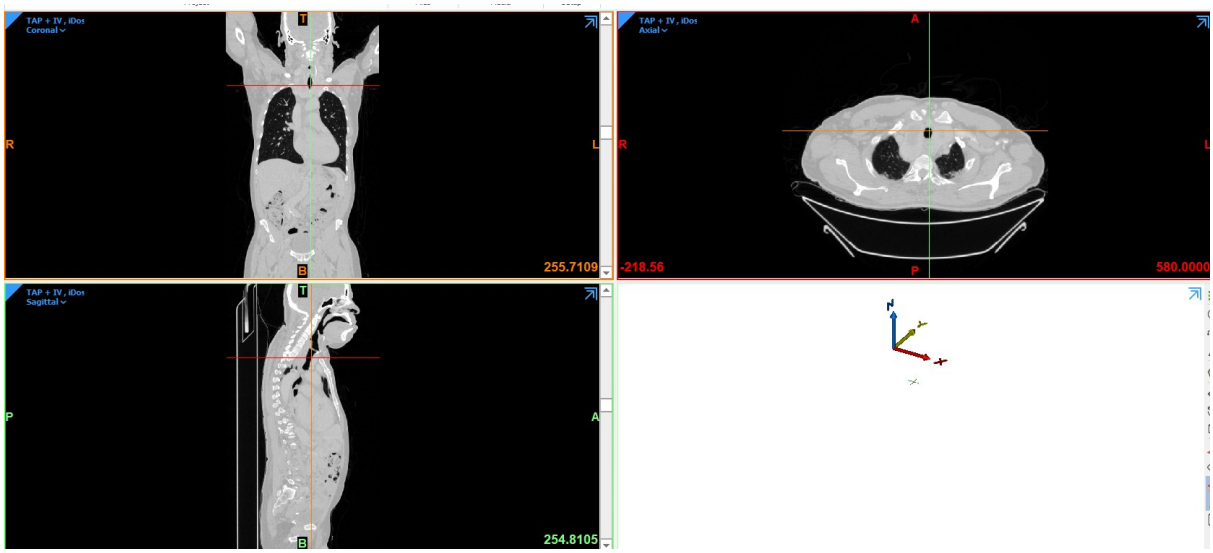


Figure 3.1. The 3 planes visible on Mimics 22.0 (coronal, axial and sagittal – clockwise from the upper left)

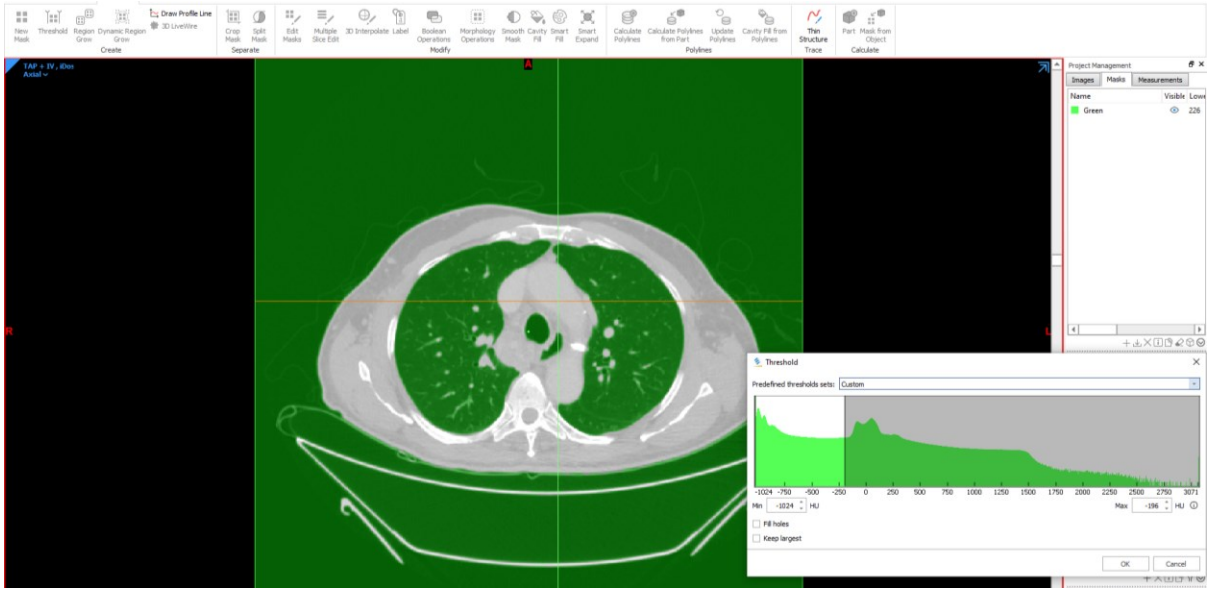


Figure 3.2. Threshold selection for selecting the airway structures in Mimics 22.0



Figure 3.3. 'leakage' from the trachea into the lung parenchyma

Once the upper and lower threshold have been selected a 'mask' is produced which includes all parts of the CT scan with HU within the range selected. The 'mask' is then split into the region of interest and everything outside of the region of interest. This is done by selecting the region of interest in multiple planes of the scan and highlighting the regions of 'non-interest'. The resulting region of interest can then be reconstructed using a 'region growing' semi-automated technique employed by the software. The 3D-reconstruction can then be viewed in the object window and checked for accuracy (see figure 3.4). If necessary, further segmentation can be performed to ensure that only area of interest is included i.e., to exclude any lung parenchyma. The reconstruction is the surface mesh that will be used to create a volume mesh for simulating airflow using CFD.

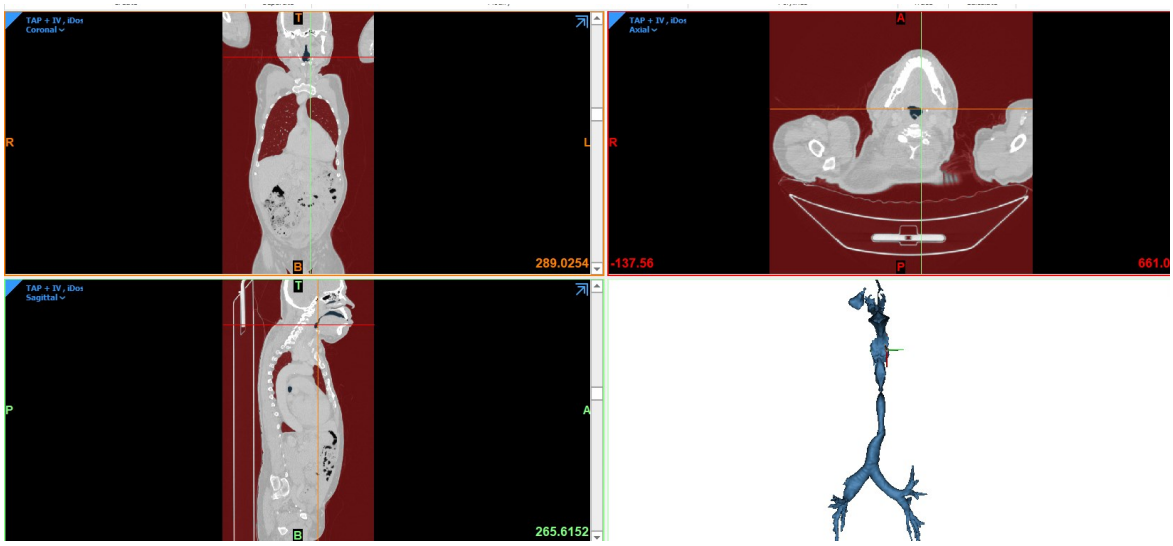


Figure 3.4. 3D reconstruction from the pre-selected threshold after region growing

The resultant 3D surface mesh can then be exported as an STL file for post-processing in Vascular Modelling Tool Kit (VMTK). This open-source software was used for the following post-processing procedures, smoothing, increasing the number of surface triangles, calculating the centerline, and performing geometric analysis of the of the virtual airway model.

Image segmentation can result in a coarse surface, especially if the image quality is low. Coarse sections on the surface can lead to spurious results in the flow, if indeed the surface is smooth in real life. The surface meshes underwent smoothing using Taubin's (52) algorithm with a smoothing factor of 0.01 and 30 iterations (see figure 3.5). Within VMTK the pre-smoothed and post-smoothed surface meshes can be compared to check that important surface features have not been reduced. A further step was taken to ensure that the surface mesh was not significantly changed by smoothing. The smallest cross-sectional area was measured in all of the pre-smoothed and post-smoothed geometries. There was <1% change seen in the post-smoothed geometry.

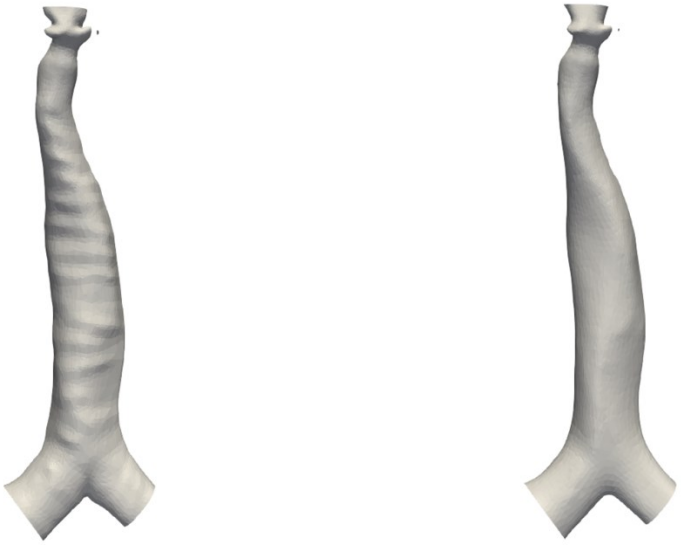


Figure 3.5. A surface mesh pre and post smoothing (left to right)

When creating a volume mesh from a surface mesh an important feature of the surface mesh is the number of surface triangles. Low resolution images produce surface meshes with fewer surface triangles which in turn can produce poor quality volume meshes. Using a smooth sub-division scheme 'Butterfly' within VTMK the surface meshes derived from low resolution CT scans were improved and the number of surface triangles increased (see figure 3.6).

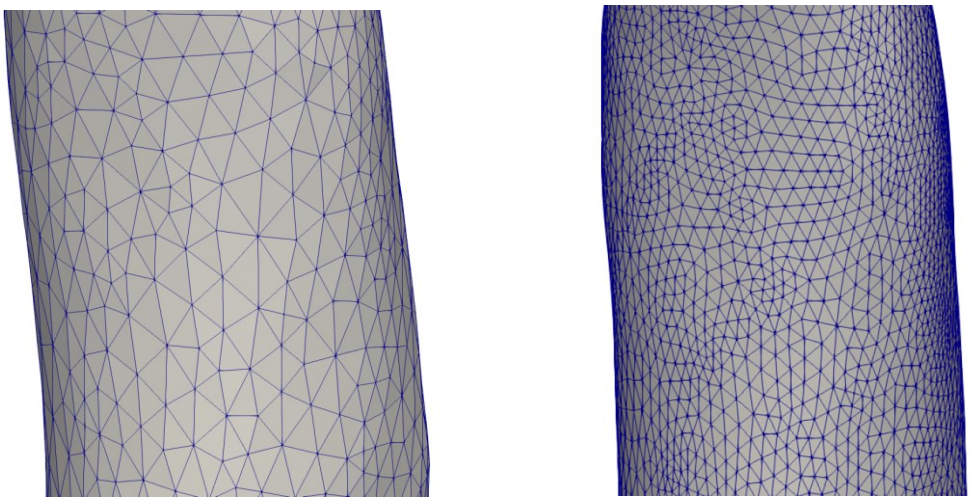


Figure 3.6. Pre and post using the subdivision scheme 'Butterfly' to increase the number of surface triangles (left to right)

Centerlines were calculated in VMTK. This was done by first using the clipping tool to open the ends of the surface mesh. The geometry was clipped above the glottis and at the level of the carina. Following this, seeds are employed at both of the clipped ends and a centerline is determined by calculating the shortest path between the two seeds. Propagation from one seed to the other is described by the Eikonal equation (9) and is computed using the 'fast marching method'. At each point along the length of the geometry the centerline path must lie at the center of the maximal inscribed sphere. These maximal inscribed spheres are referred to on Voronoi diagrams (see figure 3.7).

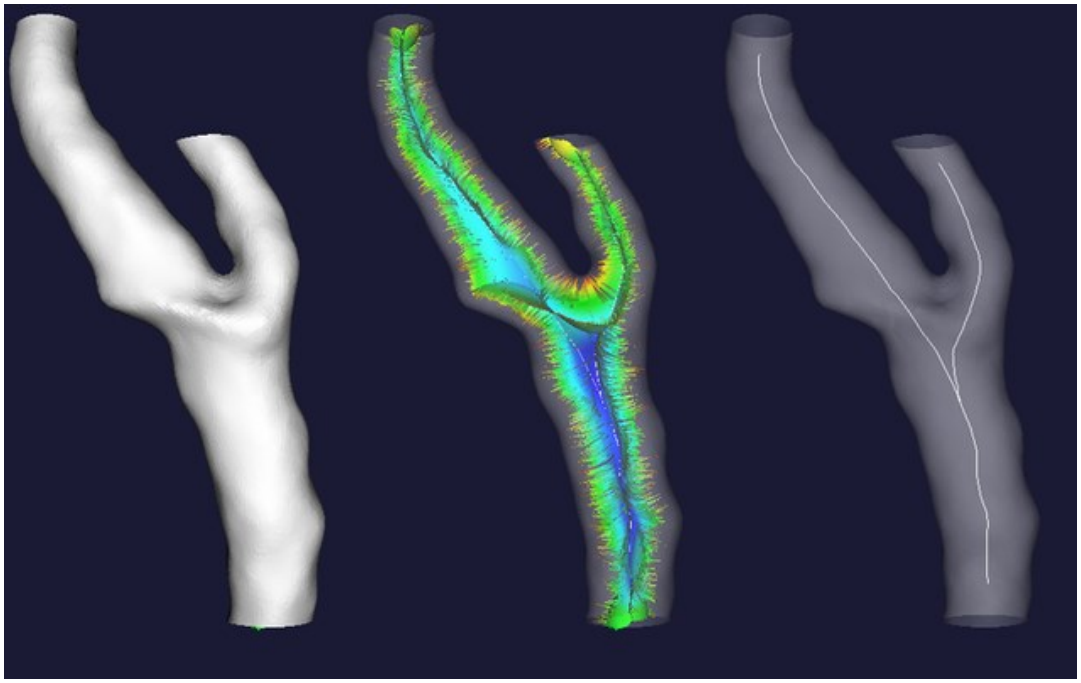


Figure 3.7. Voronoi diagram to demonstrate how a centerline is calculated (53)

Using the centerline STL file, further geometric analysis of the surface mesh was performed using the centerline attributes. This provides details of the cross-sectional area and the ellipticity of the geometry normal to the centerline.

3.3 Choice of landmarks

Ideally when modelling flow through the large airways we would include the entire upper airway to ensure that the model was as accurate as possible. However, inclusion of the entire upper airway is expensive both computationally and in terms of the time needed for

segmentation. Often the CT scan does not include the whole upper airway and sometimes it does not include the glottis. The CT scan does not always include the two main bronchi. In addition to this, the glottis is often in a variable position meaning that on one CT scan the glottis can be almost closed and, on another CT scan, the glottis can be wide open. This makes comparison of airflow in the area of interest (an area of airway compression or stenosis) between two subjects difficult. One method for reducing the computational cost would be to only model the area of interest - in other words to exclude the glottis and supra-glottic region. However, this will reduce the accuracy of the model, since the glottis presents a natural restriction, accelerating flow entering the trachea. Truncation immediately superior to the glottis likewise neglects the flow accelerations in the pharynx and the flow distortion caused by turning as flow passes from the nasal to pharyngeal airway. Thus, when deciding where to truncate an airway model a balance needs to be struck between ensuring sufficiently realistic flow distribution at entry to the modelled domain and the computational demands. Here we review the literature on the effects of the domain extent on tracheal flow modelling.

3.3.1 Effect of the upper airway

Lin et al compared simulation results between a full geometry which included the upper airway (mouth, oropharynx, and larynx) and a truncated geometry (of the same subject) which only included the intra-thoracic airway. The airway geometry was derived from the CT scan of a volunteer subject. They used an LES model to simulate airflow. They found that in the first simulation, which included the upper airway, the turbulence intensity within the trachea was between 10-20% whereas the turbulence within the trachea of the geometry without an upper airway was negligible. The presence of turbulence in the first simulation led to a threefold increase in local wall shear stress. The group concluded that simulations of airflow in the intrathoracic airway should include the larynx. (54)

Choi et al (55) used LES to show that a truncated airway model which did not include the glottis does not produce the same flow structures as seen in the airway model which includes the glottis. They found that as less of the upper airway is included in the geometry, the less accurate the CFD predicted flow fields are. Overall, the two main effects of not including the upper airway were that the flow behaved more as a laminar than a turbulent flow and that the speed was underestimated, when using a pressure boundary inlet condition. The speed at the glottic inlet was underestimated by about 50% at 15L/min. In order to improve the

accuracy of the CFD modelling when the upper airway is not included the team suggest using a mass flow inlet boundary condition.

More recently, Xiao et al (29) have shown that the breakdown of the flow jet formed by a severe tracheal constriction is affected by the level of turbulence in flow entering the trachea, confirming the need to include at least the presence of a glottis in predictions of airway resistance due to constriction.

For this study we truncated the upper airway above the level of the glottis, thereby including the glottis but not including the other complex structures of the upper airway. A mass flow inlet has been used as opposed to a pressure boundary inlet.

3.3.2 Effect of glottic closure angle

Choi et al (55) also studied inter-subject flow characteristics using LES and found that the angle of glottic closure significantly affected the flow. They found that larger glottic angles resulted in a longer jet core and there was overall less turbulence than for the subjects with smaller glottic angles. They also found that varying the opening angle of the glottis led to the laryngeal jet being aimed differently at the tracheal wall.

Work by Ritchie, 2019 (56) used a physical model of the large airways and varied the glottic closure angle in order to assess the effect on glottic angle on pressure loss. They looked at the following angles 5 degrees, 10 degrees, 33 degrees and 53 degrees. The pressure loss was found to scale with the flow rate according to a simple power law with an exponent of 1.91 for the 5-degree glottis in comparison to an exponent of 1.55 for the 53-degree glottis. This demonstrates the significant effect the glottic closure angle has on the pressure loss.

One study (57) has looked at the effect of the shape of the glottis on the laryngeal jet. They used a 3D surface geometry of the idealized mouth-throat model, which represents an average model of the extra-thoracic airway. The model was then manipulated to produce three types of glottis aperture. The three types of glottis included a quasi-circular glottis with a cross sectional area of 90mm^2, an elliptical glottis with a cross sectional area of 45mm^2, and a triangular glottis with a cross sectional area of 45mm^2. For the surface geometry they used a mesh with 650,000 cells. The authors performed a mesh independence study to show that beyond 650,000 cells the velocity profile and pressure drop between finer meshes did not change significantly. The team found that the Reynolds number at the level of the glottis ranged

from 2215 (for the quasi-circular glottis) to 8900 (for the elliptical glottis) and therefore a turbulence model was used to run CFD. They ran simulations at 15 and 30l/min flow rates. Due to their reduced cross-sectional area, both the elliptical and the triangular glottis geometries had a peak velocity of flow which was twice as high as the quasi-circular geometry, when the peak velocity of flow was measured at 0.5 diameters below the level of the glottis. However, further downstream at a distance of 2 diameters there was a difference in the peak velocity of flow between the elliptical model and the triangular model. In the elliptical model the peak velocity was 62% (15L/min) and 64% (30L/min) of the velocity measured at 0.5 diameters below the glottis, whereas in the triangular model the peak velocity was reduced to 30% (15L/min), and 32% (30L/min) of the velocity measured 0.5 diameters below the glottis. This was explained by the more complex flow and recirculation patterns seen in the triangular geometry. Thus, highlighting the significant impact that the shape of the glottis can have on the flow rates.

3.3.3 Effect on the main bronchi

Bronchial configuration does not affect the velocity profiles in the trachea during inspiration, as demonstrated by Yu et al. (13) Using CT scans of the upper airway to create 3D airway models they used a RANS k-epsilon model to simulate inspiratory airflow. The 3D airway models consisted of normal airways and airways with pathological constrictions of the main bronchi. They found that when flow entered the two main bronchi the high flow rate zone was divided into two streams, with peak velocity close to the inner bronchial wall. The flow rate was greater in the left main bronchus which has been shown in other studies and is thought to be because of the different angles between the trachea and the two main bronchi and the fact that the airway resistance is higher in the right lung.

3.3.4 Surface Mesh modifications

Following airway segmentation in Mimics 22.0 a number of modifications were implemented in order to standardize the airway model. Some of the airway models had large glottic angle openings whereas a number of the models had no connection between the trachea and the larynx due to the glottis being closed whilst the CT images were acquired. The addition of a standardized glottis to the airway models removes the variability in glottic angle opening.

A glottis which has abducted vocal folds was chosen because this would represent the appearance of a subject's glottis during inspiration. A study by Brancatisona et al (58) found that the average glottic area during mid inspiration was 120 $mm^{2.}$ The glottis used for the standard glottis in this study has an area of 120.7mm^2, however the glottis was re-sized for each tracheal geometry and therefore there is variability in the glottic area.

The standardized glottis was created by clipping the surface mesh of subject 17 at the level of the cricoid perpendicular to the centerline using the software VMTK. Each of the tracheal models was also clipped at the level of the cricoid perpendicular to the centerline. The STL file of the glottis was then imported into the software Meshmixer (see figure 3.8: note the shader used in Meshmixer is an 'overhang shader' and highlights areas of the mesh that may require support for 3D printing if this were to take place). Next, the surface mesh of one of the subjects was imported and appended to the glottis STL (see figure 3.9). Using the 'transform' tool, the size of the glottis mesh was re-sized to match the size of the subject's trachea (see figure 3.10). Importantly the size of the trachea was not manipulated in order to maintain the geometry taken from each patient's CT scan. The two meshes were then aligned as closely as possible before the 'Boolean union' was used to create a union between the glottis and the trachea. Following the union, the supraglottis and other more superior airway structures were removed using the clipping tool (see figure 3.11). A smoothing tool was used at the union site to reduce any irregularities. The viewing tool was used to view the glottis from above (see figure 3.12). With a standardized glottis adjoined to each of the 21 tracheal geometries, the glottic angle remains the same for each subject. This removes variability in the glottic jet and allows the difference in pressure loss to be attributed to the tracheal changes caused by the compressive goitre.

A small number of the airway geometries did not include the two main bronchi due to the CT scan limits. For those geometries without bronchi the same method described above has been used for attaching a standardized carina and main bronchi.

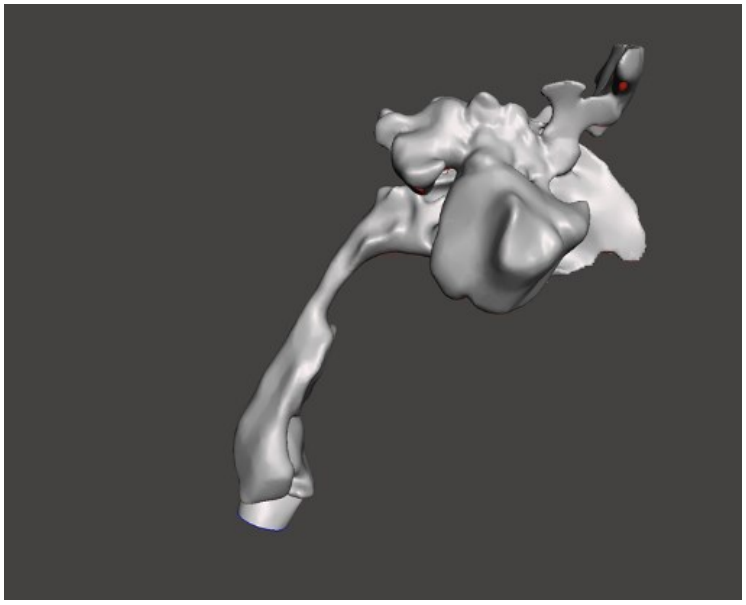


Figure 3.8. Standardized glottis

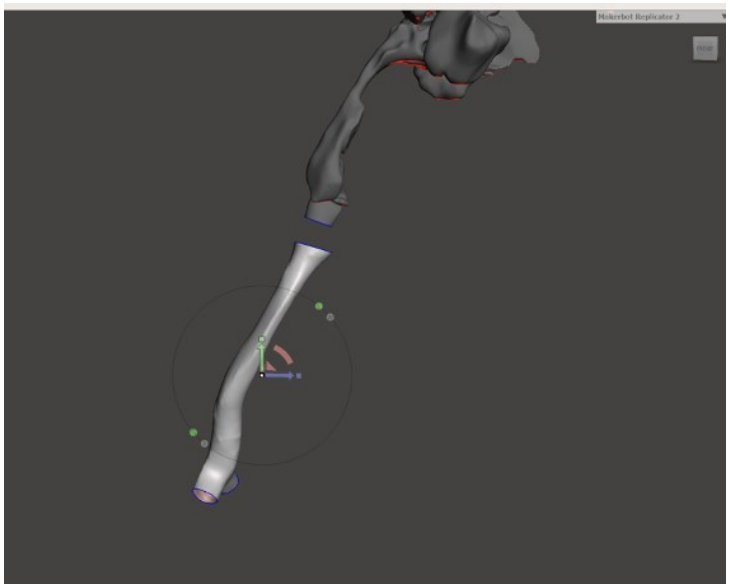


Figure 3.9. Imported and appended glottis and trachea

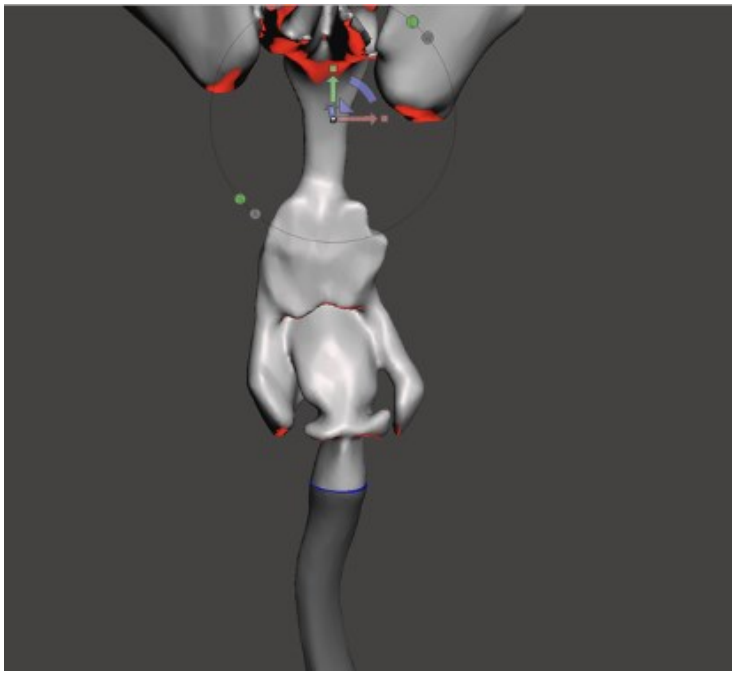


Figure 3.10. Standardized glottis re-sized to the trachea

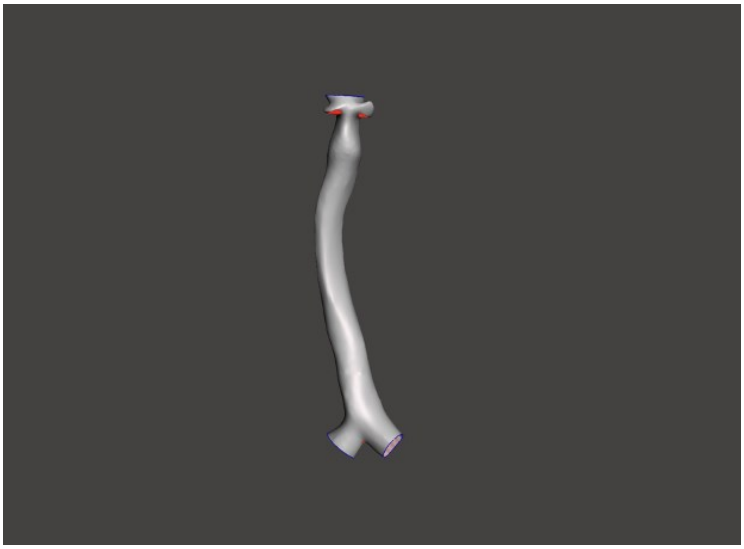


Figure 3.11. Boolean union of the glottis and trachea

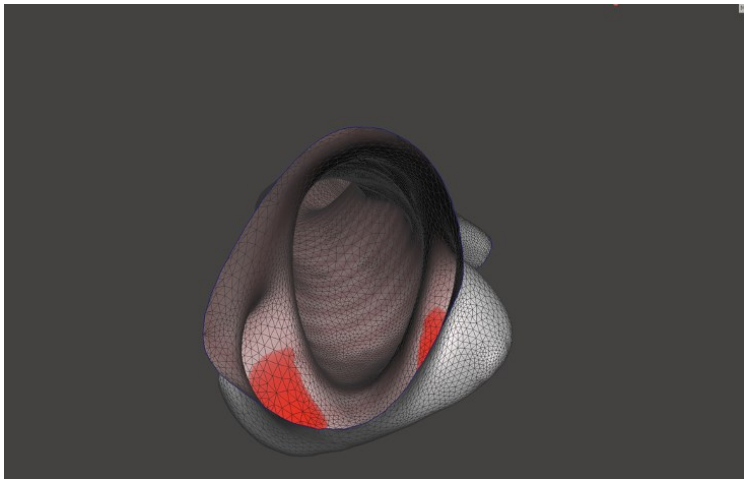


Figure 3.12. View from above the glottis to visualize the glottic opening

The rationale for appending a standardized glottis to the tracheal models was to remove the variability of glottic opening angle between the different subjects. The standardized glottis has the same opening angle for each one of the tracheal models, despite being re-sized to fit each trachea. Therefore, although the cross-sectional area of the glottis is different for each tracheal model the opening angle is the same. Figures 3.13-13.5 show the glottic opening angle for subjects 1, 13 and 18.

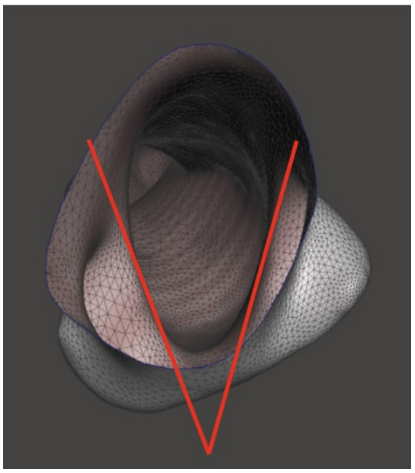


Figure 3.13. Image of subject 1's tracheal surface mesh from above showing the glottis and glottic angle

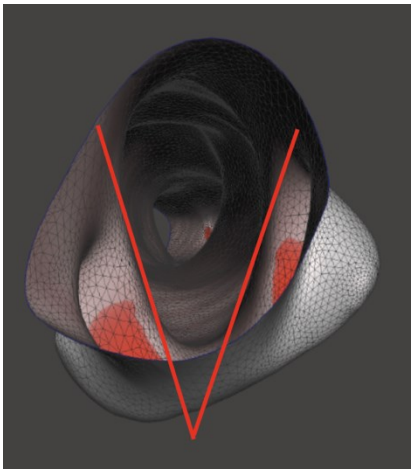


Figure 3.14. Image of subject 13's tracheal surface mesh from above showing the glottis and glottic angle

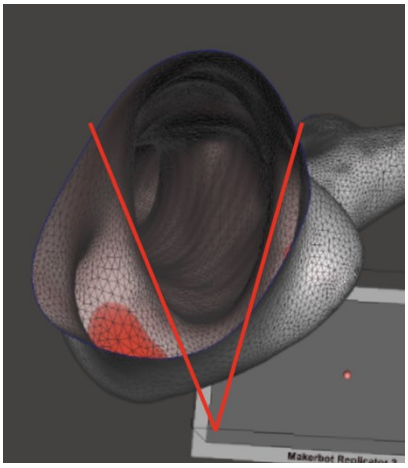


Figure 3.15. Image of subject 18's tracheal surface mesh from above showing the glottis and glottic angle

Refer to Chapter 5.2 for a table showing the tracheal geometries of the 21 subjects undergoing thyroid surgery for compressive thyroid goiters. The table shows the pre- and post-modification models. Figure 3.16 shows an example of one of the geometries pre-modification and post modification. The pre-modification surface mesh can be seen to have an almost closed glottis, and after modification, with the addition of the standardized glottis, the glottic region is much wider and is no longer the narrowest constriction of the surface mesh.

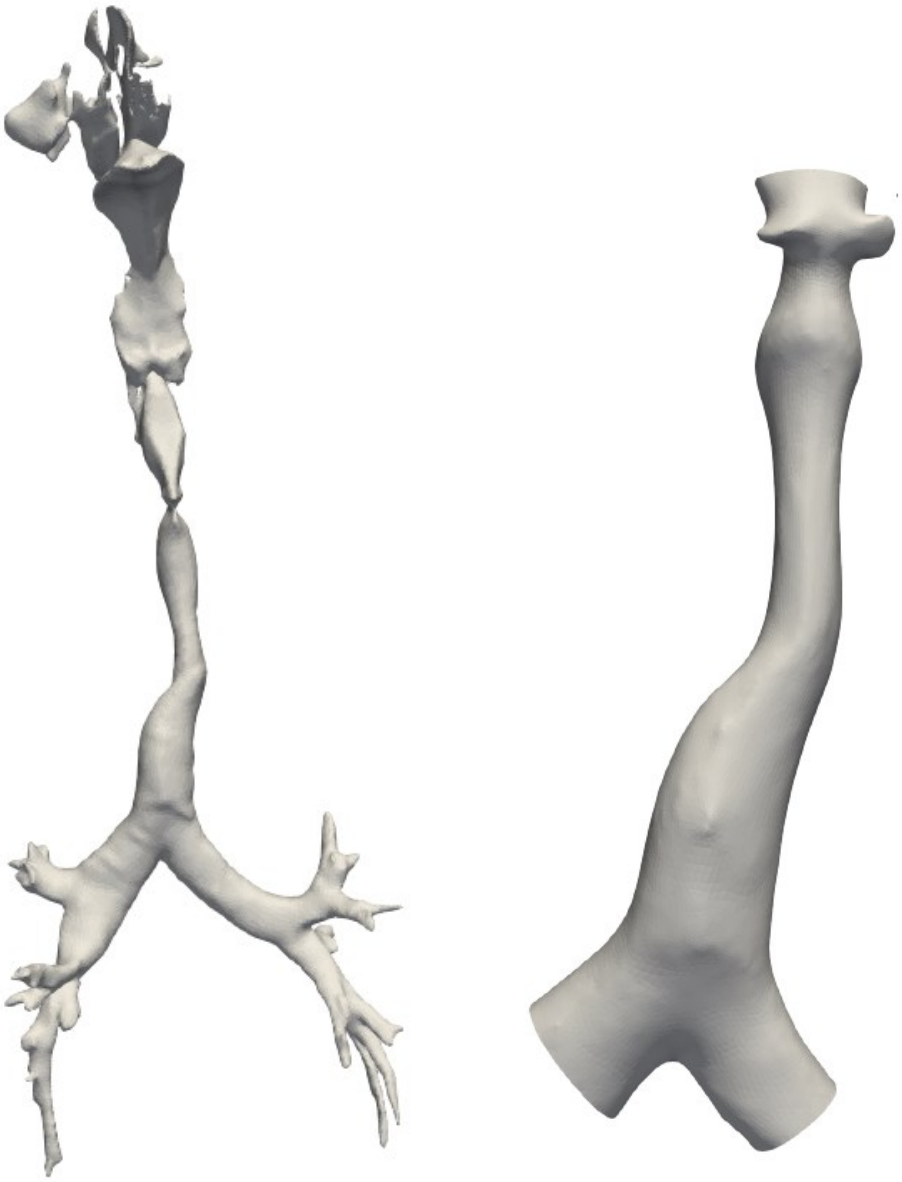


Figure 3.16. Subject 12 tracheal surface mesh pre-modifications (left) and post modifications (right)

3.4 Methods

3.4.1 Measuring the minimum diameter of the trachea and the % constriction

Using the data extracted from the surface mesh centerlines, the minimum diameter of the trachea between the first tracheal ring and the carina was recorded. The tracheal reference point

used was the diameter of the trachea 2 cm above the carina. % Diameter constriction = minimum tracheal diameter / diameter of the trachea 2 cm above the carina) *100. These measurements represent diameters of the trachea in a plane perpendicular to the centerline.

3.4.2 Measuring the minimum cross-sectional area and % area constriction

Using the data extracted from the surface mesh centerlines, the smallest cross-sectional area of the trachea between the first tracheal ring and the carina was recorded. The tracheal reference point used was the cross-sectional area of the trachea 2 cm above the carina. % Area of the tracheal constriction = (minimum tracheal cross-sectional area / cross-sectional area of the trachea 2 cm above the carina) *100. These measurements represent cross-sectional areas of the trachea in a plane perpendicular to the centerline.

3.4.3 Ellipticity

The shape of the trachea was also considered. The anterior –posterior (AP) diameter was compared with the transverse diameter. In a perfect circle the AP diameter would be the same as the transverse diameter. In an ellipse the two diameters will differ. The degree of how elliptical the trachea is can be defined as a ratio of the AP diameter: transverse diameter. The degree of ellipticity along the length of the trachea has been recorded.

3.4.4 Measuring the length of constriction

The current recommendation for considering surgery is based on a 35% or more reduction of tracheal diameter. The length of trachea >35% constricted has been measured and recorded.

3.4.5 PACS (Picture Archiving and Communications System) measurements

When assessing a patient in the outpatient clinic the clinician would typically take measurements of the diameter of the trachea from within PACS (see figure 3.17), as opposed to taking measurements from planes perpendicular to the centerline (see figure 13.8). To assess the difference in diameter measurements (between the two different methods of measuring the diameter), each CT scan was reviewed on the PACS system, and the diameter measured 2cm

above the carina rele and at the constriction. A Shapiro-Wilks test was used to check for normality and paired t-tests were used to compare the diameter measurements taken from PACS with the measurements taken from the centerline.

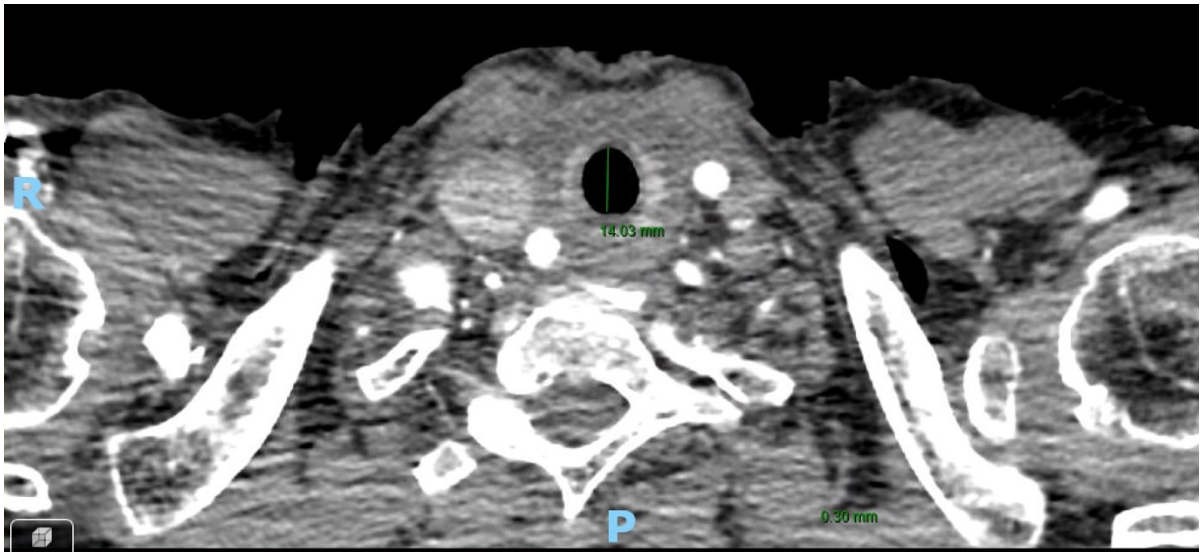


Figure 3.17. CT scan of the neck and chest in the axial plane, as it would be viewed on PACS, with a single 2D measurement being taken of the trachea

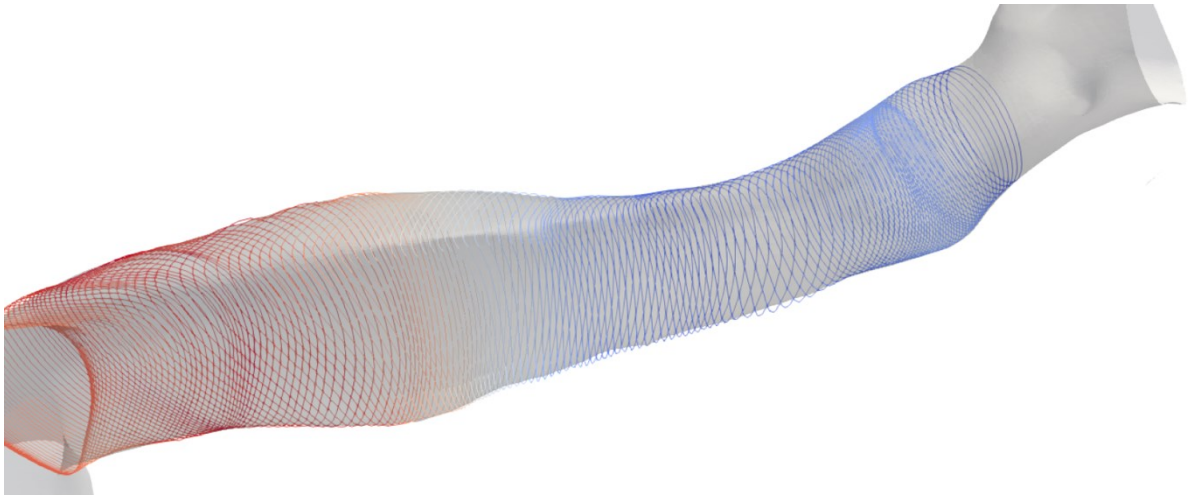


Figure 3.18. Planes of the trachea, perpendicular to the centerline, used to measure the diameter and calculate the cross-sectional area along the length of the trachea

3.4.6 Intra-user repeatability

In order to check for intra-user variability of the thresholds selected for creating the 3D tracheal models from the CT scans; a repeatability study was performed. 6 months after the initial airway segmentations were performed, the subjects' CT scans were re-segmented whilst being

blinded to the results of the original segmentation. The same method was used for segmentation. The lower threshold is set at -1024HU and the upper threshold was selected by the 'expert' user. The initial segmentation threshold was recorded as the 'original threshold' in HU, and at the time of re-test these results were hidden. The repeated segmentation threshold was recorded as the 're-test threshold' in HU. The two results were then compared. In order to see the effect these different thresholds have on the smallest cross-sectional area, for each threshold a 3D reconstruction of the trachea was created within Mimics 22.0 and a centerline was fitted. Using the measurement tool within Mimics 22.0 the minimum cross-sectional area (A_{min}) was calculated. The difference in the A_{min} between the 'original threshold' and the 're-test threshold' was calculated. A Shapiro-Wilks test was used to check for normality and a paired t-test was used to compare the original thresholds with the revised thresholds and to compare the original minimum cross-sectional area with the revised minimum cross-sectional area.

3.5 Results and discussion

Twenty airway models underwent geometric analysis. Shapiro wilks was used to test the normality of the data. Using the data extracted from planes perpendicular to the centerline, the mean minimum diameter (+/- SD) is 9.31 +/- 3.2 mm which equates to a median % reduction in diameter (+/- IQ range) of 22.3 +/- 40 when comparing the minimum diameter (D_{min}) with the diameter of the trachea 2 cm above the carina. The mean minimum cross-sectional area (A_{min}) was 103.4 +/- 51.7 mm^2 which equates to a mean % reduction in area of 42.4 +/- 24.4 % when comparing the A_{min} with the cross-sectional area of the trachea 2 cm above the carina (see table 3.1).

The mean ellipticity of A_{min} is 0.72 +/- 0.1, when referring to ellipticity as a ratio of the AP: transverse diameter, with 1 being a perfect circle. The mean length of constriction is 14.58 +/- 18.3 mm, when classifying 'constriction' as a reduction in the cross-sectional area of >35% (see table 3.2).

Parameter	Mean	Range	Standard deviation
D_{min} (mm)	9.3	2.0– 14.3	+/-3.2
% Reduction in diameter (median)	22.3	5.0- 85.0	+/- 40 (IQ)
Amin (mm^2)	103.4	14.8– 218.6	+/- 51.7
% Reduction in area	42.4	7.1– 90.8	+/- 24.4
Ellipticity of Amin	0.72	0.45 – 0.97	+/- 0.17

Table 3.1. The geometric analysis of the tracheal models using the centerline data derived from planes perpendicular to the centerline where: Dmin = minimum diameter, Amin = Minimum cross-sectional area

Parameter	Median	Range	IQ range
Length of constriction (mm)	5.83	0.00 - 62.90	+/-30.01

Table 3.2. The median, range, and IQ range of the length of constriction (when the constriction is >35%) of the 21 tracheal models

The patients can be stratified into two main groups according to the % area constriction. Nine patients have constriction <35% and twelve patients have a constriction >35%.

A paired t-test was used to compare the measurements taken from PACS with measurements taken from planes perpendicular to the centerline and this showed there was a significant difference in the measurements. The results are demonstrated in tables 3.3 - 3.5 and figures 3.19 – 3.20. The measurements taken from planes perpendicular to the centerline represent a more accurate representation of the true airway geometry. Both diameters taken from PACS are significantly larger than the diameters taken from VMTK. The mean % reduction in diameter calculated using the measurements taken from PACS is 42.4 +/- 24.3 compared to a median % reduction of 22.3 +/- 40.0 using the measurements taken from planes perpendicular to the centerline. Therefore, it's likely that the % reduction in diameter is over-estimated when the clinician takes measurements using PACS. The clinical relevance of this is that more patients would be considered for surgery than if the measurements were taken using planes perpendicular to the centerline.

Measure	Mean (mm)	Standard deviation
PACS tracheal diameter 2 cm above the carina	19.2	3.4
VMTK tracheal diameter 2 cm above the carina	13.4	1.9
PACS Minimum diameter	10.5	3.4
VMTK Minimum diameter	9.3	3.2

Table 3.3 The paired sample statistics of measurements taken from PACS and those taken from planes perpendicular to the plane (VMTK)

Measure	Mean (mm)	Standard deviation	T value	P value
Tracheal diameter 2cm above the carina	5.80	2.8	8.95	<0.001
Minimum diameter	1.15	1.5	3.47	0.002

Table 3.4. Paired differences of measurements taken from PACS with those taken from planes perpendicular to the plane (VMTK)

	Minimum	Maximum	Mean	Std. Deviation
PACS % reduction in diameter	13	81	45.0	38.7
VMTK % reduction in diameter	5	85	22.3	40.0

Table 3.5. Comparison of % reduction in the minimum diameter (minimum diameter / diameter of the trachea 2cm above the carina) between measurements taken from PACS and measurements taken from VMTK

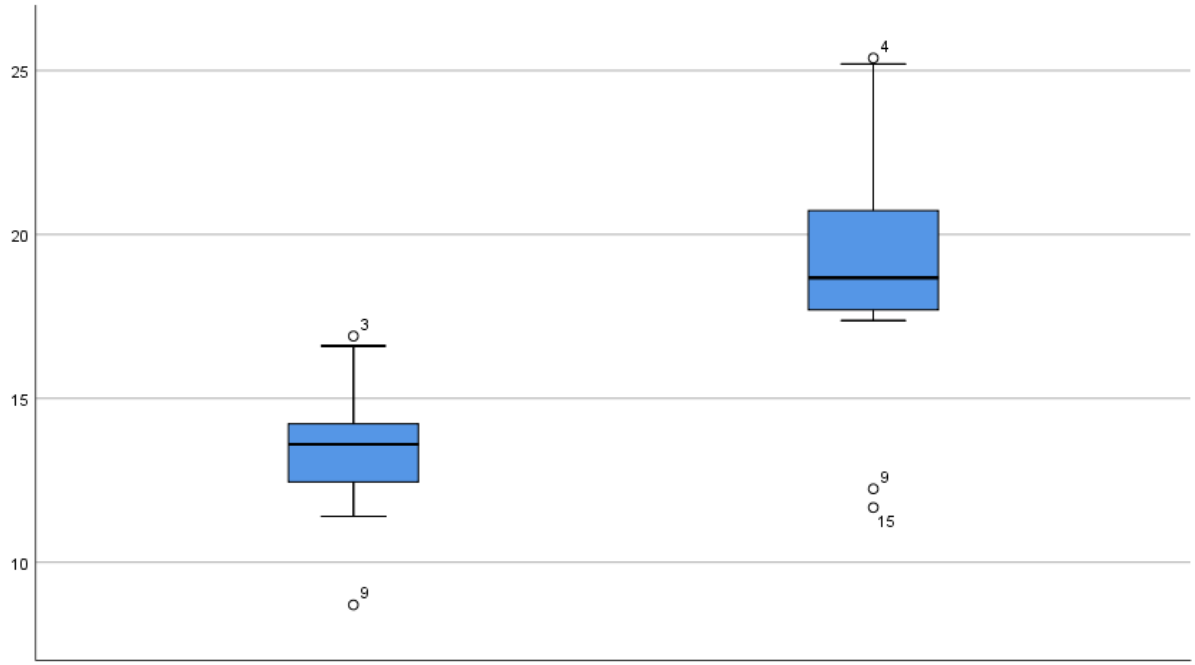


Figure 3.19. Diameter of the trachea 2cm above the carina taken from VMTK and the diameters taken from PACS

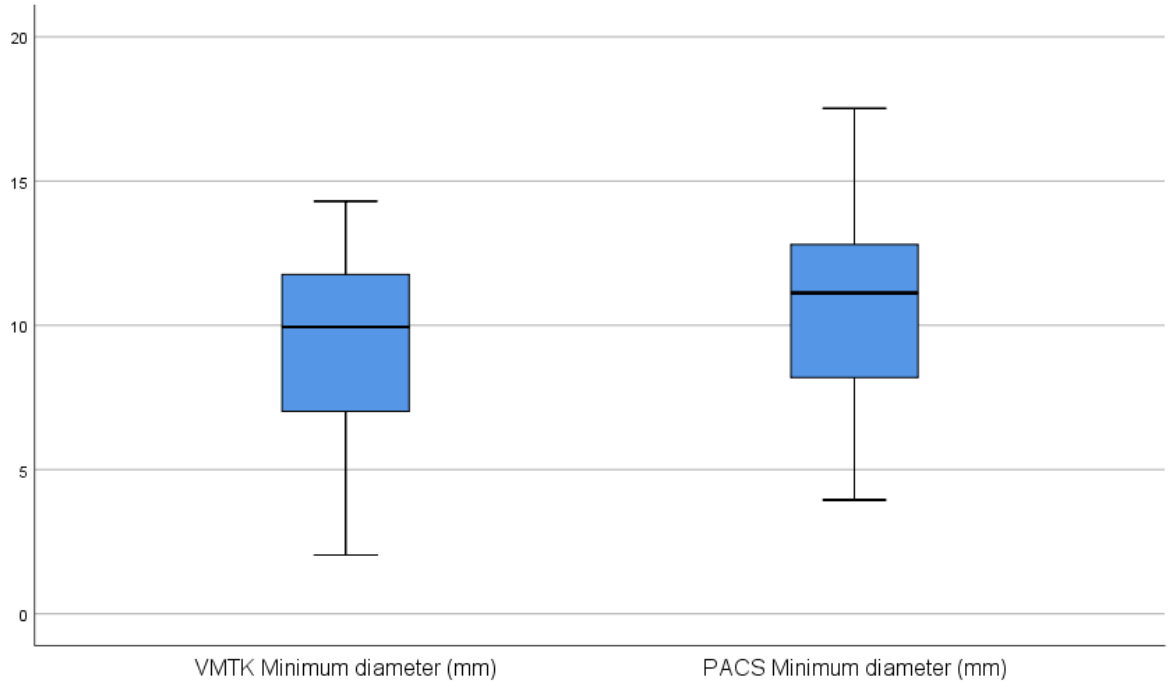


Figure 3.20. Minimum diameter taken from VMTK, and the minimum diameter taken from PACS

The ‘original threshold’ refers to threshold selected initially, whilst the ‘re-test threshold’ refers to the threshold selected by the same expert user 6 months later. The mean difference between the original threshold and re-test threshold is 18.18 HU (SD +/- 12.12) with a range of 1-47 HU. The mean difference in smallest cross-sectional area is 1.48 mm^2 (SD +/- 1.37) range is 0.01-4.99. The difference in smallest cross-sectional area between original and re-test was checked for normality using the Shapiro-Wilk test. The p-value is 0.330 and therefore the normality assumption cannot be rejected. A paired sample two tailed t-test was performed to check for a significant difference in smallest cross-sectional area between the two groups. The null hypothesis is that there is no significant difference between the two groups. The p-value = 0.71126 and therefore we accept the null hypothesis. However, this is a small sample size of 21 cases and therefore the priori power is low at 0.1031. Figure 3.21 shows the difference in thresholds (in HU) between the original upper threshold re-test threshold 6 months later. Figure 3.22 shows the difference in the corresponding smallest cross-sectional area between the original threshold and the re-test threshold.

Previous studies have shown that inter-user variability in thresholding of the airway can be as high as 230 HU. (56) However, this was a mean value taken from a group of non-medics and medics who were classified as ‘non-expert’ users. This level of variability in the selected threshold would result in much larger differences in the A_{MIN}. This repeatability study is reassuring in that the mean difference in thresholds was 18 HU and the corresponding mean difference in A_{MIN} is 1.48 mm^2. The reason for specifically analyzing the difference in A_{MIN} is due to the impact this has on the flow through the trachea model.

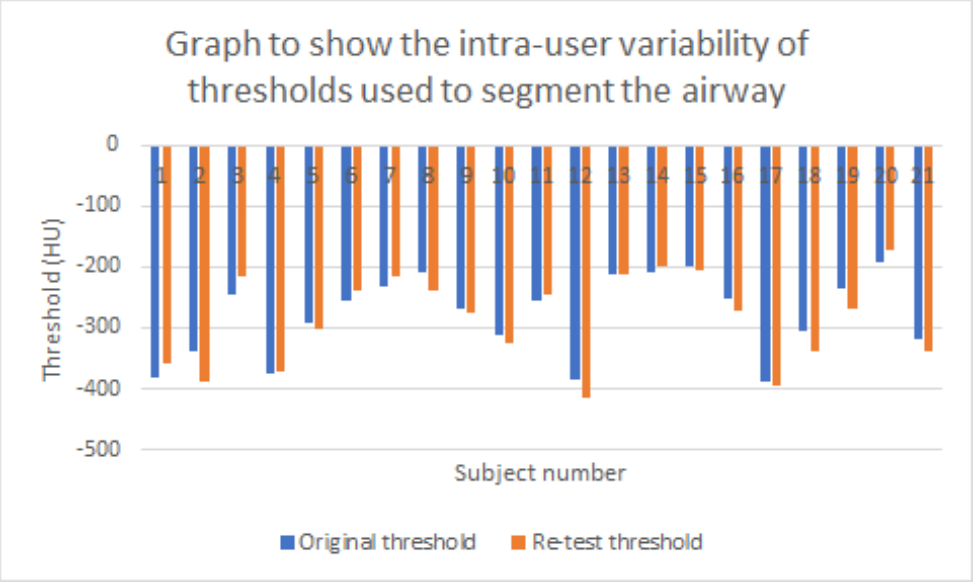


Figure 3.21. Intra-user variability of the selected upper threshold (HU) when segmenting the airway

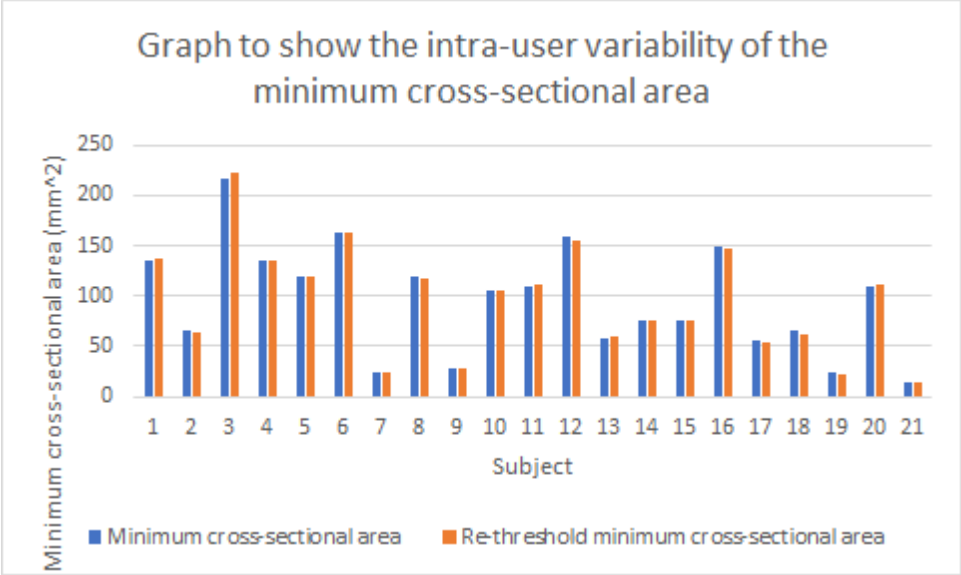


Figure 3.22. Intra-user variability of the minimum cross-sectional area (mm2) when the original thresholding was used to create the tracheal model and when the re-test thresholding was used to create the tracheal model

3.6 Conclusions

In clinical practice measurements are taken from a patient's CT scan in PACS which allows 2D measurements to be taken on a screen. However, due to the orientation of the trachea not being in a plane perpendicular to the CT scanner at the time of the scan the measurements do

not represent true measurements of the trachea. A more accurate way of measuring the trachea is to take measurements from a plane perpendicular to the centreline. This can be done once a 3D re-construction of the airway has been made.

Both the diameter of the tracheal reference point and the diameter of the minimum cross-sectional area (A_{min}) are significantly larger when taken from PACS than the same measurements taken from the planes perpendicular to the centreline. The mean % reduction in the trachea at the A_{min} is significantly larger when using PACS than the %reduction in the trachea at the A_{min} when using the centreline. The clinical relevance is that using PACS will lead to more patients being considered for surgery that if the measurements were taken from the centreline of the trachea.

When creating a 3D representation of the airway, an expert user chooses an upper threshold. All of the pixels in the CT scan which fall below this upper threshold are selected and are then included in the segmentation of the airway. There is inter- and intra-user variability. The expert user in this study re-segmented all of the airways six months after the original segmentation. The threshold selected for each subject were recorded and compared and then the re-segmentation was used to create a second series of airway models. The A_{min} of the originals tracheal model and the re-test tracheal models was compared. The mean difference in thresholds was 18 HU and the corresponding mean difference in the A_{min} was 1.48 mm^2. This suggests that using one expert user to perform the segmentation of all tracheal models in a study provides a reasonably good level of repeatability.

Chapter 4 CFD analysis of airway flows: Methods

4.1 Introduction
4.2 Generating a volume mesh
4.3 Defining boundary conditions
4.4 Choice of CFD methodology
4.5 Mesh independence tests
4.6 Effect of timestep on unsteady calculations
4.7 Experimental model and CFD validation study
4.8 Validating a steady RANS model
4.8.1 Simulating flow at 15L/min
4.8.2 Simulating flow at 30L/min
4.9 Inflow domain truncation effects
4.10 Concluding remarks

4.1 Introduction

In this chapter the methodology used to predict flow in the 21 tracheal models of subjects undergoing thyroidectomy for a compressive thyroid goitre is described. Tests to ensure convergence of the numerical solution and validity of the predicted results are presented.

The choice of appropriate methodology to predict tracheal flow depends on the nature of the flow (whether laminar or turbulent) and on the level of accuracy required. To determine the nature of tracheal flow, Dekker et al (59) performed experiments on 21 transparent cast of human tracheas and found the flow in the trachea to be turbulent above an inspiratory flow rate of 50 ml/s with the glottis described as “in the cadaveric position” and for the glottis opened to a more natural position, turbulent flow was determined to occur at an average flow rate of about 0.1 L/s.

Computational simulation of tracheal flows must thus be capable of modelling turbulence. However, computational simulation of turbulent flows without simplifying assumptions, so-called direct numerical simulation (DNS) is computationally very expensive, and impractical for the present study. The choice is thus between large eddy simulation (LES) or turbulence modelling, the latter usually some form Reynolds averaged Navier-Stokes

(RANS). In each case, the computational mesh must be sufficiently fine to be capable of resolving the spatial variations of the flow for the simulation to be accurate. In the following we first describe the process of constructing a mesh, before describing the computational procedure to be applied to each element of the mesh.

4.2 Generating a volume mesh

In order to simulate flow through an airway using computational fluid dynamics (CFD), we must first create a 3D representation of the airway in the form of a volume mesh. The first step in creating a volume mesh is to create a surface mesh, a process that is described in detail in Chapter 3.2.2. The surface mesh is then imported to STAR-CCM+ where it is used to create a volume mesh. A polyhedral mesher was used to create the volume mesh model of the trachea. Polyhedral meshers can mesh complex geometries and can produce a more accurate solution than a tetrahedral mesh. Polyhedral meshers are dependent on the quality of the surface mesh and therefore it is important to have a good quality surface mesh prior to volume meshing. The number of cells in the resulting volume mesh can be determined by the settings used to generate the volume mesh.

Work done by Bates et al 2017 (23) compared the results of LES simulations performed on a number of different tracheal volume meshes. These meshes were made from the same tracheal geometry; however, each volume mesh had a different number of cells. The purpose was to find an acceptable compromise between accuracy and computational effort. The volume meshes ranged in size from 945,000 to 9.2 million cells. They found that the mesh with 2.2 million elements, with 5 prism layers starting at 0.15mm and geometric progression of 1.3 to be sufficient for accurate estimation of flow energy loss in a pathological trachea with significant constriction and deviation. Their study provides a benchmark dataset for tracheal CFD and a good set of reference starting points. Independent mesh convergence tests were conducted for the airway geometries used for this thesis as reported further in section 4.5.

All of the volume meshes in this study contain more than 2.6 million elements;
Whilst, for the two most constricted cases, subject 9 and subject 21, it was found that a significantly finer mesh was required to achieve satisfactory convergence of the flow solution. Specifically, the mesh for subject 9 contained 5.2 million cells, whilst that for subject 21 had a volume mesh of 6.2 million cells.

The behaviour of flow near a wall poses a challenge for accurate flow simulation, since the flow speed decreases to zero velocity relative to the wall in a thin region known as the

boundary layer. In a turbulent flow, the boundary layer comprises three distinct sublayers adjacent to a wall: the viscous sublayer, the buffer layer and the overlap layer. Flow immediately adjacent to the wall is affected to a large degree by viscous forces, and as the distance from the wall increases the impact of these viscous forces reduces. The thickness of the boundary layer is determined by the distance from the wall in which these viscous forces have an effect, and the boundary layer edge is where these forces become negligible. Because the flow patterns and turbulence are different in this layer, the size of the cells in the mesh at the wall need to be smaller in order to capture the turbulence. To account for this, a prism layer is needed, to simulate the more complicated flow patterns (see figure 4.1). The prism layer can be made up of smaller cells than the rest of the mesh body. An important parameter in assessing the adequacy of a mesh is y^+ which is a dimensionless quantity, the distance from the wall measured in viscous lengths. Calculating an estimate of y^+ prior to running a simulation can aid in determining the height of the prism cells and the overall thickness of the prism layer. Bates et al 2017 (23) used a prism layer of 0.15mm and 5 cells thick. Using this benchmark dataset, simulations for this thesis were initially run with this reference point; however, if one of the simulations failed to converge, one of the checks performed was to check the maximum y+ value and if this was larger than one then the prism layer was adjusted until the maximum y+ value was less than one.

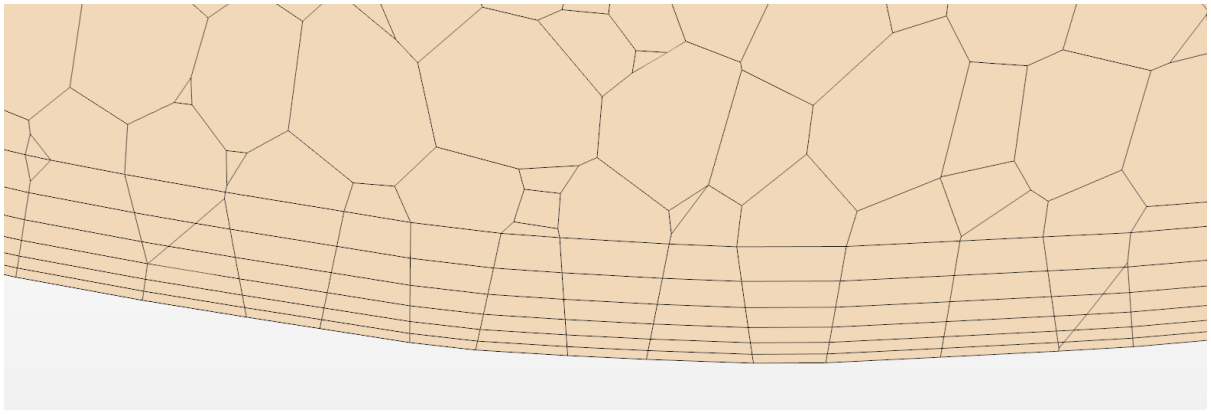


Figure 4.1. Plane through the volume mesh to demonstrate the prism layer

In order to capture the laminar sublayer whilst using a near wall model the y^+ value needs to be equal to or less than 1. Values of y+ for the wall-adjacent cells can either be estimated prior to running the simulation or calculated following an initial simulation. As an example, the y+ value can be calculated. The distance 'y' is measured directly from the volume mesh within Star-CCM+. To convert this value to y+ the following equation is used:

$$y^+ = \frac{yU_{tau}}{nu}$$

Equation 4.1

Where:

U_{tau} = the friction velocity

nu = kinematic velocity

$U_{tau} = \sqrt{(tau_w/\rho)}$

Where:

tau_w = wall shear stress

ρ = density of air

The region of highest wall sheer stress needs to be identified.

Another method of calculating the y+ value uses the report feature within the STAR-CCM+ package. The y+ values are calculated for the whole volume mesh and therefore it is possible to check that the highest y+ value is equal to or less than 1 (see figure 4.2). If the volume mesh has y+ values higher than 1, the height of the first prism layer can be reduced. Figure 4.2 demonstrates that for the mesh used to validate the simulation methods used, the maximum y+ value was 0.4.

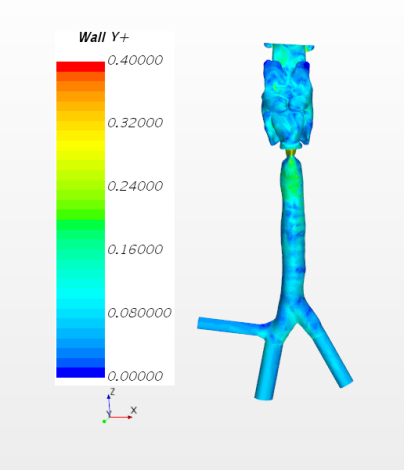


Figure 4.2. A volume mesh demonstrating the wall y+ values are all lower than 0.4.

A valid volume mesh is the most important factor contributing to a valid, converged simulation. Once the mesh is created within Star-CCM+, checking the validity of the volume mesh is the next crucial step. There is a function within Star-CCM+ which runs a mesh diagnostic report. A number of key areas are used to check for volume mesh validity: negative volume cells, face validity of the cells, cell volume change, and skewness angle. For a volume mesh to be valid, there cannot be any negative volume cells. Face validity of the cells refers to the face normal pointing outwards from the centroid of the cell. A cell with face quality of 1 is considered perfect. A cell with face quality less than 1.0e-5 is considered of unacceptable quality and therefore a valid volume mesh requires all cells to have face validity greater than 1.0e-5. Volume change of the cell refers to the ratio of volume of one cell compared to its neighbour i.e., if two cells adjacent to each other have a large volume ratio this implies a rapid change in mean cell dimension, which leads to inaccurate estimation of gradients in the flow. A volume of 1.0 indicates that the cells next to each other have an equal volume. If cells have a volume change of 0.01 or lower than this, this is considered to be poor quality. Cell skewness angle refers to the angle at which the centroids of two adjacent cells relate to one another. If the cell skewness angle is >85 degrees, then this is considered to be poor quality. The table below (see table 4.1) summarises the volume mesh validity checks performed on each of the volume meshes prior to running simulations. All the volume meshes used in this thesis were valid.

Volume Mesh Validity Check	Value required
Negative Volume Cells	0
Face Validity	>1.0e-5
Volume change	>0.01
Cell skewness angle	<85degrees

Table 4.1. Volume mesh validity checks and the values required for a valid volume mesh

4.3 Defining boundary conditions

Using a mass flow inlet, constant flow rates were distributed uniformly over the inlet of the domain with flow rates of 15 and 30L/minute to simulate quiet breathing and light exercise, respectively. Bates et al (60) showed that whilst realistic breathing conditions are cyclical, for

90% of inhalation, the flow patterns and distribution of flow change only in amplitude. The work of this thesis considers the pressure loss across the trachea during inspiration. The reason for simulating inspiration is two-fold; firstly, it is difficult to model expiration due to the lack of knowledge about the flow from the bronchi and due to the lack of geometry beyond the two main bronchi. Due to the limitations of the CT scan quality, it is extremely difficult to segment beyond the two main bronchi into any of the lower generations. Secondly, inspiration is generally more difficult than expiration (which is a largely passive process) and most patients with compressive goitres feel breathlessness during inspiration. (61)

When using a RANS model to simulate flow through the tracheal models the inlet turbulence intensity used was 10%. Turbulence intensity refers to the level of turbulence set at the inflow and is expressed as a % value. High turbulence cases are considered to be in the region of 5-20%, low turbulence cases are considered to be in the region of <1%. The tracheal models have been clipped immediately caudal to the glottis and therefore the effects of the upper airway structures on the flow are not simulated. The pharyngeal and supraglottic structures are complex and if they were included in the tracheal model would introduce turbulent flow. Brouns et al (62) found no significant difference in the turbulent kinetic energy in the trachea when using inlet settings of either 5% or 10%. Persak et al (63) used a k-omega turbulence model to investigate the effects of varying the inlet turbulence intensity in an upper airway model and likewise found no significant difference when varying the inlet turbulence intensity from 3%-30%.

A no-slip condition was used at the mesh walls and a pressure outlet boundary condition was used with a static pressure of zero.

Extruders are typically used at inlet and outlet boundaries in order to extend a volume mesh beyond the original boundaries. The pathological volume meshes used in the main body of this work have both inlet and outlet extruders. These mesh extruders allow flow to fully develop (including the boundary layer) at the inlet and also to prevent backflow at the outlet. During mesh development the length of the extruder was varied until there was no backflow from the outlet. The stretch factor of the cells within the extruder was also varied in order to avoid a big jump in cell size between the core mesh and the extruder mesh. The extruder used 60mm in length with 50 layers and a stretch factor of 6.0; the extruded section was aligned with the normal direction to the core mesh at the corresponding location. The same extruder for both inlet and outlets has been used across all the pathological geometries (see figure 4.3). For the healthy geometries with an upper airway, an artificial surface has been used, in order to seal the volume on interest and this has been done using a half sphere inlet (see figure 4.3).

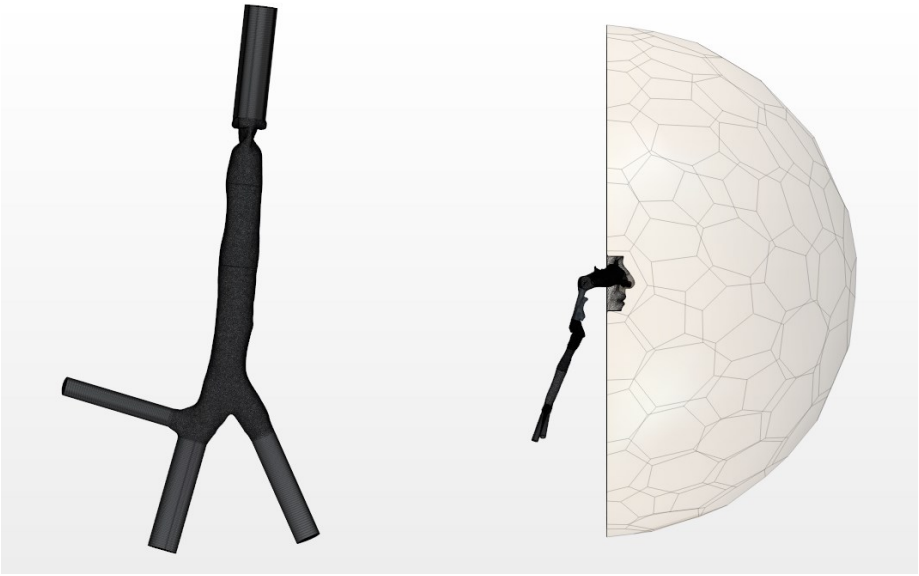


Figure 4.3. Volume mesh with both inlet and outlet extrusions (left), volume mesh with face and half sphere (right)

4.4 Choice of CFD methodology

The turbulent laryngeal jet is a dominant feature in inspiratory flow. The larynx and in particular, the constriction at the glottis introduce turbulence into the flow through the trachea. The high Reynolds numbers (>4300) seen at flow rates 15L/min require a turbulence model for simulating the flow through the airway. (55) For the purpose of this study, STAR-CCM+ 12.06.010-R8 has been used to solve the Navier-Stokes equations using a segregated flow solver and a second-order implicit discretization scheme. Two different models have been used throughout the study: LES and steady RANS.

When choosing a physics model to simulate turbulence, the main considerations are the computational cost and the accuracy. The model chosen is normally a trade-off between the two. Navier-Stokes equations can be used to predict laminar flow in very simple examples, however when the flow begins to transition to turbulence, small oscillations appear. In order to capture these small eddies, the mesh must be extremely fine which makes this computationally very expensive. Direct numerical Simulation (DNS) solves Navier-Stokes equations directly without using any turbulence models. It requires first order spatial discretization schemes. STAR-CCM+ does not provide the settings to run this type of simulation and therefore instead quasi-DNS simulations are used. These use second-order implicit temporal discretization

schemes to calculate Navier-Stokes equations. A quasi-DNS simulation was used in previous work by Bates et al (23) to provide a benchmark dataset for CFD in tracheal models. This quasi-DNS case provides validity for the turbulence models used. For the purpose of this thesis LES and RANS model were used to simulate flow.

Large Eddy Simulation (LES) is a turbulence model whereby the large-scale eddies are directly resolved, whilst the small-scale turbulence is modelled. It is thought to be more accurate than RANS, however it is more computationally expensive and requires a finer mesh. The transport equations are solved by using a spatial filter, with the solution variables being divided into a filtered, a sub-filtered and a sub-grid value. The Wall-Adapting Local-Eddy Viscosity (WALE) sub-grid scale model was used in this thesis. See table 4.2 for the physics model used in this thesis for LES simulations.

Flow model	Large Eddy Simulation
Energy model	Segregated Flow
Flow property	Constant Density
Transient term	Implicit Unsteady
Solver	Segregated Flow Solver
Wall treatment	All y+ Wall Treatment
Wall distance	Exact Wall Distance

Table 4.2. Physics model for LES simulations

Reynolds-Averaged Navier-Stokes (RANS) equations are based on the observation that the flow field contains many small eddies and oscillations which can be treated in a time-averaged sense. RANS turbulence models solve the RANS equations that govern the transport of the mean flow quantities.

Each solution variable is decomposed into its mean value $\bar{\phi}$ and its fluctuating component ϕ' :

$$\phi = \bar{\phi} + \phi'$$

Equation 4.2

Where ϕ = the solution variables; velocity, pressure, energy

There are eight different RANS models available and all of them calculate both Navier-Stokes equations with the addition of a turbulence eddy viscosity term. The models differ in the way in which the equations are computed, and they also differ in how they model the flow close to the walls. Therefore, it is important when choosing which RANS model to decide how important it is to accurately model flow next to wall. SST (Menter) k-omega model with all y+ wall treatment has been used for the main subjects in this study. See table 4.3 for the physics model used for steady RANS simulations.

Flow model	SST (Menter) k-omega RANS
Energy model	Segregated flow
Flow property	Constant density
Transient term	Steady
Solver	Segregated flow solver
Wall treatment	All y+
Wall distance	Exact wall distance
Gradient	Hybrid Gauss-Least Squared

Table 4.3. Physics model used for steady RANS

The k-omega model is a two-equation turbulence model and determines the turbulent eddy viscosity by solving the transport equations for both the turbulent kinetic energy and the specific dissipation rate. Menter introduced some modifications which helped overcome some short comings of the model, namely the sensitivity to the inlet conditions. The modifications included using a blending function far from the wall and adding a non-conservative cross diffusion term. These modifications mean that this model has the advantage of relative

insensitivity to the inlet conditions and free-stream conditions and the advantage of the accurate near-wall calculations. SST (Menter) k-omega model is effectively a blended combination of both the k-epsilon model and the k-omega model, using the k-epsilon model in the outer region of the mesh and the k-omega model in the inner region. Mylavarapu et al (64) used an airway model created from an MRI scan to validate the different CFD models. They found the results from the LES model, k-omega model, and the SST (Menter) k-omega were consistent with the experimental results. Steady RANS is computationally cheaper than an unsteady RANS model. Given that 90% of inspiration is considered to be steady, a steady RANS model should be suitable to model inspiration.

The all y+ wall treatment is a hybrid of both the low y+ and the high y+ wall treatments. Low y+ wall treatment resolves the viscous sublayer, and the transport equations are resolved all the way to the wall, although computationally expensive it provides accurate modelling of flow close the wall. Low y+ requires extremely fine meshes, especially for high Reynolds flows. High y+ wall treatment does not resolve the viscous sublayer and does not require y+ <1, and although less accurate it is used for coarser meshes. All y+ wall treatment employs either treatment in accordance with the mesh and this is the wall treatment used in this thesis for both the steady RANS and LES.

Wall distance is a measure of the distance of the cell centroid to the wall face. The exact wall distance model was used as this is more accurate than the alternative PDE wall distance.

Within each cell variable gradients are required for flow calculations due to the different values at each cell face. The Hybrid Gauss-Least Squared method was used, this allows computation of unlimited reconstruction gradients.

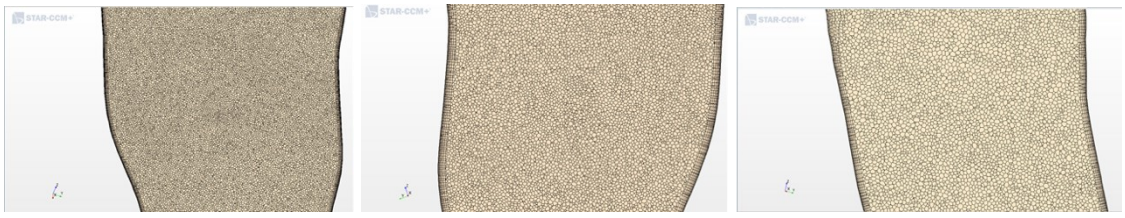
For each simulation there were a number of checks for convergence of the solution. The following monitor plots were set up, residuals and pressure loss. Typically, a simulation is considered to be loosely converged if the residuals fall below $10E^{-4}$, most will consider a simulation to be converged when the residuals fall below $10E^{-6}$. However, one cannot rely entirely on the residual plot. An important way to check for convergence is to look at quantities of interest e.g., a monitor plot of pressure loss. As the solution converges a plot of pressure loss across the trachea should flatten out i.e., a reduction in the variation of the solution outcome. The main quantity used to check for convergence was the mean pressure loss along the trachea and the amplitude and frequency of its fluctuations.

4.5 Mesh independence tests

Quasi-DNS and LES simulations require finer meshes than RANS simulations. Ideally the mesh should be made with the lowest number of cells needed to accurately capture important flow characteristics without affecting the accuracy of flow predictions. This is due to the computational cost of a) creating the volume mesh b) running the simulation. If mesh independence is achieved using LES it can be assumed that the number of cells required for mesh independence will be enough to ensure mesh independent studies for RANS. Mesh independence refers to the result of the simulation being independent of the number of cells i.e., if the same simulation was performed on an airway model with a greater number of cells, then the result would be the same. A mesh independence study was performed using a full airway with a ten-degree glottis, which represents an area of narrow constriction which behaves like an orifice loss, much like the constrictions seen in the pathological tracheas studied in this work. The cross-sectional area of the glottis is 10.2mm^2 which is smaller than the minimum cross-sectional areas of the tracheas of the subjects studied in this thesis (range of the minimum cross-sectional area 14.93 mm^2 – 218.6 mm^2. The volume mesh was created using the same surface mesh, changing the base size in order to produce three volume meshes with varying numbers of elements; 11221311 elements, 4169665 elements and 2677939 elements respectively (see table 4.4 and figure 4.4).

Volume mesh	Number of elements
One	11221311
Two	4169665
Three	2677939

Table 4.4. The number of elements in each mesh



Mesh 1 Mesh 2 Mesh 3

Figure 4.4. Sagittal slice of the volume mesh to demonstrate the density of cells in mesh 1,2 and 3

The LES model was run at a flow rate of 50L/minute with a time step of 5e-5 seconds and with first order temporal discretization. The pressure loss was calculated using (pressure inlet - pressure outlet). The results are displayed in table 4.5.

Mesh	Number of elements	Pressure loss (Pa)	Relative difference (%)
One	11221311	116.49	-
Two	4169665	116.81	0.27
Three	2677939	117.73	1.05

Table 4.5. Pressure loss across the trachea for volume meshes 1,2 and 3

The results are in keeping with a study by Bates et al (23), who described a benchmark dataset of CFD in the human trachea using LES. They found that the best compromise between computational expense and accuracy was a mesh of 2.2 million elements.

The following scalar images (see figure 4.5) demonstrate the changes seen in the detail of simulated vorticity in the three volume meshes. There is a slight reduction in the detail of the vorticity between mesh one to mesh three.

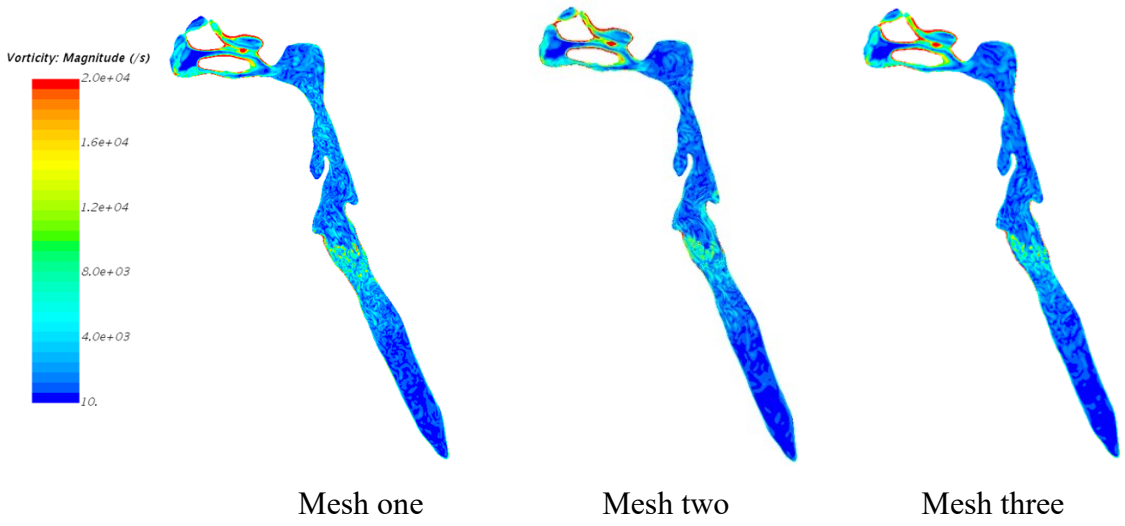


Figure 4.5. Sagittal plane of vorticity for the three volume meshes

Following the mesh independence test it was decided that the minimum number of elements used for the mesh would be a minimum of 2.6 million cells. With a relative error of only 1.05% between a volume mesh of 11.2 million elements and a volume mesh of 2.6 million elements, then the reduction in computational cost outweighs the introduction of a relatively small error.

4.6 Effect of time step for unsteady simulations

The timestep effects the accuracy of the unsteady simulations and for LES the turbulent time scale must be considered. The cell size and fluid velocity should be taken into account when deciding on the time step for a simulation. This can be estimated using the Courant number (C).

$$C = \frac{U\Delta t}{\Delta x}$$

Equation 4.2

Where:

U = fluid velocity

Δt = time step

Δx = cell length

The maximum Courant number in the LES simulation at 30L/min on the 10-degree glottis trachea, with a time step of 1e-4s, used for the validation studies was 0.9. Ideally, the Courant number should be less than 1. If the Courant number is more than 1 then the simulation may diverge and the timestep should be reduced.

An excessively small time-step will be computationally expensive; however, a large time step can lead to inaccurate results as important flow characteristics may not be captured. A time-step test was performed using a full airway model with a 10-degree glottis and an LES model a flow rate of 30L/min. The time steps used were 1e-5 seconds, 5e-5 seconds, and 1e-4 seconds. The pressure loss was calculated using pressure inlet-pressure outlet. A timestep of 1e-4 seconds resulted in a relative error of 1.38% which is considered acceptable for the reduced computational time required to run the simulation (see table 6).

Timestep (s)	Pressure loss (Pa)	Relative error (%)
1e-5	39.85	-
5e-5	40.78	2.33
1e-4	40.40	1.38

Table 4.6. Results of the pressure loss with differing timesteps

4.7 Experimental model and CFD validation study

Experimental work carried out by Ritchie 2019 (56), demonstrated the validity of CFD flow predictions through the trachea for a laminar flow model. This thesis will use the same experimental model to validate CFD flow predictions using both LES and a steady RANS model. The experimental model set up will be described in brief here. A contrast enhanced CT neck and thorax scan was acquired using a Philips iCT 256 helical scanner with the patient in the standard supine position. The patient was taking a breath whilst the images were obtained. The DICOM file consisted of 323 slices 2mm thick, a FOV of 430mm and pixel size 0.56mm. The DICOM files were imported into Mimics version 18.0 and the images were semi-automatically segmented using user-selected thresholding. The segmentation included the airway from the nostrils down to the carina and included the main bronchi. A number of models were created with varying vocal fold apertures however for the purpose of this validation study, we will only consider the model with a 10-degree glottic aperture. This model was chosen for this validation study due to the constriction created by a small glottic opening which in theory will produce a similar jet to the constrictions seen in the subjects in the study. The model was smoothed using first order Laplacian smoothing with a smoothing factor of 0.4 and 10 iterations.

The 3D surface mesh of the trachea and upper airway was exported as an STL file into Materialise 3-Matic where it was prepared for 3D-printing. A 3mm wall was built around the surface mesh. In addition, 37 pressure taps were incorporated to allow for monitoring the pressure loss along the length of the trachea during the experiment (see figure 4.6*).* The model was printed using an Object Connex 350 3D printer using an ABS-like material made of two subtypes of plastic (RGD515 AND RGD353). Both a micromanometer and an alcohol manometer were used to measure the pressure across the 37 taps during the airflow experiment.

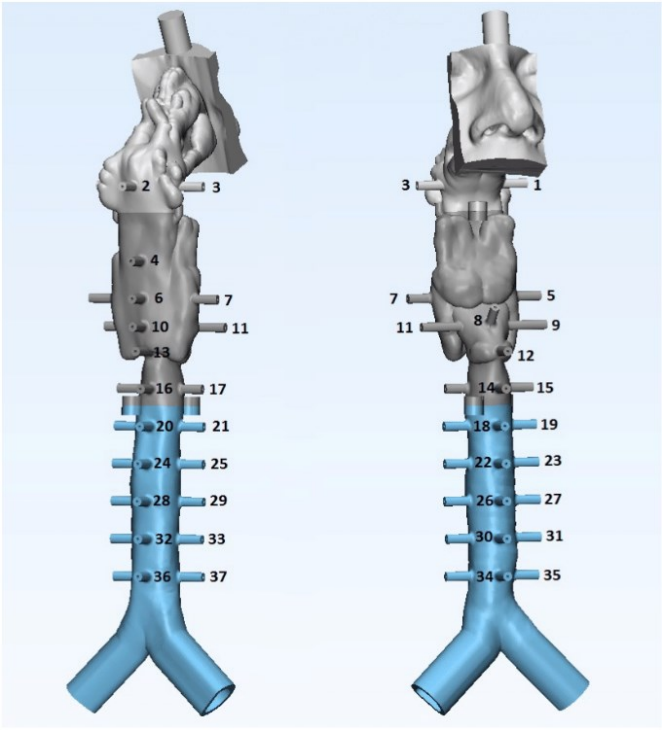


Figure 4.6. A schematic of the 3D printed airway model demonstrating the position of the 37 pressure recording taps

Different flow rates were applied (range of 30L/minute – 80L/minute) and the pressure was recorded at the 37 taps along the airway. The results at 50L were compared with a quasi-DNS, laminar, LES, and RANS model using CFD. Of note, the experimental model used an air pressure value of 101325 Pa whereas the CFD uses a reference value of 0 Pa. Therefore, in order to compare the results, the pressures were aligned by making tap 37 a 'zero' reference pressure. The results were not found to be significantly different using an independent t-test and a p value of <0.05. This comparison between the physical experimental model and the CFD model validated the use of the CFD technique for estimating the pressure loss along the airway.

In order to validate the LES and steady RANS model used in this thesis the same airway surface geometry has been used and a volume mesh created within STAR-CCM+. Measurements of static pressure were taken at the exact location as the pressure taps used in the experimental model. An LES at 30L/minute with a time step of 5e-5 was performed in STAR-CCM+ (please refer to chapter 4.4 for the simulation set up) and the results of the pressure at the tap locations were compared. The results from the experimental model have an error of +/-3.5Pa (the known error from the CANDaq pressure transducer used in the physical experiment). The pressure recordings from the LES model all fall within the +/- 3.5Pa error bar apart from the first second, third and fourth taps which have a difference in pressure of 4.11,

4.48, and 3.61 Pa respectively. The measurements from these taps are in the pharyngeal region which is not studied in the work of this thesis and therefore these differences are not considered important.

A steady RANS model (please refer to chapter 4.4 for the simulation set up) was used to run the simulation at 30L/minute and the steady RANS model was a close fit to the experimental data with all of the static pressure measurements along taps 1-37 being within +/- 3.5 Pa. See figure 4.7 which shows the static pressure recordings along the length of the trachea for the experimental and the CFD models: LES and steady RANS. The +/- 3.5 Pa error bars have been fitted to the experimental data. Figure 4.8 demonstrates a sagittal section of the airway model with the locations of the measured pressure demonstrated, these correspond to the exact locations of the pressure taps on the 3D model used for the physical experiment. Figures 4.9 and 4.10 demonstrates the cross-sectional area and the pressure loss along the length of the trachea respectively as estimated using the steady RANS model. At the level of the glottis there is a marked drop in both the cross-sectional area of the trachea and correspondingly a marked drop in the pressure.

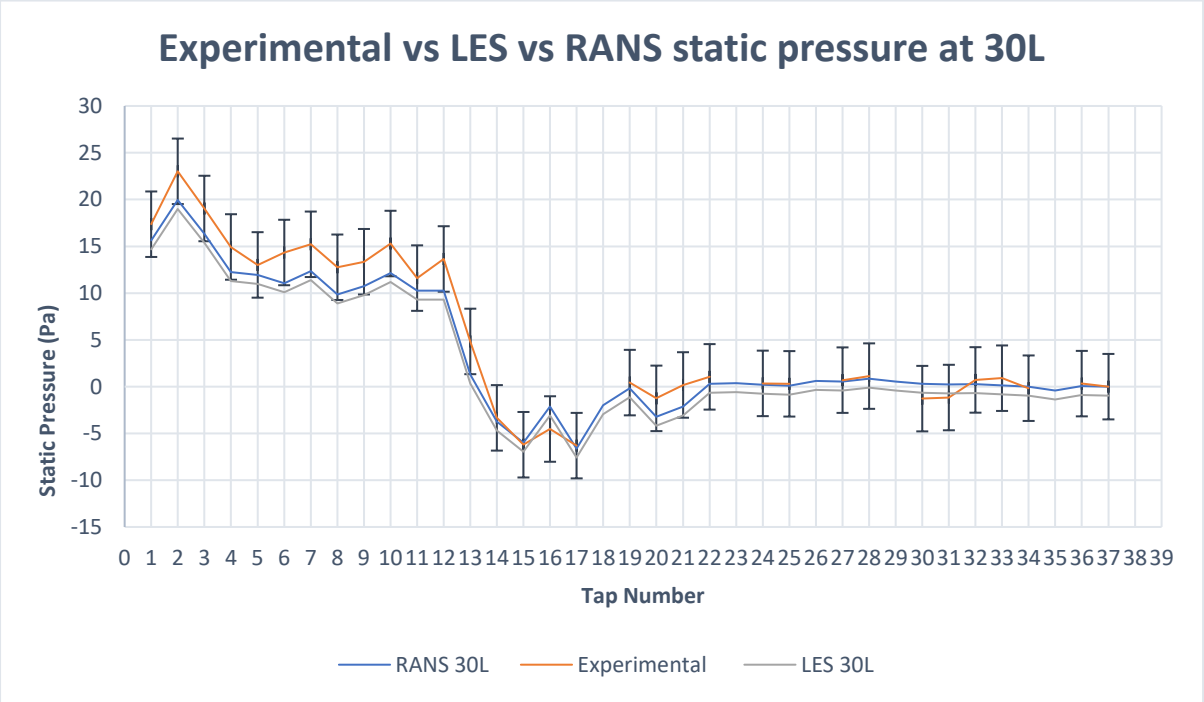


Figure 4.7. Static pressure along the length of the trachea from tap 1-37 comparing the experimental, LES and steady RANS results

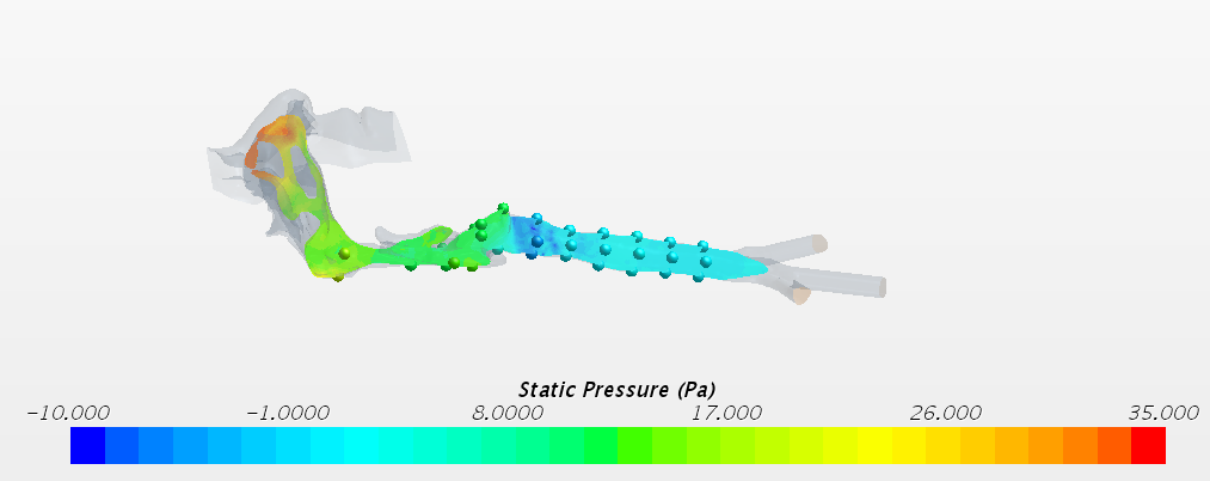


Figure 4.8. Sagittal section of the airway model and the static pressure

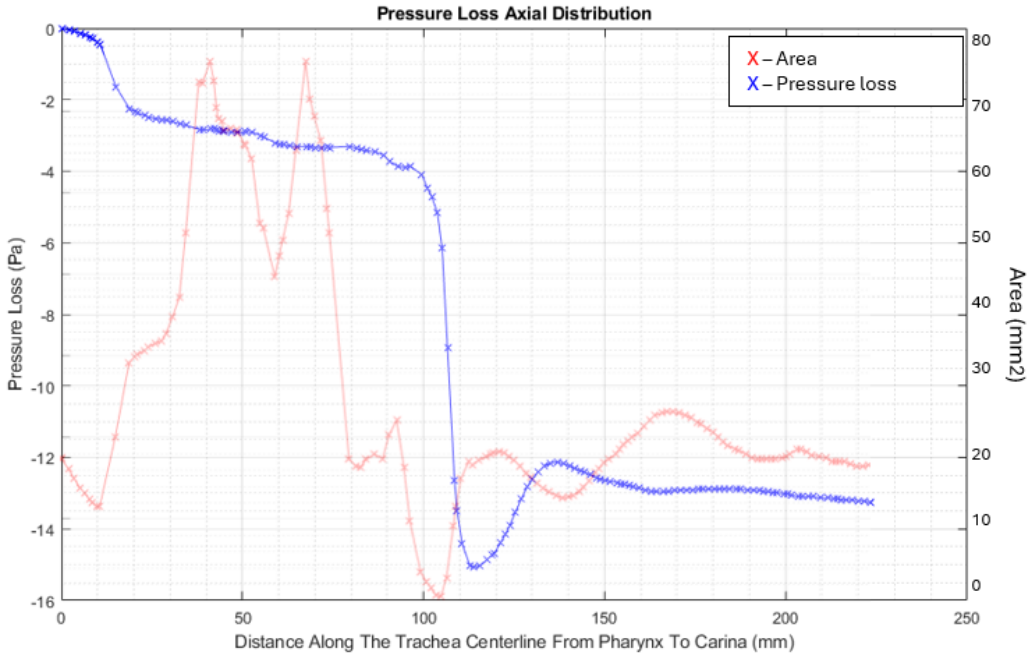


Figure 4.9. Pressure loss and Cross-sectional area distribution along the length of the airway

The steady RANS model has also been used to run simulations at 50L, 60L and 80L and the results for static pressure for taps 1-37 have been compared with experimental data of the same flow rates (see figure 4.11, 4.12, and 4.13 respectively). At a flow rate of 30L/min and 50L/min the steady RANS matches the experimental data (+/- 3.5 Pa) from the glottis

region down to the carina, however in the pharyngeal model the relative error is greater. At a flow rate of 60L/min the steady RANS matches the experimental data (+/- 3.5 Pa) below the glottis down to the carina however there is more than +/- 3.5 Pa difference at the level of the glottis and the relative error again increases at a flow rate of 80L/minute. These results indicate that steady RANS model is a reliable model to simulate flow for the glottis and trachea for flow rates of 30L/min and 50L/minute.

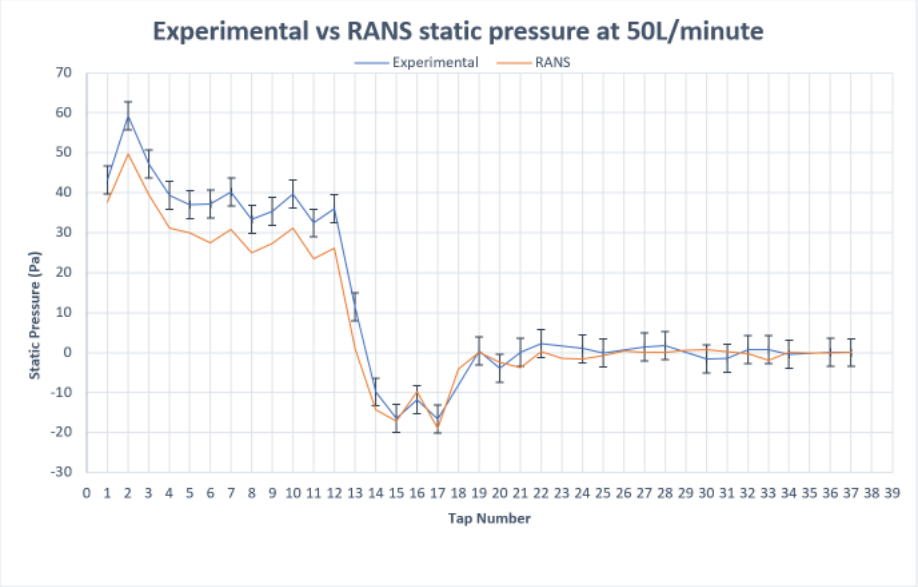


Figure 4.10. Static pressure loss along the length of the trachea for the experimental model and the steady RANS model at a flow rate of 50L/min

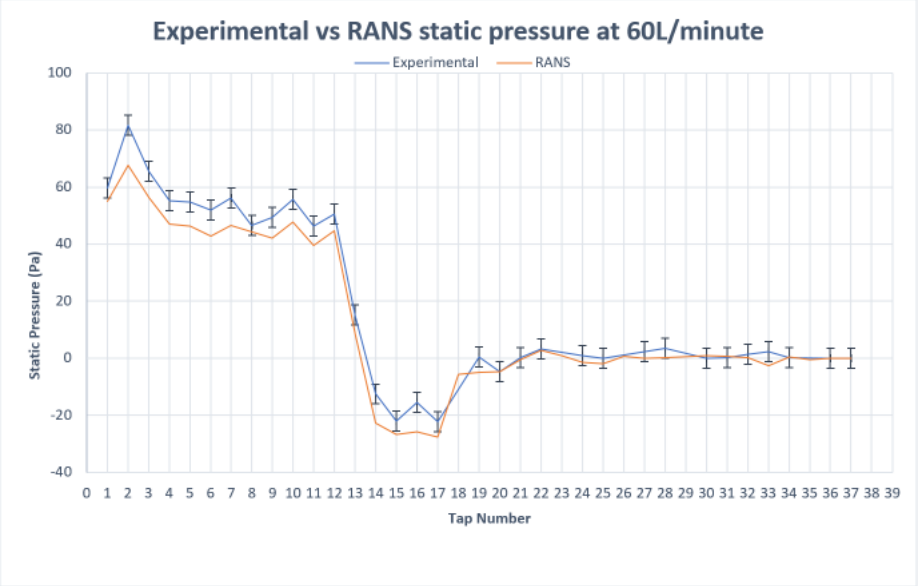


Figure 4.11. Static pressure loss along the length of the trachea for the experimental model and the steady RANS model at a flow rate of 60L/min

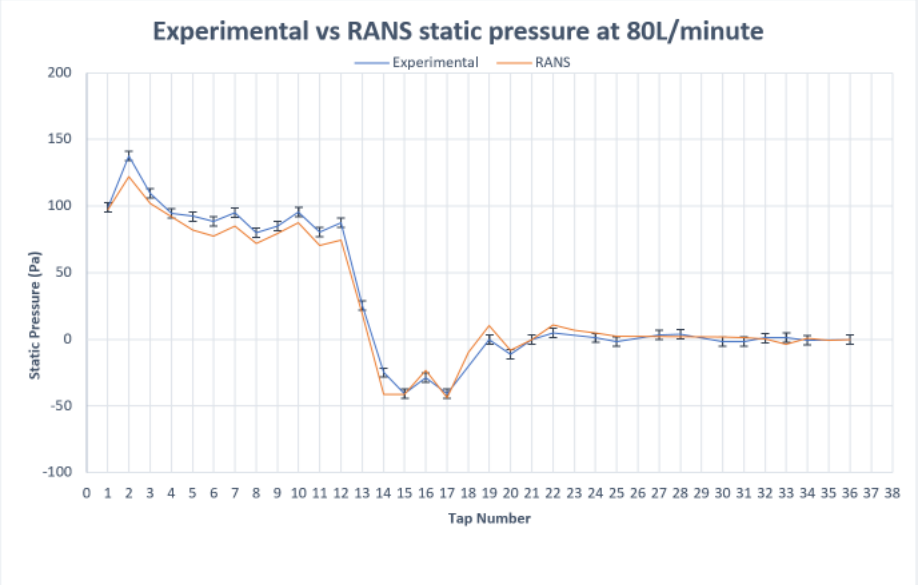


Figure 4.12. Static pressure loss along the length of the trachea for the experimental model and the steady RANS model at a flow rate of 80L/min

4.7 Validating a steady RANS model in the truncated airway

A steady RANS model is computationally much cheaper than an LES model and could provide a relatively quick estimate of pressure loss across the trachea. If accurate enough, a steady RANS model would be preferable due to the reduced computational time required to provide an estimate of pressure loss. Both LES and RANS models have been validated against the experimental model for a full airway model (see chapter 4.6). To look in more detail at the

differences between LES and steady RANS in the truncated airway model, the following simulations were run and compared:

1) LES and a steady RANS simulation for a truncated airway model with a moderate constriction (subject 19, minimum cross-sectional area 49.5mm^2) at a flow rate of 15L/min
2) LES and a steady RANS simulation for a truncated airway model with a severe constriction (subject 9, minimum cross-sectional area 25.7 mm^2) at a flow rate of 15L/min
3) LES and a steady RANS simulation for a truncated airway model with a severe constriction (subject 9, minimum cross-sectional area 25.7 mm^2) at a flow rate of 30 L/min
4) LES and a steady RANS simulation for a truncated model with the most severe constriction in the series of tracheas used for the main body of this thesis (subject 21, minimum cross-sectional area 14.8 mm^2).

The first experiment compared LES with a steady RANS model in the truncated model with a moderately constricted trachea (subject 19). The flow rate was 15L/minute. Please refer to chapter 4.4 for a full description of the settings used for the simulations. The same volume mesh (3562888 elements) was used for both simulations. The pressure loss was calculated using pressure inlet-pressure outlet. The relative difference in pressure loss between the simulations was 3.2%, the actual difference being only 0.48 Pa (see table 4.7)

The second experiment compared LES with a steady RANS model in the truncated model with a severely constricted trachea (subject 9). The flow rate was 15L/minute. Please refer to chapter 4.4 for a full description of the settings used for the simulations. The same volume mesh (3481734 elements) was used for both simulations. The pressure loss was calculated using pressure inlet-pressure outlet. The relative difference between the simulations was 8.3%, the actual difference being 7.31Pa (see table 4.7). Most of the study subjects' airway models are mild - moderately constricted, and the severely constricted case (minimum cross-sectional area 25.7 mm^2) used in the second experiment lies outside of the interquartile range for the minimum cross-sectional area (see figure 4.14).

Simulation	Pressure loss (Pa)	Relative difference (%)
LES -moderately constricted	15.12	-
RANS - moderately constricted	14.64	3.2

LES - severely constricted	87.55	-
RANS – severely constricted	80.24	8.3

Table 4.7. Pressure loss as estimated using LES model and a steady RANS model in the truncated airway model with a moderate and a severe constriction at a flow rate of 15L/min

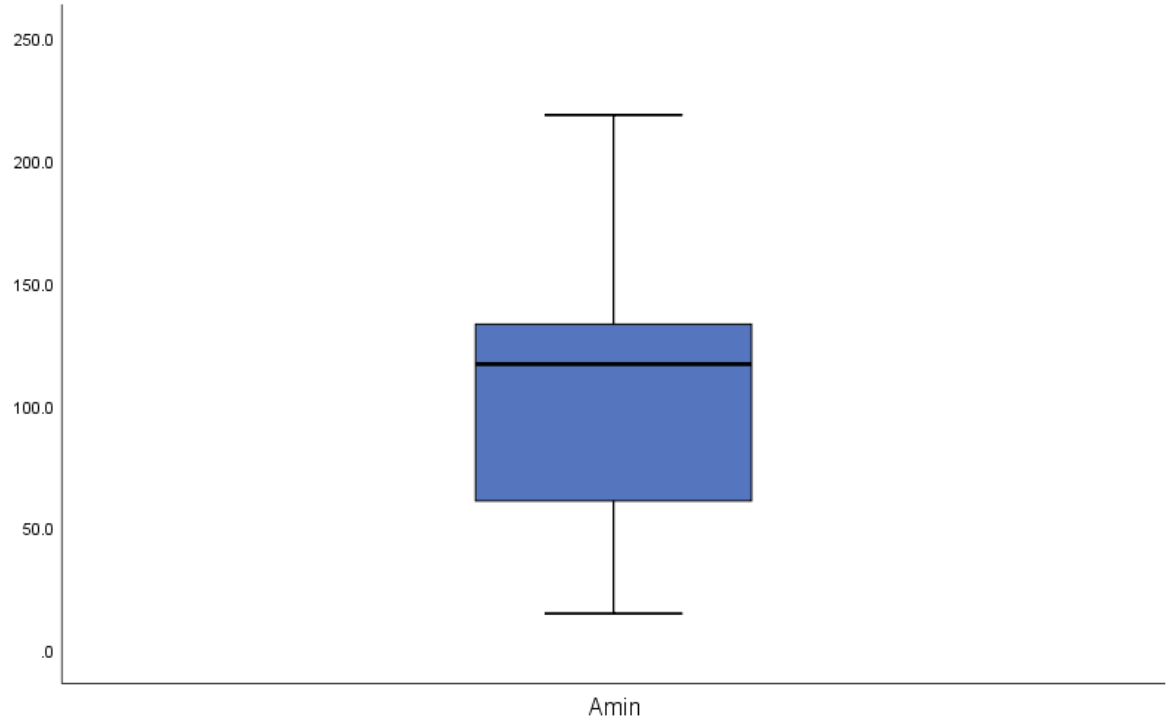


Figure 4.13. Minimum cross-sectional area (Amin) of the subjects' tracheas

The third experiment compared LES with a steady RANS model in the truncated model with a severely constricted trachea (subject 9) with a flow rate of 30 L/minute. Please refer to chapter 4.4 for a full description of the settings used for the simulations. The same volume mesh (3481734 elements) was used for both simulations. The pressure loss was calculated using pressure inlet-pressure outlet. The estimated pressure loss across the trachea (inlet-outlet) for Subject 9 using an LES model was 234.0 Pa and the estimated pressure loss using a steady RANS model was 235.7 Pa The relative difference was small at 0.72% (see table 4.8). Therefore, we are confident to use a steady RANS model for both flow rates 15L/min and 30L/min to estimate the pressure loss across the tracheas in subjects with a minimum cross-sectional area that is $\geq 25.7 mm^2$.

Simulation at 30L/min	Pressure loss (Pa)	Relative difference (%)
Subject 9 LES	234.0	-
Subject 9 Steady RANS	235.7	0.72

Table 4.8. Pressure loss as estimated using LES model and a steady RANS model in subject 9 at 30L/min

The most constricted trachea in this thesis is that of subject 21. The minimum cross-sectional area is 14.8 mm^2. The plan for the fourth experiment was to compare the pressure loss as estimated by a steady RANS simulation and an LES simulation. A steady RANS simulation was used to simulate the airflow through this tracheal geometry; however, the simulation did not converge to a satisfactory degree for a flow rate of 30L/min. The mean pressure loss across the trachea was fluctuating at +/- 10 Pa and the residuals were not resolved. Due to the severe constriction, the geometry for subject 21 was too complex to obtain a converged steady RANS solution. For this subject an LES model was used to predict the pressure loss across the trachea for the main results.

4.9 Inflow domain truncation effects

Creating an airway model which includes the face, oral cavity, nasal cavity, pharynx, larynx and trachea is technically more challenging and takes considerably longer than creating a truncated airway model. Ideally a volume mesh should closely represent the real-life environment however in clinical practice only a few of the CT scans performed include all of the anatomy required to produce a full representation of the airway. Often the CT scan stops just outside the area of clinical interest, which in the case of compressive thyroid goitres only includes the trachea. Many of the subjects' CT scans did not include the pharynx or any of upper airway beyond the larynx. Creating a truncated model of the airway simplifies the process and saves time. Choi et al (55) concluded that the glottis is an important structure to include when studying flow through the trachea.

To look at the effects of truncating the airway model an experiment was carried out to compare the results of a steady RANS simulation at 30L/min for a full airway model (see figure 4.15) and a truncated airway model (see figure 4.16). The model was truncated above the glottis and at the two main bronchi and flow extensions of 60 mm in length added to the both the inlet

and outlets. For full details of creating the volume mesh please refer to chapter 4.2. For full details of the simulation settings please refer to chapter 4.4.

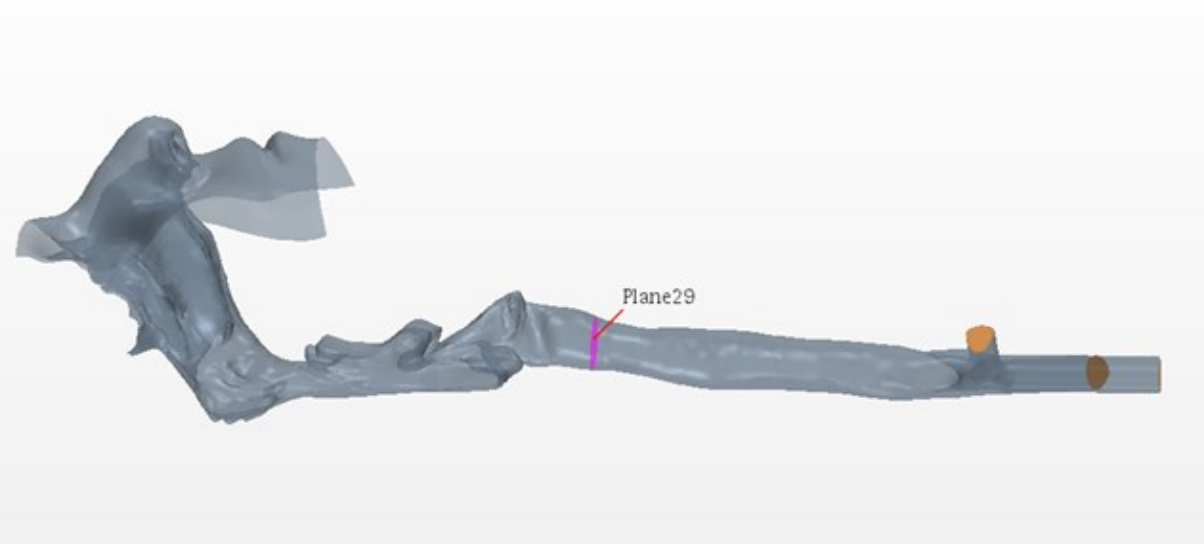


Figure 4.14. Full airway model with outlet extensions with the plane of peak turbulence highlighted

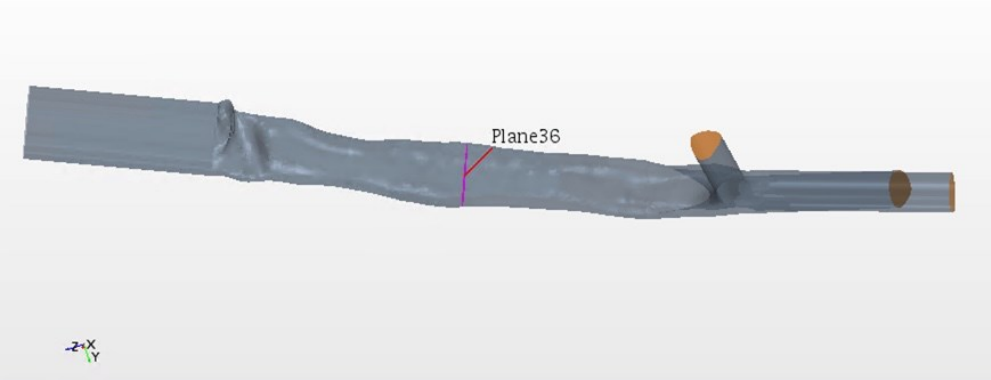


Figure 4.15. Truncated airway model with inlet and outlet extensions with the plane of peak turbulence highlighted

To measure the relative difference in pressure loss between the two models, measurements were taken from identical planes (inlet plane was taken above the glottis and outlet plane taken just above the carina). The pressure loss from the full airway model at 30L/minute was 11.7 Pa, whilst the pressure loss from the truncated airway model was 12.5 Pa. The 0.8 Pa pressure difference is minimal and although truncating the airway model introduces a small amount of relative error, the speed of making the volume mesh and reduced computational time make this small error worthwhile.

Figure 4.17 demonstrates the difference in mean total pressure along the length of the airway model. In the full airway model, there is a drop in the mean total pressure in the pharyngeal region which isn't present in the truncated model. This is likely due to flow disturbances in the upstream structures of the full airway model that aren't present in the truncated model. There is slower recovery of the pressure loss in the truncated model. Overall, the graph shows that the pressure loss seen at the level of the glottis is very similar between the two airway models.

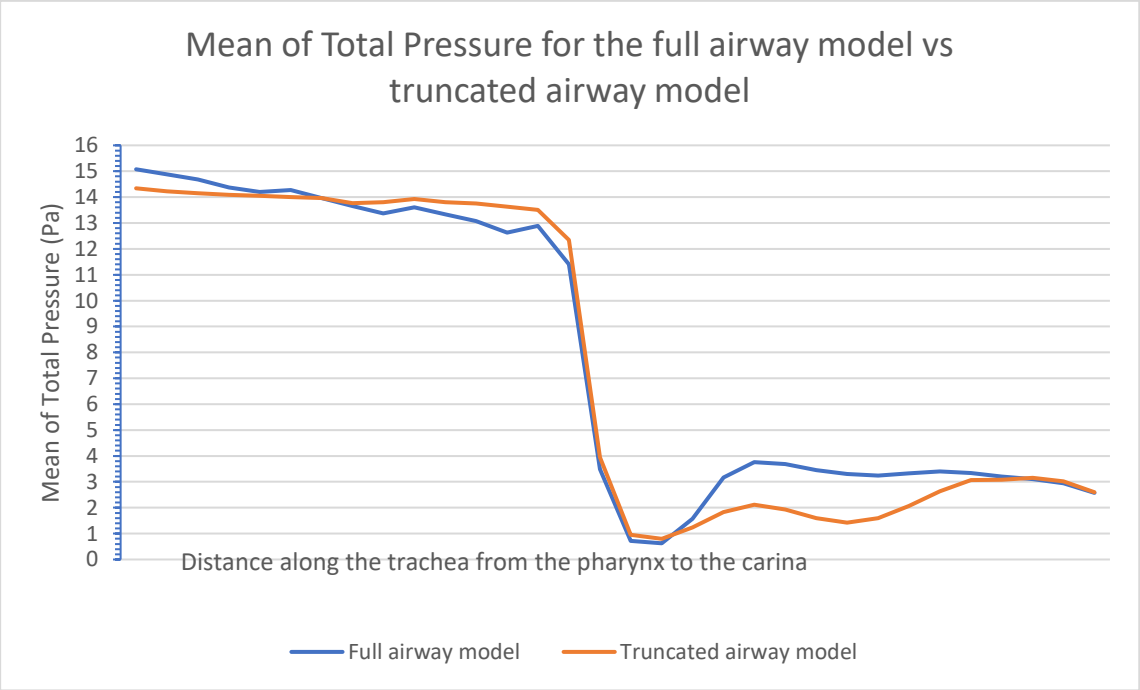


Figure 4.16. The mean of total pressure along the length of the airway comparing the full airway model with the truncated airway model at 30L/min using a steady RANS model

Figure 4.18 shows the velocity along the length of the airway models and demonstrates that there is a reasonable concordance in velocity along the whole length. The velocity of flow peaks around the level of the glottis in both airway models, as would be expected due to the jet produced by the narrowing of the glottis.

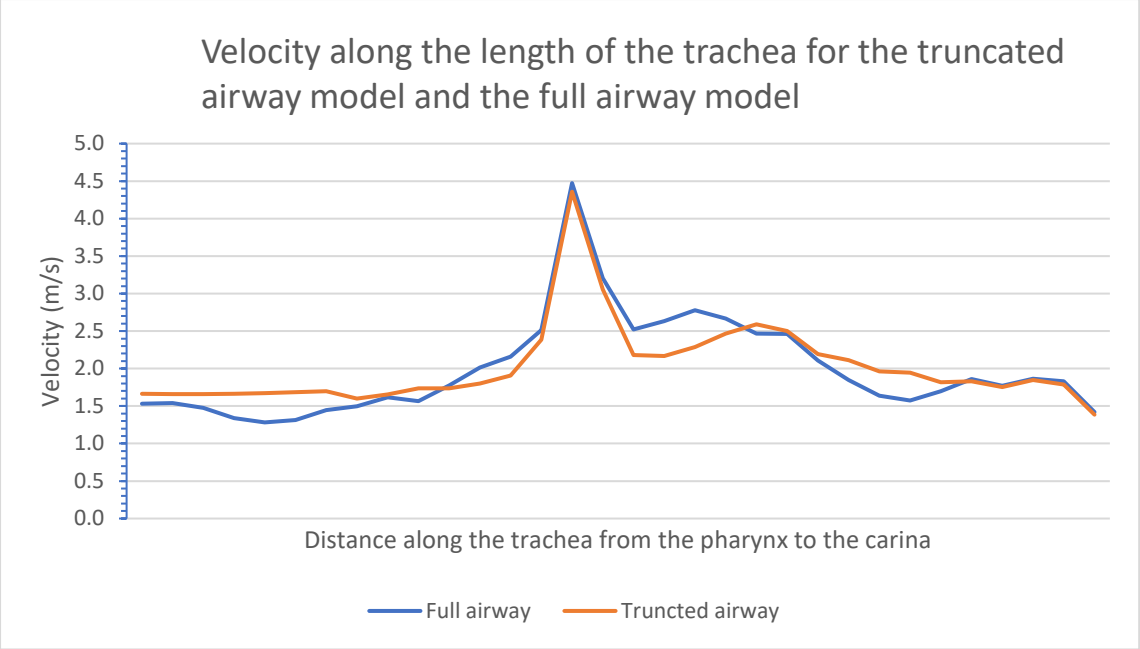


Figure 4.19. The velocity along the length of the airway comparing the full airway model with the truncated airway model

Both of the steady RANS simulations (full airway and truncated airway) have an initial setting of 5% turbulence. Figure 4.19 shows a graph of the turbulent kinetic energy along the length of both airway models. The peak in the turbulence is further upstream the trachea in the full upper-airway model than in the truncated model. Figure 4.20 shows a sagittal plane through the full upper-airway model and the truncated airway model to demonstrate the difference in turbulent kinetic energy distribution throughout the airway model. This is similar to findings by Choi et al (55) who demonstrated that truncating the airway model above the glottis led to a delay in the transition of the laryngeal jet from laminar to turbulent flow. This is due to the lack of the upstream disturbances from the other upper airway structures.

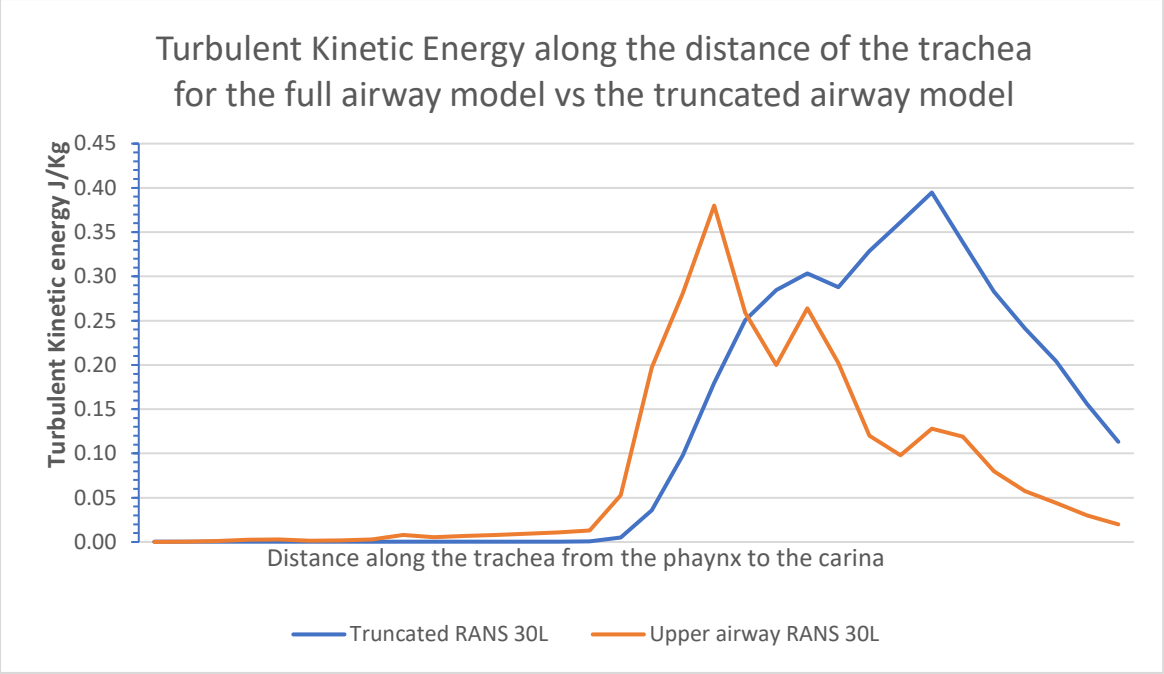


Figure 4.18. The turbulent kinetic energy along the length of the trachea comparing the full airway model with the truncated model

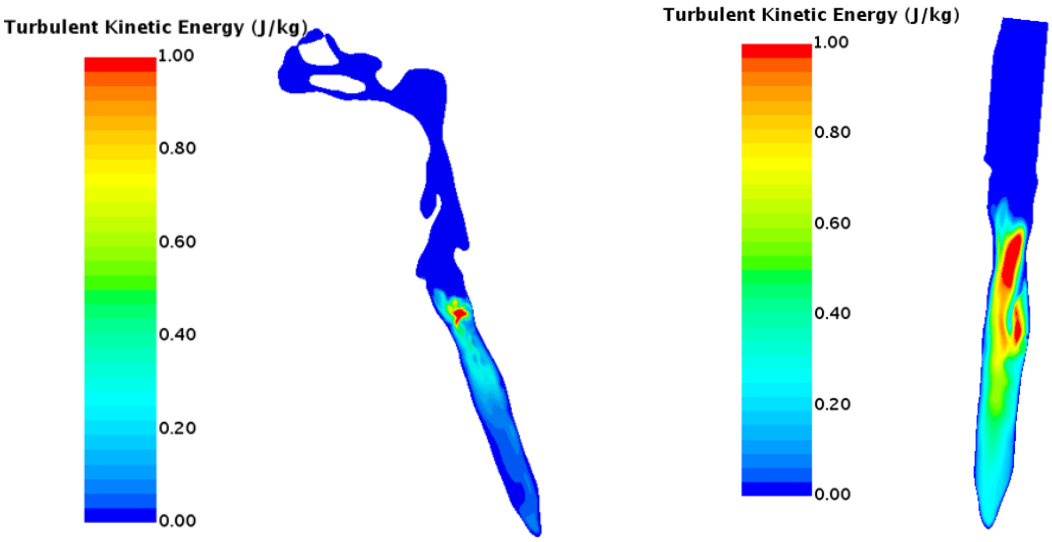


Figure 4.19. Sagittal plane demonstrating the change in turbulent kinetic energy along the length of the airway comparing the full airway model with the truncated model at 30L/min using a steady RANS model

4.10 Concluding remarks

This chapter presented the methods used to generate a volume mesh of a human trachea for the purpose of simulating airflow through the airway and the choice of turbulence model used. For

moderately constricted tracheas, with a minimum cross-sectional area ≥ 25.7 mm^2 a volume mesh with 2.6 million cells is sufficiently fine enough. However, with greater constrictions a finer mesh is required in order to achieve a converged simulation. For capturing flow behaviour near the wall, the height of the prism layer and the height of the cells within the prism layer, are important. As a starting point we used a prism layer of 0.015 mm, 5 cells thick with a stretch factor of 1.3. Y+ values greater than 1 will require smaller cells within the prism layer, therefore it is important to check the maximum y+ value after running an initial simulation.

Choi et al (6) demonstrated that using a mass flow inlet boundary condition on a truncated airway geometry (truncated above the glottis), provides an accurate representation of the flow, despite not including the entire upper airway. A mass flow inlet was used at the inlet of the tracheal models in this study. For the RANS model, an inlet turbulence intensity of 10% was used. A no slip condition was used at the mesh walls and a no pressure outlet boundary condition used with a static pressure of zero. Extruders were used at both the inlet and outlet, in order to allow flow to fully develop at the inlet and prevent backflow at the outlet. The extruders used were 60mm in length with 50 layers and a stretch factor of 6.0.

In order to capture the flow characteristics in laminar, transitional and turbulent regimes computational fluid dynamics was used to simulate the flow through the 21 tracheal volume meshes. To reduce the computational cost of running the simulation, a steady RANS (SST (Menter) K-omega) model of turbulence was used. This RANS model in particular has the advantage of relative insensitivity to the inlet conditions and free stream conditions and the advantage of near-wall calculations.

A steady RANS model was found to provide a converged solution for 20 of the 21 models. However, for the most constricted trachea model, subject 21, we were unable to obtain a converged solution at a flow rate of 30L/min and therefore an LES model was used instead. A timestep of 1e-4 was found to be sufficiently accurate to model the flow through the tracheal mesh. For this dataset, a steady RANS model was suitable for modelling flow through tracheal models with a minimum cross-sectional area ≥25.7mm^2.

Chapter 5 CFD Assessment of compressive goitre

5.1 Introduction
5.2 RANS model of pressure loss at 15L and 30L
5.2.1 Overview of geometries and pressure losses
5.3 Patterns of flow
5.4 Correlating geometric analysis with pressure loss
5.5 Loss predictions using A_{min}
5.6 Hydraulic diameter
5.7 Area of the glottis
5.8 Discussion and conclusions

5.1 Introduction

As described in the introduction (1.3), the work performed in each breath is the integrated product of the pressure that the body needs to generate at each instant multiplied by the incremental change in the lung volume. Air moves from a region of high pressure to a region of lower pressure and in the airway this pressure gradient is created between the pressure at the airway at the nose or mouth (normally atmosphere, often referred to as barometric pressure) and that at the alveoli.

There is some confusion regarding terminology relating to pressures in the respiratory system. As explained by Loring (65) transpulmonary pressure (P_L) is defined as the difference between pressure at the airway opening (P_{ao}), usually the mouth or nose, minus the pressure in the pleural space (P_{pl}), i.e., $P_L = P_{ao} - P_{pl}$. We can split the transpulmonary pressure into the pressure drop across the airway ($P_{ao} - P_{alv}$), with P_{alv} denoting alveolar pressure, and the pressure drop across the lung tissue, which is referred to as the elastic recoil pressure of the lung. [$Pe_{l(L)} = P_{alv} - P_{pl}$]. Therefore, whilst $P_L = (P_{ao} - P_{alv}) + (P_{alv} - P_{pl})$, it is only the part $(P_{ao} - P_{alv})$ that is responsible for overcoming the viscous stresses that resist the motion of the air. The magnitude of the viscous stresses depends on several factors, chief among which are the geometry of the airways and the rate of airflow.

Airway resistance (normally measured in $cmH_2O/L/s$) is defined as the ratio of the pressure drop across the airways to the flow rate, as expressed in the following equation:

$$R = \frac{\Delta P}{\dot{V}} \ (cmH_2O/l/s) \qquad \text{(Equation 5.1)}$$

Here R = resistance;

ΔP= difference in pressure, $(P_{ao} - P_{alv})$;

$\dot{V}$ = flow rate.

For a simple laminar flow in a pipe, the flow rate is directly proportional to the pressure drop between entry and exit of the pipe, so the resistance is independent of flow rate. However, for a turbulent flow or for a more complicated geometry, resistance itself depends on flow, for example resistance is directly proportional to flowrate for an orifice, as described further below.

During inspiration, the inspiratory muscles contract and expand the chest wall and flatten the diaphragm. As a result, the thoracic volume increases and thus the intra-thoracic pressure decreases. This creates the necessary pressure gradient between the atmosphere and the alveoli such that air flows into the airways. During quiet expiration the inspiratory muscles relax and there is a resultant decrease in the intra-thoracic volume and the intra-thoracic pressure increases, additionally there is an inward elastic recoil of the lungs.

The work of breathing can broadly be divided into the elastic work i.e., the work necessary to overcome the compliance of the lungs (elastic recoil) and chest wall, and resistive work i.e., the work necessary to overcome the airway flow resistance. It is estimated that 60-70% of the work of breathing during inspiration is the elastic work and therefore around 30% of the work during inspiration is resistive work. (66) Otis et al (67) described three aspects to the work of breathing and calculated estimates of the contribution of each: 63% of the total work of breathing is required to overcome the elastic forces of the lungs and chest wall during inspiration, 29% is required to overcome the resistance associated with the movement of air through the respiratory tract and 8% is required to overcome the deformity of tissues.

Large increases in either the elastic or resistive components of the work of breathing can be caused by a range of pathologies, including pulmonary fibrosis, pneumonia, and ARDS, which affect compliance, or asthma, and tracheal stenosis which affect resistance. An enlarged thyroid goitre can result in compression of the trachea which in turn can result in an increase in the airflow resistance through this section of the airway. Patients with compressive thyroid

goitres often complain of dyspnoea and although the mechanisms are not fully understood it is thought that this is due to the compression of the trachea which leads to an increase in the airway resistance and a subsequent increased work of breathing.

Unfortunately, measurement of the total work of breathing is difficult being either invasive or requiring specialised equipment. Likewise, determining the component of the work of breathing associated with resistance to airflow is difficult, and the measurements that exist all involve some assumptions and approximations, particularly in their neglect of the time-varying course of breathing.

Frank et al (68) compared four methods of determining inspiratory airway resistance (in 9 healthy male subjects, 31-58 years), and found values in the range 1.2-1.9 $cmH_2O/L/s$, according to the different measurement methods. While Loring et al (65) drawing on Frank and other references state pulmonary resistance to be normally ~ 1 $cmH_2O/L/s$. In the absence of a means to measure patient-specific airway resistance, we rely on these approximate values as representative values in the healthy adult.

Pathological changes to the trachea, such as those seen in patients with a compressive retrosternal goitre, can result in a sizable increase in the flow resistance in this part of the airways. (1) This increase in airflow resistance will contribute to the patient's sensation of breathlessness and will also increase the work of breathing. When we consider flow through the airways, the contribution of the trachea to the total flow resistance in a healthy individual is normally small, in the region of around 5%. (29)

During quiet breathing (15 L/min), airway resistance is estimated to be 1.5-2 $cmH_2O/L/s$, which is equivalent to around 200 Pa/L/s. Therefore, the total pressure loss of the airway at 15 L/min is estimated to be around 100 Pa (calculated using equation 5.1). (69) If we estimate that the tracheal contribution to the airway resistance is around 5% of the total airways resistance, then in a healthy individual we would expect to see a pressure loss of around 5 Pa during quiet breathing (15 L/min). An estimate of the normal airway resistance of the trachea at a flow rate of 15 L/min would be 0.02 Pa/ml/s. Olson et al (70) calculated estimates of the pressure drop throughout the respiratory tract in a healthy individual and found that the pressure drop across the trachea was estimated to be 7 Pa at 30 L/min, (corresponding to a resistance of 0.014 Pa/ml/s.)

Airway resistance and thus pressure loss will increase with increasing flow rates. We would expect that compression of the trachea from a retrosternal goitre would lead to an increase in airway resistance in the trachea and therefore an increase in the pressure loss. If we consider a normal tracheal airway resistance to be around 0.02 Pa/ml/s and a normal tracheal

pressure drop to be around 5 Pa at a flow rate of 15L/min, then we would expect higher pressure drops to be found in patients experiencing shortness of breath from their compressive goitres.

The diaphragm is considered to be the primary muscle of inspiration, accounting for up to 70% of the tidal volume exchanged during normal inspiration. The other inspiratory muscles include the external intercostals, the parasternal and scalene muscles and the sternocleidomastoids. The principal muscles of expiration are the internal intercostals and the abdominal muscles. The afterload on the respiratory muscles may be assessed by measuring the work of breathing. The work of breathing can be calculated by integrating the change in pressure (P) and the change in volume (dV):

$$work\ of\ breathing = \int P\ dV \qquad \text{(Equation 5.2)}$$

In a patient with a tracheal compression and increased airways resistance, a greater increase in pressure will be required in order to provide the same change in volume when compared to a healthy patient. This is reflected as an increased work of breathing. The inspiratory muscles will have to work harder in order to expand the lungs to a given volume. The total work of breathing is approximately 0.5 Joules/L of ventilation in healthy adults. (71) Powell et al performed a series of experiments in healthy adults whereby individuals performed exercise tasks whilst having an applied resistive load at their mouth whilst breathing through a pneumotach. The work of breathing was calculated and it was found that even small increases in airway resistance results in large increases in the work of breathing. (66)

When we consider the losses that we have in the trachea we should refer to both the major and minor losses. In the large airways, where the flow is considered to be turbulent due to the high Reynolds number (>4300), Poiseuille flow is not a good approximation. In the large airways we have to consider flow distortion from entrance effects, curvature of the airway away from the midline, unsteadiness, flow separations following narrowing of the airway and sudden expansions, and turbulence.

The pressure available to drive a flow, i.e. the pressure head, is usually shortened to ‘head’ and pressure losses referred to as head losses. Head loss due to pipe friction dominates in long pipe networks; it is consequently termed major loss. This loss can be estimated using

the Darcy-Weisbach equation. Minor losses, despite the name, dominate in the large airways and are made up of losses due to constrictions creating flow jets, curvature away from the midline resulting in flow asymmetry, vocal folds creating a flow jet which leads to entrance effects, sudden expansions following a constriction leading to separation of the flow and turbulence due to the complex structure of the upper airways. Minor losses are expressed as a loss co-efficient multiplied by the dynamic head. $\frac{1}{2}\rho\overline{U}^2$, where $\overline{U}$ is the average flow velocity, which can be expressed in terms of the flowrate, Q and cross-sectional area A as $\overline{U} = \frac{Q}{A}$. The pressure loss due to a constriction is thus expressed as:

$$\Delta P_L = K_L . \frac{\rho Q^2}{2A_{min}^2}$$

(Equation 5.3)

where:

P_L = pressure loss

K_L = loss coefficient

Q = flow rate

A_{min} = area at constriction

Computational fluid dynamics has been used to analyse airflow through the human airway and a recent review by Faizal et al (21) summarises the extensive use of CFD for assessing the airway in different pathologies, ranging from asthma to obstructive sleep apnoea. Bates et al (72) provided a benchmark dataset for using CFD to study the human trachea in both the healthy and pathological state.

Calculating an estimate of the pressure loss across a pathological trachea could provide clinically useful information. In the case of patients with a compressive thyroid goitre, in whom the decision to operate is not straightforward, having access to this data would prove to be helpful in the decision-making process. If, for example a patient with multiple co-morbidities in whom the risks of operating are high, complains of dyspnoea and it is not clear from a CT scan if compression of the trachea is contributing to this in a significant way, then an estimate of the pressure loss across the trachea would provide clinically relevant information. If the

pressure loss across the trachea was within the region of what is considered normal (around 5 Pa pressure loss at 15L/min), then it is unlikely that surgery to remove the goitre is going to improve the airway resistance significantly and therefore reduce the pressure drop across the trachea.

Currently, the guidelines for surgery are based on a 2D measurement being taken from a CT scan of the patient's airway, however, this 2D measurement does not take into account the curvature of the airway or the length of tracheal compression, both of which can contribute significantly to tracheal losses. (72) CFD can be used to estimate pressure loss across a compressed trachea and this pressure loss can be used as an indicator of the severity of tracheal compression. However, calculating pressure loss across the pathological trachea using CFD is not something that is currently available to clinicians. In the interim therefore, it is worth assessing if there is a tracheal measurement that correlates strongly with pressure loss; such a measure could provide a useful clinical guide to the severity of pressure loss. The % tracheal constriction and the minimum cross-sectional area of the trachea are two such measurements.

If we hypothesise that the loss across the constricted area of the trachea in a patient with a compressive goitre is a type of 'orifice loss', then pressure loss is given by equation 5.3 Pressure loss can be estimated using the minimum cross-sectional area of the trachea and a loss co-efficient 'K' for varying flow rates. If it were assumed that the major source of loss within the compressed trachea is due to the constriction, the formula in equation 5.3 could be used to provide a simple predictive rule for estimating the pressure loss

However, although orifice type losses may dominate in the constricted trachea, the pressure loss may not correlate perfectly with the minimum cross-sectional area or with the %tracheal constriction. Thus, we need to consider what other factors contribute to the severity of the pressure loss i.e., the trachea may not be circular at the level of the trachea, in which case the hydraulic diameter may be a useful measurement.

The sensation of dyspnoea, also referred to as shortness of breath, is the subjective sensation of running out of breath, not being able to breathe deeply or freely, or feeling discomfort when breathing. The sensation is a result of complex interactions between peripheral and central receptors feeding back to the respiratory centre in the brain. When a patient with a compressive goitre complains of shortness of breath, we assume that the mechanism is related to the increased work of breathing, and the increased pressure loss across the compressed trachea. However, pressure loss may not explain the sensation of dyspnoea in its entirety and therefore

we should consider other mechanisms, a point that we return to later in the discussion (Chapter 5.7), after the pressure loss analysis.

This chapter presents the results of a study in which CFD analysis was performed to predict flow during the established phase of inspiration in the trachea for twenty-one goitre patients who had been referred for surgery. In the following, we begin by presenting the key geometric measurements and predicted pressure loss for each subject, before describing the flow analysis and results of the CFD analysis in greater detail. Furthermore, we will consider:

- If there is a strong correlation between pressure loss and the tracheal measurements: %tracheal constriction, minimum cross-sectional area and hydraulic diameter
- If there is a simple predictive calculation of pressure loss using a loss co-efficient '*K*'
- Which other tracheal factors contribute to the severity of pressure loss
- Which mechanisms contribute to the sensation of dyspnoea in these patients

5.2 RANS model of pressure loss at 15 and 30 L/min

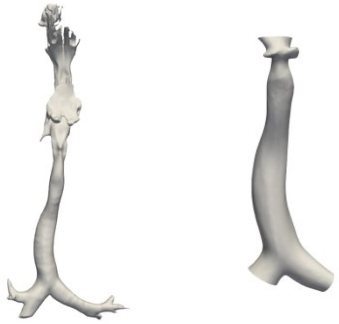
Airflow was simulated at two steady flow rates, 15 L/min and 30 L/min, for each of the pathological tracheas. A mean flow rate of 15 L/min, assuming equal inspiratory and expiratory phases (I:E ratio of 1:1), corresponds to a minute volume of 7.5 litres; for an I:E ratio of 1:2, the corresponding minute volume is 5 litres. Flow rates of 15L/min and 30L/min are used widely throughout the CFD literature to represent quiet breathing and light exercise, respectively. Patients who are severely affected by shortness of breath complain of breathlessness at rest i.e., during quiet breathing or during light exercise. In order to present data that would be both clinically useful and in order to compare our data with other data sets in the literature, the flow rates of 15 L/min and 30 L/min were selected for the CFD analysis.

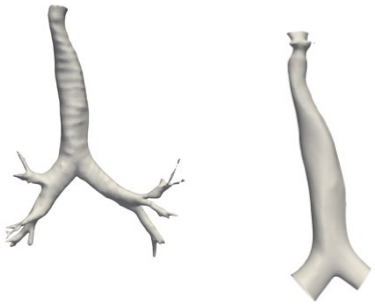
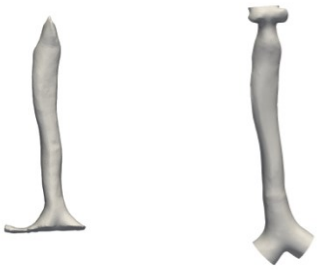
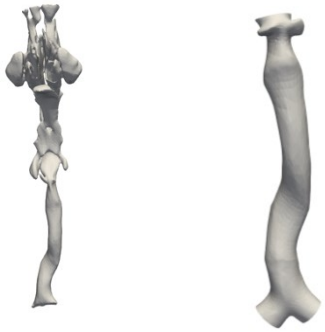
Flow computations were performed using an SST (Menter) k-omgea steady RANS model for nearly all cases; for full details of the computational modelling, refer to Chapter 4.2. Subject 21 displayed a severe constriction of the trachea, with a minimum cross-sectional area of 14.8mm^2. Due to the severity of this constriction, a steady RANS model would not converge sufficiently to provide a repeatable estimate of pressure loss in this trachea. Consequently, an implicit unsteady LES model was used to estimate the pressure loss across the trachea for subject 21.

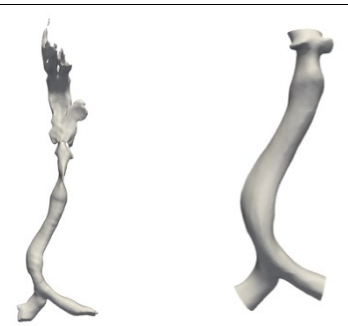
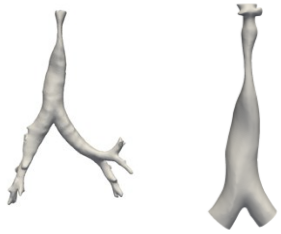
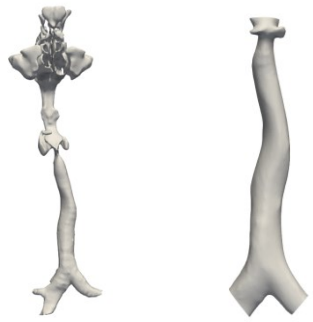
5.2.1 Overview of geometries and pressure losses

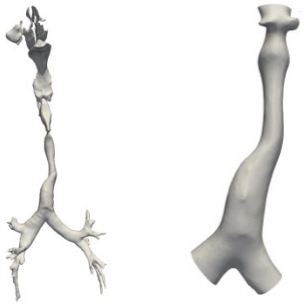
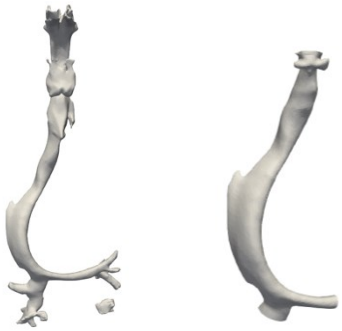
Table 5.1 below summarises key geometric and flow measures obtained for each case.

The tracheal models are depicted in two forms: on the left shows the tracheal model prior to undergoing any surface mesh modifications and on the right shows the tracheal model following surface mesh modifications. (Refer to Chapter 3.1 for details on preparing the surface mesh). Due to variability in the limits of the CT scan performed on each subject there is a wide range in the anatomical limits of each surface mesh. A large number of the tracheal image data did not show the glottis and/or main bronchi due to the limited scan area of the corresponding CT study. For those tracheas for which the image data included a glottis, the position of the glottic folds was variable and on some of the surface meshes the glottis was almost completely closed. The size of the glottic opening has a large impact on the airflow through the trachea. Therefore if we want to study the effects of the tracheal compression on airflow through the trachea it would be preferable to have models with the same relative size glottic opening. Due to the wide variability in the subjects' glottic opening, all the surface meshes were cropped at the level of the cricoid and the same standardised glottis was appended to each trachea. Further surface mesh modifications were performed on each of the tracheas including; for those tracheas without two main bronchi, the mesh was cropped at the level of the carina followed by the addition of a standardised pair of main bronchi. The surface meshes underwent smoothing and an increase in the number of surface triangles.

Subject	Anterior-posterior view of 3D tracheal geometry (pre-processing on the left and post-processing on the right)	Subject details
1		A_{min}=133.1mm^2 % constriction = 51.0 $A_{glottis}$=115.3 Pressure loss (Pa) at: 15L/min= 3.4 30L/min= 11.1

2		A_{min}= 78.8 mm^2 % constriction =66.7 $A_{glottis}$=69.8mm^2 Pressure loss (Pa) at: 15L/min= 11.4 30L/min= 41.6
3		A_{min}= 218.6 mm^2 % constriction = 8.92 $A_{glottis}$=186.4mm^2 Pressure loss (Pa) at: 15L/min= 1.5 30L/min= 5.2
4		A_{min}= 130.7 mm^2 % constriction = 16.1 $A_{glottis}$=153.5 mm^2 Pressure loss (Pa) at: 15L/min= 3.0 30L/min= 9.9
5		A_{min}=127.3 mm^2 % constriction = 7.1 $A_{glottis}$=125.6 mm^2 Pressure loss (Pa) at: 15L/min= 5.0 30L/min= 16.5
6		A_{min}= 116.8 mm^2 % constriction = 28.9 $A_{glottis}$=110.5 mm^2 Pressure loss (Pa) at: 15L/min= 5.0 30L/min= 15.6

7		A_{min}= 156.9 mm^2 % constriction = 28.8 $A_{glottis}$=189.9 mm^2 Pressure loss (Pa) at: 15L/min= 2.9 30L/min= 9.4
8		A_{min}= 99.3 mm^2 % constriction = 19.4 $A_{glottis}$=103.5 mm^2 Pressure loss (Pa) at: 15L/min= 5.5 30L/min= 18.3
9		A_{min}= 25.7 mm^2 % constriction = 86.3 $A_{glottis}$=60.3 mm^2 Pressure loss (Pa) at: 15L/min= 80.2 30L/min= 235.7
10		A_{min}=119.1 mm^2 % constriction = 38.9 $A_{glottis}$=110.3 mm^2 Pressure loss (Pa) at: 15L/min= 4.3 30L/min= 14.1
11		A_{min}= 103.0 mm^2 % constriction = 28.4 $A_{glottis}$=110.3 mm^2 Pressure loss (Pa) at: 15L/min= 4.4 30L/min= 15.0

12		A_{min}= 120.1 mm^2 % constriction = 56.1 $A_{glottis}$=139.1 mm^2 Pressure loss (Pa) at: 15L/min= 2.9 30L/min= 10.6
13		A_{min}= 166.1 mm^2 % constriction = 21.8 $A_{glottis}$=111.3 mm^2 Pressure loss (Pa) at: 15L/min= 3.0 30L/min= 10.9
14		A_{min}= 60.9mm^2 % constriction = 67.2 $A_{glottis}$=126.5 mm^2 Pressure loss (Pa) at: 15L/min= 7.0 30L/min= 24.9
15		A_{min}= 67.1 mm^2 % constriction = 43.8 $A_{glottis}$=83.5 mm^2 Pressure loss (Pa) at: 15L/min= 13.66 30L/min=44.9
16		A_{min}= 145.0 mm^2 % constriction = 20.9 $A_{glottis}$=144.3 mm^2 Pressure loss (Pa) at: 15L/min= 3.1 30L/min= 10.3

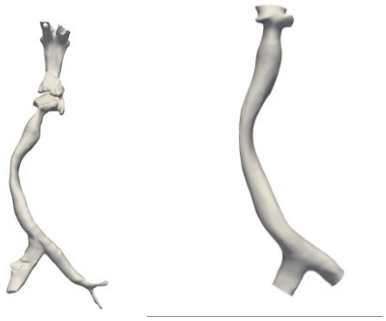
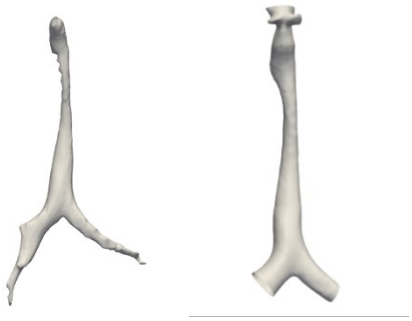
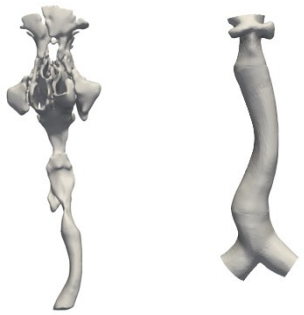
17		A_{min}= 49.7 mm^2 % constriction = 58.3 $A_{glottis}$=120.7 mm^2 Pressure loss (Pa) at: 15L/min= 13.0 30L/min= 45.5
18		A_{min}= 42.9 mm^2 % constriction = 50.1 $A_{glottis}$=110.1 mm^2 Pressure loss (Pa) at: 15L/min= 19.0 30L/min= 74.1
19		A_{min}= 49.8 mm^2 % constriction = 68.3 $A_{glottis}$=115.9 mm^2 Pressure loss (Pa) at: 15L/min= 14.6 30L/min= 45.5
20		A_{min}= 145.0 mm^2 % constriction = 32.2 $A_{glottis}$=125.3 mm^2 Pressure loss (Pa) at: 15L/min= 3.1 30L/min= 10.3
21		A_{min}= 14.8 mm^2 % constriction = 90.8 $A_{glottis}$=120.0 mm^2 Pressure loss (Pa) at: 15L/min= 298.0 30L/min= 1057.3

Table 5.1 The anterior-posterior view of the trachea (pre-processing on the left and post-processing on the right) for the 21 subjects and the results of the pressure loss as estimated by a steady RANS model of turbulence (and using an LES model for subject 21) at steady flow rates of 15L/min and 30L/min

The estimated pressure loss using a RANS model in this series of subjects shows a range of 1.5 - 298.0 Pa at a flow rate of 15 L/min, and a range of 5.2 – 1057.3 Pa at a flow rate of 30 L/min. The % constriction of the trachea refers to the reduction of the cross-sectional area of the most constricted part of the trachea relative to the cross-sectional area at a fixed reference point in the particular trachea geometry (at a position 2 cm above the carina for the respective trachea geometry). Note that whereas two geometries may have a similar % constriction, however the minimum cross-sectional area may be vastly different e.g., subjects 1 and 18 have a % constriction of 51.0 and 50.1 respectively whilst their minimum cross-sectional areas are 133.1 mm^2 and 42.9 mm^2.

For a given flow rate, the minimum cross-sectional area of a constriction determines the maximum velocity attained by the flow at the narrowest point. If the airflow experiences anything other than a gradual increase in area downstream of the narrowest point, the flow, rather than decelerating uniformly across the width of the lumen, will separate, forming a core jet of high velocity flow. The kinetic energy of this accelerated flow is then rapidly dissipated in the downstream turbulent breakup of the jet. Even if the airway area increases so gently as to avoid jet formation, the pressure losses associated with elevated wall shear stress likewise depends on the maximum velocity attained. The degree of constriction thus has to be considered in conjunction with the minimum area.

In order to place the CFD results obtained here into context, we attempt a brief summary of previous studies relevant on tracheal resistance. Of these, studies, Shih et al (73) investigated the pressure drop across a trachea with a compression, secondary to a lung tumour, both before and after the placing of a tracheal stent. They used a k-epsilon model of turbulence and found that a compression corresponding to a 75% constriction led to a pressure drop of 22.89 and 77.23 Pa across the trachea at 15 L/min and 30L/min respectively. Following a stent insertion, the compressed area had a constriction of 38% and the pressure drop reduced to 2.15 Pa at 15 L/min and 7.05 Pa at 30 L/min respectively. As would be expected they found that as the flow rate through the trachea increased, the pressure drop correspondingly increased. The results obtained in that study are similar to the findings for the tracheas investigated in this study: Subject 10 has a trachea which has been compressed by 38.9% and has an estimated pressure loss of 4.3 and 14.1 Pa at flow rates of 15L/min and 30L/min respectively. Subject 10 has a

constriction due to a thyroid goitre compression without a large deviation of the trachea away from the midline which makes the pressure loss results comparable to a trachea with a subglottic stenosis of similar constriction.

Large retrosternal goitres can lead to a fixed compression of the trachea, similar to the fixed constriction seen in subglottic stenosis patients. Subglottic stenosis (SGS) leads to a fixed constriction below the level of the glottis. The Cotton-Meyer classification system is a commonly used method of describing the severity of the obstruction: grade I stenosis <50%, grade II 51 – 70%, grade III 71-99%, grade IV no detectable lumen. Patients with subglottic stenosis tend to report a sudden and rapid decline in their breathing when their airway stenosis reaches 75% of the tracheal lumen. (62)

Lin et al (44) carried out a study to investigate the relationship between the degree of obstruction and airflow limitation in SGS. The authors hypothesised that the Bernoulli Obstruction Theory better predicts the airway resistance than the Hagan-Poiseuille equation. The Hagan-Poiseuille equation predicts that airflow resistance is inversely proportional to the fourth power of the tube diameter. However, the equation is only valid for flow that is fully formed and laminar. Airflow in the human upper airways is at best transitional between laminar and turbulent. The Bernoulli Obstruction Theory predicts a fourfold increase in the airway resistance with a fourfold decrease in the airway cross-sectional area.

In the Lin et al study, the team simulated the effect of varying degrees of subglottic stenosis using a standard 5 mm long cylindrical segment which was re-scaled to represent cross-sectional areas of 40%, 50%, 60%, 70% and 90% obstructions. Each cylinder was then inserted into a healthy 3D tracheal model at the level of the subglottis. A steady state airflow simulation with a k-omega turbulence model was used to calculate the pressure drop across each airway. The pressure drop was then used to calculate the airway resistance between the nostrils and the carina. Airway resistance (R) was defined as:

$$R = \frac{\Delta P}{Q} \qquad \text{Equation 5.4}$$

Where:

ΔP = Change in pressure between the nostrils to the carina

Q = inhalation rate

They estimated the pressure drop to be 23.1 Pa between the nostrils to the carina in their healthy adult tracheal model. This is considerably higher than the pressure drop seen in the less obstructed subjects studied for this thesis. In part this is because the tracheal models in this thesis did not include the nasal or pharyngeal airways and only measure the pressure drop between the surpraglottis and the carina. It may also be because the glottis in the healthy tracheal model used in the Lin et al study may be partially abducted (although this information is not provided).

The study calculated the airway resistance in the trachea to be roughly 0.4 Pa/s/ml in the model representing a 90% 5mm long subglottic stenosis. This is very similar to the estimated airway resistance for subject 9, with an 86% obstruction at a flow rate of 15 L/min the airway resistance was 0.32 Pa/s/ml. A direct comparison cannot be made because the study did not provide the exact flow rates for each simulation. A negative pressure outlet was used to obtain a flow rate of 15 L/min in the healthy trachea and the same pressure outlet was then used across the obstructed tracheas. (44)

Wasserman et al (74) developed a bronchoscope technique for the assessment of airway resistance in patients with benign glottic or subglottic stenosis. Thirteen patients with glottic or subglottic stenosis were studied, and seven control subjects were studied. Each patient recorded their level of breathlessness on a visual analogue scale 100 mm in length, with 0 representing “no shortness of breath” and 100 representing “shortness of breath as bad as can be”. The patients underwent a diagnostic flexible bronchoscopy whilst being sedated with 5mg Midazolam and 25-50mg of Pethidine. A pressure catheter was introduced (1 mm in diameter) through the working port of the bronchoscope and pressure measurements were taken above the glottis and below the level of the subglottic stenosis. Patients were asked to take deep breaths in and out and flow rates reached up to 2 L/s. The mean inspiratory airway resistance of the controls was measured to be 0.36 +/- 0.13 Pa/s/ml in the control group and 7.11 +/- 7.19 Pa/s/ml in the group that required intervention. No correlation was found between the dyspnoea score and the airway resistance measurements. Considering the airway resistances measured by Wasserman et al, we note that their values are much higher than the airway resistances estimated by CFD in the subjects studied in this thesis (range 0.02 -2.11 Pa/s/ml). This may be for a number of reasons, the first being that the patients in the Wasserman et al study were sedated at the time of the airway resistance measurements. Sedation leads to a degree of upper airway obstruction due to the collapse of the upper airway. Although this collapse would have taken place upstream of the pressure transducer, this would change the airflow structure as the air entered through the larynx into the trachea. A second reason that could explain the much

higher airway resistance is the higher flow rates achieved by the patients, reaching up to 2L/s, whilst a lower flow rate of 0.25-0.5 L/s was used in this thesis. A third reason is the introduction of a pressure transducer through the glottis and through the subglottic stenosis which itself would impede the airflow through the trachea and introduce more airway resistance.

Pedley et al (75) predicted the pressure loss and airway resistance using measurements from a rigid model of the anatomy of the trachea and bronchial tree based upon data from lungs fixed at 75% of the total lung capacity. Their findings were in agreement with experimental studies using human subjects, excised lungs and on models of the bronchial tree. The studies all showed that the major source of airways resistance were the larger airways and that under normal conditions the peripheral airways contribute little resistance. The largest airway resistance and therefore pressure drop is seen in generations 4-6. They calculated the viscous resistance using the following equation:

$$(R_R)_n = (R_P)_n . \frac{C}{4\sqrt{2}} (Re \frac{d}{L})^{\frac{1}{2}} \qquad \text{Equation 5.5}$$

Where:

R_R= real viscous resistance

R_P = Poiseuille viscous resistance

Re = Reynolds number

d = average diameter of the airway at this generation

L = average length of the airway at this particular generation

They estimated the pressure drop across the model trachea (from above the glottis to the level of the carina) to be 4.4 Pa at a flow rate of 10 L/min. The airway resistance of the trachea in this model is 0.02 Pa/ml/s, which is in line with the airway resistance seen in the tracheal models studied in this thesis (range 0.02-2.2 Pa/ml/s). The tracheal model used by Pedley et al represents a healthy non-constricted trachea.

A sum of all the airway resistance estimations for their airway model has been taken from a figure showing the airway resistance at each generation (from 0-18) at a flow rate of 10 L/min and is equal to 290 $cmH_2O/L/s \times 10^{-3}$. If the tracheal resistance is 34.9 cm $cmH_2O/L/s \times 10^{-3}$, then this would mean that the trachea accounts for 12% of the airway resistance in this model of the airways. This is higher than other estimations for the tracheal contribution of airway resistance quoted in the literature and highlights the difficulty in acquiring accurate real-life data. A more accurate way to measure tracheal pressure loss and the airway resistance

across the trachea would be to insert pressure gauge needles above the level of the glottis and at the level of the carina in an awake, self-ventilating patient which would of course be invasive, high risk for complications and entirely unethical.

In the healthy trachea, the glottis is a major source of losses. Brancatisano et al (58) found that the average glottis size during mid-inspiration at rest was 126 mm^2 in a study of both men and women. For the tracheal models used in this thesis a standardized glottis was attached to each of the tracheas in order to remove the variability in glottic aperture. The mean glottic area for the 21 tracheal models was 120.5 mm^2. Brouns et al (62) used a tracheal model to study the effects of tracheal stenosis. The glottic area of their tracheal model was 125 mm^2. They estimated the pressure drop across the glottis using CFD to be 15 Pa at 30 L/min which was equivalent to the pressure drop seen across a 40-50% stenosis. They found that when the stenosis exceeded 50% there was a sudden increase in the pressure drop seen across the trachea.

Markow et al (76) studied the effect of glottic area on airway resistance in patients who had undergone surgery for bilateral vocal fold paralysis. They found that when the glottic area was less than 40 mm^2 there was a sudden and sharp rise in the airway resistance. This is similar to the findings in this thesis, subjects 18, 19, and 21 have a tracheal minimum cross-sectional area of 42.9, 25.7, and 14.8 mm^2 respectively and demonstrate a sudden increase in the pressure loss (at flow rates of 30L/min) of 74.1, 235.7, and 1057.3 Pa respectively.

Chen et al (77) investigated the pre- and post-operative pressure drops in a series of 12 paediatric patients with vascular rings compressing the trachea. Due to the much lower flow rates used in the simulations the pressure losses across the trachea were much lower however they found that post-operatively when the degree of compression was reduced there was a reduction in the pressure loss. Verbanck et al (78) used forced oscillation testing in tracheal stenosis patients to demonstrate that respiratory resistance is a function of airflow rates and the minimum cross-sectional area of the trachea. The same pattern can be seen here with the goitre subjects. Overall, there is an increase in pressure loss as the minimum cross-section reduces, and there is an increase in the pressure loss as the flow rate increases (see table 5.2 which shows the subjects in ascending order of minimum cross-sectional area.)

Subject	Amin (mm^2)	%Constriction	Pressure loss (Pa) at 15 L/min	Pressure loss (Pa) at 30 L/min
21	14.8	90.8	298.0	1057.3
9	25.7	86.3	80.2	235.7
18	42.9	50.1	19.0	74.1
17	49.7	58.3	13.0	44.5
19	49.8	68.3	14.6	45.5
15	67.1	43.8	13.6	44.9
14	71.4	61.5	7.0	24.9
2	78.8	66.7	11.4	41.6
8	99.3	19.4	5.5	18.3
11	103.0	28.4	4.4	15.0
6	116.8	28.9	5.0	15.6
10	119.1	38.9	4.3	14.1
12	120.1	56.1	2.9	10.6
5	127.3	7.1	5.0	16.5
4	130.6	16.1	3.0	9.9
1	133.1	51.0	3.4	11.1
20	143.0	32.2	3.2	10.6
16	145.0	20.9	3.1	10.3
7	156.9	28.8	2.8	9.4
13	166.1	21.8	3.0	10.9
3	218.6	17.5	1.5	5.2

Table 5.2 The estimated pressure loss across the trachea for each subject as calculated using CFD (steady RANS model) for the flow rates 15 L/min and 30 L/min in order of the minimum cross-sectional area of the trachea (ascending order). The most constricted case (subject 21) shows the estimated pressure loss calculated using an LES model for the flow rates 15 L/min and 30 L/min.

5.3 Patterns of flow

Three subjects have been selected to represent a mildly constricted trachea (subject 6), a moderately constricted trachea (subject 18) and a severely constricted trachea (subject 21). Table 5.3 shows a summary of each of these tracheas, which we will look at in detail.

Subject	%Constriction	Amin (mm^2)	Pressure loss at 15L/min (Pa)	Pressure loss at 30L/min (Pa)
6 (mild constriction)	28.9	116.8	5.0	15.6
18 (moderate constriction)	50	42.9	19.0	74.1
21 (severe constriction)	90.8	14.9	298.0	1057.3

Table 5.3. Key geometric and flow measures obtained for the three subjects representing a mild constriction, a moderate constriction, and a severe constriction

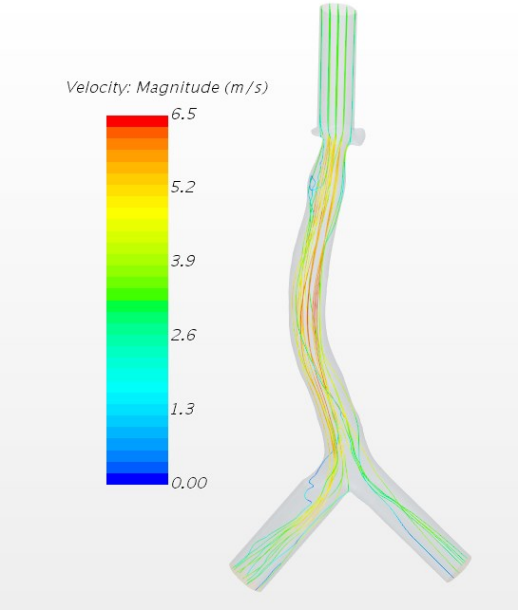
Figure 5.1 demonstrates the increasing complexity of flow with increasing restriction of the trachea at a flow rate of 30 L/minute. The three subjects have a minimum-cross sectional area (A_{min}) equal to 116.8, 42.9 and 14.9 mm^2 respectively. In subject 6 (mildly constricted), the cross-sectional area of the glottis ($A_{glottis}$) is smaller than the cross-sectional area of the trachea, $A_{min.}$ whereas in the moderately and severely constricted subjects, the cross-sectional area at the tracheal constriction is smaller than the area of the glottis. The streamlines in the mildly constricted trachea are relatively straight with only minor disturbance to the flow in the glottic region and downstream of the glottis, so in this mildly constricted case the glottis behaves like a low-resistance orifice and leads to little downstream disturbance in the flow. The corresponding pressure losses (15.6 Pa at a flow rate of 30 L/min.) are mild,

By contrast, the streamlines in the moderately constricted trachea show a large disturbance to the flow in the area of separation following the constriction and deviation of the trachea. Likewise, there is a large disturbance to the flow in the severely constricted trachea in the area of separation following the length of constriction.

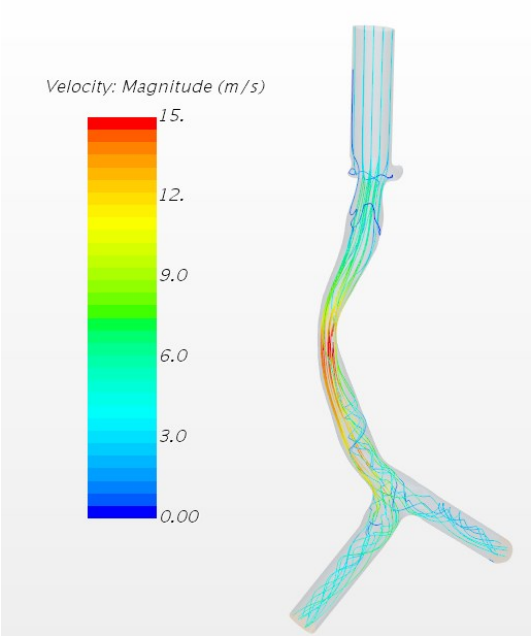
Whereas the peak velocity of flow in the mildly constricted trachea is around 6.5m/s in the region of the glottis, the peak velocity of flow in the severely restricted trachea reaches a velocity of around 60m/s (see figure 5.1) in the region of the constriction

These findings are in keeping with Brouns et al (62). The team studied the flow patterns in artificially modified tracheal stenoses. Using a Yang-shih k-epsilon turbulence model they demonstrated the increased complexity of flow dynamics as the tracheal stenosis increased in severity. In a non-stenosed trachea they demonstrated the peak flow of velocity in the vicinity of the laryngeal jet, this peak velocity of flow shifted to the area of stenosis when the stenosis

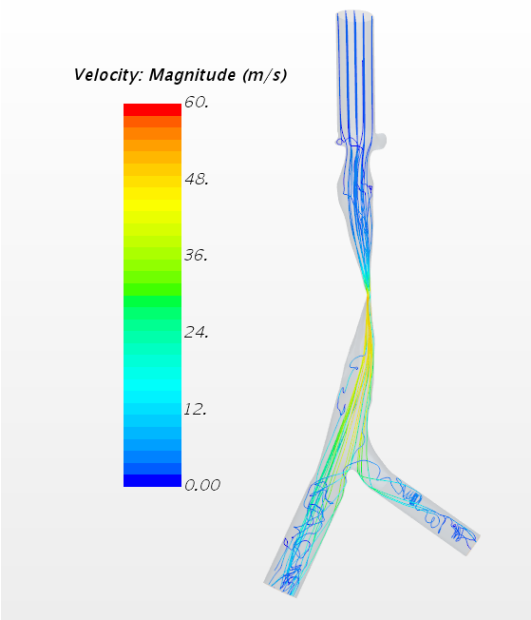
exceeded a 50% constriction. Regarding the present study, we note that Subject 18 has a constriction of 50% and subject 21 has a constriction of 90.8%. Both of these cases demonstrate the peak velocity of flow is in the region of the constriction, whilst subject 6, which has a constriction of 28.9%, demonstrates peak velocity in the region of the glottis. Bates 2014 (79) demonstrated flow patterns within the trachea using CFD. The glottic opening results in a jet which impinges on the anterior wall of the trachea which leads to detachment from the trachea wall and recirculation of flow with secondary vortices. The same patterns of flow have been demonstrated here in figure 5.1.



Subject 6: mildly constricted trachea



Subject 18: moderately constricted trachea

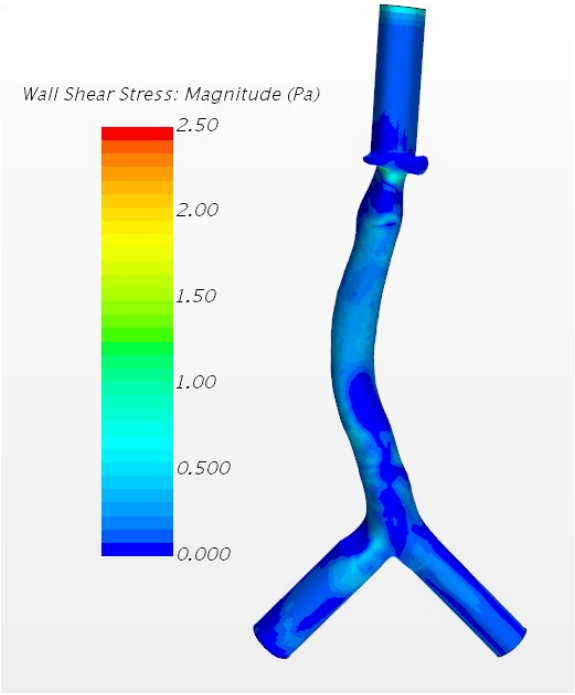


Subject 21: severely constricted trachea

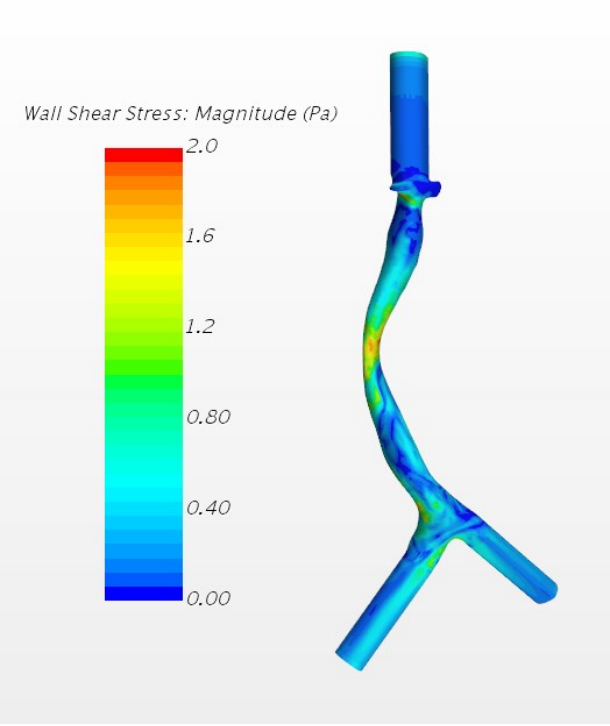
Figure 5.1. Streamlines to demonstrate the disturbance in flow and the velocity of flow through three tracheas at a flow rate of 30L/min

(Subject 6 representing a mildly constricted trachea, subject 18 representing a moderately constricted trachea and subject 21 representing a severely constricted trachea. Note the change in the scale on the colour bars, necessary in order to capture the range of velocities seen throughout the different tracheas.)

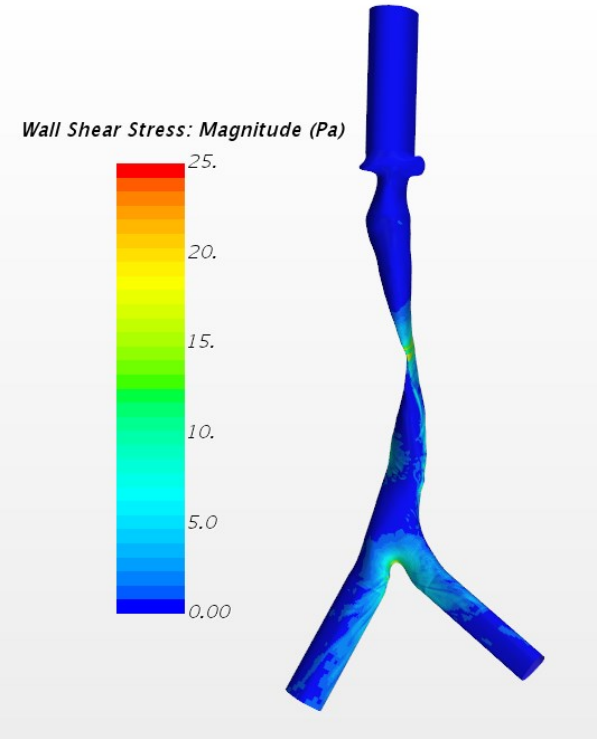
Areas of local acceleration (constriction induced high velocity in flow) lead to an increase in wall shear stress (WSS). Figure 5.2 demonstrates the WSS seen in the three subjects 6, 18 and 21; note the change in scale of the plot legend when comparing these. The maximal WSS is seen at the level of the glottis in the mildly constricted subject 6 and reaches maximal levels of around 2.5 Pa. In subject 18, the moderately constricted trachea, the maximal WSS is in the region of the constriction, with a modest increase in maximal levels of 2 Pa. Subject 21 has a prominent region of high WSS around the narrow constriction with maximal levels of 25 Pa. These areas of maximum wall shear stress correlate with the areas of maximum velocity. Choi et al (80) noted the same pattern of wall shear stress around areas of constriction induced high velocity flow in the trachea.



Subject 6: mildly constricted trachea



Subject 18: moderately constricted trachea



Subject 21: severely constricted trachea

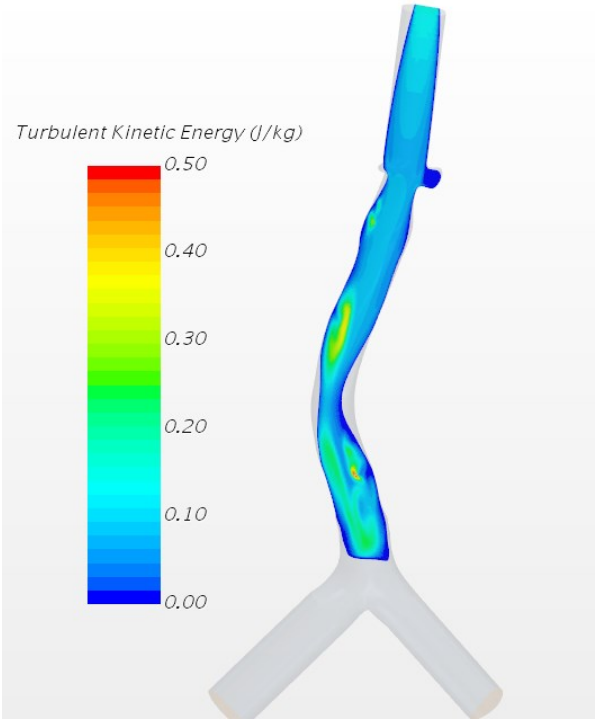
Figure 5.2 Magnitude of Wall Shear Stress (Pa) for subjects 6, 18 and 21 at a flow rate of 30L/min

(Note the change in the scale on the colour bars, necessary in order to capture the range of velocities seen throughout the different tracheas.)

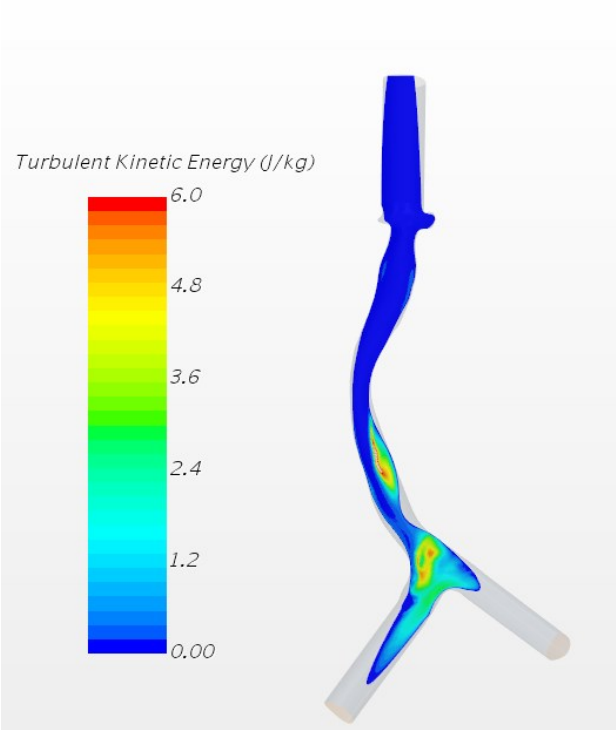
In order to look more closely at the patterns of flow within each of the three tracheas, planes have been selected for subject 6 and 18 and a volume render has been taken for subject 21. Subject 21 has a severe restriction that prevents a complete plane from being selected.

Turbulent kinetic energy can provide a useful indicator of the state of flow as described by Bates 2014 (79). Turbulence can be seen in the trachea when there is disturbance in flow, such as when there is a separation following a constriction. Figure 5.3 shows the turbulent kinetic energy in subjects 6 and 18. In the mildly constricted trachea (subject 6), there is a small increase in turbulent kinetic energy (TKE) in the region of the laryngeal jet. In the moderately constricted trachea, there are two areas of increased turbulence. The first is following the constriction where the trachea also deviates away from the midline. The deviation of the trachea at this point means that the constriction jet is aimed at the lateral aspect of the tracheal wall leading to an area of separation and turbulence adjacent to this. Due to the second deviation in

the trachea back towards the mid-line the direction of flow is then back towards the midline as it enters into the two main bronchi, leading to a second region of flow disturbance and turbulence.



Subject 6: mildly constricted trachea

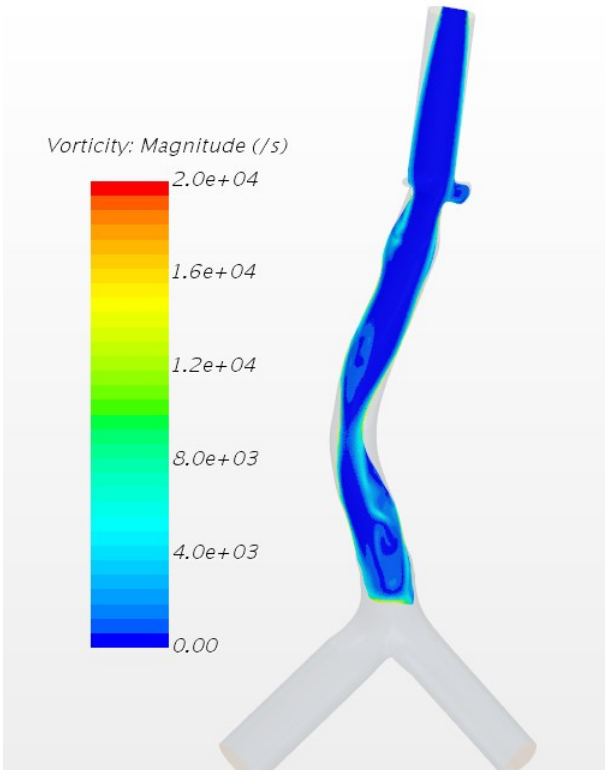


Subject 18: moderately constricted trachea

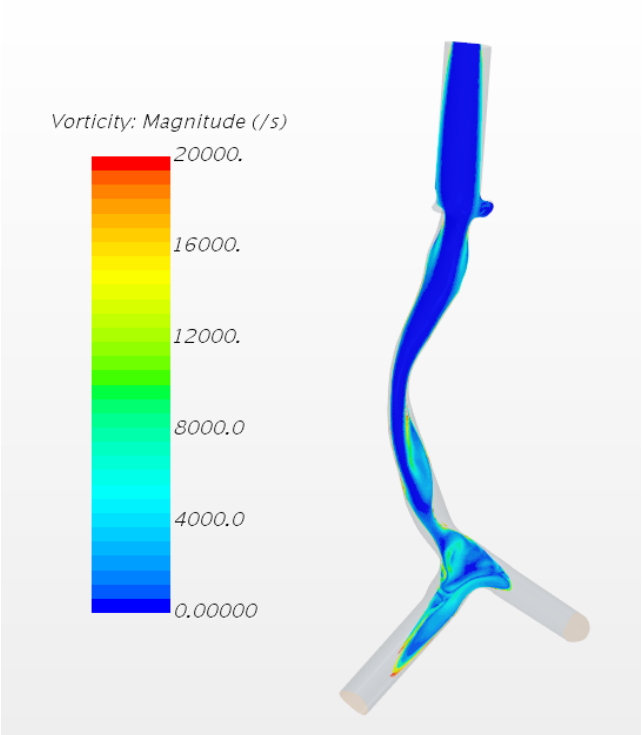
Figure 5.3. Turbulent kinetic energy (J/Kg) for subjects 6 and 18 at a flow rate of 30L/min

(Note the change in the scale on the colour bars, necessary in order to capture the range of velocities seen throughout the different tracheas.)

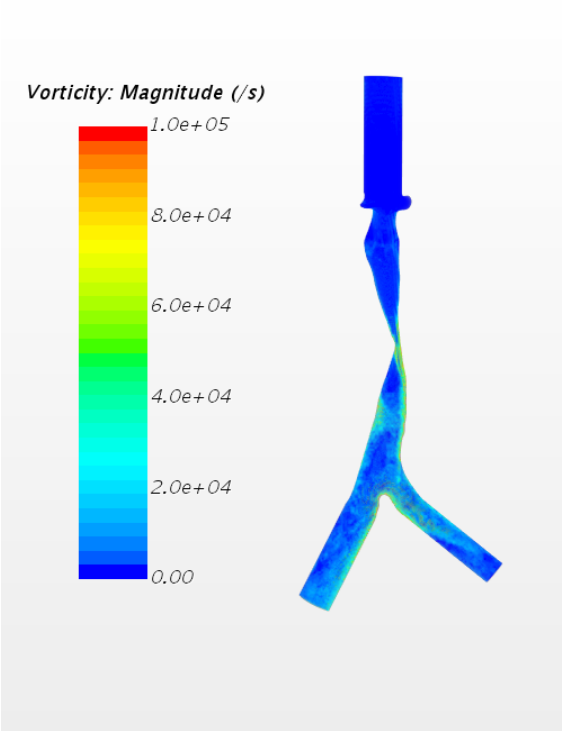
Vorticity is the curl of velocity field and measures the rotational distortion of a fluid element. Areas of vorticity indicate gradients in the flow and rapid changes in velocity, and areas of high vorticity indicate a high level of energy dissipation. Examining the magnitude of vorticity throughout the trachea helps to identify areas with unsteady flow. Figure 5.4 shows the magnitude of vorticity throughout the tracheas of the three subjects. The peak vorticity in subject 6 is around 12,000, whilst the peak vorticity in subject 18 is around 20,000 and in subject 21 it is around 100,000. The breakdown of separated shear layers leads to the major source of fluctuations in airway flow and the areas of high vorticity identify these areas. There is breakdown of separated shear layers parallel to the laryngeal jet, and parallel to the constriction seen in subject 6 and 18. The volume render of subject 21 demonstrates a region of high vorticity at the level of the severe constriction. These findings mirror the findings of Martonen et al (81) who studied the fluid dynamics of the larynx and upper tracheobronchial tree and demonstrated the formation of vortices secondary to the breakdown of flow adjacent to the laryngeal jet. Tracheal constrictions lead to a similar pattern of flow due to the formation and subsequent breakdown of the constriction jet.



Subject 6: mildly constricted trachea



Subject 18: moderately constricted trachea



Subject 21: severely constricted trachea

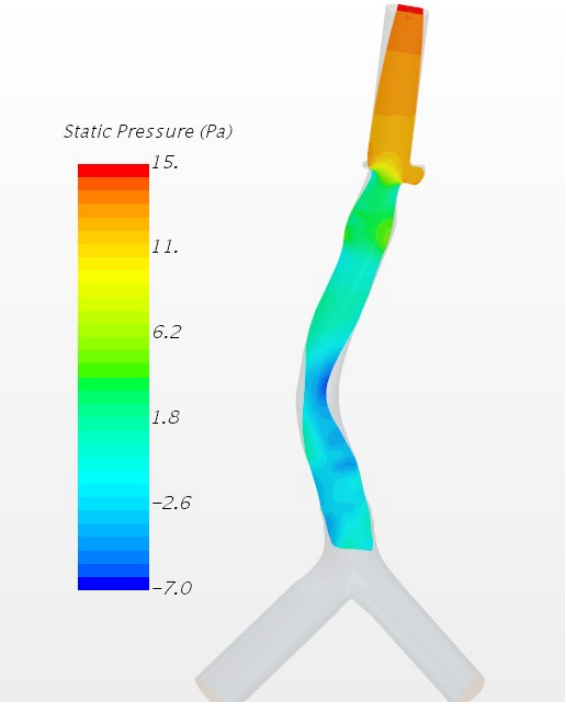
Figure 5.4. Magnitude of Vorticity (/s) for subjects 6, 18 and 21 at a flow rate of 30L/min

(Note the change in the scale on the colour bars, necessary in order to capture the range of velocities seen throughout the different tracheas.)

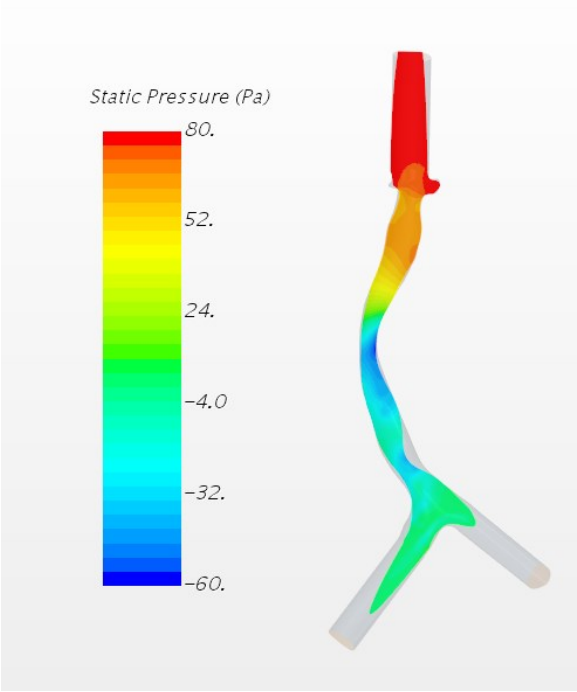
Figure 5.5 shows the static pressure throughout the tracheal models and demonstrates which locations the pressure loss takes place. It's important to note that static pressure is not the same as pressure loss, however it does give an indication of the location of forces which could lead to tracheal collapse further downstream of the compression. The largest fall in static pressure takes place at the region of the glottis in the mildly constricted trachea. In the moderately constricted trachea, there is static pressure drop appreciated at both the glottis region and the region of the constriction. Partial recovery can be seen after the region of constriction. The large drop in static pressure seen in the severely constricted trachea can also be seen to partially recover in the post-constriction region.

As flow travels through a constriction, flow accelerates and, due to the Bernoulli effect, there is a drop in pressure. Following a constriction, when there is a widening of the trachea, there is a deceleration in the flow and a resulting recovery in pressure. If there is separation in the flow following the constriction, turbulent flow leads to a loss of energy and there isn't a

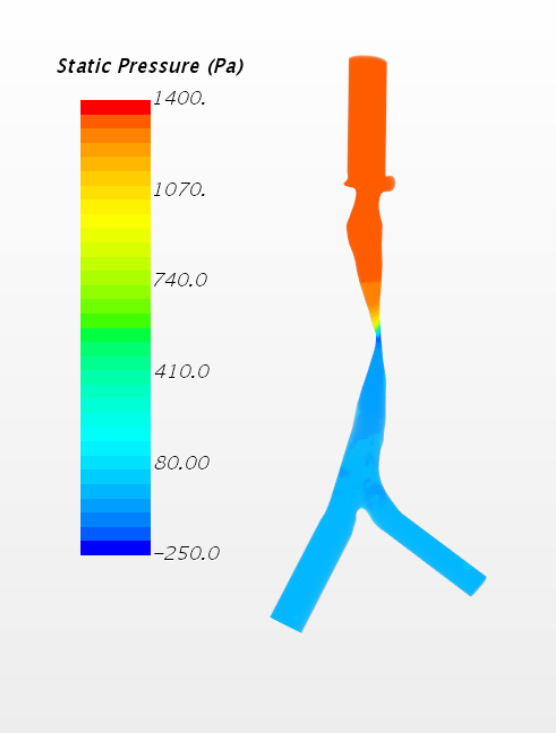
full recovery in the pressure. Bates 2014 (79) found similar recovery in static pressure following a constriction jet.



Subject 6: mildly constricted trachea



Subject 18: moderately constricted trachea



Subject 21: severely constricted trachea

Figure 5.5. Static pressure (Pa) for subjects 6, 18 and 21 at a flow rate of 30L/min

(Note the change in the scale on the colour bars, necessary in order to capture the range of velocities seen throughout the different tracheas.)

5.4 Correlating geometric analysis with pressure loss

There is a moderately positive correlation between the %constriction of the trachea and the pressure loss, as estimated by CFD at both 15 L/min and 30 L/min and this is statistically significant (see table 5.4). A scatter plot to show this relationship demonstrates that as the percentage constriction of the trachea increases there is an increase in pressure loss across the trachea (see figure 5.6).

% Constriction of the trachea vs	Spearman's rho	p value
Pressure loss at 15L/min	**0.602**	**0.005***
Pressure loss at 30L/min	**0.687**	**0.001***

Table 5.4 Correlation between the % constriction of the trachea and the pressure loss (outliers removed: cases 9, 17 and 21)

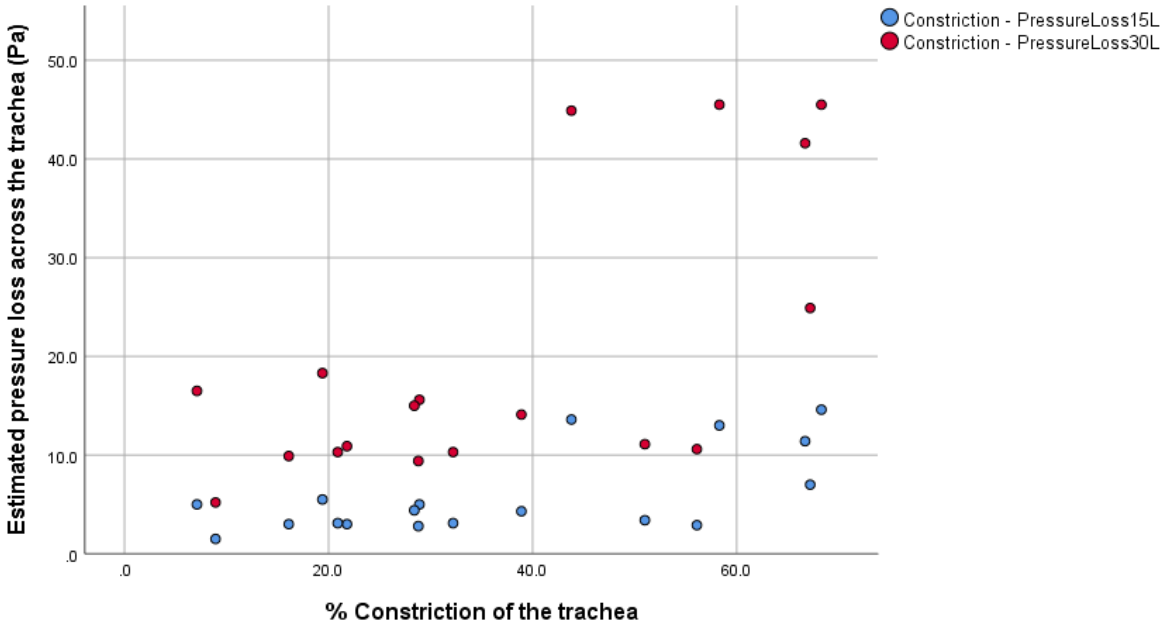


Figure 5.6. Pressure loss across the trachea against the % constriction of the trachea at flow rates 30L/min and 15l/min (outliers removed: subjects 9, 17 and 21)

There is a very strong negative correlation between the minimum cross-sectional area of the trachea and the pressure loss at both 15 L/min and 30 L/min, and this is statistically significant (see table 5.5 and figure 5.7). As the minimum cross-sectional area of the trachea reduces in size, the pressure loss across the trachea increases. Interestingly, the absolute size of the compression (A_{min}) correlates more strongly with the pressure loss than the relative compression (%constriction). This would indicate that a smaller trachea is more likely to be affected by a less severe compression than a larger trachea. This may lead us to hypothesise that it is more relevant to look at the minimum cross-sectional area of the trachea rather than the %constriction when considering surgery in these patients. As can be seen in the graph in

figure 5.7, there is a sharp rise in the pressure loss when the minimum cross-sectional area falls below 50 mm^2. This is similar to the findings by Brouns et al (62).

Minimum cross-sectional area of the trachea vs	Spearman's rho	p value
Pressure loss at 15L/min	**-0.930**	**0.000***
Pressure loss at 30L/min	**-0.946**	**0.000***

Table 5.5. Correlation between the Amin of the trachea and the pressure loss (outliers removed: subjects 9 and 21)

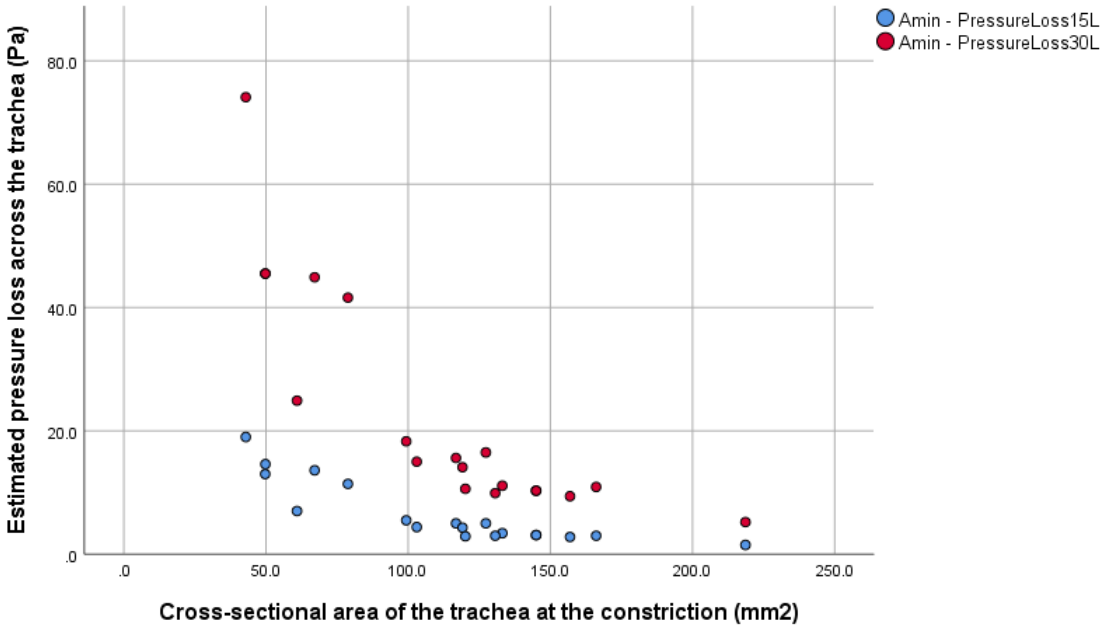


Figure 5.7. Pressure loss across the trachea against the minimum cross-sectional area of the trachea at flow rates 30L/min and 15l/min (outliers removed: cases 9 and 21)

There is a moderate negative correlation between the % constriction of the trachea and the minimum cross-sectional area and this is significant (see table 5.6 and figure 5.8). This is to be expected, as the tracheas vary greatly in size and therefore, we would not expect perfect correlation, however broadly speaking as the % constriction of the trachea increases the minimum cross-sectional area of the trachea decreases.

% Constriction of the trachea vs	Spearman's rho	p value
Minimum cross-sectional area	**-0.731**	**0.000***

Table 5.6. Correlation between the % constriction of the trachea and the minimum cross-sectional area

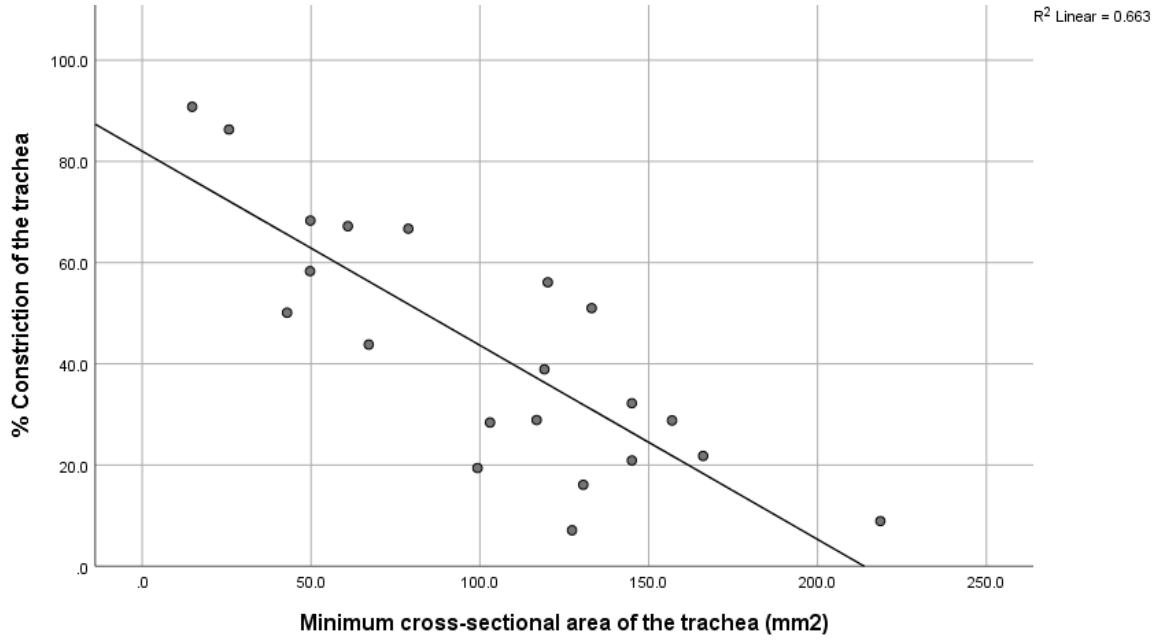


Figure 5.8. %constriction of the trachea against the minimum cross-sectional area of the trachea

There was no significant correlation found between the length of constriction of the trachea and the pressure loss (see table 5.7). Although we know that length of constriction does affect the pressure loss, a short severely compressed trachea leads to a greater degree of pressure loss due to the disruption of flow in a sudden expansion, compared to a moderately compressed trachea which is longer in length. (14, 62) The correlation calculated in this work is confounded by the fact that the tracheas all have varying degrees of compression and varying lengths as opposed to a fixed degree of compression with varying lengths. Lin et al (44) found that the length of compression did not affect the airway resistance as much as the degree of compression when looking at different lengths of simulated subglottic stenosis.

Length of constriction of the trachea (>35%) vs	Spearman's rho	p value
Pressure loss at 15 L/min	0.533	0.091
Pressure loss at 30L/min	0.371	0.291

Table 5.7. Correlation between the length of constriction of the trachea (for those tracheas where the degree of constriction was >35%) and the pressure loss

As discussed earlier in this chapter, if we hypothesise that the loss across the constricted area of the trachea in a patient with a compressive goitre is a type of 'orifice loss' then pressure loss is given by equation 5.3, i.e. $\Delta P = K.\frac{\rho}{2}.\left(\frac{Q}{A_{min}}\right)^2$, with K conventionally assumed constant.

If we discard the assumption that K is a constant, then we can calculate the loss co-efficient 'K' for each subject for the flow rates 15 L/min and 30 L/min using equation 5.3. To assess if there is a relationship between the % constriction of the trachea and the loss co-efficient, we can plot a graph of the two. Figure 5.9 shows the % constriction of each trachea against the loss co-efficient plotted for each subject for flow rates 15 L/min and 30 L/min respectively. For both flow rates we can see that the loss co-efficient is different for each subject and that there is a fair negative correlation between the loss co-efficient and the % constriction (see table 5.8). A study by Brouns et al (62) found that as the % constriction increased so did the loss co-efficient. Another study by Fulcher et al (82) calculated the loss co-efficient for a physical model with varying glottic openings. The loss co-efficient was larger for the glottic openings with a smaller cross-sectional area. The data from the 21 tracheal geometries does not reflect the same pattern as the studies in the literature. This is likely to be because each geometry is very different and the size of the constriction is not the only variable, as it is in the Brouns et al and Fulcher et al studies. The other factors will include the shape of the trachea at the constriction i.e., circular or elliptical, the size of the glottis which also produces a jet flow, the curvature of the trachea away from the midline and the length of the constriction.



Figure 5.9. Loss co-efficient 'K' at a flow rate of 15L/min and 30L/min against the % constriction of the trachea

% Constriction of the trachea vs	Spearman's rho	p value
Loss coefficient at 15L/min	**-0.454**	**0.039***
Loss coefficient at 30L/min	-0.393	0.078

Table 5.8 Loss co-efficient between the % constriction and the loss co-efficient at 15L/min and at 30L/min

The loss co-efficient is dependent not only on the shape of the constriction (geometry dependent) but is also dependent on the velocity profile upstream of the constriction – which explains why there is difference in the K values for the two different flow rates 15 L/min and 3 0L/min. Figure 5.10 is a graph of the loss co-efficient plotted against the minimum cross-sectional area and shows that as the minimum cross-sectional area increases so does the loss co-efficient. This relationship is fairly positive (see table 5.9).

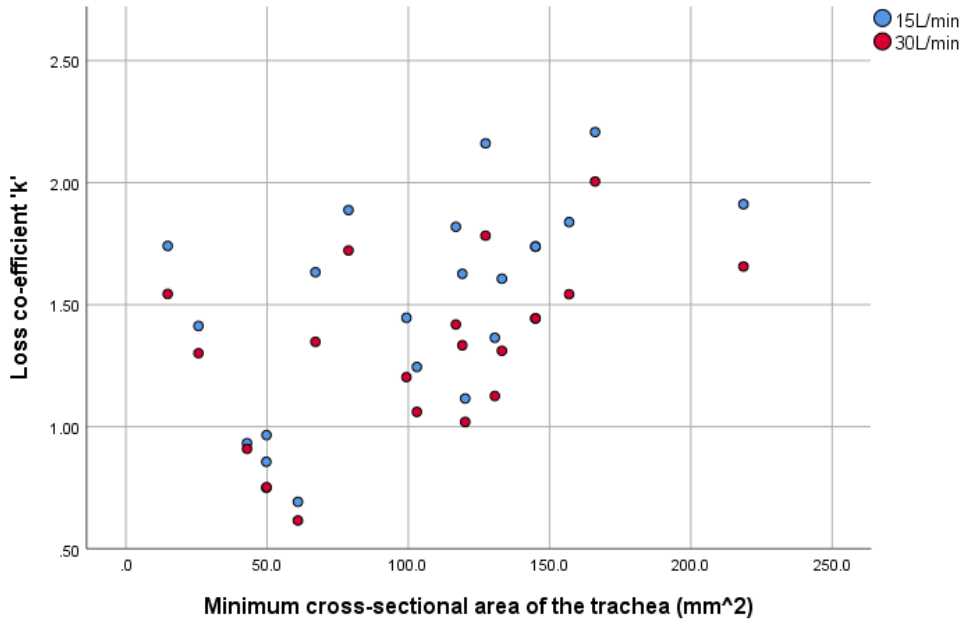


Figure 5.10. Loss co-efficient 'K' at a flow rate of 15 L/min and 30 L/min against the minimum cross-sectional area of the trachea

Minimum cross-sectional area of the trachea (mm^2) vs	Spearman's rho	p value
Loss coefficient at 15L/min	**0.565**	**0.008***
Loss coefficient at 30L/min	**0.517**	**0.017***

Table 5.9 Correlation between the minimum cross-sectional area of the trachea and the loss coefficient at 15L/min and at 30L/min

5.5 Loss predictions using A_{min}

Brouns et al (62) suggested using a 'blanket' loss co-efficient of 1.2 when estimating pressure loss across the trachea for simplicity. To estimate the pressure loss across the trachea for each subject, assuming a loss co-efficient of 1.2, equation 5.3 was used. Figures 5.11 and 5.12 graph the estimated pressure loss using equation 5.3 and a loss co-efficient of 1.2 plotted alongside the pressure loss as estimated using CFD for flow rates 15 L/min and 30 L/min. As can be observed, the estimated pressure loss assuming a loss co-efficient of 1.2 appears to be a reasonably good fit in both graphs and certainly follows the same pattern of pressure loss as the minimum cross-sectional area reduces in size. Both methods of estimating the pressure loss

see the same sharp rise in pressure loss once the minimum cross-sectional area reduces below 50mm^2. Wilcoxon signed rank test was used (non-parametric related samples) to look for significant differences between the two methods of estimating pressure loss, using either CFD or equation 5.3 and a loss co-efficient of 1.2 (see table 5.10). At 15 L/min there is a significant difference between the two sets of data, however there is not a significant difference between the two methods at 30 L/min.

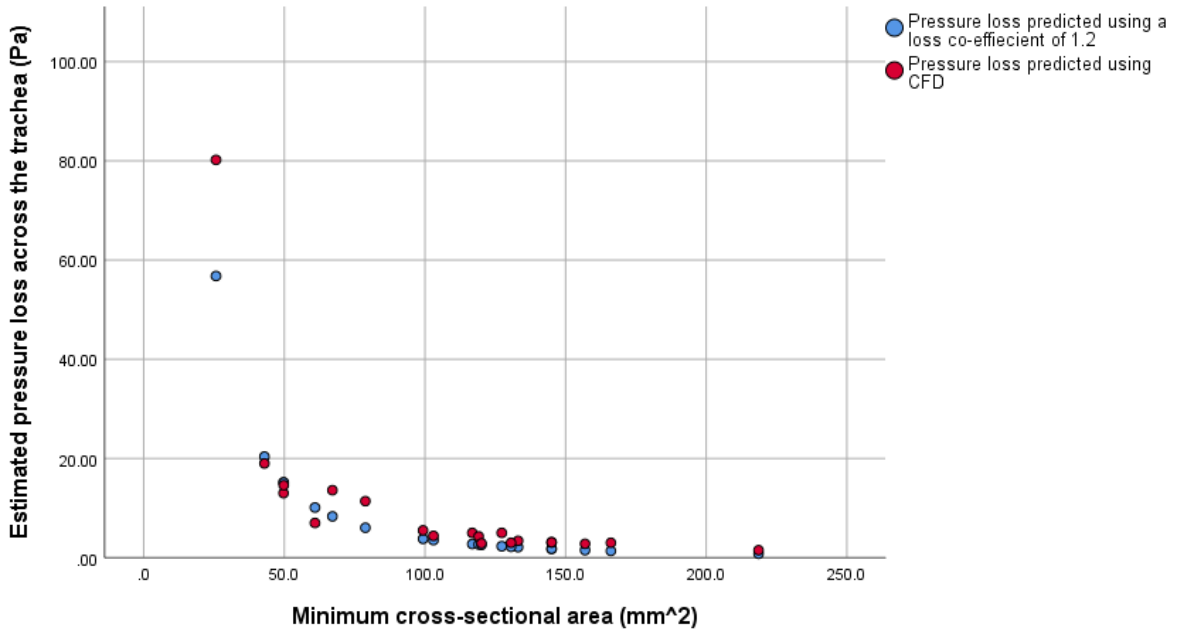


Figure 5.11. Estimated pressure loss using CFD and using a loss co-efficient of 1.2 against the minimum cross-sectional area at a flow rate of 15L/min



Figure 5.12. Estimated pressure loss using CFD and using a loss co-efficient of 1.2 against the minimum cross-sectional area at a flow rate of 30L/min

Pressure loss as estimated by CFD vs an estimated pressure loss using a loss co-efficient of 1.2	Wilcoxon Signed Rank Test p value
At a flow rate of 15L/min	0.021 (reject the null hypothesis)
At a flow rate of 30L/min	0.079 (retain the null hypothesis)

Table 5.10. Wilcoxon signed rank test of differences between the pressure loss as estimated using CFD and the pressure loss as estimated using a loss co-efficient of 1.2

The loss co-efficient was calculated for each subject using the pressure loss as estimated by CFD using equation 5.3. The median loss coefficient K is 1.6 for 15 L/min and 1.3 for 30 L/min. Figures 5.13 and 5.14 are graphs of the estimated pressure loss calculated using equation 5.3 and loss co-efficient 1.6 and 1.3 respectively plotted alongside the pressure loss as estimated using CFD for flow rates 15L/min and 30L/min.

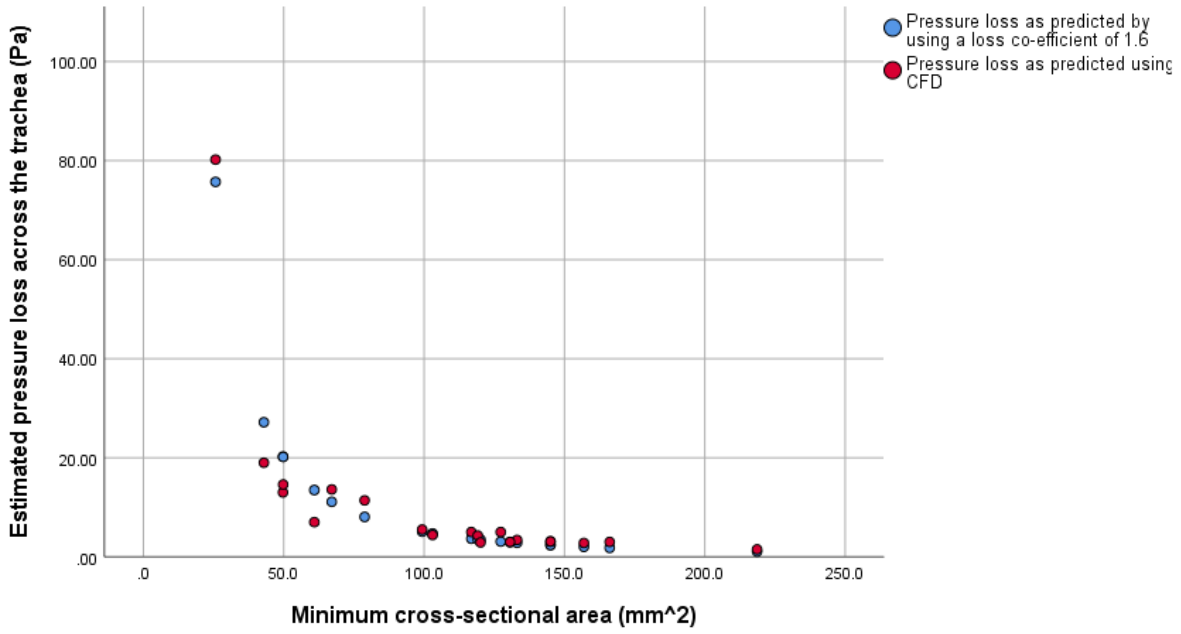


Figure 5.13. Pressure loss across the trachea as estimated by CFD (red) and as estimated using a loss co-efficient of 1.6 (blue) at a flow rate of 15L/min against the minimum cross-sectional area of the trachea

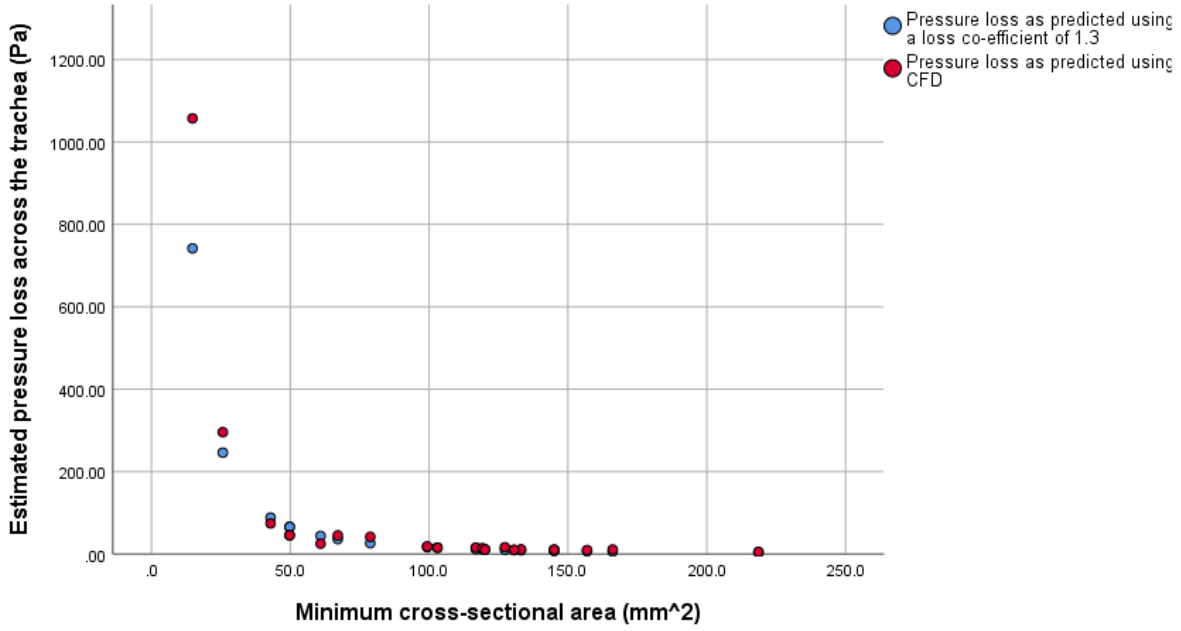


Figure 5.14. Pressure loss across the trachea as estimated by CFD (red) and as estimated using a loss co-efficient of 1.30 (blue) at a flow rate of 30L/min against the minimum cross-sectional area of the trachea

Wilcoxon signed rank test demonstrated no significant difference between the two methods of estimating the pressure loss when using a loss coefficient of 1.6 for a flowrate of 15 L/min and 1.3 for a flowrate of 30 L/min (see table 5.11). This provides the opportunity for predicting the

pressure loss across the trachea, using the $A_{min,}$ in a patient with compressive symptoms in whom the decision to operate is not straightforward, without needing to perform CFD.

Pressure loss as estimated by CFD vs an estimated pressure loss using a loss co-efficient	Wilcoxon Signed Rank Test p value
1.6 at a flow rate of 15L/min	0.37 (retain the null hypothesis)
1.3 at a flow rate of 30L/min	0.14 (retain the null hypothesis)

Table 5.11. Wilcoxon signed rank test between the pressure loss as estimated using CFD and the pressure loss as estimated using a loss co-efficient of 1.6 and 1.3

Lin et al (44) studied the effect of varying degrees and length of tracheal stenoses on the airway resistance and calculated resistance using $R = \Delta P/Q$ where P = pressure loss across the trachea and Q =flow rate. Using a k omega turbulence model and a flow rate of 15 L/min they found that an increasing severity of constriction led to an increase in airway resistance in a pattern that was in line with the Bernoulli obstruction theory, as opposed to Poiseuille's law. Using a series of six tracheas (with artificially inserted tracheal stenosis segments), they found that the airway resistance could be accurately estimated using tracheal measurements alone. This finding is similar to the finding of this thesis that using a loss co-efficient of 1.6 and 1.3 for flow rates of 15 L/min and 30 L/min can accurately predict the pressure loss across the constricted trachea, using the minimum cross-sectional area in this series of tracheas.

A scatter plot of the Pressure loss (Pa) against $1/A_{min}^2$ (mm^2) for flow rates of 15 L/min and 30 L/min shown below demonstrates the relationship between the two (see figure 5.15). As $1/A_{min}^2$ increases, the pressure loss across the trachea also increases. As would be expected, this loss is greater at greater flow rates.

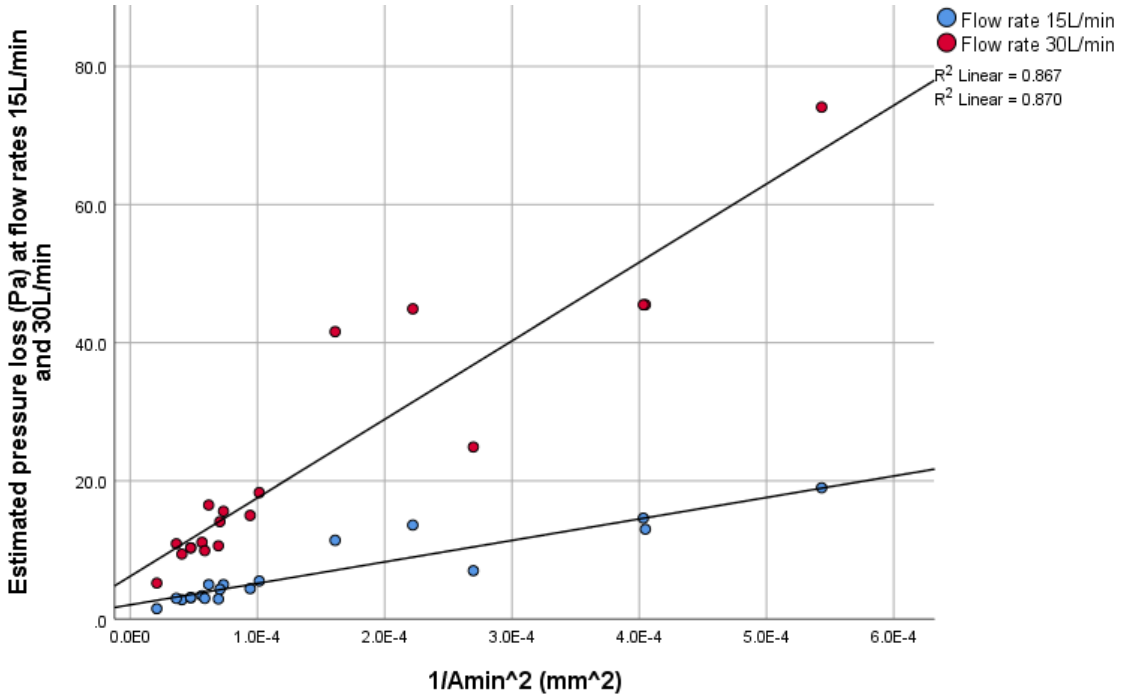


Figure 5.15. Pressure loss (Pa) against 1/Amin2 (mm2) for flow rates of 15 L/min and 30 L/min (outliers removed: subject 9 and 21)

Spearman's rho test was used to assess for correlation between the minimum cross-sectional area of the trachea and the pressure loss across the trachea for flow rates 15 L/min and 30 L/min. The results can be found in table 5.12. There is a very strong correlation between the pressure loss across the trachea and $1/A_{min}^2$ and this was significant at the $p>0.05$ level for both flow rates.

	Spearman's rho correlation	P value
$1/A_{min}^2$ vs Pressure loss (Pa) at 15 L/min	**0.940**	**>0.001***
$1/A_{min}^2$ vs Pressure loss (Pa) at 30 L/min	**0.946**	**>0.001***

*Table 5.12. Correlation between 1/Amin2 and the pressure loss as estimated by CFD at flow rates of 15 L/min and 30 L/min. *denotes significant results (outliers removed: subjects 9 and 21)*

If we stratify the group into <35% constricted (10 subjects) and >35% constricted (11 subjects), we can then assess the correlation with pressure loss for the two groups. Spearman's rho test

was used to assess for correlation. The results can be found in tables 5.13 and 5.14. Scatter plots of the two groups can be seen in figure 5.16 and figure 5.17. $1/A_{min}^2$ and the pressure loss across the trachea is more strongly correlated for the subjects with a constriction of >35% than for subjects with a constriction of <35%, although there is a very strong correlation between both sets of results at a flow rate of 15 L/min.

For tracheas constricted >35%	Spearman's rho correlation	P value
$1/A_{min}^2$ vs Pressure loss (Pa) at 15 L/min	**0.903**	**0.000***
$1/A_{min}^2$ vs Pressure loss (Pa) at 30 L/min	**0.961**	**0.000***

Table 5.13. Correlation between pressure loss (Pa) against 1/Amin2 (mm2) for subjects with a constriction >35%

For tracheas constricted <35%	Spearman's rho correlation	P value
$1/A_{min}^2$ vs Pressure loss (Pa) at 15 L/min	**0.844**	**0.004***
$1/A_{min}^2$ vs Pressure loss (Pa) at 30 L/min	**0.714**	**0.031***

Table 5.14. Correlation between pressure loss (Pa) against 1/Amin2 (mm2) for subjects with a constriction <35% (outlier removed: subject 3)

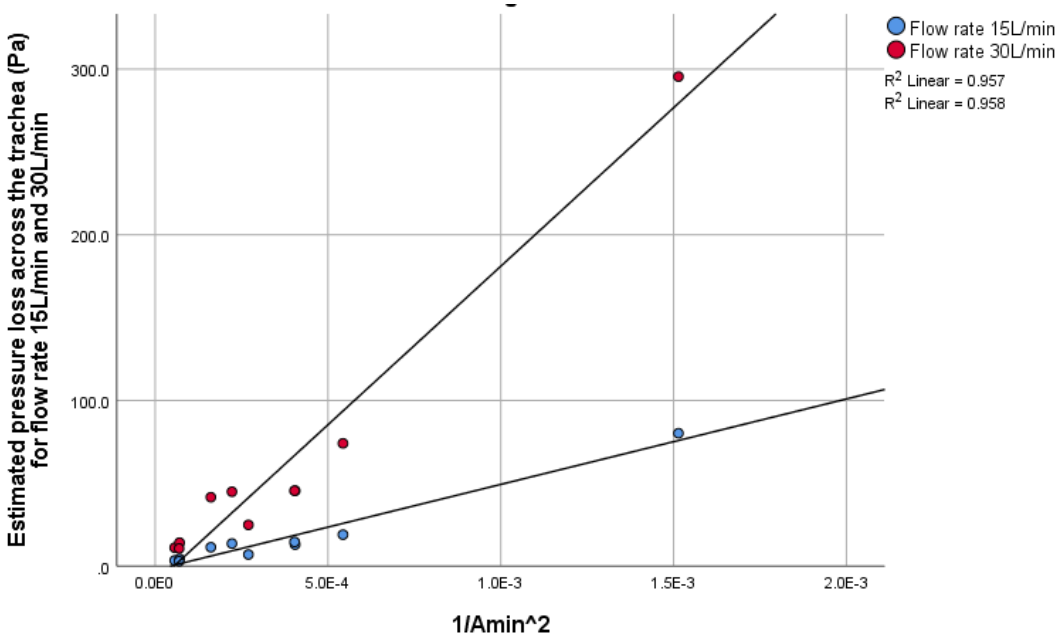


Figure 5.16. Pressure loss (Pa) against 1/Amin2 (mm2) for subjects with a constriction >35%

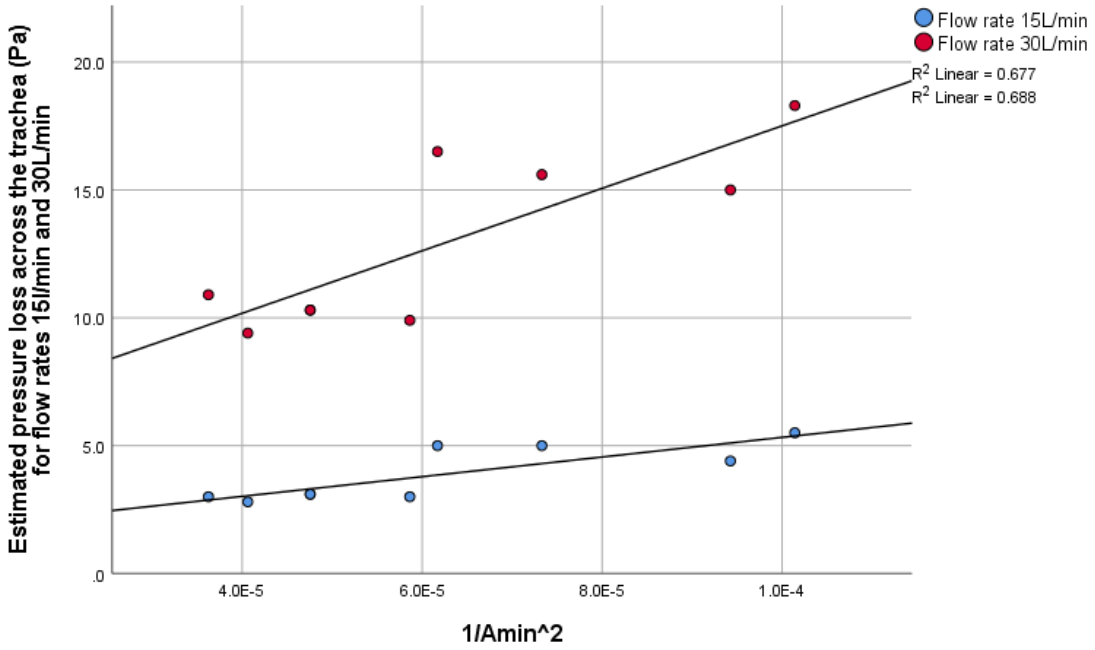


Figure 5.17 Pressure loss (Pa) against 1/Amin2 (mm2) for subjects with a constriction <35% (outlier removed: subject 3)

If we don't assume that the loss co-efficient K is a constant and instead consider it to be geometry dependent, then we have the equation:

$$\Delta P = k_{geom} \cdot \frac{\rho}{2} \cdot \left(\frac{Q}{A_{min}}\right)^2$$

Equation 5.6

Where P = Pressure loss (Pa)

K_{geom} = geometry dependent loss co-efficient

ρ = density of air

Q = flow rate

A_{min} = Minimum cross-sectional area of the trachea

P/Q^2 has been calculated for each geometry for the two flow rates 15 L/min and 30 L/min. If equation 5.5 holds, then ΔP should scale with the square of flow rate, so the ratio of results for flow rates 1 and 2 ($\Delta P_1/Q_1^2$) over ($\Delta P_2/Q_2^2$) should be close to 1. The results of $\Delta P/Q^2$ for each subject at the two flow rates and the corresponding ratio is shown in table 5.15. In most of the geometries the ratio is close to 1. Subject 16 is an outlier with a ratio of 1.68. If equation 5.6 were to hold true then this would assume that the losses are primarily due to the constriction jet. Many of the tracheas in this series have a ratio close to one which suggests that most of the tracheal losses are due to the constriction jet. Subject 16 has a geometry which is severely deviated from the centreline and the trachea is curved and constricted, therefore it is likely that the loss profile in subject 16 is in part due to these other factors and not just the constriction alone.

Subject	$(\Delta P_1 / Q_1^2)$	$(\Delta P_2 / Q_2^2)$	Ratio
1	54.70	44.26	1.24
2	181.60	166.24	1.09
3	23.84	20.86	1.14
4	47.12	39.41	1.20
5	79.41	66.07	1.20
6	79.42	62.68	1.27
7	45.58	37.50	1.22
8	87.20	73.15	1.19
9	1283.84	942.8	1.36
10	68.48	56.20	1.22
11	71.84	59.99	1.20
12	45.76	41.56	1.10
13	46.40	43.42	1.07
14	220.96	225.27	0.98
15	220.00	170.63	1.29
16	167.84	99.76	1.68
17	208.00	179.72	1.16
18	50.08	41.17	1.22
19	234.19	181.90	1.29
20	304.00	296.40	1.03
21	4768.00	4229.2	1.12

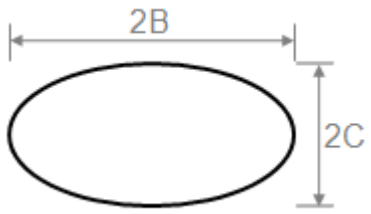
Table 5.15. ΔP /Q2 using the pressure loss estimation from CFD (steady RANS) simulations for each geometry. Q1 is the flow rate 15 L/min and Q2 is the flow rate 30 L/min

5.6 Hydraulic diameter

Hydraulic diameter is used when considering flow in a non-circular pipe. The minimum diameter, maximum diameter and 'ellipticity' of each tracheal model was extracted from the centreline using VMTK at the level of the maximum constriction (A_{min}) (see table 5.16). In a circular pipe the ellipticity would be 1 and the more 'squashed' the pipe is the smaller the ellipticity. Flow behaves differently in non-circular pipes as there is more contact with the boundary layer and wall sheer stress will be increased. The hydraulic diameter for each geometry has been calculated using equation 5.6.

When considering flow through a compressed trachea, the shape of the trachea is also important. In the case of subject 21, the pressure loss is much greater than the other geometries, which can in part be attributed to the very small cross-sectional area of 14.8mm^2, but furthermore we can consider that the hydraulic diameter is considerably smaller than the other geometries and the shape of the trachea at this point is a very narrow ellipse with an ellipticity of 0.22.

The correlation between hydraulic diameter and pressure loss at both 15 L/min and 30 L/min has been calculated using Spearman's rho (see table 5.17). There is a strong negative correlation, which is statistically significant. Therefore, as the hydraulic diameter of the trachea reduces the pressure loss across the trachea increases. The strength of the correlation is similar to the correlation between pressure loss and $A_{min.}$



$$D_h = \frac{4BC(64 - 16E^2)}{(\mathrm{B} + \mathrm{C})(64 - 3E^4)}$$

(Equation 5.7)

Where:

D_h = Hydraulic diameter

2B= maximum radius

2C= minimum radius

$$E = \frac{(\mathrm{B} - \mathrm{C})}{(B + C)}$$

Subject	Minimum diameter (mm)	Maximum diameter (mm)	Hydraulic diameter (mm)	Ellipticity
1	12.0	14.3	13.0	0.84
2	8.9	11.6	10.0	0.77
3	14.3	18.8	16.2	0.76
4	11.2	15.4	12.9	0.72
5	11.9	13.9	12.8	0.86
6	11.6	16.5	12.5	0.86
7	11.0	18.5	13.6	0.60
8	9.9	12.8	11.1	0.77
9	3.9	8.26	5.1	0.47
10	11.2	15.0	12.8	0.75
11	7.5	15.2	9.7	0.49
12	9.2	16.4	11.6	0.56
13	13.0	15.4	14.1	0.84
14	6.6	14.7	8.8	0.45
15	6.9	12.7	8.8	0.55
16	11.8	15.5	13.4	0.76
17	5.7	11.4	7.4	0.50
18	5.1	11.1	6.7	0.46
19	7.0	8.3	7.6	0.84
20	11.8	15.9	13.4	0.73
21	2.0	9.4	3.0	0.22

Table 5.16 The minimum diameter, maximum diameter, hydraulic diameter and ellipticity of the trachea at the minimum cross-sectional area

Hydraulic diameter at A_{min}	Spearman's rho correlation	P value
Pressure loss at 15L/min	**-0.914**	**0.000***
Pressure loss at 30L/min	**-0.928**	**0.000***

Table 5.17 Correlation between the hydraulic diameter at the minimum cross-sectional area of the trachea and the pressure loss across the trachea

5.7 Area of the glottis

The glottis refers to the portion of the larynx which contains the vocal folds and the opening between the vocal folds. The glottis extends from the junction between the true and false cords to a line one centimetre below the inferior aspect of the vocal folds. (83) The glottic cross-sectional area refers to the area of the opening between the vocal folds. Nine of the twenty-one subjects had a glottic cross-sectional area that was smaller than the minimum cross-sectional area (refer to table 5.1). If the $A_{glottis}$ is smaller than the A_{min} then the glottis will be the major source of orifice type losses rather than the constriction itself. To assess if using the smaller of the two measurements improves the correlation between the tracheal geometry and the estimated pressure loss, as calculated by CFD, the $A_{glottis}$ is used instead of the A_{min} if it was the smaller of the two measurements. Spearman's rho correlation was used and the calculated correlation for the flow rate 15 L/min was –0.925 which is very similar to the correlation using only A_{min} (-0.930). The correlation for the flow rate 30 L/min was –0.951, which is a slightly stronger correlation than when using only A_{min} (-0.946) (see table 5.18). Using the minimum cross-sectional area of the glottis when it was smaller than the minimum cross-sectional area of the constriction did not make a significant difference in the correlation with the pressure loss across the trachea.

Amin or Aglottis (the smaller of the two)	Spearman's rho correlation	P value
Pressure loss at 15L/min	**-0.925**	**0.000***
Pressure loss at 30L/min	**-0.951**	**0.000***

Table 5.18. Correlation between the pressure loss as estimated by CFD and the minimum cross-sectional area of the trachea (either the glottis or the constriction - the smaller of the two measurements)

5.7 Discussion and conclusions

Computational fluid dynamics was used to estimate the pre-operative pressure loss across the trachea in 21 subjects who underwent total thyroidectomy for compressive symptoms. An SST (Menter) k-omega steady RANS model of turbulence was used to simulate flow through the trachea at flow rates 15 L/min and 30 L/min for twenty of the subjects, and an unsteady LES model was used for the most constricted subject (subject 21).

In a healthy individual it is estimated that the pressure loss across the trachea of around 5 Pa at a flow rate of 15 L/min, with a total pressure loss across the whole airway (from the mouth to alveoli) of around 100 Pa at this flow rate. In a healthy individual the predicted pressure loss across the trachea at a flow rate of 30L/min is 7Pa. All of the tracheas in this study have an estimated pressure loss >7Pa at 30L/min. 12 of the 21 subjects have an estimated pressure loss >14Pa which is more than twice the estimated pressure loss in a healthy individual.

The range of estimated pressure loss across the trachea in this cohort of subjects is 5.2 to 298.0 Pa for the flow rate of 15 L/min. Thirteen of the subjects have an estimated pressure loss of less than 20 Pa. Although this seems to be a small pressure loss, if we consider that a pressure loss of 20 Pa is four times what a healthy individual would expect across their trachea at a flow rate of 15 L/min, and this in turn leads to a 15% increase in their overall pressure loss across the whole airway, then maybe it is unsurprising that these patients are complaining of shortness of breath and/or positional dyspnoea. For those subjects with a minimum cross-sectional area of ≤ 40 mm^2 the pressure loss across the trachea becomes increasingly large with a range of 235.7 – 1057.3 Pa at a flow rate of 30L/min. The finding of an inflexion point at certain degree of constriction is also seen in tracheal stenosis. Furthermore, as the flow rate increases so does the pressure loss. We have only considered the flow rates of 15 L/min and 30 L/min which roughly equate to breathing at rest and light exercise. The pressure losses seen at moderate and strenuous exercise are likely to be much greater.

The sensation of dyspnoea, also referred to as shortness of breath, is the subjective sensation of running out of breath, not being able to breathe deeply or freely, or feeling discomfort when breathing. The sensation is a result of complex interactions between peripheral and central receptors feeding back to the respiratory centre in the brain. Functional MRI scans involving patients with CO_2 induced air hunger showed activation of the following brain regions: fusiform gyrus and anterior insular cortex, cingulate cortex, limbic and paralimbic areas, hypothalamus, midline cerebellum, pons and ventral and dorsal medulla. (84)

Mechanoreceptors are found throughout the airway and the thorax, within the trachea, lungs and within pulmonary vessels. These mechanoreceptors, and central and peripheral chemoreceptors signal back to the complex network of brain regions involved in the perception of dyspnoea. A number of theories have been developed for the mechanism of dyspnoea sensation. Scwartzstein et al (85) developed the “mismatch theory of dyspnoea”. This mismatch theory has been further refined by Fukushi et al. (84) They propose that the

perception of dyspnoea is a result of the mismatch between respiratory effort and the feedback from the respiratory system (mechanoreceptors and chemoreceptors). It is postulated that when a motor command is transmitted from the lower brainstem to the respiratory system, a copy of this command is also sent to the limbic system and cerebrum where it is perceived as the 'respiratory effort'. The ventilatory output from this command, is then monitored by mechanoreceptors throughout the chest, lung and airways and then fed back to the brainstem, limbic system and cortex where the information is processed as a 'mechanical respiratory sensation'. The mechanical respiratory sensation and the motor command are counter-compared and a mismatch leads to the sensation of dyspnoea. (84)

According to the mismatch theory, if a patient has a tracheal compression secondary to a large thyroid goitre, the increased tracheal airway resistance will lead to a mismatch in the mechanical respiratory sensation and the motor command when they are counter-compared in the higher respiratory centres, which in turn will lead to the sensation of dyspnoea.

The trachea itself is extremely sensitive, and this is demonstrated in patients with a tracheostomy (a surgical opening into the front of the trachea in order to provide a patient with an alternative airway). Whilst passing a soft suction tube down into the trachea through a tracheostomy in an awake patient to aid removing mucous from the airway, if the tubing touches the inside wall of the trachea, this results in extreme discomfort and elicits the cough reflex. Pressure being exerted on the outside of the trachea, as is the case in compressive thyroid goitres, leads to the sensation of discomfort through the mechanoreceptors signalling to the respiratory centre. The discomfort or feeling of pressure in the neck experienced by patients with a compressive thyroid goitre may, in part, contribute to the feeling of dyspnoea.

When looking in more detail at the flow patterns in three of the study tracheas, there is increasing complexity of flow within the trachea with increasing constriction. In a mildly compressed trachea (28.9% compression) the peak velocity of flow was observed in the region of the laryngeal jet and in a moderately (42.9.% compression) and severely compressed trachea (90.8% compression) the peak velocity was seen in the region of the constriction jet. Peak turbulent kinetic energy can be observed in the same region, adjacent to the constriction jet where there is breakdown of the jet and separation flow. The breakdown of separated shear layers leads to the major source of fluctuations in airway flow and the areas of high vorticity identify these areas. The static pressure shows the largest pressure drops are at the level of the glottis in the mildly constricted trachea and the at the level of the constriction in both the moderately and severely restricted tracheas.

Within this series of subjects, the minimum cross-sectional area of the trachea (A_{min}) is very strongly correlated with pressure loss across the trachea, whilst the % constriction of the trachea is moderately correlated with the pressure loss. There is no significant correlation with the length of constriction, and this is likely due to the varying degrees of length and % constriction of each trachea. The hydraulic diameter of the trachea, measured at the level of the constriction, is also very strongly correlated with the estimated pressure loss across the trachea. For this series of tracheas, both the A_{min} and the hydraulic diameters provide useful tracheal measurements for surrogate markers of the severity of pressure loss one might expect to see across the trachea.

Using the minimum cross-sectional area of the trachea and a loss co-efficient 'K' of 1.6 and 1.3 for flow rates of 15L/min and 30L/min respectively, to calculate an estimate of the pressure loss across the trachea has shown to reproduce very similar results to the pressure loss as predicted by CFDs for this series of subjects. This opens up the opportunity for predicting the pressure loss across the trachea, using the A_{min} and equation 5.3, in a patient with compressive symptoms in whom the decision to operate is not straightforward, without needing to perform CFD.

The main limitations of this study are that the airflow was studied in relation to static parameters such as the cross-sectional area and the %constriction of the trachea. These parameters do not capture the dynamic nature of the airway. The static image used to create a 3D reconstruction of the airway may have been captured at different points in the breathing cycle and therefore we may not be capturing the full extent of airway collapse for each individual subject. In addition to this, simulations represent the average flow rate during inspiration (e.g., 15 L/min and 30 L/min) and do not take into account the airflow during the full cycle of inspiration. The study is entirely computational in nature and does not include any in vivo measurements to validate the estimated values of pressure loss across the trachea.

The findings of this chapter may have clinical implications for patients with tracheal compression secondary to a retrosternal thyroid goitre. The results suggest that we can accurately predict an estimate of the pressure loss across the trachea using the minimum cross-sectional area and a loss co-efficient. A quick calculation using a measurement from a CT scan could provide an estimated pressure loss for breathing at rest. In a healthy trachea, the estimated pressure loss is thought to be around 5 Pa at 15L/min. Comparing the estimated pressure loss across the trachea in a patient with a compressive goitre with a normal pressure loss of 5 Pa, could add more useful information when deciding whether to operate.

A further study could be performed to correlate the pre-operative symptoms with predicted pre-operative pressure loss using A_{min} and to correlate post-operative improvement in symptoms with predicted pre-operative pressure loss. The work of this thesis looks at these parameters for 21 subjects however larger numbers will be needed to validate predicted pressure loss using a loss co-efficient as a tool to aid surgical decision making.

In young, fit and well patients with an enlarged goitre thyroid goitre resulting in compressive symptoms the decision to operate is more straight forward. In elderly patients with co-morbidities, when the risks of operating are much greater, surgeons and patients are presented with a more challenging decision. Currently, the guidelines recommend considering surgery if there is more than a 35% constriction of the trachea. In this series of subjects, the estimated pressure loss was only moderately correlated with the % constriction of the trachea whereas the A_{min} and hydraulic diameter were found to be very strongly correlated with pressure loss. This would indicate that the A_{min} and the hydraulic diameter of the trachea are better surrogate markers of the pressure loss across the constricted trachea. Markow et al (76) found that there was a sudden increase in airway resistance when the glottic area was $<40mm^2$, there is a similar finding in the work of this thesis. When the A_{min} $<40mm^2$ there was a dramatic rise in the estimated pressure loss. Further work could be carried out to see if there is a consistent inflexion point (of the A_{min}) where there is a sudden increase in the reported breathlessness. This inflexion point could be used as a guide to when to consider performing a thyroidectomy for high-risk patients.

Chapter 6 Potential application of CFD for surgical planning and pathophysiological understanding of the airway

6.1 Introduction
6.2 Simulating post-operative improvement in tracheal flow
6.3 Comparison of a sudden expansion vs a gradual expansion
6.4 Simplifying the tracheal geometry
6.5 Concluding remarks

6.1 Introduction

In this chapter we consider the potential application of CFD for surgical planning using manipulated tracheal models. Firstly, taking a constricted tracheal model and manipulating the geometry to expand the constricted region so that the trachea represents a post-operative trachea. Secondly, running a CFD simulation to estimate the pressure loss in this "post-operative trachea". Calculating the difference in pressure loss between the pre-operative trachea and the simulated "post-operative trachea" leads to an estimate of the improvement in pressure loss the patient would experience if they were to undergo surgery.

When there is a sudden expansion following a tracheal constriction, flow separation occurs due to adverse flow gradients. To investigate the effects of separation in flow on the pressure loss within a constricted trachea two tracheal models were developed; the first with a constriction followed by a sudden expansion, and the second model with a constriction followed by a more gradual expansion. CFD was used to simulate flow through both tracheal models and the effects of a sudden expansion within the trachea are explored.

Simulating flow through a simplified tracheal geometry would be computationally less expensive than using a non-simplified tracheal model. Simplified models of three tracheal geometries were made using the centreline co-ordinates and the diameter of the tracheal planes perpendicular to the centreline. CFD was used to simulate flow through the three simplified

geometries and the estimated pressure loss was compared with the estimated pressure loss across the original geometries to assess the accuracy of using a simplified model.

6.2 Simulating post-operative improvement in tracheal flow

Computational fluid dynamics has been used throughout the medical field to evaluate post-operative findings whether this be i) evaluating real-life post-operative findings using post-operative imaging or ii) simulating post-operative changes by manipulating pre-operative imaging as part of surgical planning. Song et al (86) used CFD to investigate patients with obstructive sleep apnoea post intervention with oral devices and found significant decrease in the airflow resistance in the pharynx. Capelli et al (87) used CFD to model cardiac interventions to check for feasibility in 12 patients prior to performing the procedures. Sundareswaran et al (88) have utilised CFD to investigate the different flow outcomes with pulmonary arteriovenous malformations with surgical simulation as part of operative planning.

One way to evaluate patients with retrosternal goitres is to assess the pre-operative pressure loss using CFD (refer to chapter 5). This provides pre-operative information about the patient. A further step could be to simulate the predicted changes that would be seen post-operatively and calculating the simulated post-operative pressure loss across the trachea. This would give an estimated improvement in tracheal pressure losses if the patient were to undergo a thyroidectomy. It is difficult to validate this as a method as most patients do not undergo any post-operative cross-sectional imaging and therefore the tracheal changes would be those "expected" to be seen once a thyroidectomy has been performed.

In order to investigate the use of CFD in simulating post-operative improvement in tracheal flow, the tracheal geometry for subject 21 was modified using Meshmixer. The modification included expanding the trachea to remove the area of constriction, as might be expected following a thyroidectomy. See figures 6.1 and 6.2 for the pre- and simulated post-operative tracheas for subject 21. Following the modification of the trachea, a steady RANS simulation was used to model the flow through this simulated post-operative trachea (see chapter 4 for simulation methods). The cross-sectional area of the pre- and simulated post-operative tracheas are shown in figure 6.3.

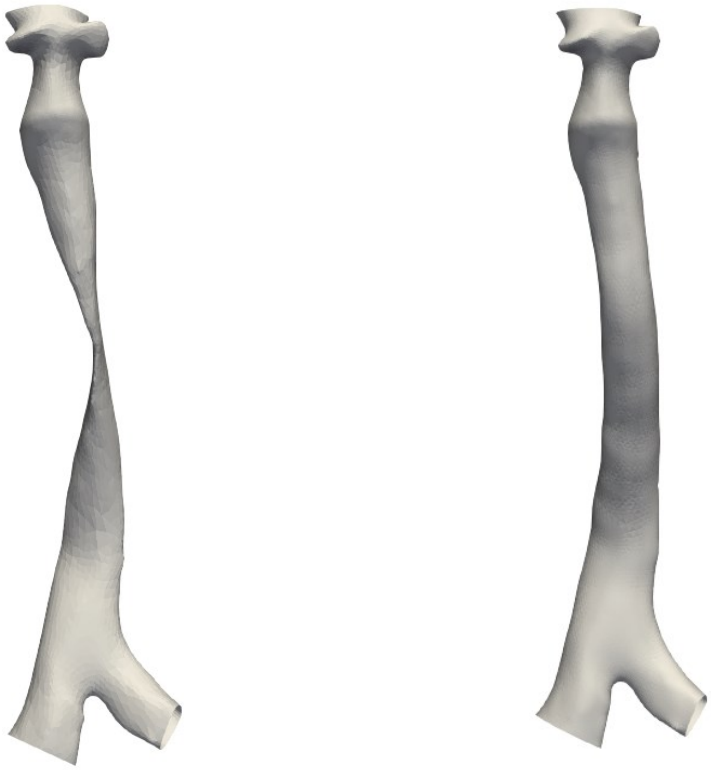


Figure 6.1. Anterior view of subject 21's trachea i) pre-operative ii) simulated post-operative

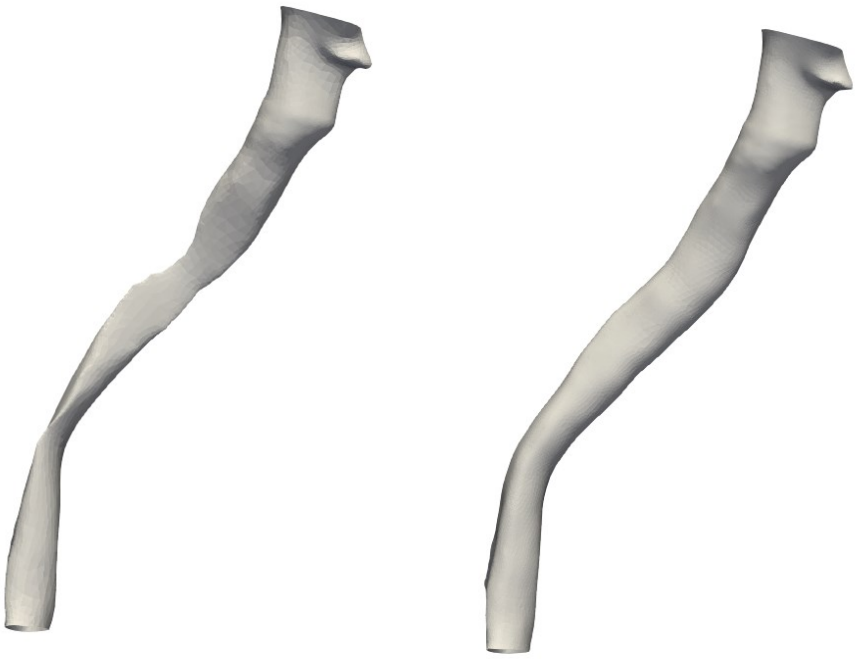


Figure 6.2. Lateral view of subject 21's trachea i) pre-operative ii) simulated post-operative

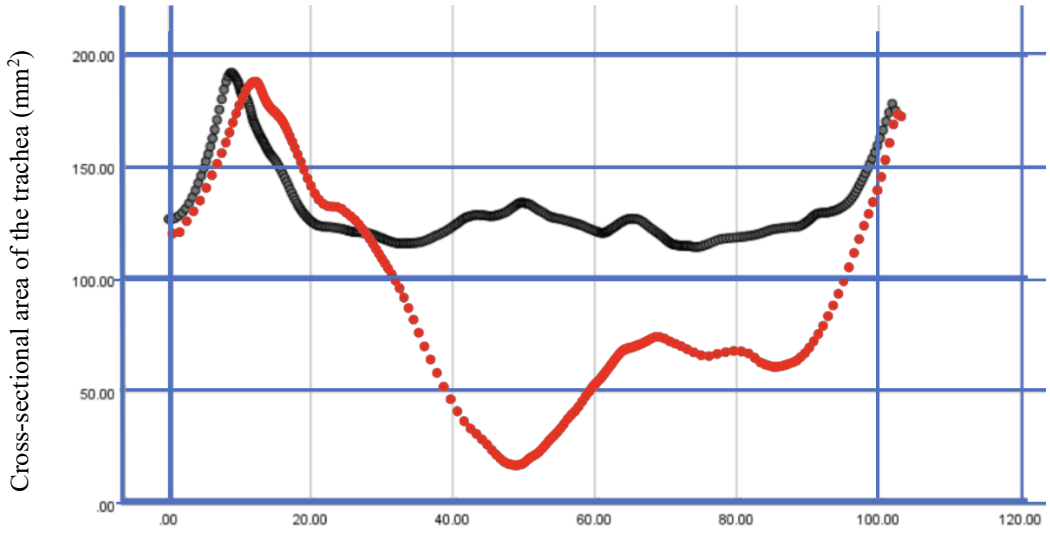


Figure 6.3. Cross-sectional area of the trachea along the distance of the trachea in i) subject 21 pre-operatively ii) subject 21 simulated post-operative trachea

The total pressure from inlet to outlet at 30L/min in the pre-operative trachea is 1057.3 Pa as estimated by LES. In the simulated post-operative trachea, the total pressure loss from inlet to outlet at 30L/min is estimated to be 18.7 Pa. This is an improvement of 1,038.6 Pa once the subject underwent simulated tracheal modifications that we might expect to see following a thyroidectomy. To look more closely at the pre-operative and simulated post-operative flow through the trachea we will now consider the velocity of flow, the wall shear stress, vorticity, and static pressure.

The streamlines of the magnitude of velocity show the increase of velocity (up to 60 m/s) at the constriction in the pre-operative trachea (see figure 6.4). Once this constriction has been removed the velocity remains fairly constant across the length of the trachea. The streamlines in the simulated post-operative trachea show a reduction in the flow disturbance in the distal trachea.

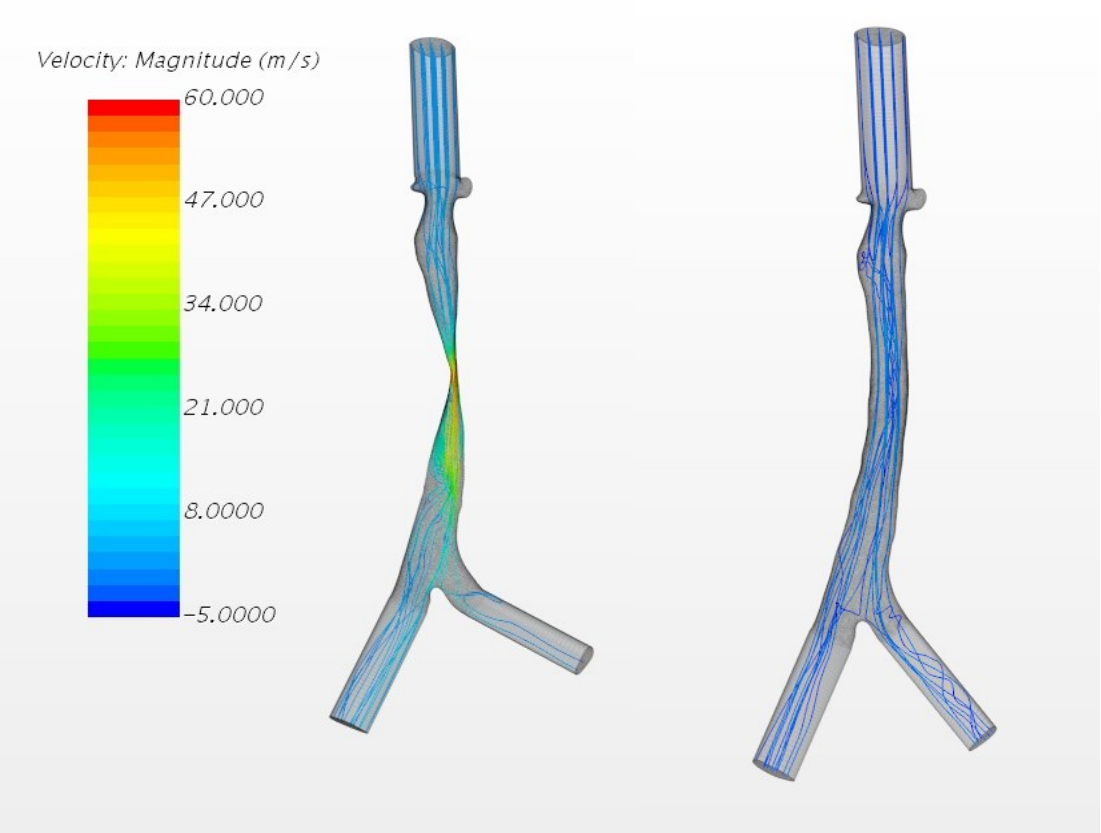


Figure 6.4. Streamlines demonstrating the magnitude of velocity (m/s) in subject 21 i) pre-operative trachea ii) simulated post-operative trachea

The wall shear stress (WSS) rises to 15 Pa at the level of the constriction in the pre-operative trachea (see figure 6.5). This rise in WSS is not present once the constriction has been removed and the only rise in WSS seen in the simulated post-operative trachea is at the level of the glottis where there is a small glottic jet.

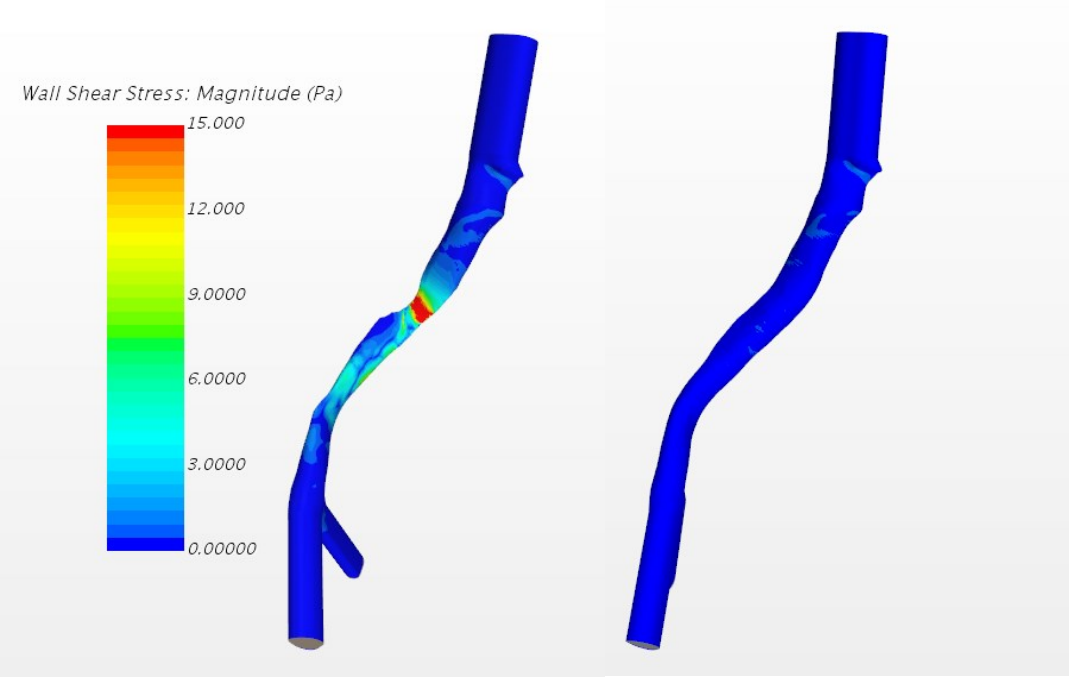


Figure 6.5. Tracheal surface mesh demonstrating the wall shear stress (Pa) in subject 21 i) pre-operative trachea ii) simulated post-operative trachea

There is a marked difference in the magnitude of vorticity when comparing the pre and simulated-post operative tracheas (see figure 6.6). The sharp rise in vorticity is no longer present in the simulated post-operative trachea. A volume render of the tracheas demonstrating the static pressure along the length of the trachea is shown in figure 6.7. Note the difference in scales for the two tracheas due to the large difference in pressure loss across the two tracheas. The simulated post-operative trachea shows that most of the pressure loss in this trachea takes place at the level of the glottis, whereas the pre-operative model shows that most of the pressure loss takes place at the constriction. The pressure loss profile has been markedly changed due to removing the severe restriction.

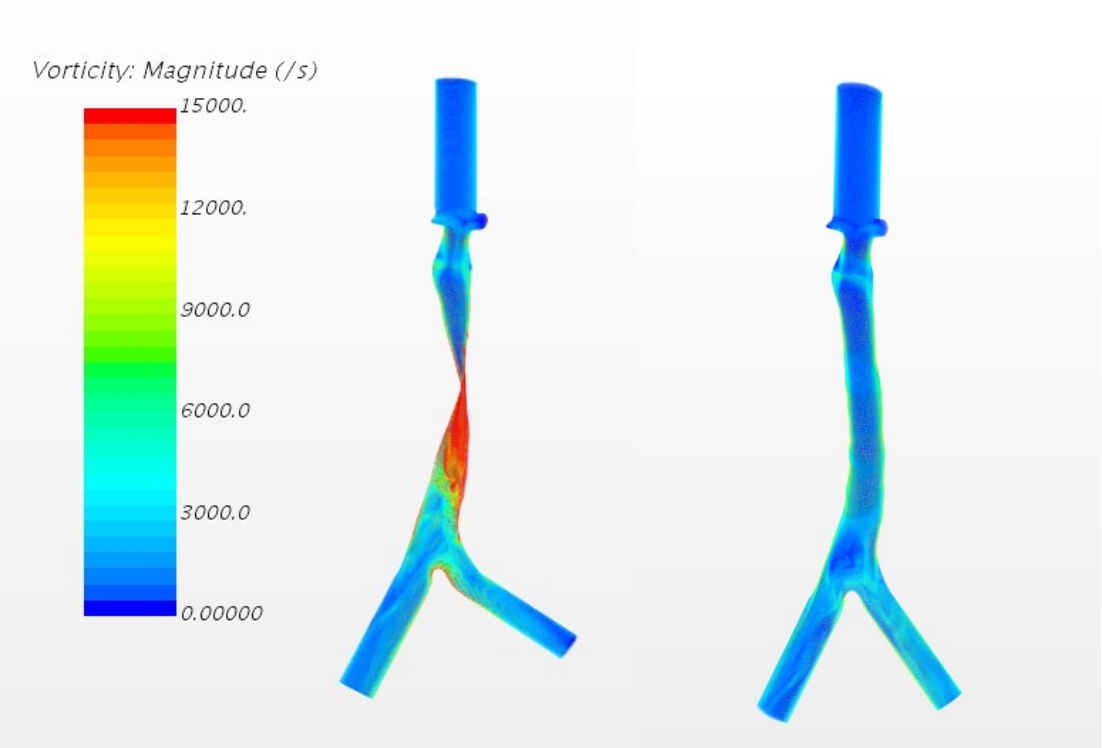


Figure 6.6. Volume render of the trachea demonstrating the vorticity in subject 21 i) pre-operative trachea ii) simulated post-operative trachea

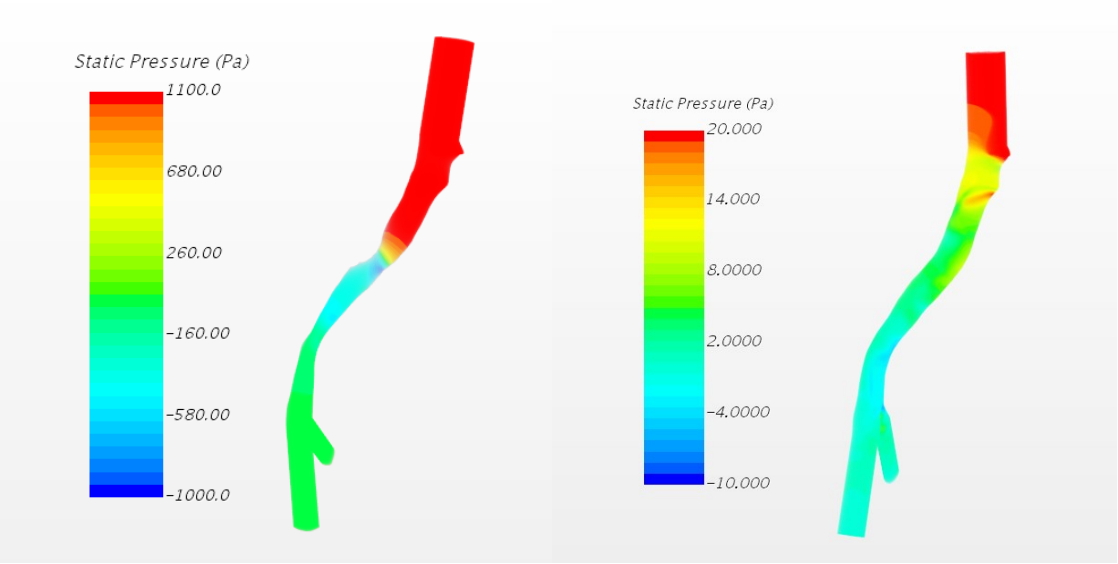


Figure 6.7. Volume render of the trachea demonstrating the static pressure (Pa) in subject 21 i) pre-operative trachea ii) simulated post-operative trachea

Simulating post-operative reduction in pressure losses in compressed tracheas provides an interesting way of assessing the patient pre-operatively when considering surgery. The subjects who were included in this thesis didn't undergo post-operative cross-sectional imaging and therefore we do not have the true post-operative tracheas.

Earlier work carried out by Xiao (2019) (29) looked at a progressive tracheal constriction secondary to a large thyroid goitre in one subject. The subject had two pre-operative CT scans, with a time interval of eleven months, and a post-operative CT scan. The tracheal geometries have been demonstrated in figure 6.8. The post-operative trachea demonstrates a complete resolution of the constricted segment of the trachea in this subject. Due to the compressible nature of the trachea and the fact that the constriction of the trachea is due to external forces from a thyroid goitre, it isn't unreasonable to expect that there would be complete resolution of a constricted segment following thyroidectomy.

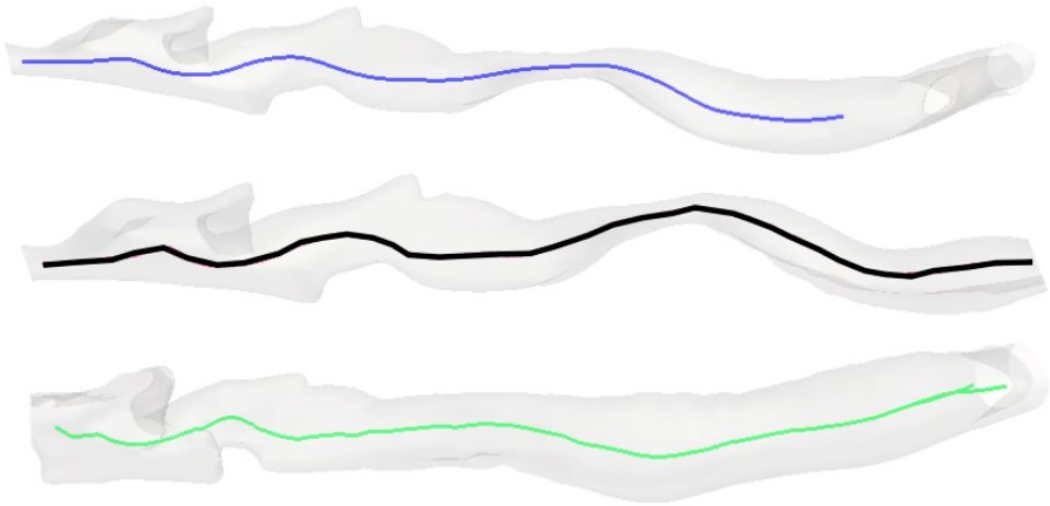


Figure 6.8. Three tracheal geometries placed in a sagittal orientation with centrelines i) pre-operative ii) pre-operative 11 months later iii) post-operative

One rare complication of thyroidectomy for compressive, retrosternal thyroids is post-operative tracheomalacia. Tracheomalacia is weakening of the tracheal structure due to softening of the cartilaginous framework. There are other causes of tracheomalacia, but in the context of thyroid goitres it is thought to occur secondary to the longstanding compression of the trachea, then following thyroidectomy there is collapse of the weakened trachea during expiration leading to >50% collapse of the airway. It is diagnosed either with dynamic imaging

or by bronchoscopy during spontaneous breathing. If a patient develops post-operative tracheomalacia they may present as an airway emergency and require tracheostomy. The post-operative trachea may remain compressed on static imaging. However, this is an extremely rare complication of thyroidectomy. A recent literature review and retrospective study of thyroidectomies performed over a thirty-month period at a UK tertiary referral centre, found that none of the patients developed post-operative tracheomalacia. (89) The study looked at 334 thyroidectomies, with 62 patients having pre-operative tracheal compression diagnosed on a CT scan. The study defined tracheal compression with a tracheal diameter of <5mm as critical compression. 18 of the patients in this study cohort had critical compression and none of these developed post-operative tracheomalacia.

Although extremely rare, it is an important complication to consider. However, predicting which patients may go on to develop this rare complication is difficult. Known risk factors include long duration of goitre and presence of a retrosternal goitre. Due to the rare nature of the complication the risk factors are not further defined. Therefore, it is not unreasonable when considering what the post-operative outcome of tracheas following thyroidectomy for as compressive goitre, to assume that there would be complete resolution of the compressed section of the trachea, as was the case in the study by Xiao (2019) (29).

Takeishi et al (90) studied the pre and post-operative tracheal flow in infants (<8 months old) who had undergone surgery for congenital tracheal stenosis (narrowing of the trachea). Six of the patients had pre- and post-operative imaging and they were able to model the flow both pre- and post-operatively using CFD. One patient was found to have a worse outcome post-operatively, and when the flow was modelled, it was found that post-operatively there had been a wide expansion of the trachea and this expansion led to further pressure losses. The pressure loss due to the post-operative expansion was greater than the pre-operative pressure loss due to the tracheal stenosis. Although this is an interesting paper, the findings are not entirely relevant to adult surgery affecting the trachea. Infants' tracheas have much softer and more malleable cartilaginous rings forming the structure of the trachea. Furthermore, the type of surgery performed to correct the tracheal stenosis is not discussed in the paper. It is unlikely that thyroidectomy in an adult with a compressive goitre would lead to a significant post-operative expansion in the trachea.

6.3 Comparison of a sudden expansion and a gradual expansion

In situations where there is a sudden and large expansion in flow, within the trachea, there are mechanical energy losses due to the turbulence created and the re-circulation of flow. Losses due to an expansion and flow separation are described by the Borda-Carnot equation:

$$\Delta E = \xi \tfrac{1}{2} \rho (v_1 - v_2)^2,$$

Equation 6.1

- ΔE is the fluid's mechanical energy loss,
- ξ is an empirical loss coefficient, which is dimensionless and has a value between zero and one, $0 \leq \xi \leq 1$,
- ρ is the fluid density,
- v_1 and v_2 are the mean flow velocities before and after the expansion

Where there is a sudden and a wide expansion the loss co-efficient is equal to one. If the expansion were to be graduated, rather than sudden and wide, the loss co-efficient would be reduced. In the case of an expansion that is gradual enough to avoid any flow separation then the loss co-efficient would be zero or close to zero. This is of particular interest when considering the shape of constriction seen in patients with thyroid goitres. Following the principle of the Borda-Carnot equation, if there is a narrow constriction at the level of the thyroid goitre followed by a sudden expansion, then we would expect the losses to be greater than a more gradual constriction, despite the fact the length of constriction in the gradual constriction will be longer. Without carefully considering separation losses, one might assume that a narrow constriction that is long in length would lead to greater energy losses than a short constriction of the same degree of constriction.

Flow separation occurs due to adverse pressure gradients. When streamlines diverge there is a decrease in the mean velocity and an overall increase in pressure due to the Bernoulli effect. If this rise in pressure is large enough this creates an adverse pressure gradient with the pressure drop that takes place due to friction. The adverse pressure gradient and wall friction slow down the layer of fluid at the wall, whilst the layer above continues to move this thin layer of fluid forward due to viscous effects. Once the adverse pressure is large enough the fluid at the wall may reverse its direction and this is where a separation region develops. The point at

which the separation region develops is referred to as the separation point (see figure 6.9). Turbulent eddies form within the separation region and this leads to large energy losses. (91)

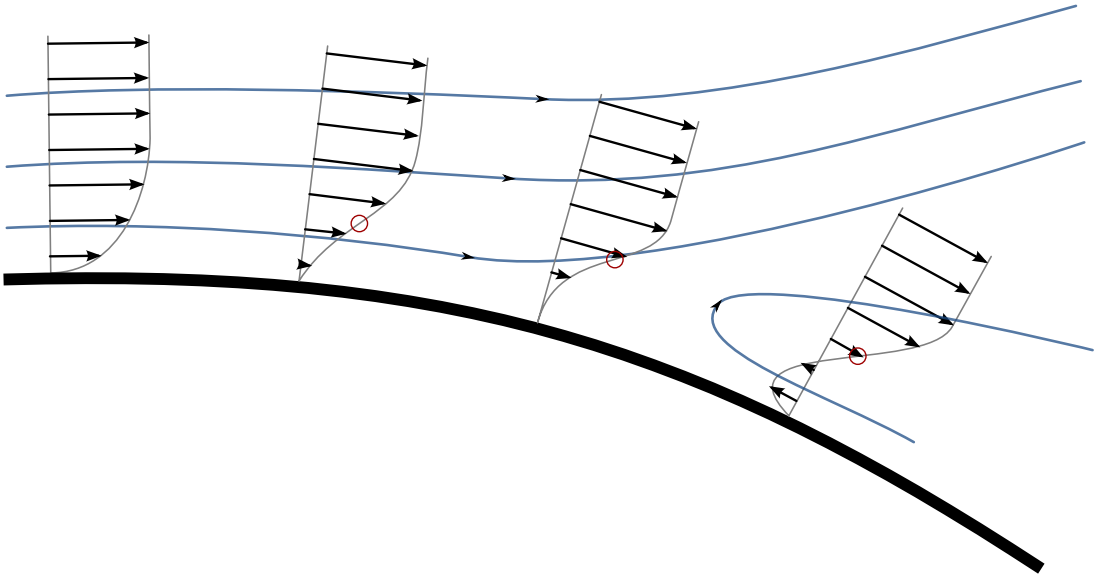


Figure 6.9. Graphical representation of the velocity profile in the boundary layer. The last profile represents reverse flow which shows separated flow (92)

To investigate the separation seen with a tracheal constriction, a healthy tracheal model was manipulated to produce 1) a trachea with a narrow constriction followed by a sudden expansion and 2) a trachea with a narrow constriction followed by a more gradual expansion. The minimum cross-sectional area, at the level of the constriction, was the same in both tracheas. Figures 6.10 and 6.11 show the surface meshes of the two manipulated tracheal models. To assess the difference in cross-sectional area along the length of the trachea, in both models, a centreline was calculated using VMTK and planes normal to the centreline were created. Figure 6.12 shows the cross-sectional area of the tracheal models along the length of the trachea from the first tracheal ring to the carina. The tracheal model with a sudden expansion has the same cross-sectional area as the tracheal model with a gradual expansion up until the point of constriction, where both tracheas have the same minimum cross-sectional area. Further downstream of this there is a rapid increase in the cross-sectional area of the trachea with a sudden expansion and the cross-sectional area exceeds that of the first tracheal ring. The tracheal model with the gradual expansion shows a much slower rate of increase in the cross-sectional area and the length of constriction (>35% reduction in the cross-sectional

area when compared with the trachea 2cm above the carina) is considerably longer. Further downstream the two tracheas meet again with the same cross-sectional area prior to the carina.

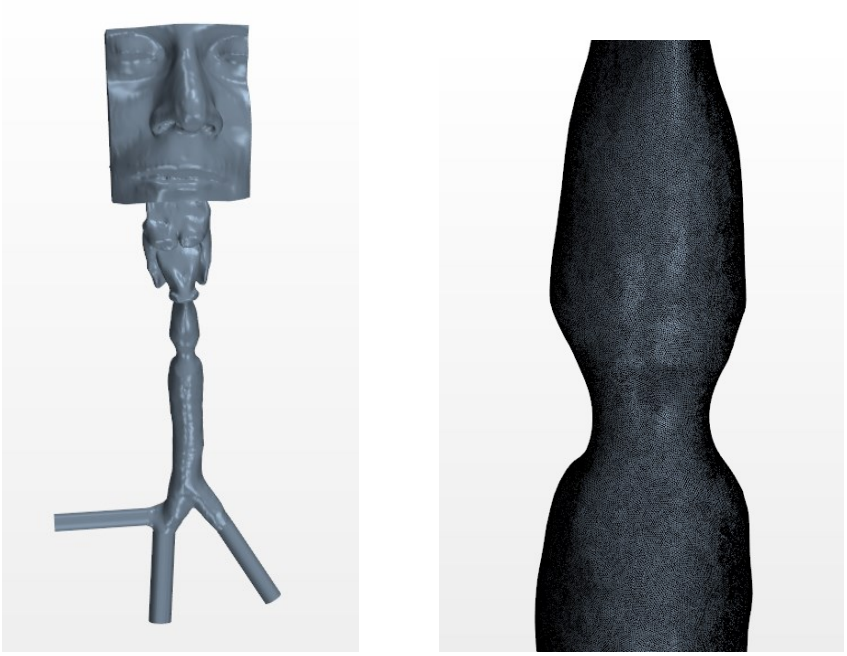


Figure 6.10. i) surface mesh representation of the tracheal constriction followed by a sudden expansion and ii) a magnified view of the mesh demonstrating the constriction

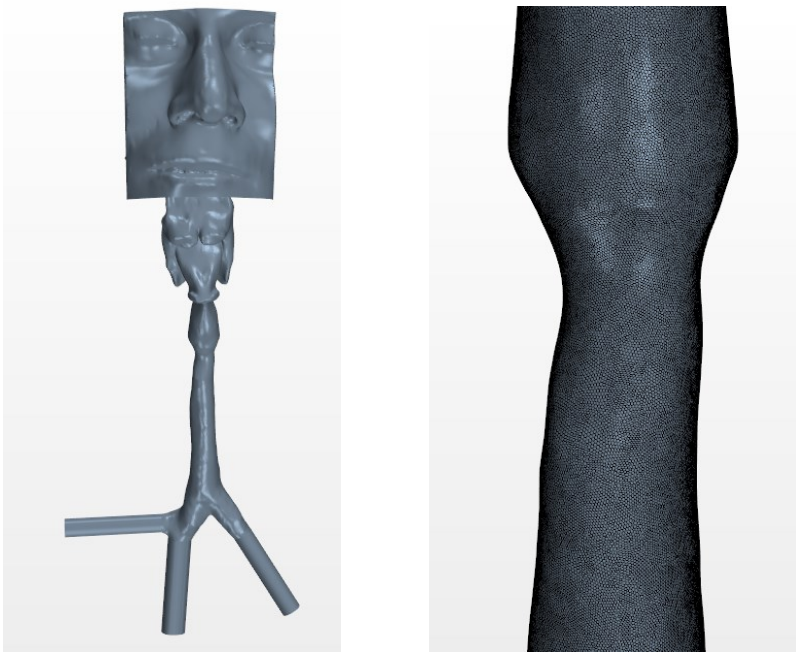


Figure 6.11. i) surface mesh representation of the tracheal constriction followed by a gradual expansion and ii) a magnified view of the mesh demonstrating the constriction

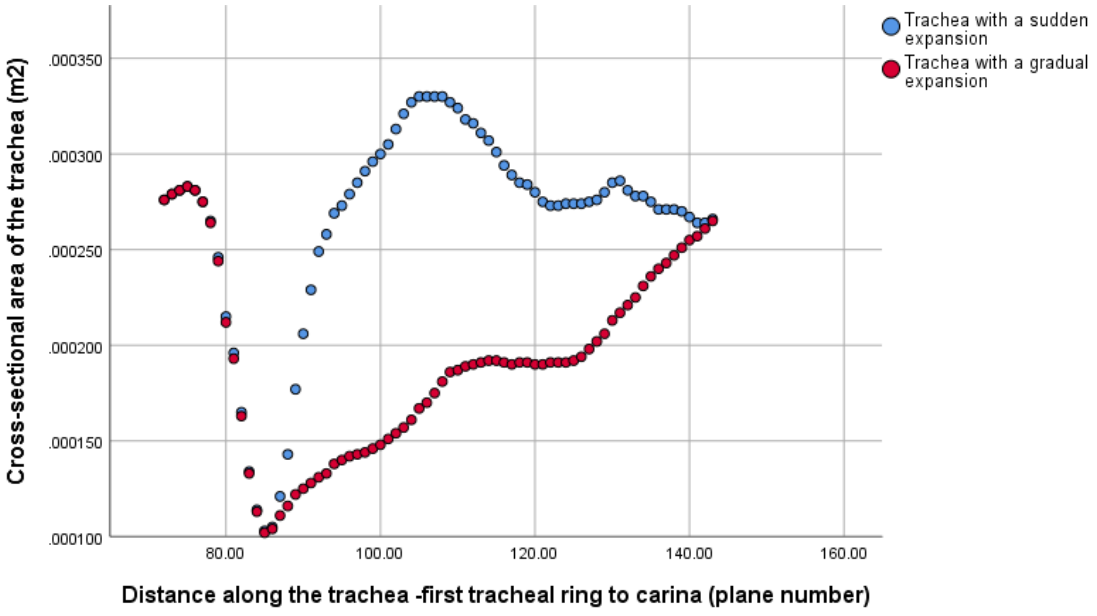


Figure 6.12. Cross-sectional area of the trachea along the length of the trachea (first ring to the carina) for the sudden expansion (blue) and the gradual expansion (red)

Using an LES model of turbulence, the pressure loss across the constricted trachea is 45.0 pa and 43.0 Pa for the sudden expansion and the gradual expansion respectively at 15L/min. Figure 6.13 shows the total pressure along the length of the trachea for both tracheal models. Although the difference in pressure loss is small it is interesting to see the distribution of loss. The total pressure drop seen in the trachea with a sudden expansion is larger and takes longer to recover than that of the trachea with the gradual expansion. This may indicate that there is less disturbance to the flow in the more gradual expansion. Within both tracheal models there is a slight recovery in the pressure loss following the drop in pressure and this is likely to be due to the redistribution of high velocity flow across the trachea. Figure 6.14 shows the static pressure along the length of the trachea for both tracheal models. The static pressure shows an earlier and better recovery in the tracheal model with a gradual expansion.

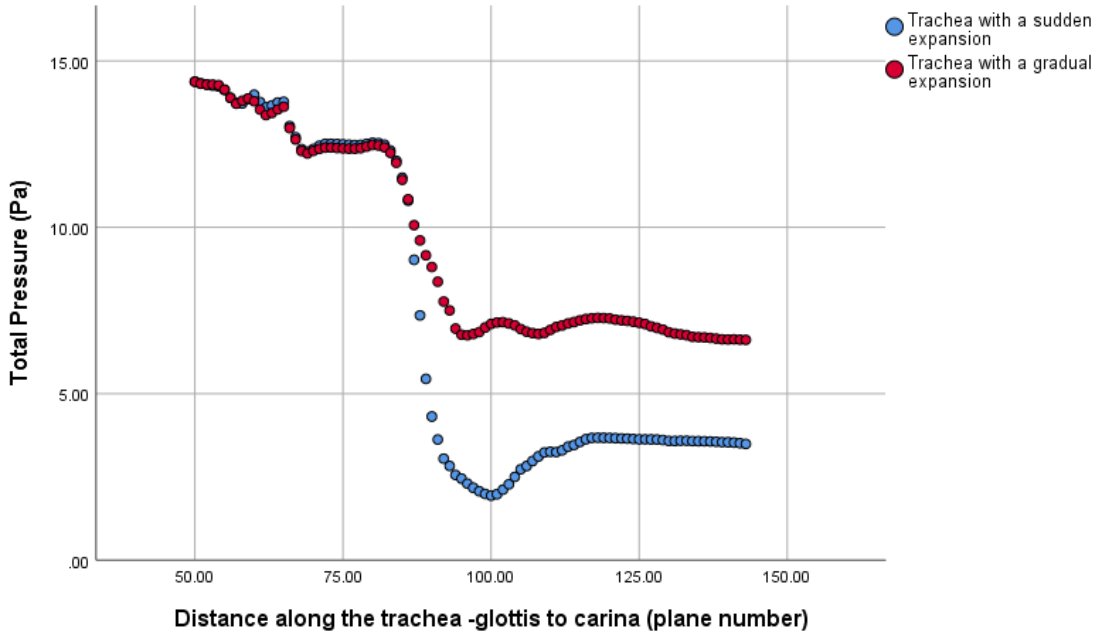


Figure 6.13. Total pressure (Pa) along the length of the trachea (glottis to the carina) for the sudden expansion (blue) and the gradual expansion (red)

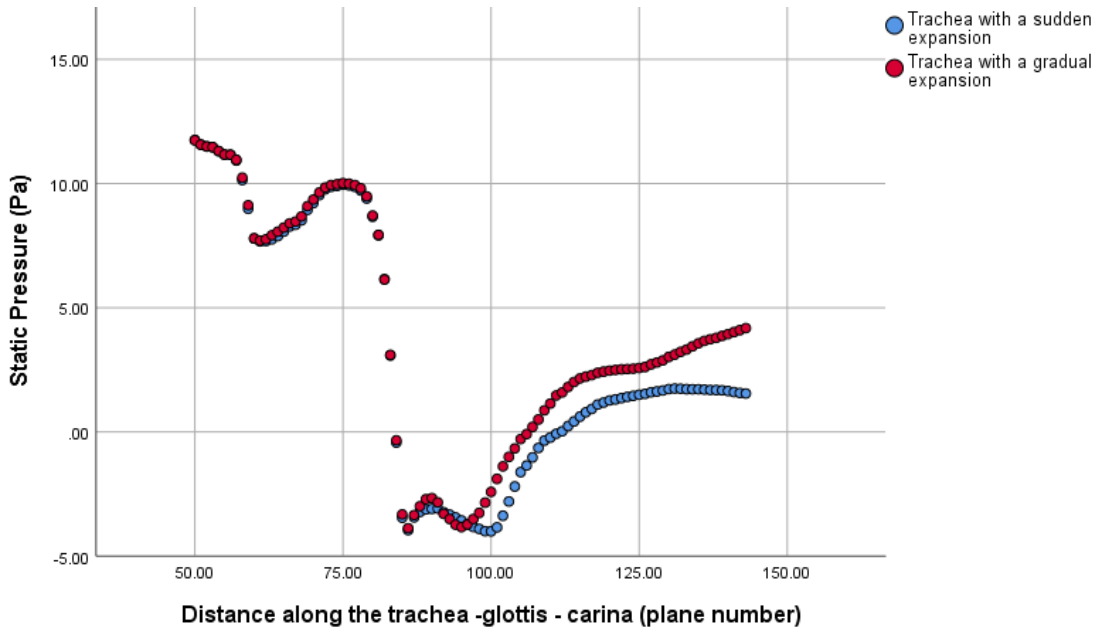


Figure 6.14. Static pressure (Pa) along the length of the trachea (glottis to the carina) for the sudden expansion (blue) and the gradual expansion (red)

To look more closely at the flow patterns in the two tracheal models isoplanes of the magnitude of velocity, static pressure, and vorticity and surface mesh representations of the wall shear stress were assessed. Looking at the isoplanes of the magnitude of velocity (see figure 6.15), both tracheal models demonstrate a jet of high velocity flow arising at the level of the constriction. The jet appears to be slightly longer in the gradual expansion model and follows the walls of the trachea more closely. The redistribution of high velocity flow following the jet breakdown is more evenly spread in the gradual expansion model. Both tracheal models demonstrate separation of the flow adjacent to the constriction jet, however the area of flow separation is much larger in the sudden expansion model.

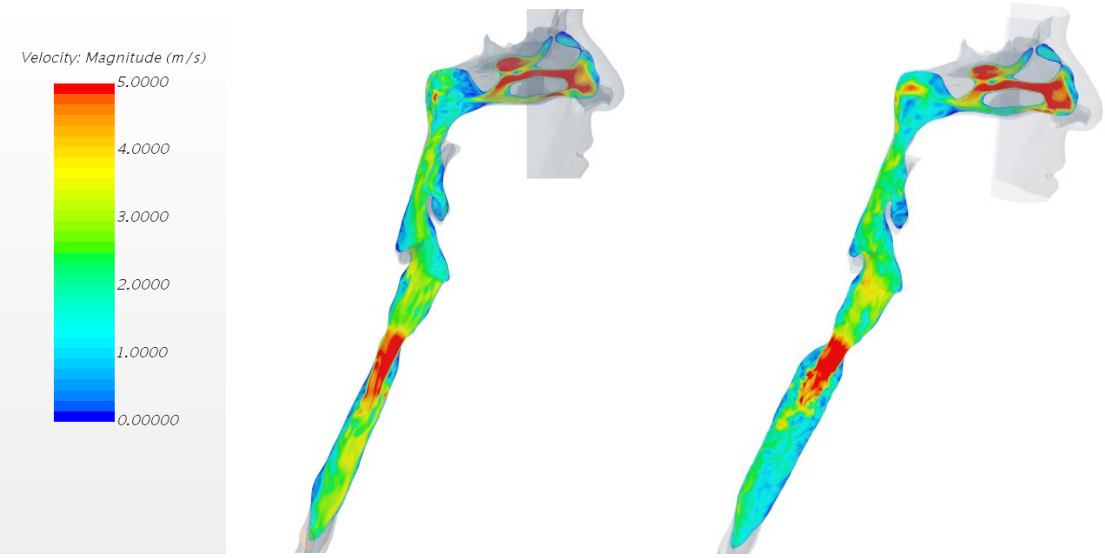


Figure 6.15. Isoplane of the magnitude of velocity (m/s) in i) gradual expansion and ii) sudden expansion

The drop in static pressure looks similar across both models with a large drop in static pressure taking place at the level of the constriction (see figure 6.16). In both tracheas there is slight recovery in the static pressure further downstream of the constriction.

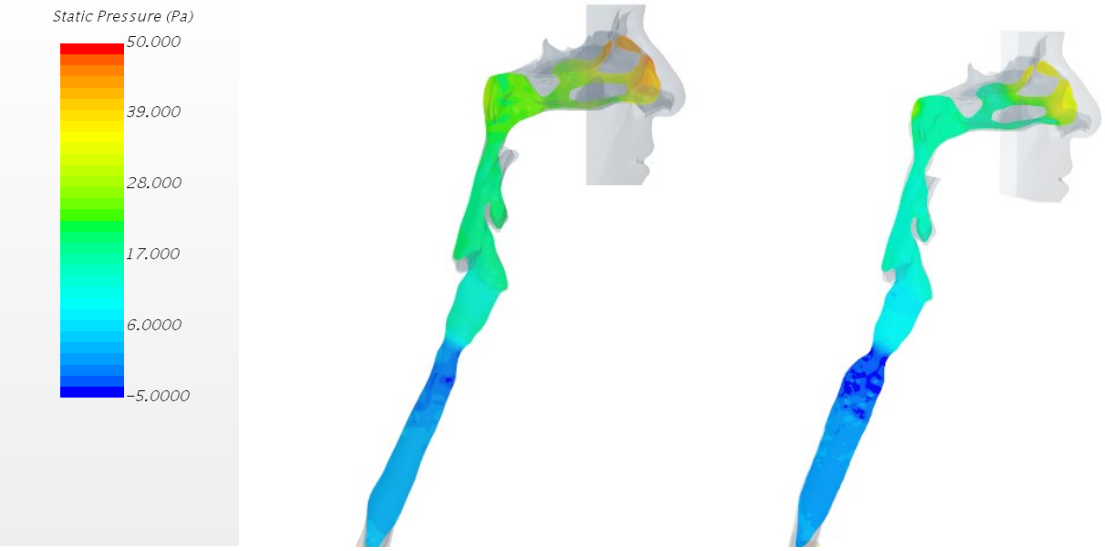


Figure 6.16. Isoplane of the static pressure (Pa) in i) gradual expansion and ii) sudden expansion

High wall sheer stress is seen in both tracheal models at the level of constriction and at the level of the glottis (see figure 6.17). There appears to be a more complex pattern of wall

shear stress further downstream of the constriction in the sudden expansion model which could be accounted for by the greater degree of disturbance in the flow.

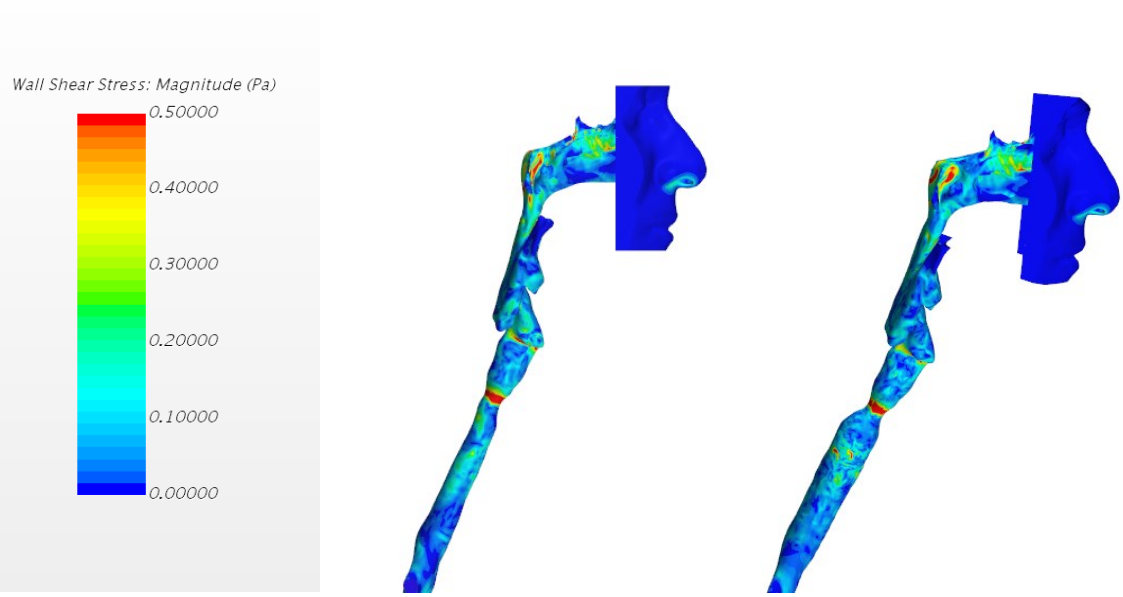


Figure 6.17. Surface mesh representation of the magnitude of wall shear stress (Pa) in i) gradual expansion and ii) sudden expansion

This greater degree of flow disturbance is demonstrated when examining the difference in vorticity between the two models (see figure 6.18). Both models have areas of high vorticity adjacent to the constriction jets, however, the vorticity remains higher for a longer length of trachea in the sudden expansion model.

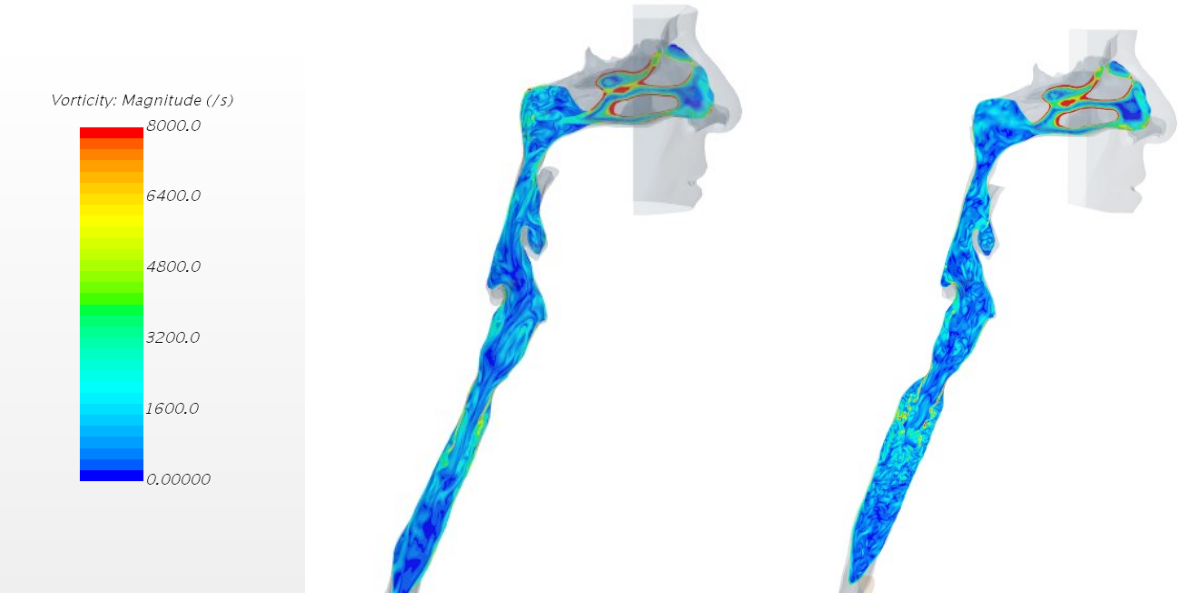


Figure 6.18. Isoplane of the vorticity in i) gradual expansion and ii) sudden expansion

Taherian et al (93) studied the flow characteristics of a trachea with a stenotic segment followed by an expansion further downstream in the trachea. They observed that there was flow acceleration through the stenotic segment with peak velocity in this region, and an area of flow separation and flow recirculation post-stenosis. They describe a "Coanda" type wall re-attachment. The Coanda flow was observed to result in an increased turbulence at the stenosis and downstream of the stenosis. The findings are similar to the findings seen here in this study. Similarly, Liu et al (94) used LES to model flow through the obstructed upper human airways and found that a strong jet produced in the pharynx resulted in jet separation and reversal of flow. They found the flow was unsteady and turbulent even at low Reynolds numbers of <500. Takeishi et al (90) studied pre and post-operative paediatric tracheas and found that improving a stenotic segment did not improve the pressure loss due to the post-operative expansion resulting in separation losses.

Although the model with a gradual expansion shows a reduction in the degree of flow separation and disturbance, the pressure losses across the constriction are still similar to the more sudden expansion tracheal model. It is possible that a tracheal model be created where the constriction diverged at an angle gradual enough that the flow wouldn't separate and thereby reducing the pressure loss due to the separation. Sparrow et al (95) used a method of numerical simulation to examine the separation of flow with divergent pipes of differing angles. They performed simulations with angles of divergence of 5, 10 and 30 degrees. They

also varied the Reynolds number of the flow. For a divergence angle of 5 degrees flow separation was found to take place at Reynolds numbers <2000. Above 2000 there was no flow separation observed. The flow at the inlet was laminar and fully developed. The situation becomes more complex in the trachea if there is a constriction close to the glottis where flow has already formed a glottic jet and there is flow separation immediately upstream of a second constriction point.

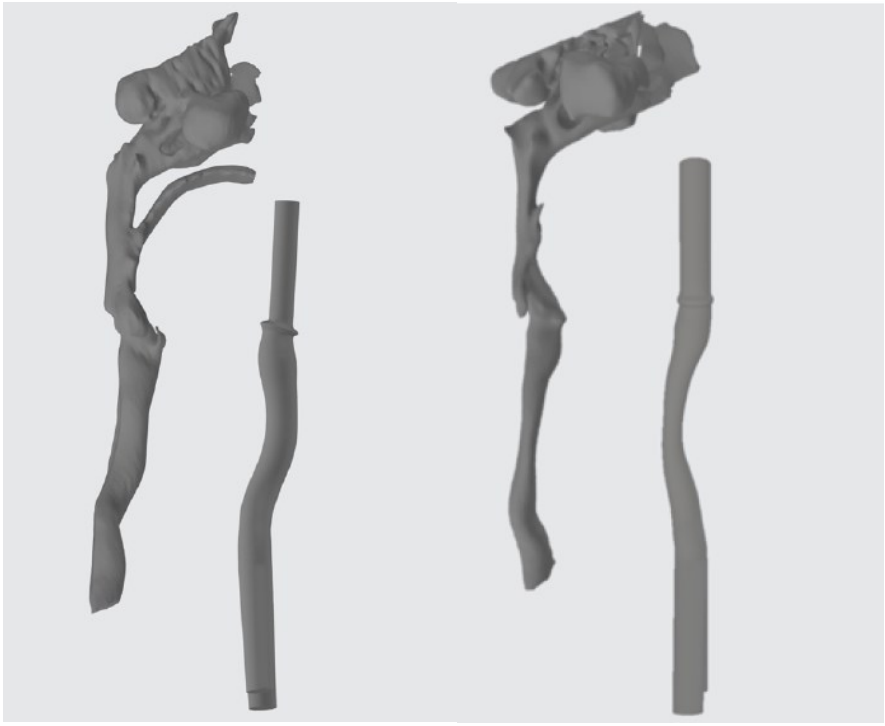
6.4 Simplifying the tracheal geometry

Yang (2020) (96) carried out work in collaboration with this thesis project. The aim of the work was to assess if a simplified tracheal geometry could accurately reproduce the CFD results of the non-simplified tracheal geometry (reference geometry), with an aim to reduce the computational cost of running simulations. Yang (2020) took three tracheal geometries; subjects 5, 19 and 21, and simplified these geometries. A steady RANS computation was used to calculate the pressure loss across the simplified tracheal model and the results of this have been compared here with the results from chapter 5.

For the simplified model construction, the centreline co-ordinates, diameters, and cross-sectional areas were extracted from the tracheal geometries using VMTK. These were interpolated to segment a smaller number of sections for reconstruction. Bernstein-Bezier curves were then used to smooth the centreline, to avoid any steps in the reconstruction. The centreline was then used as a centre point for reconstructing the trachea. The maximum diameter of the tracheal geometry at each segment along the centreline was used to produce a circular ring around the corresponding centre line point. This series of circular rings around the centreline were then used to reconstruct the trachea. This method was used for subjects 5 and 19. However, due to the severe flattening of the trachea of subject 21, if the normal diameter was used for creating circular rings, then this would lead to a gross over-representation of the cross-sectional area of the trachea at the point of maximum constriction. At this point the difference between the minimum and maximum diameter is 7.38mm. Therefore, instead the hydraulic diameter was used for subject 21.

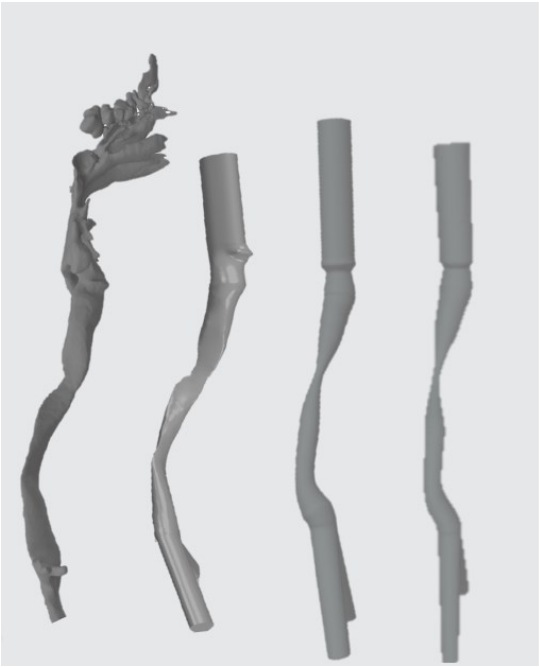
Figure 6.19 shows the comparison between the reference geometry of subject 5 with the simplified tracheal model reconstructed using the normal diameter and the comparison between the reference geometry of subject 19 with the simplified tracheal model reconstructed

using the normal diameter. Figure 6.20 shows the comparison between the tracheal geometry for subject 21 in its un-modified form, modified in preparation for CFD, and the simplified tracheal model reconstructed using the normal diameter, and the hydraulic diameter.



Subject 5 Subject 19

Figure 6.19. From left to right tracheal geometry of subject 5 compared with the simplified geometry, reconstructed using the normal diameter and the tracheal geometry of subject 19 compared with the simplified geometry, reconstructed using the normal diameter



Subject 21

Figure 6.20. From left to right: the un-modified tracheal geometry of subject 21 and the modified tracheal geometry, compared with the simplified geometry, reconstructed using the normal diameter and the tracheal geometry.

A steady RANS computation was performed at 15L/min on the simplified tracheal models and the total pressure loss (inlet pressure -outlet pressure) calculated. The results were compared with the steady RANS computation performed on the main subjects' tracheal geometries (see table 6.1). The total pressure losses across the simplified geometries are surprisingly very comparable to the total pressure loss across the reference tracheal geometries. Although the relative difference for subject 5 is large at 37.5%, however the actual difference in pressure loss is small at 3.0 Pa. The relative difference in total pressure loss for subject 19 is 2.1% and the actual difference in pressure loss is 0.3 Pa. The relative difference in pressure loss for subject 21 is 1.4% and the actual difference in pressure loss is 3.9 Pa.

Subject	%Constriction	Total pressure loss (Pa) reference	Total pressure loss (Pa) simplified	Relative difference %
5	33.00	5.0	8.0	37.5
19	68.27	14.6	14.3	2.1
21	92.05	298.0	294.1	1.4

Table 6.1. Total pressure loss (Pa) across the trachea for subjects 5, 19 and 21 and the total pressure loss (Pa) across the simplified tracheal models for subjects 5, 19 and 21, and the relative difference

Volume renders were made of subject 21 including the reference geometry, the simplified tracheal geometry rebuilt using the hydraulic diameter and the simplified tracheal geometry rebuilt using the normal diameter. Figure 6.21 shows the volume renders of the static pressure. The pattern of static pressure loss across the trachea is similar between the reference geometry and the simplified geometry rebuilt using the hydraulic diameter. There is a large pressure drop across the tracheal compression. The same magnitude of pressure drop is not seen in the simplified geometry using the normal diameter. This is due to the nature of the tracheal constriction seen in subject 21. The tracheal constriction is extremely flattened by the surrounding thyroid goitre which is wrapped around the trachea at this point. Therefore, if the normal diameter is used, the cross-sectional area at the point of constriction will be much larger than the reference geometry.

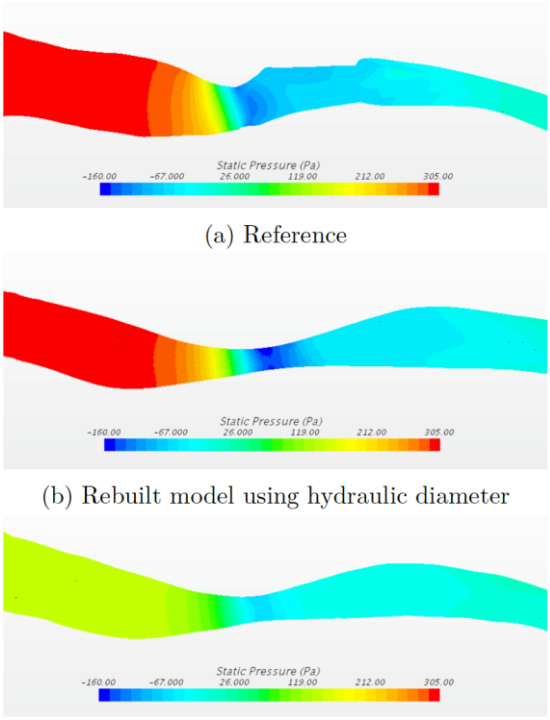


Figure 6.21. Volume renders of static pressure (Pa) for subject 21 a) reference geometry b) tracheal geometry rebuilt using the hydraulic diameter and c) tracheal geometry using the normal diameter

There are similar findings when looking at the total pressure loss (figure 6.22). The volume render of the magnitude of velocity shows peak velocity in the region of the constriction and there is a constriction jet in all three geometries (figure 6.23). Once again, the geometry rebuilt using the hydraulic diameter is a much closer fit than that of the geometry rebuilt using the normal diameter.

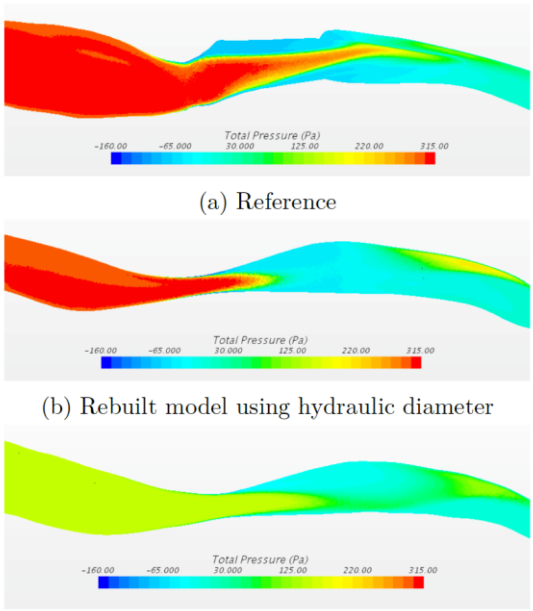


Figure 6.22. Volume renders of total pressure (Pa) for subject 21 a) reference geometry b) tracheal geometry rebuilt using the hydraulic diameter and c) tracheal geometry using the normal diameter

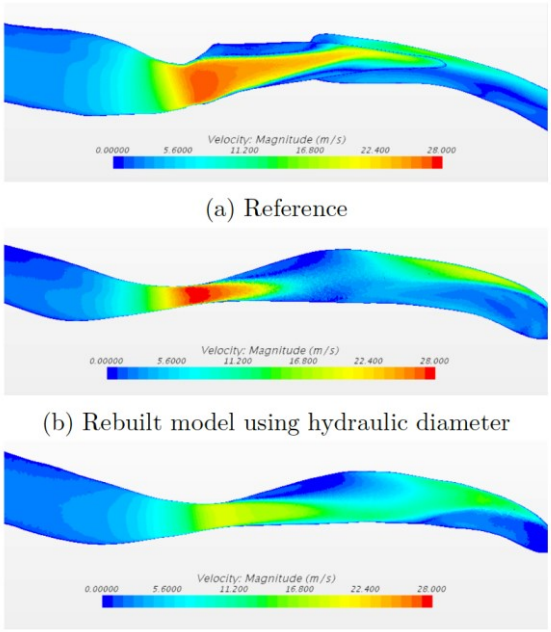


Figure 6.23. Volume renders of velocity (m/s) for subject 21 a) reference geometry b) tracheal geometry rebuilt using the hydraulic diameter and c) tracheal geometry using the normal diameter

The simplified geometries accurately reproduce the pressure loss across the trachea when compared to the reference geometries. Yang (2020) has recorded the methods of reproducing the simplified geometries using either the normal diameter or the hydraulic diameter. This has

the potential for reducing the computational costs of estimating the pressure loss across pathological tracheas. The steps involved for this piece of work included: exporting CT scans of the subject from the hospital imaging system (PACS), using Mimics software to create a 3D model of the trachea, exporting the STL file of the tracheal geometry to VMTK and creating a centreline, the centreline data was then used to create multiple sections of trachea along the centreline and from these sections the normal diameter or hydraulic diameter was calculated. There is potential for this process to be simplified further. A few key parameters taken from the CT scan may be enough to recreate a much more simplified tracheal geometry. For example: the diameter taken at the first tracheal ring of the trachea, the diameter at the constriction, and the length of constriction. These measurements can be easily measured either by a clinician or by a radiologist. Further work needs to be done to assess if these parameters would produce a simplified tracheal geometry that could accurately predict the estimated pressure loss when compared to the reference geometry.

6.5 Concluding remarks

Manipulating tracheal geometries in order to simulate post-operative findings is an interesting way of assessing if a patient is likely to benefit from surgery. This technique has been used in other specialities. An interesting way of validating this technique for patients with compressive thyroid goitres would be to use a series of patients who had post-operative imaging for other reasons and the simulated “post-operative” trachea could be compared with the actual post-operative trachea. The improvement in pressure loss across the trachea when comparing pre- and post-operative results could be correlated with the clinical outcomes as reported by the patient.

The study assessing the effect of a sudden expansion in a constricted trachea demonstrated that there is a greater disturbance in the flow when compared to a constricted trachea with a more gradual expansion. It is important to consider the type of constriction and whether or not there is a sudden expansion when assessing these patients and when considering surgical intervention.

Simplified geometries can reduce the computational cost of running simulations. Work performed by Yang (2020) (10) showed that simplified tracheal geometries can accurately represent the original geometries when considering the pressure loss across the trachea. The work demonstrated that using the hydraulic diameter to create the simplified geometry is more

accurate when the geometry is elliptical. There is potential for an even more simplified tracheal geometry to be created which would markedly reduce the number of steps needed, however, further work is needed.

Chapter 7 Lung function tests

7.1 Introduction

7.1.1 What is spirometry and how is it performed?

7.1.2 Issues with spirometry

7.1.3 Flow Volume Loop Curve appearance

7.2 Studies using spirometry to assess subjects with upper airway obstruction

7.2.1 Positional Spirometry

7.2.2 Work of breathing and pressure loss across the trachea

7.3 Aims

7.4 Methods

7.4.1 Spirometry

7.4.2 Difference in pre- and post-operative lung function tests

7.4.3 Visual inspection of flow volume loops

7.4.4 FEV_1/PEF ratio

7.4.5 Upright and Supine Lung function tests

7.4.6 Correlation between tracheal measurements and lung function tests

7.4.7 Calculating an estimate of the pressure loss using the flow volume loop

7.5 Results

7.5.1 Pre- and post-operative lung function tests

7.5.2 Visual inspection of the flow volume loops

7.5.3 FEV_1/PEF ratio

7.5.4 Correlation between tracheal measurements and lung function tests

7.5.5 Upright and Supine Lung function tests

7.5.6 Calculating an estimate of the pressure loss using the flow volume loop

7.6 Conclusions

7.1 Introduction

7.1.1 What is spirometry and how is it performed?

Spirometry is a non-invasive set of lung function tests which measures flow, volume, and time. This provides information about a subject which can be used to diagnose, to monitor disease progression over time and to assess response to treatment. Spirometry provides the following key information:

- Forced expiratory volume in 1 s (FEV_1)
- Forced vital capacity (FVC) which is the maximum volume of air exhaled by a subject when exhaling out as fast as possible
- FEV_1/FVC ratio
- Peak expiratory flow (PEF) which is the maximal flow that can be blown out when exhaling at a steady rate
- Forced expiratory flow (FEF)
- Forced inspiratory flow (FIF)
- Inspiratory vital capacity (IVC), the maximum amount of air which can be inhaled after a full expiration

The European Respiratory Society (32) has guidelines on how to perform spirometry, in order to provide reliable and reproducible results. Lung function tests for an individual subject are normally compared to a set of reference values or predicted values. For each subject, a predicted set of values can be produced prior to testing according to the subjects age, height, weight, sex, and race. The results of spirometry are presented as a list of values and in a graph, form showing the flow volume loop (see figure 7.2). Spirometry can be used to diagnose obstructive disease, restrictive disease, and mixed diseases of the airways.

Prior to performing spirometry, the equipment must be calibrated in accordance with the guidelines. (32) The subject's height, weight, race, sex, and age are recorded, and any inhaler/drug therapy use is noted. The standard position for spirometry is with the subject sat upright with their feet flat on the ground, legs uncrossed without any tight fitted/restrictive clothing. A nose clip is applied, and the subject is asked to form a tight seal around the

spirometer mouthpiece (see figure 7.1). In order to measure FVC and FEV_1 the subject is asked to take in a deep breath, as large as possible and then to blow out as fast as they possibly can and to keep blowing out until they have no more air left to blow out. PEF is obtained from the same manoeuvre. The IVC manoeuvre follows on from the FVC/FEV_1 manoeuvre and is performed by asking the subject to take a fast, deep breath back in after breathing all of the way out. The manoeuvres are repeated to ensure that there is reproducibility and that the repeated results meet the minimum accepted criteria. Three of the best test results need to be within 5% of each other.

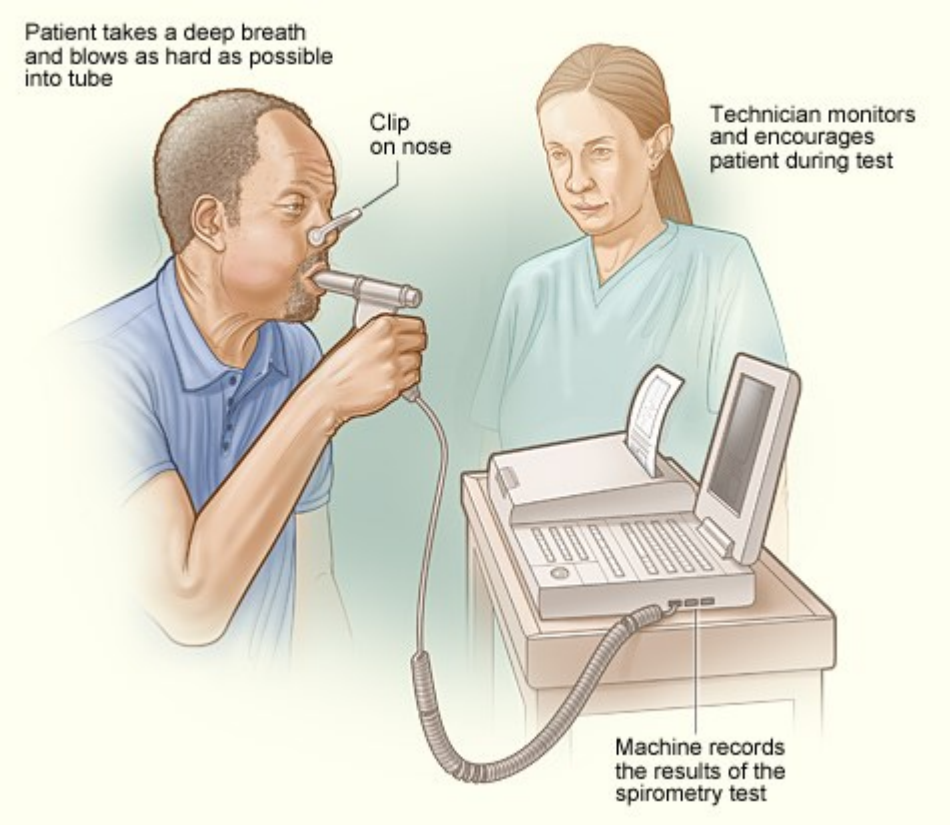


Figure 7.1. Schematic of a subject undergoing spirometry (97)

In order to assess the subject for central and upper airway obstruction, at least three repeatable flow volume loops are required. The flow volume loop is plotted as a graph of inspiratory and expiratory flow (on the y axis) against the volume (on the x axis) (see figure 7.2). It is crucial that the subject has used maximal inspiratory and expiratory effort and the person performing the tests should make note of the subject's effort and ability to clearly follow the instructions. The person performing the spirometry should use active encouragement to ensure the subject is using maximal effort. Guidelines from the European Respiratory Society

(ERS) Task Force have been published on the criteria on acceptable quality for spirometry results. (98)

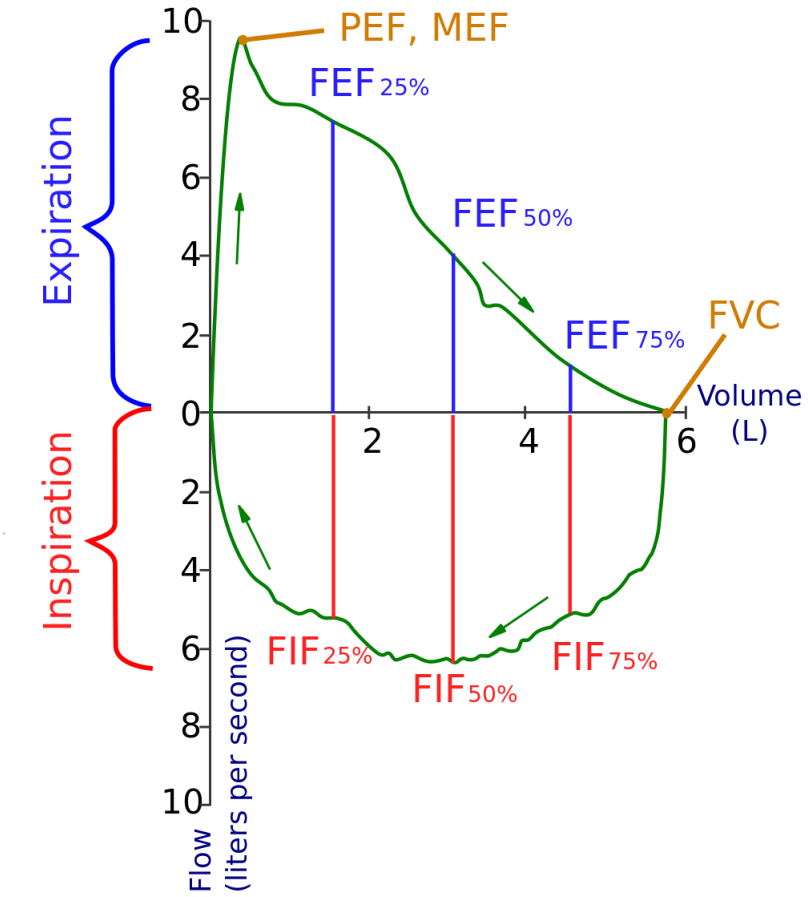


Figure 7.2. Schematic of a flow volume loop demonstrating a successful FVC manoeuvre. PEF = peak expiratory flow, MEF = maximal expiratory flow, FEF = forced expiratory flow, FVC = forced vital capacity, FIF = forced inspiratory flow (99)

7.1.2 Issues with spirometry

Lung function testing relies on the subject to understand instructions, co-operate in performing the tests and to use maximal effort. Because the tests are effort dependent it is crucial that the subject is performing to the best of their ability, and this can be encouraged through verbal encouragement from the technician. Due to being user-effort dependent there is intra-user test variability and therefore to overcome this there does need to be a significant change in a subject's lung functioning test results before the change can be thought to be due to a disease process. (38)

7.1.3 Flow Volume Loop Curve appearance

For the purpose of this thesis, the focus will be on upper airway obstruction, as might be seen in a subject with a compressive goitre. Figure 7.3 demonstrates the different types of flow-volume loops that can be seen in airway obstruction. Three classic patterns of upper airway obstruction can be found on the flow volume loop. The first is variable extra thoracic obstruction. During expiration the intra-tracheal pressure exceeds atmospheric pressure which helps to stent open the airway and prevents/reduces the obstruction. However, during inspiration the intra-tracheal pressure is reduced and is below atmospheric pressure and the extra-thoracic segment of trachea collapses inwards. This leads to a flattening of the inspiratory limb, whilst the expiratory limb remains unchanged. In variable intra-thoracic obstruction, during expiration the intra-pleural pressure is higher than intra-tracheal pressure and the intra-thoracic section of the trachea collapses inwards during expiration. This leads to flattening of the expiratory limb whilst inspiration remains unchanged. Fixed airway obstruction leads to flattening of both limbs because airflow is affected throughout the whole breath cycle. (100)

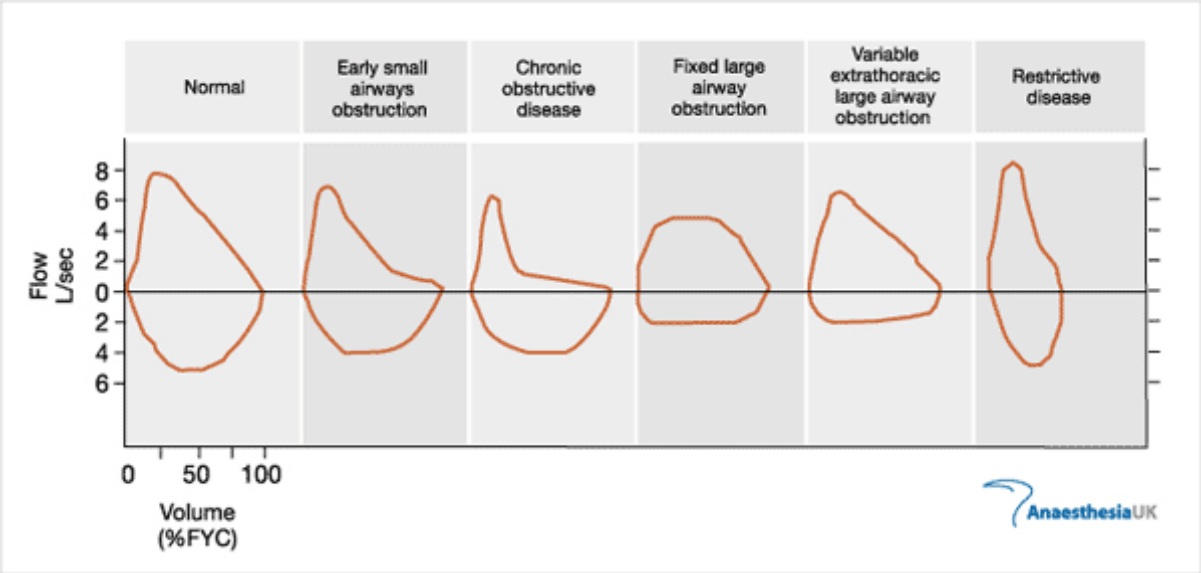


Figure 7.3. Schematic of flow-volume loops demonstrating the different types of airway obstruction (101)

7.2 Studies using spirometry to assess subjects with upper airway obstruction

Geraghty et al (102) studied the pre- and post-operative flow volume loops of 51 subjects who underwent thyroidectomy for a thyroid goitre. Four of these subjects had retrosternal goitres and the remaining subjects had cervical goitres. The subjects were subdivided according to tracheal changes seen on pre-operative imaging; group A had tracheal narrowing, group B had a deviated trachea but no tracheal narrowing, group C had normal tracheas. They found that group A showed a significant increase in the mean inspiratory maximal flow rate post operatively. Pre-operatively this group had a mean inspiratory maximal flow rate of 3.9 +/- 0.2 L/s and post operatively the group had a mean inspiratory maximal flow rate of 4.9 +/- 0.2 L/s. No other significant changes were seen in any other aspects of the FVL curve. They did not find a correlation in the weight of the resected gland and the improvement in mean inspiratory maximal flow rate.

A study by Albareda et al evaluated the presence of upper airway obstruction in subjects with retrosternal goitres and the relationship between the FVL with subjects' symptoms and CT scan measurements. They assessed fifty subjects with retrosternal goitres. These subjects underwent a questionnaire, lung function tests and a CT scan. Upper airway obstruction on the FVL was diagnosed as i) extra thoracic if visually there was flattening of the inspiratory limb, as ii) intrathoracic if there was a plateau of the forced expiratory flow, along with the lack of forced inspiratory plateau, or as iii) fixed if there is flattening of both the inspiratory and expiratory limbs. The curves were assessed by three blinded, independent expert pneumonologists. In addition, they used the alternative cut off points $FEF_{50}/FIF_{50} > 1.2$ and $FEV_1/PEF > 8$ as alternative methods of diagnosing upper airway obstruction. Tracheal narrowing was evaluated using CT scans of the chest and the narrowest AP diameter was expressed as a quotient of the diameter of the tracheal diameter 2 cm above the carina.

The analysis of the FVLs showed that 26% of the subjects in the study had evidence of upper airway obstruction: twelve of the subjects had signs of extra thoracic airway obstruction, none of the subjects had intrathoracic obstruction and one subject had a fixed obstruction. They found that 54% of the subjects had clinical symptoms of compression however there was no correlation with the presence of upper airway obstruction on the FVL. Nor was there any correlation found between the presence of upper airway obstruction and tracheal compression or deviation. The authors concluded that due to the lack of correlation with subject reported symptoms and radiological parameters they did not feel that FVLs should be used in the decision-making process for subjects considering surgery for compressive goitres. (103)

Miller et al (104) carried out a study in 1989 to look at the methods of detecting upper airway obstruction in subjects with thyroid goitres. 144 subjects were included in the study. All subjects underwent lung function tests including FVLs. The FVLs were interpreted by one expert user. Evidence of upper airway obstruction was determined by assessing the FVL for a period of relatively constant expiratory flow (<10% variation) lasting over a volume period of at least 20% of the FVC and this period of constant flow had to include the peak flow. Of the 144 subjects, 31% were diagnosed as having upper airway obstruction and 65% had normal FVLs, a further 4% had intrapulmonary airway obstruction as evidenced on their FVL. When comparing the group with UAO to the group without UOA they found that the PEF in the UAO group was significantly lower and that the $FEV_{50\%}$, $FEV_{50\%}/FIF_{50\%}$ and FEV_1/PEF were significantly higher.

44 of the 144 subjects underwent thyroid surgery, 29 of which had upper airway obstruction on their FVL. 28 of these subjects reported an improvement in their symptoms following surgery. The authors compared the pre-operative lung function tests with the post-operative lung function tests of all the subjects who underwent surgery. They found that the subjects who had pre-operative evidence of UAO showed a significant post-operative drop in the FEV_1/PEF ratio and there was no significant change in the subjects who had no pre-operative evidence of UAO. The PEF increased significantly in both groups post-operatively with a 34% rise in the subjects with pre-operative UAO and a 9% rise in those subjects without. It was concluded that these results demonstrate that FVL can be used to predict which subjects will benefit from undergoing thyroidectomy for compressive goitre symptoms. The criteria used by the authors for diagnosing UAO was specific, and it is unclear how they were able to analyse the schematic of a FVL so precisely.

A further study by Melissant et al (105) assessed 28 subjects with goitres in an attempt to find a simple radiologic measurement which would reflect the degree of tracheal compression in subjects with UAO. The subjects were divided into three groups according to the results of their FVL: variable extra thoracic obstruction (n = 6), variable intrathoracic obstruction (n = 11), and fixed obstruction (n = 11). Variable extra thoracic obstruction was defined as an inspiratory plateau on the inspiratory limb of the FVL and a PEF_{50}/PIF_{50} ratio of >1.1. Variable intrathoracic obstruction was defined as an expiratory plateau with a PEF_{50}/PIF_{50} ratio of <0.9. Fixed obstruction was defined as a plateau on both the inspiratory and expiratory limbs of the FVL and PEF_{50}/PIF_{50} ratio of 0.9-1.1. CT scans of the neck and chest were performed, and the minimal cross-sectional area of the trachea was measured and

compared with the diameter of the trachea at 2cm above the carina, a ratio of these two measurements was calculated. The only significant correlation found between CT measurements and lung function indices was between airway resistance and the cross-sectional area of the trachea 2cm above the carina. No other correlations were found between the CT measurements of the trachea and the lung function tests and they concluded that the measurements on the CT scan could not be used to predict which subjects should undergo surgery for compressive thyroid goitres. They found that lung function abnormalities tended to be greatest in subjects with variable extra thoracic obstruction when compared to the other two groups. The authors postulated which lung function test is the most accurate way to reflect the degree of UAO; FEV_1 is thought to grossly underestimate the degree of UAO and PEF is thought to be less accurate because it is effort dependent. PEF_{50} and MIF_{50} (maximal inspiratory flow at 50% of forced vital capacity) are thought to be better predictors because these are both forced manoeuvres which will reflect any tracheal narrowing. These measurements do not however reflect quiet breathing. (105)

One group looked at the normalization of abnormal flow volume loops following surgery for symptomatic goitres. Twenty-five subjects who were undergoing surgery had pre- and post-operative lung function tests. The post-operative lung function tests were performed one month following surgery. 60% of the subjects had pre-operative lung function tests which indicated upper airway obstruction. Surgery resulted in normalization of the abnormal pre-operative flow volume loops in all 15 subjects. The group used visual inspection of the flow volume loop as the diagnostic criteria for UAO for the pre-operative lung function tests and for determining normalization of the flow volume loop. (106)

Sorensen et al (43) performed pre and post lung function tests on subjects undergoing surgery for symptomatic benign goitres. They measured the FVC, FEV_1, FEV_1/PEF and $FEF_{50\%}/FIF_{50\%}$. They then correlated the changes in lung function parameters with changes in the tracheal A_{min}, as measured on pre- and post-operative MRI scans. They found that tracheal narrowing correlated significantly with pre-operative lung function parameters. However, there was no correlation between HRQOL, as measured using the ThyPro, and tracheal narrowing or lung function parameters. FVC was almost unchanged by surgery, $FIF_{50\%}$ did show a small but significant improvement, and there was a small improvement in the mean FEV_1/PEF ratio. Prior to surgery 19 of the 65 subjects studied had a FEV_1/PEF >8, indicating UAO and following surgery this was significantly reduced to 7 subjects.

7.2.1 Positional Spirometry

Upper airway obstruction from a goitre can lead to symptoms of positional dyspnoea. The compression of the trachea from a goitre has the potential to worsen when the subject is supine due to the effects of gravity. In fact, many subjects with goitres complain of worsening symptoms when they lie flat. We could be missing diagnoses of upper airway obstruction in subjects if spirometry is only performed in the seated position.

Meysman et al (107) performed both upright and supine spirometry on two subjects with goitres who complained of positional dyspnoea. They used the following values for determining the presence of upper airway obstruction: FEF_{50}/FIF_{50}, PEF/PIF, $FEV_1/FEV_{0.5}$, FEV_1/PEF1. When performed in the upright position the lung function tests did not show evidence of upper airway obstruction in either subject and the flow volume loops did not demonstrate a characteristic pattern of upper airway obstruction. However, on further testing in the supine position both subjects showed evidence of upper airway obstruction. One of the two subjects underwent surgery and following surgery showed an improvement in both symptoms and spirometry results. There was less flattening of the inspiratory curve of the flow volume loop and lower (more normal) UAO ratios. The authors concluded that subjects with goitres and symptoms of positional dyspnoea should undergone lung function tests in both upright and supine positions.

7.2.2 Work of breathing and pressure loss across the trachea

Pulmonary resistance in a healthy subject is in the region of ~1 $cmH_2O \cdot l^{-1} \cdot s$. This resistance is largely made up of the large airways resistance and the resistance of the lung tissue. This resistance can increase when the subject has airway disease. For example, in the case of subjects with COPD the pulmonary resistance can increase to 5-15 $cmH_2O \cdot l^{-1} \cdot s$. (65) This affects the work of breathing. In a subject with COPD breathing at 12 breaths per minute with a tidal volume of 500ml and an inspiratory: expiratory ratio of 1:4 and an inspiratory flow rate of 0.5 l/s then increasing the pulmonary resistance from 1 to 10 $cmH_2O \cdot l^{-1} \cdot s$ would increase the resistive component of the work of breathing from 0.25 to 2.5 $cmH_2O \cdot l$ per breath. This is a considerable increase in the work of breathing. (108)

Chen et al (77) used CFD to calculate the pressure loss in subjects with tracheal stenosis secondary to vascular rings prior to and post corrective surgery. They calculated pressure loss at 0.01, 0.1 and 1m/s to simulate airflow at rest, mild exercise, and exercise. They found that the pressure loss was greater at higher flow rates. For one of their subjects the pressure loss along the stenotic trachea was 3.76 Pa at the inspiratory inlet velocity of 1m/s. After surgery the pressure loss was reduced to 1.76 Pa. They studied 12 subjects and found a significant reduction in the pressure loss across all flow rates following corrective surgery.

Wassermann at al (74) sought to find an inspiratory resistance cut-off that would help determine when subjects with tracheal stenosis required surgery. Using in-vivo measurements they showed that if there was a sevenfold increase in inspiratory airway resistance then the subject required surgery.

One study looked at the pressure loss across tracheal stenosis in subjects with left pulmonary artery slings. They used CFD to model the pressure loss in the trachea and found a range of pressure loss of 78.9 to 914.5 Pa at flow rates calculated according to the patient's weight and estimated tidal volume. They also ran a simulation for a healthy subject and found a pressure loss of 0.7 Pa at a flow rate of 0.125 L/s. (109)

Brouns et al performed CFD on models of tracheal stenosis at differing severities of stenosis and at different flow rates; 15 and 30l/min. Using CFD they calculated the pressure loss across the stenotic segments of trachea. Using these simulations, they derived a formula to be used in clinical practice to estimate the pressure loss across the trachea, taking into account frictional losses in the trachea and the frictional losses induced by the degree of stenosis.

$$\Delta P_{1-3} = \rho \frac{V_3^2}{2}\left(1 - \frac{S_3^2}{S_1^2}\right) + \sum_i \Delta P_i^{loss} \qquad \text{Equation 7.1}$$

Where:

P = Pressure

1, 2 and 3 refer to the inlet to the model, the stenosis, and the outlet of the model.

ρ = 1.2kg/m^3 (the density of air)

V = local velocity

S = cross-sectional area

P^{loss} refers to the pressure loss across the stenosis. To calculate the pressure loss across the stenosis they derived the following formula:

$$\Delta P^{loss}_{(stenosis)} = \rho K \frac{Q^2}{2S_2^2} \qquad \text{Equation 7.2}$$

Where:

Q = flow rate

K is a constant which is determined by the degree of stenosis

The group produced a graph of K values which can be used as an idealised estimate coefficient to calculate pressure loss across tracheal stenoses relative to the degree of stenosis. To simplify the formula for clinical practice, they recommend using a K value of 1.2 to estimate the pressure loss across a tracheal stenosis using equation 7.2. (62)

7.3 Aims

The subjects studied in the main body of this thesis underwent thyroidectomy for compressive thyroid goitres. They underwent pre- and post-operative lung function tests, including flow volume loops. The lung function tests have been studied in detail with an aim to:

- Determine if there is a significant improvement in lung function parameters following surgery
- Assess if study subjects demonstrate upper airway obstruction on standard pre-operative lung function tests in the upright position as defined by the appearance of the flow volume loop
- Assess if study subjects demonstrate upper airway obstruction on standard pre-operative lung function tests in the upright position as defined by FEV_1/PEF ratio >8

- Assess if study subjects demonstrate upper airway obstruction on supine pre-operative lung function tests
- Determine if there is a significant difference between the subjects' upright and supine lung function tests
- Determine if there is a relationship between pre-operative lung function tests and CT evaluation of the trachea (degree of tracheal narrowing and length of tracheal narrowing)

7.4 Methods

7.4.1 Spirometry

Subjects underwent pre-operative and post-operative (>6 months following surgery) spirometry as per the European Respiratory Society (ERS) Task Force guidelines. (98) The spirometer used was the Carefusion Vyntus spirometer. Standard and positional spirometry was requested for all subjects. The following parameters were used to determine a diagnosis of upper airway obstruction: visual inspection of the flow volume loop and FEV1/PEF ratio.

7.4.2 Difference in pre- and post-operative lung function tests

The pre- and post-operative FEV_1, FEV_1(% predicted), FEV_1/PEF, PEF, PEF(%predicted) results have been reported for the subjects and compared using either Wilcoxon sign rank test or paired t-test according to the data being non-parametric or parametric, respectively.

7.4.3 Visual inspection of flow volume loops

The flow volume loop was visually assessed by a clinician for the appearance of upper airway obstruction. Pre- and post-operative flow volume loops were divided into four categories: normal, extra thoracic obstruction, intrathoracic obstruction, or a fixed obstruction. Flow volume loops were considered to show extra thoracic obstruction if there was flattening of the inspiratory limb, intrathoracic obstruction if there was flattening of the expiratory limb in addition to a lack of forced inspiratory plateau, or a fixed obstruction if there was flattening of both the inspiratory and expiratory limb. For those subjects who had upright and supine spirometry, differences between the flow volume loops was recorded. For those subjects who

had both pre- and post-operative flow volume loops, improvement in the post-operative appearance was recorded. Figure 7.4 demonstrates an example of a pre- and post-operative flow volume loop recorded for subject 7. The pre-operative flow volume loop shows three loops i) ”pred” the loop predicted according to the subject demographics ii) “pre” the loop recorded with the subject sat upright and iii) “post” the loop recorded with the subject supine (lying flat). In the example displayed, the post-operative flow volume loop was only recorded with the subject in the upright position. Comparing the “pre” loop of each graph it can be seen that the inspiratory limb on the pre-operative loop is markedly flattened, thus indicating extra thoracic obstruction. This flattening has improved in the post-operative loop.

The software Engauge Digitizer 12.0 was used to extract the data points from the flow volume loop schematic for both pre- and post-operative flow volume loops. The inspiratory limb could then be plotted on the same graph for visual comparison. Figure 7.5 shows the inspiratory limb of the flow volume loop for subject 7 for both the pre and post-operative FVL. The pre-operative flow volume loop is flattened, indicating the presence of variable extra thoracic obstruction. Post-operatively the appearance of the loop is much improved with a much greater flow rate.

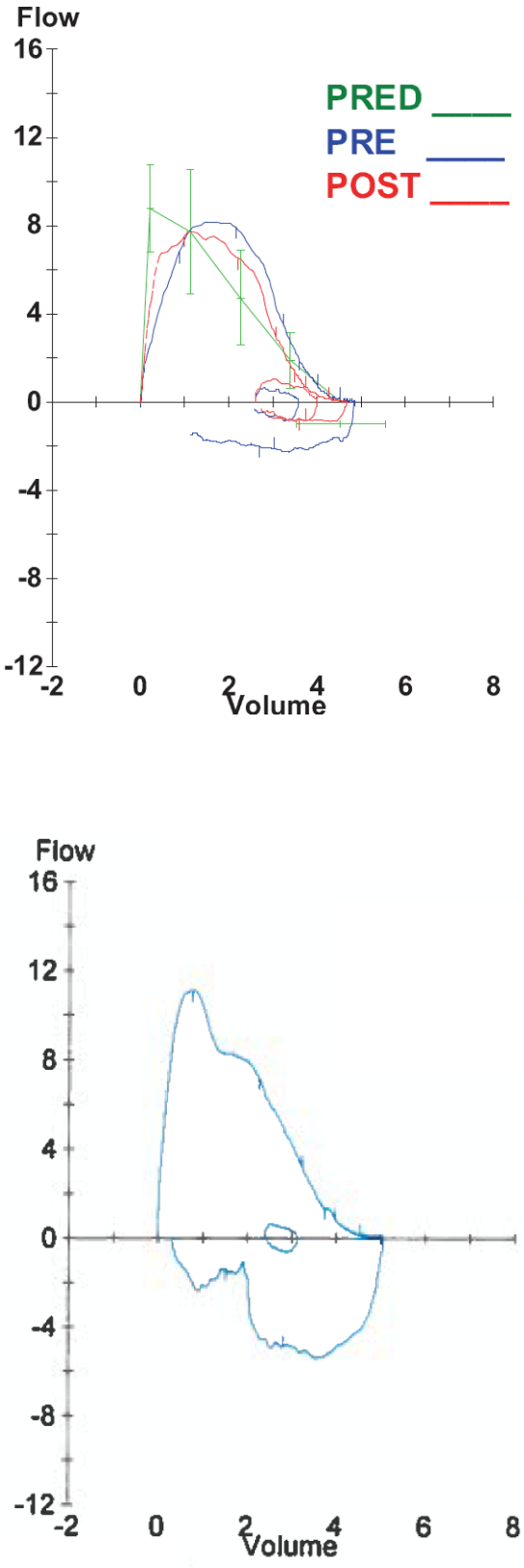


Figure 7.4. Example pre-operative flow volume loop (left) and post-operative flow volume (right) from subject 7

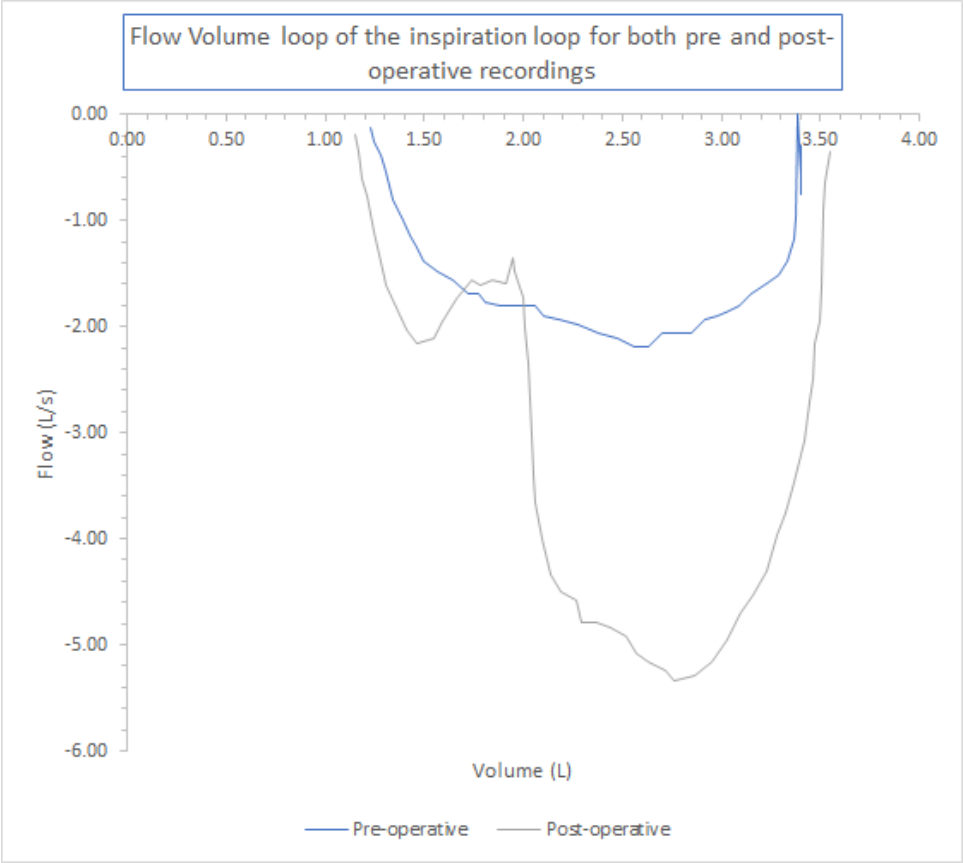


Figure 7.5. Re-plotted inspiratory data from the original flow volume loops of one subject both pre- and post-operatively for subject 7

7.4.4 FEV_1/PEF ratio

The FEV_1/PEF ratio was calculated for subjects for both pre- and post-operative assessments. FEV_1 and PEF are automatically calculated by the spirometer software. This ratio considers FEV_1 in ml and PEF in L/min. If the FEV_1/PEF ratio was >8 the subject was considered to have a diagnosis of UAO. Upright and supine FEV_1/PEF ratios were compared. The pre- and post-operative FEV_1/PEF ratios were compared to see if there was an improvement post operatively. A paired t-test was used to calculate if this improvement was significant.

7.4.5 Upright and Supine Lung function tests

All subjects had both standard and supine lung function tests requested at their pre-operative appointment. The protocol is identical for both sets of lung function tests apart from the

position of the subject. For the supine test the subject is lying flat. The upright and supine lung function tests were compared to see if there was a significant difference using a paired samples test.

7.4.6 Correlation between tracheal measurements and lung function tests

The following tracheal measurements were correlated with the lung function test results for each subject; smallest cross-sectional area (A_{min}), minimum diameter, the % reduction in the trachea when comparing the A_{min} with the cross-sectional area of the trachea 2cm above the carina, the minimum diameter of the trachea as measured on the DICOM scan using PACS, the ellipticity of the trachea and the length of constriction (if we consider >35% constriction). Spearman's rank correlation was used for FEV_1 and for length of constriction and Pearson's rank correlation was used for all other lung function tests and tracheal measurements.

7.4.7 Calculating an estimate of the pressure loss using the flow volume loop

The flow volume loops provided by the spirometer are schematics and the data points used to form the schematic are not provided by the spirometer software. Typically, the flow volume loop is assessed by the clinician visually. The open-source software Engauge Digitizer 12.0 was used to extract data points from the flow-volume loop schematics. Using Excel, the data points were then replotted on a graph and a best fit polynomial line was fitted to the points. The equation of the best fit line could then be used to find a sum of the flow rates over time.

$$\text{Flow rate} = \frac{\text{Change in volume}}{\text{Change in time}} \qquad \text{Equation 7.3}$$

Using the numerical data, the total time taken for the breath and the total volume change can be calculated. Using the equation above the average flow rate over the course of the breath can be calculated from the change in volume divided by the change in time. The average flow rate has been calculated for the inspiratory limb of the flow volume loops for each subject, both pre and post operatively. The pre- and post-operative average flow rates, as calculated from the FVLs, have been compared using a paired t-test.

One way to think about breathing is to think of the work of breathing as measured by the power needed to drive air through the airway.

Inspiratory power of breathing $= \frac{1}{2}\rho\kappa\frac{Q^3}{A_c^2}$ Equation 7.4

Where ρ=density of air

κ=loss co-efficient

Q=flow rate

A_c=minimum cross-sectional area of the trachea

The estimated power of the inspiratory component of the breath for the flow volume loop has been calculated for each subject for both pre- and post-operative flow volume loops using equation 7.4. The inspiratory component of the breath used for the flow volume loop represents the subject breathing at their maximal effort and therefore the flow rates far exceed those that the subject would be used to breathing at rest or during light exercise. For some context, it is estimated that most of us breathe at 0.5 L/second whilst lightly exercising, whereas the flow rate for the flow volume loop can exceed 5 L/second. The power of the inspiratory component of the breath for the pre-operative flow volume loop has been compared with the power of the post-operative breath using Wilcoxon signed rank test. For the pre-operative power of breathing calculation, the smallest cross-sectional area has been used, whilst for the post-operative power of breathing calculation it is assumed that the compressed part of the trachea returns to an uncompressed state and therefore as an estimate, the area of the first tracheal ring has been used.

Constrictions in pipe flows can create flow jets, entrance effects, flow separation, all of which are referred to as minor losses, despite the fact that they can be orders of magnitude greater than the pipe friction losses. Minor losses tend to be expressed in terms of their loss co-efficient. Tracheal compression leads to an orifice type loss. The pressure loss across the trachea can be estimated using the 'orifice loss' equation (equation 7.5). The pressure loss across the trachea has been estimated for each subject using the flow rate of the pre- and post-operative inspiratory limb of the flow volume loop. Pre- and post-operative results have been compared using a Wilcoxon signed rank test. For the pre-operative pressure loss calculation, the minimum cross-sectional area has been used, whilst for the post-operative pressure loss

calculation it is assumed that the compressed part of the trachea returns to an uncompressed state and therefore as an estimate, the area of the first tracheal ring has been used.

$$\Delta P = k.\frac{\rho}{2}.\left(\frac{Q}{A_{min}}\right)^2$$ Equation 7.5 (refer to Equation 5.4)

7.5 Results

7.5.1 Pre- and post-operative lung function tests

Eighteen patients had pre-operative lung function tests. Twelve patients underwent both pre- and post-operative lung function tests. The pre-operative lung function tests results are shown in table 7.1 and the post-operative lung function test results are shown in table 7.2. Shapiro-Wilks test was used to check for normality of the data. The pre-operative FEV_1 is not normally distributed and therefore the median values are displayed for these tests, and for comparison between pre- and post-operative tests the post-operative FEV_1 result is displayed as a median value. The post-operative median FEV_1 shows a modest improvement as from 2.15 to 2.23. The post-operative mean % predicted of the FEV_1 also shows an improvement from 93.3% to 107%. There is an improvement in the post-operative mean PEF from 6.17 to 7.05 and the mean %predicted PEF from 92.4% to 98.6. The group mean pre-operative FEV_1/PEF does not meet the criteria for diagnosing upper airway obstruction (>8). There is an improvement (reduction) in the post-operative FEV_1/PEF ratio from 6.55 to 5.68.

Lung Function test	Mean +/- SD	Median +/- IQ range	Range
FEV_1		2.15 +/- 0.74	1.36 - 4.04
FEV_1 (% predicted)	93.3 +/-17.8		69.5 - 129
FEV_1/PEF	6.55+/- 1.96		4.38 – 11.74
PEF	6.17 +/- 2.04		2.33 – 10.97
PEF (% predicted)	92.4 +/- 32.3		9.6 – 134

Table 7.1. Pre-operative lung function tests

Lung Function test	Mean +/- SD	Median +/- IQ range	Range
FEV_1		2.23 +/- 1.21	1.13 -4 .01
FEV_1 (% predicted)	107 +/- 22.3		76 - 143
FEV_1/PEF	5.68 +/- 1.08		4.19 – 7.3
PEF	7.05 +/- 2.09		4.85 – 11.15
PEF (% predicted)	98.6 +/- 14.5		77 – 114

Table 7.2.Post-operative lung function tests

Two sample tests (both parametric and non-parametric) were carried out to look for significant differences between the pre-operative mean or median lung function tests and the post-operative tests (see table 7.3 and 7.4). A significant difference was not found between the following lung function tests: FEV_1, FEV_1 (% predicted), FEV_1/PEF, PEF, PEF (% predicted).

Lung Function test	Wilcoxon Signed Rank Test significance	Reject or retain null hypothesis
FEV_1	0.695	Retain

Table 7.3. Wilcoxon Signed Rank Test to test for a significant difference between the pre- and post-operative median lung function tests FEV_1 and FEV_1/PEF

Lung Function test	Paired mean difference	T value	P value
FEV1 (% predicted)	-2.84 +/- 10.7	-0.703	0.508
FEV_1/PEF	1.05 +/- 1.97	-1.826	0.095
PEF	-0.43 +/- 1.81	-0.790	0.450
PEF (% predicted)	-4.99 +/- 22	-0.601	0.507

Table 7.4. t-test to assess for a significant difference between the pre- and post-operative mean lung function tests FEV_1 and FEV_1/PEF

Boxplots comparing the spread of data for the pre-operative FEV_1, PEF, and FEV_1/PEF are shown in figures 7.6-7.8. The boxplot of the pre- and post-operative FEV_1 doesn't appear to show any real difference between the two sets of data. The boxplot of the pre- and post-operative PEF shows that although the group medians do not vary greatly, there is a trend in

the data to show an overall improvement post operatively with a greater PEF, which is what one might expect to see. The FEV_1/PEF is considered to demonstrate evidence of upper airway obstruction if the ratio is >8. The boxplot demonstrating the pre- and post-operative FEV_1/PEF ratio shows that post-operatively there is an overall improvement (reduction) in the FEV_1/PEF ratio.

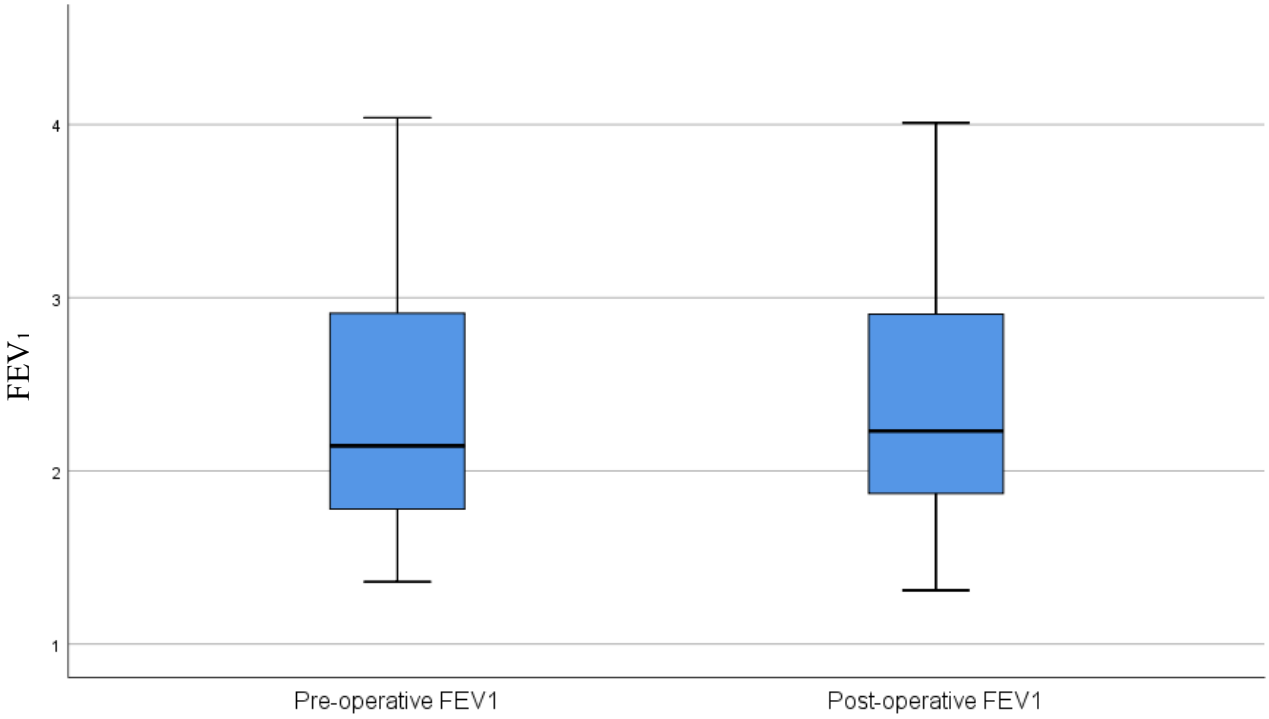


Figure 7.6. Pre- and post-operative FEV1 results for the main subjects

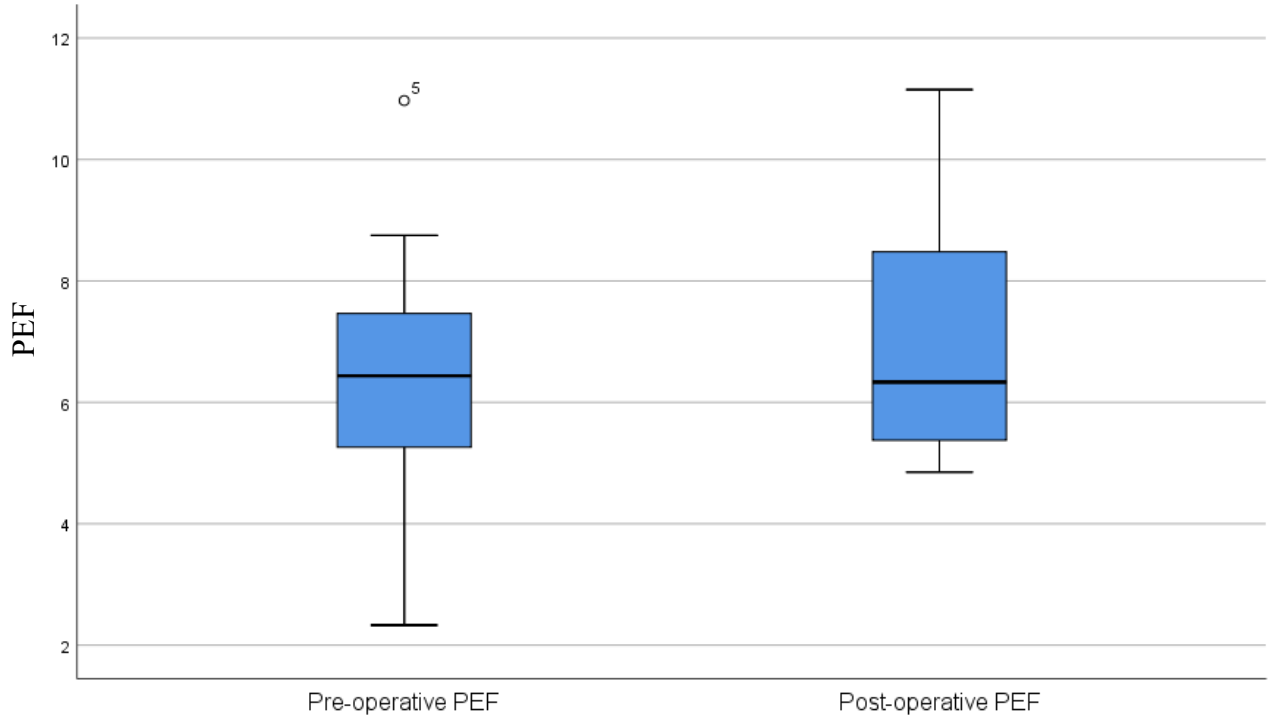


Figure 7.7 Pre- and post-operative PEF results for the main subjects

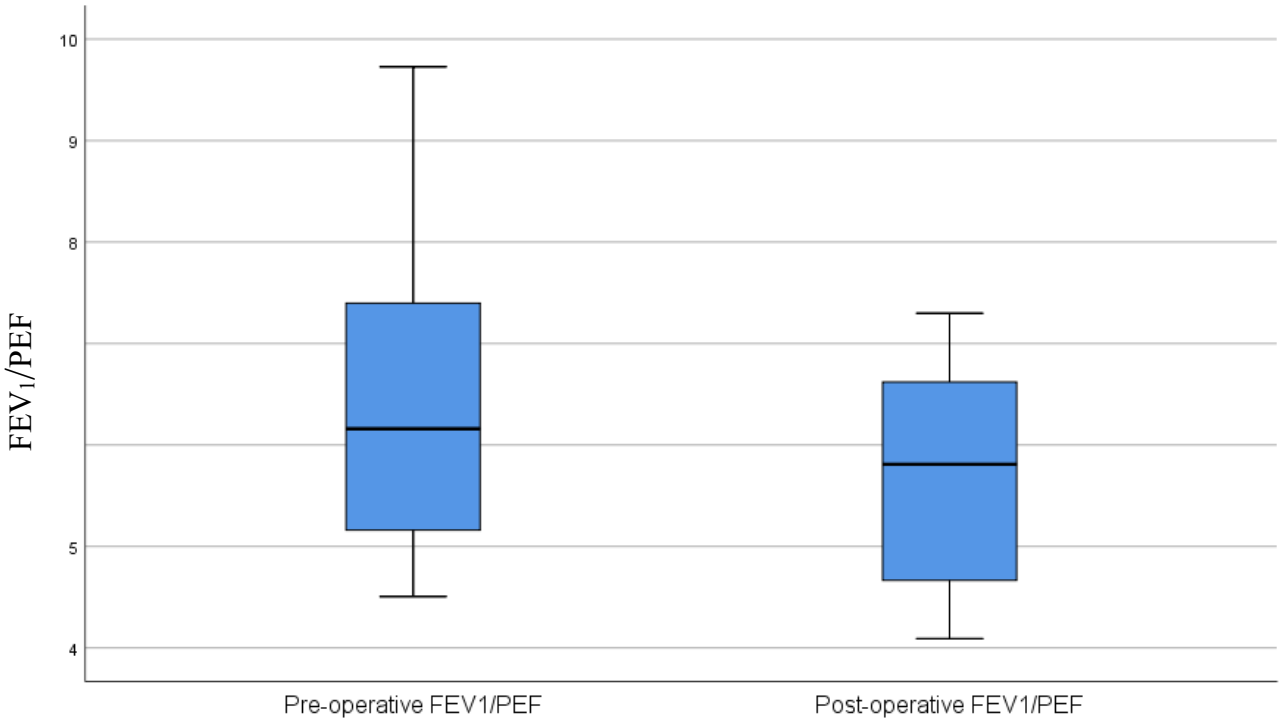


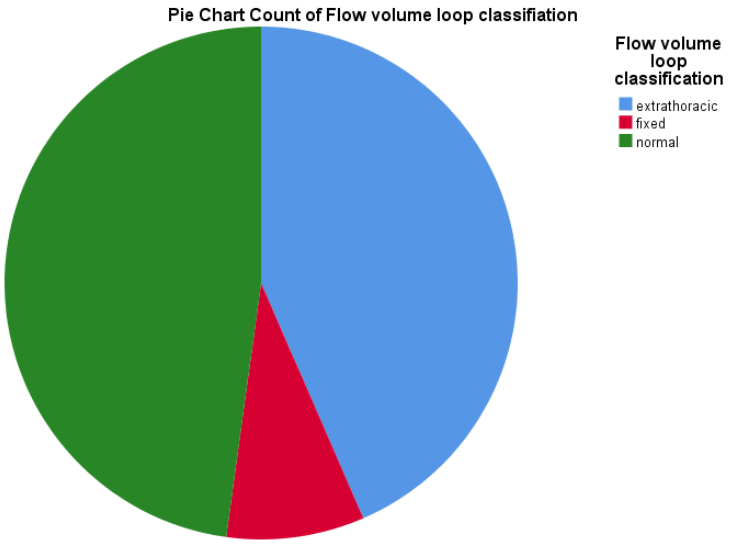
Figure 7.8. Pre- and post-operative FEV1/PEF results for the main subjects

Although not significant, there is an overall improvement in the post-operative lung function tests. Miller at al (104) also found that there was no significant difference in the pre- and post-operative lung function tests in those patients who did not have pre-operative evidence on the flow volume loop of upper airway obstruction. Sorenson et al (110) found a small but insignificant improvement in the FEV_1/PEF ratio postoperatively, similar to the findings in this study.

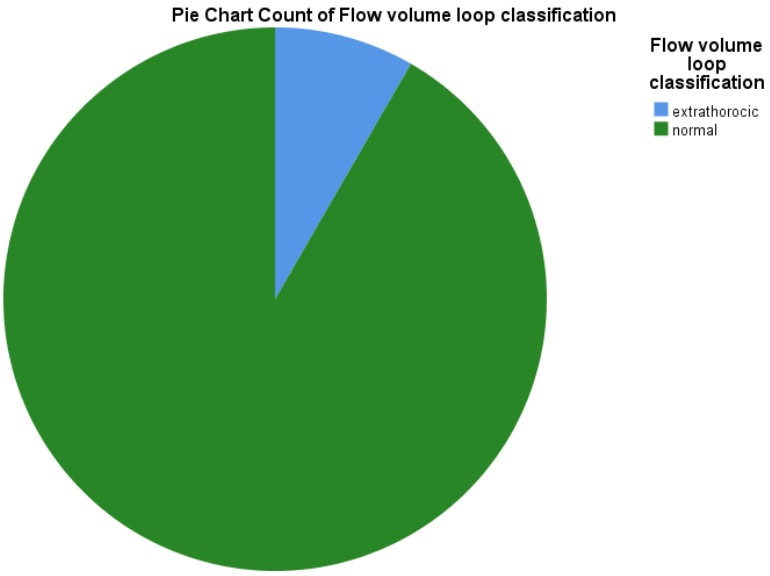
7.5.2 Visual inspection of the flow volume loops

Although the protocol for lung function pre- and post-operatively was for the study subjects to undergo both upright and supine flow volume loops, unfortunately this only took place in a small number of the subjects (4 subjects), and most had only upright flow volume loops recorded. On further investigation with the lung function testing team, the reasons for not performing the supine flow volume loops included: it was felt that a subject would be unable to lie flat in order to record a flow volume loop, or the details of the request were overlooked.

The pre-operative flow volume loops were inspected visually and classified into two main groups: normal and abnormal. The abnormal group was further subclassified into, extra thoracic obstruction, intrathoracic obstruction, or fixed obstruction. Using visual inspection of the pre-operative flow volume loops 75% had abnormal flow volume loops. 66.7% were classified as extra thoracic obstruction with flattening of the inspiratory limb, 8.3% were classified as having a fixed obstruction with flattening of both the inspiratory and expiratory limb (see figure 7.9) and 25% had a normal flow volume loop (FVL). Of the abnormal FVLs which also underwent post operative lung function testing – all but one of the FVLs improved to become normal post-operatively. This is in line with the findings by Thusoo et al (106) who found that of a group of patients with compressive thyroids undergoing surgery 60% of them had abnormal flow volume loops, all of which improved post operatively. The findings are also in keeping with Albareda at al (103) who found that out of 13 patients who had abnormal flow volume loops, 12 showed evidence of extra thoracic obstruction with flattening of the inspiratory curve, none of them showed variable intrathoracic obstruction and one showed fixed obstruction.



a) Pre-operative flow volume loops



b) Post-operative flow volume loops

Figure 7.9. a) Pre and b) post-operative flow volume loop classification

A small number of subjects (4 subjects) underwent both pre-operative sitting and supine flow volume loops. The sitting flow volume loop was abnormal in 3 of the subjects and normal in 1 subject. The appearance of the flow volume loops remained abnormal in the 3 subjects and remained normal in the 1 subject when lying flat.

7.5.3 FEV_1/PEF ratio

In the literature if the FEV_1/PEF ratio is >8 the subject is considered to have a diagnosis of UAO. Pre-operatively the mean (+/- SD) FEV_1/PEF ratio was 6.55 (+/- 1.96) with a range of 4.38-11.74. Four subjects had a FEV_1/PEF ratio of >8 whilst tested in the upright position. For the 4 subjects who underwent additional supine lung function testing, 2 subjects had an FEV_1/PEF ratio >8. These 2 subjects didn't have an FEV_1/PEF ratio>8 whilst tested sitting up. All 4 subjects who had supine lung function testing had a worse FEV_1/PEF ratio whilst lying down when compared to sitting up. Despite this being a very small number of subjects, this demonstrates that in order to capture the effect of the compressive goitre on the lung function tests the subject should ideally be tested in the supine position.

Post operatively the mean (+/-SD) was FEV_1/PEF ratio 5.68 (+/- 1.08). Using a paired sample t-test there is not a significant difference between the pre- and post-operative FEV_1/PEF ratios. The mean difference is 1.05 (t-1.826) p = 0.095. All four subjects who had an FEV_1/PEF ratio >8 pre-operatively improved post operatively with a FEV1/PEF ratio <8. All four of these subjects had pre-operative flow volume loops which showed extra thoracic upper airway obstruction with flattening of the inspiratory curve.

Sorenson et al (110) found that 30% of patients undergoing surgery for compressive thyroidectomy had an FEV_1/PEF ratio>8 and this fell to 11% postoperatively. Although the subjects in this thesis had a smaller proportion of those with an FEV_1/PEF ratio>8 pre-operatively, all of these patients had a post-operative FEV_1/PEF ratio<8.

7.5.4 Correlation between tracheal measurements and lung function tests

Table 7.5 details the correlation between the following tracheal measurements; smallest cross-sectional area (A_{min}), minimum diameter, the % reduction in the trachea when comparing the A_{min} with the cross-sectional area of the tracheal 2cm above the carina, the minimum diameter of the trachea as measured on the DICOM scan using PACS, the ellipticity of the trachea and the length of constriction (if we consider >35% constriction). Spearman's rank correlation was used for FEV_1 and for length of constriction and Pearson's rank correlation was used for all other lung function tests and tracheal measurements.

There is a positive, fair correlation between FEV_1 and the ellipticity of the trachea. As the ellipticity increases i.e., becomes less narrowed and more circular- the subject's FEV_1 increases. There are no significant correlations with the lung function tests: FEV_1 (%

predicted), FVC, FVC (%predicted), FEV_1/FVC. Interestingly, FEV_1/PEF, PEF, and PEF (% predicted) have a number of significant correlations with tracheal measurements. FEV_1/PEF has a negative fair correlation with the minimum cross-sectional area of the trachea - as the minimum cross-sectional area of the trachea reduces the FEV_1/PEF ratio increases, see figure 7.10. This is logical, given that a FEV_1/PEF>8 is thought to be diagnostic of upper airway obstruction. Likewise, there is a fair negative correlation between FEV_1/PEF and the minimum diameter and the %reduction in cross-sectional area of the trachea. There is a fair positive correlation between the FEV_1/PEF and the length of constriction, indicating that as the length of constriction increases the FEV_1/PEF ratio also increases. There is a moderate positive correlation between PEF and the minimum cross-sectional area of the trachea, the minimum diameter of the trachea and a moderate negative correlation with the % reduction in cross-sectional area of the trachea. This indicates that as the trachea is reduced in size, by the compressive goitre the PEF is also reduced.

Sorensen et al (43) carried out a similar analysis and found that the pre-operative FVC, FEV_1, and FEV_1/PEF correlated significantly with pre-operative tracheal $A_{min.}$ In our study we have found that the tracheal A_{min} correlates significantly with FEV_1/PEF, PEF, and PEF (% predicted).

Correlation coefficients and p values with spirometry values								
	FEV_1	**FEV1 (% predicted)**	**FVC**	**FVC (% predicted)**	**FEV_1/PEF**	**FEV_1/FVC**	**PEF**	**PEF (% predicted)**
A_{min}	0.294 p=0.236	-0.45 p=0.803	0.478 p=0.052	0.065 p=0.804	**-0.562 p=0.015**	0.034 p=0.896	**0.664 p=0.003**	**0.588 p=0.013**
Min Diameter	0.265 p=0.287	-0.81 p=0.757	0.456 p=0.66	0.072 p=0.782	**-0.562 p=0.015**	-0.012 p=0.963	**0.61 p=0.07**	**0.529 p=0.029**
% Reduction	-2.470 p=0.324	0.012 p=0.963	-0.402 p=0.110	-0.110 p=0.673	**0.573 p=0.013**	-0.037 p=0.889	**-0.618 p=0.006**	**-0.627 p=0.07**
Min Diameter PACS	0.284 p=0.226	0.014 p=0.955	0.463 p=0.053	0.113 p=0.656	**-0.549 p=0.014**	0.110 p=0.663	**0.626 p=0.003**	**0.579 p=0.012**
% Reduction PACS	0.046 p=0.848	-0.009 p=0.971	0.181 p=0.473	0.035 p=0.89	**-0.555 p=0.011**	0.162 p=0.521	0.365 p=0.113	0.406 p=0.095
Ellipticity	**0.475 p=0.046**	-0.177 p=0.483	0.463 p=0.053	-0.034 p=0.893	-0.428 p=0.076	-0.040 p=0.874	**0.587 p=0.010**	0.408 p=0.093
Length of constriction	-0.150 p=0.553	0.025 p=0.923	-0.292 p=0.255	-0.100 p=0.701	**0.575 p=0.013**	0.00 p=1.00	**-0.526 p=0.025**	-0.465 p=0.060

Amin = smallest cross-sectional area of the trachea, as measured using the centreline

Min Diameter = minimum diameter of the tracheal constriction, as measured using the centreline

% Reduction = % reduction in the diameter of the trachea when comparing the tracheal diameter at the trachea 2cm above the carina vs the diameter at the constriction as measured using the centreline

Min Diameter PACS = minimum diameter of the tracheal constriction, as measured using PACS

% Reduction PACS = % reduction in the diameter of the trachea when comparing the tracheal diameter 2 cm above the carina vs the diameter at the constriction as measured using PACS

Ellipticity = a measure of how elliptical the smallest cross-sectional area is

Length of constriction = length of trachea which is >35% constricted as measured using the centreline

Significant values are highlighted in **bold**

Table 7.5. Correlation co-efficient and p values for tracheal measurements and lung function tests for the study subjects

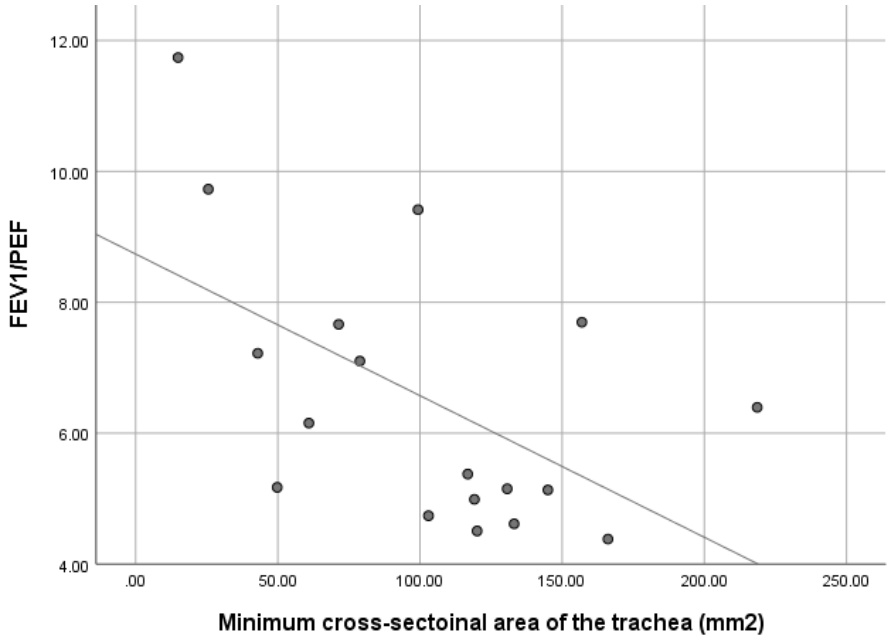


Figure 7.10. Pre-operative FEV1/PEF plotted against the minimum cross-sectional area of the trachea

7.5.5 Upright and Supine Lung function tests

4 subjects underwent upright and supine lung function tests. Below is table 7.6, showing the mean (+/- SD) of the upright and the supine tests (the data is parametric). The mean PEF and FEV_1 are reduced when the subjects are supine for their lung function testing. The FEV_1/PEF ratio is higher (indicating a greater degree of airway obstruction) when the subjects are supine. A paired sample test was used to look for a significant difference in the upright and the supine lung function tests (see table 7.7). A significant difference was not found between the lung function tests using a p value of <0.05, however the sample size is very small with only four subjects. Similar results were found by Meysman et al (107) who found that the lung function test performance measures worsened when the patient was supine when compared to sitting upright.

Lung function test	Upright Mean +/- SD	Supine Mean +/-SD
PEF	7.38 +/- 3.10	6.48 +/- 2.26
FEV_1	2.77 +/- 1.12	2.65 +/- 1.04
FEV_1/PEF	5.15 +/- 1.46	6.90 +/- 1.62

Table 7.6. Mean +/- standard deviation of upright and supine pre-operative lung function tests

Lung function test	Paired mean difference	t value	P value
PEF	0.90	2.00	0.139
FEV_1	0.12	1.68	0.192
FEV_1/PEF	-0.48	-1.92	0.150

Table 7.7. Paired samples t-test to assess for significant differences between the upright and supine pre-operative lung function tests

7.5.6 Calculating an estimate of the pressure loss using the flow volume loop

The pre-operative and post-operative flow volume loops were used to calculate the average pre- and post-operative flow rate of the inspiratory limb (see table 7.8). The mean pre-operative flow rate is lower than the mean post-operative flow rate. Overall, there appears to be an improvement in the post-operative flow rate. The difference is not statistically significant (see table 7.9). The pre- and post-operative power of the inspiratory limb of the breath have been estimated using equation 7.4 and shows that the median inspiratory pre-operative power is higher than the median inspiratory post operative power. If the pre-operative resistance across the trachea is higher than it would be expected that the inspiratory power across the trachea would be greater than post-operatively when the resistance across the trachea is lower (due to a reduction in the tracheal compression). The difference between the pre- and post-operative estimated inspiratory power is not statistically significant (see figure 7.10).

The estimated pressure-loss was calculated using equation 7.5, the pre-operative tracheal A_{min} and the pre-operative average flow rate of the inspiratory limb, as calculated from the flow volume loop. The post-operative estimate of the pressure loss was calculated using equation

7.5, the tracheal measurement of the first tracheal ring and the post-operative average flow rate of the inspiratory limb, as calculated from the flow volume loop. The post-operative pressure loss is significantly lower than pre-operative pressure loss (see table 7.8).

Parameter	Mean +/- SD	Median +/-IQ	range
Pre-operative flow rate (L/s)	1.73 +/- 0.69	-	0.59 - 2.83
Post-operative flow rate (L/s)	2.12 +/- 0.92	-	1.14 - 4.08
Pre-operative power of inspiration (W)	-	0.29 +/- 1.08	0.038 – 2.00
Post-operative power of inspiration (W)	-	0.14 +/- 0.24	0.044 – 1.48
Pre-operative pressure loss (Pa)	-	113.48 +/- 541.59	39.02 – 1508.63
Post-operative pressure loss (Pa)	-	88.53 +/- 138.05	32.40 – 515.00

Table 7.8. Pre- and post-operative measures of average flow rates, estimates of power of inspiration across the trachea and estimates of pressure loss across the trachea

Parameter	Mean of differences +/- SD	T value	P value
Flow rate (L/s)	-0.353 +/- 1.02	-1.20	0.256

Table 7.9. Paired samples test between pre- and post-operative measures of flow rate

Parameter	Wilcoxon signed rank test p value	Null Hypothesis
Power of breathing (W)	0.182	Retain
Pressure loss (Pa)	**0.026**	**Reject**

Table 7.10. Wilcoxon signed rank test between pre- and post-operative estimates of the power of breathing and pressure loss

As a means of assessing the mechanical burden that tracheal constriction imposes on a subject's ventilation, it is worth comparing the work required to drive air past the constriction with the total effort required during inspiration. A considerable number of studies have been performed on the work of breathing. Four different methodologies (oesophageal pressure catheter, plethysmographic, forced pressure oscillations and airway interrupter) have been used in the different studies, as described in Frank et al (68). However, only the first of these allows the total work required to expand the lungs and chest as well as to overcome airway resistance to be determined. Essentially the total work can be described in terms of three components: work to overcome the elastic resistance to inflate the lungs, work to overcome the airway resistance and work to accelerate the air. In order to perform the requisite work to inflate the lungs by a volume V, the difference between pleural pressure and pressure at the airway opening (taken as barometric pressure unless the subject is connected to a mechanical ventilator) amounts to the sum:

$$P = KV + R\frac{dV}{dt} + I\frac{dV^2}{dt^2} \qquad \text{Equation 7.6}$$

The last term (the inertance or resistance to acceleration) of the air is small and is generally neglected; whereas K is assumed constant, R is properly assumed to depend on dV/dt, as it is in Otis et al (67) but is often constant for a given flow rate, as in Officer et al (111).

A good description of the oesophageal pressure technique is provided in the study of Mancebo et al (112), who investigated the effect of breathing through different devices providing intermittent inspiratory support during normal ventilation and during CO_2 induced hyperventilation. Of interest for this study are the results they obtained from 7 healthy volunteers who had normal, unassisted ventilation. The mean age of this cohort was 29 years (range of 24-35 years). Airflow at the mouth was measured with a pneumotachograph. Airway pressure at the airway opening was measured using a pressure transducer at the mouth. Balloon catheter probes were used to measure the oesophageal and gastric pressures. Signals of flow, tidal volume and pressure were recorded for each breath. The work of breathing was calculated for each breath as the area enclosed between the inspiratory part of the tidal pressure-volume loop and the relaxation curve of the chest wall. The oesophageal pressure was used as a surrogate measure for pleural pressure. The chest wall is assumed to expand elastically according to the predicted value for chest wall compliance in normal subjects and is estimated

to be around 4% of the vital capacity. (113) Given that vital capacity is determined by sex and age, the estimated chest compliance range is 120-200ml/cmH_20. For the 7 healthy volunteers the minute volume was 6.7±1.5 L/min, for which the equivalent mean steady flow rate is approximately 16.75 L/min. The power of breathing for spontaneous breathing at this flow rate was calculated to be 2.4±0.7 J·min-1 which is equivalent to 0.04±0.01 Watts. Normally, the resistive component of breathing is around 25% of the total work of breathing. Therefore, the resistive component of breathing using the values from this study would be approximately 0.4 J/min.

Another study, by Cross et al (114), quantified the resistive and elastic work of breathing in 9 healthy subjects during graded exercise. At the lowest level of exercise, the minute volume was 20L/min. The tidal volume was approximately 1L and the respiratory rate was 21 breaths/minute. The corresponding steady flow rate at this minute volume is approximately 50L/min. Figure 7.12 shows a graph of the data from the Cross et al study to show the average minute volume plotted against the average estimated work of breathing in 9 healthy study subjects. The graph shows that in healthy individuals the work of breathing is estimated to be approximately 10 Joules/min (or 0.17 Watts) at a steady flow rate of approximately 20L/min.

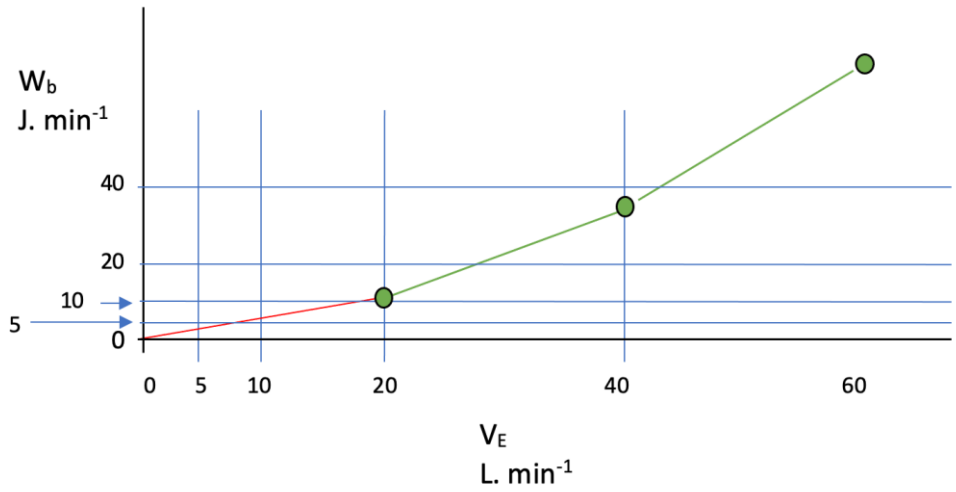


Figure 7.12 A graph taken from Cross et al (114) to show the minute volume (VE) plotted against the estimated work of breathing (Wb)

Equation 7.4 has been used to estimate the work of breathing for the main subjects in this thesis using the pressure loss, as estimated using CFD, at flow rates of 15L/min and 30L/min.

Assuming that inspiratory flow occurs 40% of the time, at a constant flow rate of 15L/min, the minute volume (V_E) is 6 L/min, and at a constant flow rate of 30L/min, the minute volume is 12L/min. For quiet breathing at a respiratory rate of 15 breaths/min, this would give a tidal volume of 400mls, and for light exercise this would give a tidal volume of 800mls. Let TRW denote tracheal resistive work.

For assumed steady flow in inspiration, the amount of work required in one minute to overcome tracheal airflow resistance is expressed as:

$$\text{TRW/min} = \Delta P \text{ across the trachea} \times V_{E.} \qquad \text{Equation 7.7}$$

where: Pa.L = Joules, J the standard unit of work. Alternatively we can calculate an average power as: $Pa.L.s^{-1} = J.s^{-}1$ = Watts, W the standard unit of power.

Flow rate (L/min)	ΔP range	TRW/min (J)	TRW/breath at RR of 15 (J)	TRW/L.s^{-1}
15	1.5 – 298	0.009 – 1.79	0.0006 – 0.12	0.0015 – 0.29
30	5.2–1057	0.06 – 12.684	0.004 – 0.85	0.01 – 2.12

Table 7.11 Estimated inspiratory tracheal resistive work of breathing for the main subjects

Therefore, for the subjects considered here, the estimated inspiratory tracheal resistive work of breathing at a flow rate of 15L/min and assuming a breathing rate of 15 breaths/min ranges from 0.009 – 1.79 J/min. Using the values from the Mancebo et al (112) paper, the estimated resistive component of breathing in healthy individuals would be approximately 0.4 J/min. In the relatively non-compressed trachea with an estimated inspiratory tracheal resistive work of breathing of 0.009 J/min, this would mean that the trachea was contributing around 2.25% of the resistive component of breathing. In a healthy individual it is estimated that the tracheal contribution to the resistive work of breathing is around 5%. In the most compressed trachea with an estimated inspiratory tracheal resistive work of breathing of 1.79 J/min, the tracheal component alone is approximately 4.5 times greater than the total estimated resistive work of breathing in a healthy individual. Further work could be carried out to investigate at what point does tracheal resistance, as a proportion of the total work of breathing, become great enough to significantly impact on the patient's symptoms.

7.6 Conclusions

Overall, there was an improvement in the post-operative FEV_1, PEF and a reduction in the FEV_1/PEF ratio, however these findings were not statistically significant. Visual inspection of the flow volume loops found that 75% had an abnormal flow volume loop and of these subjects 92% improved post operatively and had a normal flow volume loop. An FEV_1/PEF ratio >8 is used as a way of diagnosing an upper airway obstruction. 33% of subjects met these criteria on upright lung function testing. Post-operatively all 4 of these subjects had an FEV_1/PEF ratio <8.

The lung function parameters which correlated significantly with the minimum cross-sectional area were FEV_1/PEF, PEF, and PEF% of predicted. As the minimum cross-sectional area of the trachea reduces the FEV_1/PEF ratio increases. As the minimum cross-sectional area of the trachea reduces the PEF and PEF% predicted also reduce.

Four subjects underwent pre-operative upright and supine lung function testing. The lung function tests improved with the patient in the upright position indicating that in order to fully assess patients with compressive goitre the lung function testing could be carried out with the patient in the supine position. A significant difference was not found between the pre- and post- operative test results, although this is a likely to be due to the small sample size.

Post-operative pressure loss across the trachea, as estimated using equation 7.5 and the average flow rate as calculated from the post-operative flow volume loop, was significantly lower than the pre-operative pressure loss.

The estimated inspiratory power of breathing was estimated using equation 7.4 for the main subjects at a flow rate of 15L/min and 30L/min using equation 7.4. If we consider the estimated resistive component of breathing in healthy individuals to be approximately 0.4 J/min. In the most compressed trachea the estimated inspiratory tracheal resistive work of breathing is 1.79 J/min. In this subject the tracheal component alone is approximately 4.5 times greater than the total estimated resistive work of breathing in a healthy individual.

Spirometry is not routinely used in our practice to aid the surgical decision-making process and the helpfulness is debated in the literature. If it is going to be used as part of the pre-operative assessment, it seems from the literature and from our limited study of upright and supine testing, the clinician should consider performing supine lung function testing in order to capture the effects of a compressive goitre. A further study of pre-operative lung function tests in patients with compressive goitres, with larger numbers would certainly be useful.

Chapter 8 Quality of Life Questionnaires

8.1 ThyPro questionnaire and MRC dyspnoea scale
8.1.1 ThyPro Questionnaire
8.1.2 Validity and reliability of ThyPro
8.1.3 MRC dyspnoea scale
8.2 Aims
8.3 Methods
8.4 Results
8.4.1 ThyPro
8.4.2 MRC breathlessness scale
8.5 Conclusions

8.1 ThyPro questionnaire and MRC dyspnoea scale

As part of the main study in this thesis, patients undergoing thyroid surgery for retrosternal goitres were assessed both pre- and post-operatively using the ThyPro questionnaire and the MRC dyspnoea scale. Here, we will discuss the validity and reliability of these tools and their use in the literature, and why they were chosen to be used for this body of work.

8.1.1 ThyPro Questionnaire

Health related quality of life (HRQOL) is now an integral part of assessing and managing patients in the clinical setting. Measuring HRQOL can be done using generic or disease specific questionnaires. Disease specific questionnaires are more sensitive and responsive to detecting change in a disease specific group of patients than generic questionnaires. Studies looking at the sensitivity of generic HRQOL in patients undergoing thyroid surgery for benign thyroid goitres found no improvement after surgery when using the Short Form Health Survey (SF-36) and the EuroQOL-5D questionnaires. (115, 116) Watt et al (117) developed the ThyPro to be a thyroid specific quality of life (QOL) questionnaire which covers the wide range of symptoms experienced by patients with and undergoing treatment for thyroid diseases. (118) ThyPro is

now a widely used and thoroughly validated tool for use in clinical practice and is useful for detecting small changes in a patient's HRQOL over time and in response to treatment.

ThyPro is comprised of 84 items and is subdivided into the following domains (or scales); goitre symptoms, hypothyroid symptoms, hyperthyroid symptoms, eye symptoms, tiredness, cognition, anxiety, emotional susceptibility, impaired social life, impaired daily life, cosmetic complaints, and overall quality of life impact. The patient is asked to complete the questionnaire independently and score each item on a Likert scale of 0-4 with 0 being no symptoms/problems and 4 being severe symptoms/problems. The average scores across a scale are then divided by 4 and multiplied by 100 to give a scale score of 0-100. The higher the score the worse the health status of the patient. (119)

8.1.2 Validity and Reliability of ThyPro

Clinical validity and test-retest reliability of the ThyPro were investigated using a cross sectional study of 907 patients with thyroid disorders. The patients were divided into subgroups according to the type of thyroid disease they had. A body of thyroid experts were asked to predict which subgroups would be likely to score highly in each one of the domains e.g., patients with hyperthyroid Grave's disease would be expected to score highly in the hyperthyroid symptom domain. The body of experts were also asked to predict which subgroups of patients would be likely to score low in each one of the domains e.g., euthyroid patients with a non-toxic goitre would be likely to score low in the hyperthyroid domain. The patients then completed the questionnaire and the results showed significant differences between subgroups for each domain as predicted by the panel of experts. The questionnaire was, therefore, deemed to have clinical validity.

87 of the 907 patients who took the questionnaire were given the questionnaire a second time, two weeks after completing the first questionnaire. The test-retest reliability was 0.77-0.89. The threshold of test-retest probability of 0.7 is considered necessary for comparing between patient groups and the upper limit of 0.9 is considered necessary for comparing an individual patient at different points in time. Therefore, the questionnaire was deemed to have acceptable test-retest probability. (120)

Wong et al (121) performed a systematic review of HRQOL questionnaires for patients with thyroid diseases. 742 studies were included in the search and of these there were 23 studies which used 14 standardized HRQOL questionnaires. The remaining studies used non-validated questionnaires and were therefore not included. The questionnaires were graded on

methodological quality and level of evidence using the COSMIN checklist. The COSMIN checklist covers three separate domains: reliability, validity and responsiveness. The two most used and evaluated tools were the ThyPro and the Grave's ophthalmopathy-specific QOL (GO-QOL) questionnaire. The following questionnaires were rated the highest: ThyPro, GO–QOL, and the Thyroid Treatment Satisfaction Questionnaire. The authors recommended the use of ThyPro as a tool for assessing the HRQOL in patients with benign thyroid disease.

8.1.3 MRC Dyspnoea Scale

Breathlessness is one of the most common symptoms perceived by patients with a compressive thyroid goitre. This symptom is not normally measured subjectively in clinical practice and the assessment approach in this patient group is normally binary – the patient is normally asked a series of questions to assess if they experience compressive symptoms or not. It is within the clinical practice of some thyroid surgeons to request lung function tests including a flow-volume loop (FVL) as a way of assessing for evidence of upper airway obstruction however this is not normally quantified, and the assessment is based on the visual appearance of the FVL. In this thesis, the MRC dyspnoea scale was used as a simple and efficient way of quantifying patients' breathlessness symptoms both pre- and post-operatively.

The MRC dyspnoea scale (also known as MRC breathlessness scale) measures 'perceived respiratory disability'. It is a series of statements on a scale 1-5 which indicate the level of perceived breathlessness experienced by a patient. Patients complete the scale independently and are asked to circle the number which correlates to their level of breathlessness. The scale is as follows:

1) I get short of breath only on strenuous exercise
2) I get short of breath when hurrying on the level or up a slight hill
3) I walk slower than people of the same age on the level because of breathlessness or have to stop for breath when walking at my own pace on the level
4) I stop for breath after walking 100 yards or after a few minutes on the level
5) I am too breathless to leave the house

The MRC dyspnoea scale was originally developed to assess lung disease amongst coal workers but has since been widely used in the literature and in clinical practice for the assessment of lower airways disease however, it also has its uses in assessing patients with

upper airway obstruction. Nouraei et al (122) began using the MRC dyspnoea scale as part of the clinical assessment of patients with laryngotracheal stenosis and this was then later assessed for its sensitivity and responsiveness in the patient group. The authors concluded that the MRC dyspnoea scale is a useful tool for assessing dyspnoea associated with laryngotracheal stenosis.

Dyspnoea or 'breathlessness' is a symptom perceived by the patient and therefore the measurement of breathlessness is subjective. In clinical practice we attempt to measure the symptom in an objective way using lung function tests. There is a significant correlation between perceived dyspnoea and the FEV_1 as measured using lung function tests, however there is a very large spread of data which demonstrates the wide variability in how patients perceive dyspnoea. There are patients who have severe airway obstruction who report no dyspnoea and there are patients who report severe dyspnoea with very little evidence of airway obstruction. In an observational study looking at 438 patients with COPD, 32% of the patients with mild airflow obstruction, as shown on lung function tests, reported moderate to severe dyspnoea. Therefore, although there is an overall correlation of symptoms with objective measures when looking at a large population of patients, this may be less useful on an individual patient basis. (123) We are then left with the question – which measurement is more important or more clinically relevant? The objective or the subjective measurement?

An interesting point raised by Banzett et al (124) is that our objective measures to assess dyspnoea might just be inadequate. Within the airways there are thousands of enteroceptors which signal to the brain if there is inadequate gas exchange, and this is perceived on a conscious level by the patient as 'breathlessness'. The complex functioning of these enteroceptors is far away from the simplicity of spirometry and therefore surely the subjective measure of perceived dyspnoea is more valuable as an assessment tool than surrogate measures in the form of lung function tests? Dyspnoea severity is a strong predictor of 5-year mortality in COPD patients and is a better predictor than lung function parameters. It is also a better predictor of cardiac outcomes than angina in patients with cardiac disease and an overall strong predictor of mortality in the general population.

8.2 Aims

- Assess if there is a change in HRQOL in patients undergoing thyroid surgery for benign retrosternal goitres using the ThyPro HRQOL questionnaire

- For any domains of the ThyPro where there is a significant change between the pre- and post-operative score, calculate the effect size using Cohen's d
- Compare the HRQOL, using the ThyPro, of the study sample with a 'normal' population
- Determine if there is a correlation between pre-operative ThyPro scores and pre-operative lung function tests, weight of the thyroid gland excised, pre-operative tracheal measures, and estimates of pre-operative pressure loss
- Assess if there is a change in MRC dyspnoea scores pre- and post-operatively
- Determine if there a correlation between pre-operative MRC dyspnoea scores and pre-operative ThyPro Goitre symptom scores, lung function tests, weight of the thyroid gland excised, pre-operative tracheal measures, and estimates of pre-operative pressure loss

8.3 Methods

Subjects were administered the ThyPro and the MRC dyspnoea questionnaires to complete independently in the outpatient clinic following their consultation, prior to surgery and again in clinic at >6 months post operatively. If the patient was lost to follow up, they were contacted via post to complete the questionnaire with a pre-paid envelope. A follow up phone call was made if the questionnaire was not returned.

Shapiro-Wilks's test has been used to check for normality of the data. In the case of normality, parametric statistical tests have been used and, when the assumption of normality has been rejected, non-parametric statistical tests have been used.

In order to assess if there was a significant difference between the pre- and post-operative group median scores a Wilcoxon signed rank test was used. The standardized effect size has been calculated for relevant scales.

For each subject the improvement in their ThyPro score was recorded for each domain by comparing their pre-operative and post-operative score. This was recorded as a positive value if the subject's score improved and scored as a negative value if the subject's score worsened.

The normal population mean scores (+/- SD) for each scale of the ThyPro have been compared with the group mean scores of the pre- and post-operative goitre groups. A Danish study of >700 individuals taken from the national registry was used as the 'normal population'. (117)

Subjects also underwent pre- and post-operative lung function tests, as detailed in Chapter 7. Pearson's correlation was used to assess for correlation between pre-operative goitre symptom scores of the ThyPro and pre-operative lung function parameters (PEF, FEV_1, and FEV_1/PEF). Spearman's rank correlation was used to look for significant correlation between the weight of the thyroid gland removed and the pre-operative goitre symptoms domain of the ThyPro.

Subjects' pre-operative tracheal geometry underwent analysis, as described in Chapter 3. Pearson's rank correlation was used to look for correlation between pre-operative tracheal geometric analysis (smallest cross-sectional area), and the pre-operative goitre symptoms domain. Spearman's rank correlation was used to correlate the pressure loss in Pa, as estimated using CFD, for each subject with the pre-operative goitre symptoms.

The scores for the pre- and post-operative MRC dyspnoea scale were analysed. Both Pearson's and Spearman's correlation were used to assess for a relationship between the pre-operative MRC dyspnoea scale and other pre-operative variables. The correlation between the post-operative MRC dyspnoea score and the post-operative ThyPro Goitre symptom score was calculated using Spearman's rank correlation.

8.4 Results

8.4.1 ThyPro

21 patients completed pre- and post-operative ThyPro questionnaires. A number of the ThyPro item results were not normally distributed and therefore results have been displayed as median and interquartile range for consistency and comparison (see table 8.1). The non-parametric Wilcoxon signed rank test has been used to assess for a significant difference between the pre- and post-operative results for each item (see table 8.2). The score 0 depicts perfect health and the score 100 depicts worst possible health.

ThyPro Scale	Pre-operative median score (IQ range)	Post-operative median score (IQ range)
Goitre symptoms	75.00 (45.78)	0.00 (8.33)
Hyperthyroid	12.50 (43.75)	16.67 (16.67)
Hypothyroid	31.25 (37.50)	41.67 (25.00)
Eyes	0.00 (33.30)	25.00 (41.67)
Tiredness	58.30 (41.67)	66.70 (16.70)
Cognitive impairment	41.67 (50.00)	41.67 (41.67)
Anxiety	16.7 (50.00)	25.00 (24.97)
Depressivity	41.67 (41.63)	41.67 (16.70)
Emotional susceptibility	41.67 (33.37)	25.00 (24.97)
Impaired social life	0.33 (33.30)	25.00 (24.97)
Impaired daily life	25.00 (24.97)	50.00 (41.70)
Cosmetic complaints	33.30 (16.60)	8.33 (16.70)
Overall QOL	50.00 (50.00)	25.00 (50.00)

Table 8.1 Pre-operative and post-operative median scores (inter quartile range) for the ThyPro items as reported by the subjects

The two ThyPro scales which showed a significant improvement in score following thyroidectomy were Goitre symptoms and Cosmetic complaints (see table 8.2). There wasn't a significant change in the other items. We wouldn't expect there to be a significant difference in the other symptoms post-operatively because the surgery was performed for euthyroid patients undergoing thyroidectomy for benign goitres. The Overall QOL of life median score improved post operatively however the result is not significant. A study by Watt et al (5) reported that the only scales that would be expected to be high (worse HRQOL) in the pre-operative benign goitre group are Goitre symptoms and Cosmetic complaints. The finding that these are the two scales which show a significant post-operative improvement is therefore a reassuring finding.

ThyPro Scale	Wilcoxon Signed Rank test (P value)
Goitre symptoms	**0.001***
Hyperthyroid	1.000
Hypothyroid	0.343
Eyes	0.161
Tiredness	0.753
Cognitive impairment	0.646
Anxiety	0.593
Depressivity	0.721
Emotional susceptibility	0.115
Impaired social life	0.550
Impaired daily life	0.346
Cosmetic complaints	**0.016***
Overall QOL	0.178

*Table 8.2. Wilcoxon signed rank test for pre- and post-operative ThyPro scores *significant result at the p<0.05*

All patients showed an improvement in their goitre symptoms (table 8.3). Despite the fact that all patients were biochemically euthyroid post-operatively, 42.9% recorded a worsening in their hypothyroid symptoms, although this difference was not significant. All patients were placed on Levothyroxine post-operatively and their post-operative thyroid function tests were checked to ensure they were biochemically euthyroid. The majority (60%) of patients reported an improvement in their post-operative Overall QOL.

ThyPro Scale	No change (%)	Improved (%)	Worsened (%)
Goitre symptoms	0	100	0
Hyperthyroid	46.2	30.8	23.1
Hypothyroid	23.1	30.8	46.2
Eyes	35.7	21.4	42.9
Tiredness	6.67	46.7	46.7
Cognitive impairment	33.3	33.3	33.3
Anxiety	28.6	35.7	35.7
Depressivity	21.4	42.8	35.7
Emotional susceptibility	7.14	71.4	21.4
Impaired social life	28.6	35.7	35.7
Impaired daily life	7.14	35.7	57.1
Cosmetic complaints	33.3	53.3	13.3
Overall QOL	13.3	60.0	26.7

Table 8.3. % of subjects who experienced no change, an improvement in symptoms or worsened symptoms for each item of the ThyPro questionnaire when reported pre and post operatively

Looking specifically at the ThyPro scales Goitre symptoms and Cosmetic complaints, the Cohen's D effect size was calculated (see table 8.4). Cohen's D effect size assumes normality and is a way of assessing the standardised effect size of an intervention. Both sets of results for these items were normally distributed, as determined by Shapiro Wilks test. The effect of thyroidectomy on the patients' goitre symptoms is large, the effect on the patients' cosmetic complaints is moderate. Goitre symptoms is a scale which we would expect to improve post operatively, in keeping with other studies. The improvement in goitre symptoms seen in this group is greater than that of other studies (4,8), and this is likely to be because this group all had retrosternal goitres, which are likely to have a greater impact on goitre symptoms pre-operatively leading to a greater post-operative improvement. We would expect that patients' cosmetic complaints would improve post operatively if patients were bothered by the appearance of their goitre pre-operatively, although not all patients had visible goitres. Post-operatively patients have a midline scar on the neck, although in the long term these scars can become barely visible, most of these patients completed their post-operative questionnaire within 12 months of their procedure and therefore their post-operative scars may have still been

prominent. Despite this, overall, there was a significant improvement in the post-operative score of the scale Cosmetic complaint and the effect size was moderate.

ThyPro Scale	Cohen's D effect size	
Goitre symptoms	2.79	Large effect (>0.80)
Cosmetic complaints	0.59	Moderate effect (0.5-0.8)

Table 8.4. Cohen's D effect size

A Danish study developed a control group for the ThyPro questionnaire. 1200 random participants were identified using the Danish National registry and they were sent the questionnaire. (117) The mean and standard deviation (SD) for each domain is presented for this 'normal' population (see table 8.5). This 'normal' data is used to compare with the outcomes with the study participants from the work of this thesis. Interestingly, the mean score for goitre symptoms is the same in the post-operative goitre group mean and the normal population. The scores for the other scales are worse in both the pre- and post-operative goitre groups, this may reflect the demographic differences between the groups of individuals.

ThyPro Scale	Mean score (+/- SD) normal population	Mean score (+/- SD) pre-op goitre group	Mean score (+/- SD) post-op goitre group
Goitre symptoms	5 (+/- 9)	72 (+/-24)	5 (+/-7)
Hyperthyroid symptoms	12 (+/- 14)	-	20 (+/-6)
Hypothyroid symptoms	14 (+/- 16)	33 (+/-20)	36 (+/-5)
Eyes	8 (+/-11)	-	25 (+/-7)
Tiredness	35 (+/- 21)	58 (+/- 23)	64 (+/-6)
Cognitive complains	14 (+/- 17)	37 (+/-24)	35 (+/-7)
Anxiety	13 (+/- 16)	23 (+/-25)	30 (+/-6)
Depressivity	21 (+/- 18)	36 (+/-22)	41 (+/-7)
Emotional susceptibility	23 (+/- 19)	46 (+/-20)	-

Table 8.5. Mean scores for ThyPro scales for a normal population and the pre- and post-operative goitre group (where the data is not normally distributed and therefore a mean value cannot be given, the data is not presented)

Pearson's rank correlation was used to look for a relationship between pre-operative lung function tests (Peak expiratory flow (PEF), Forced expiratory volume in 1s, (FEV_1), and FEV_1/PEF) and the pre-operative ThyPro scale Goitre symptoms. A fair positive correlation was found between pre-operative goitre symptoms and the pre-operative lung function test FEV_1/PEF, and this was found to be significant (see table 8.6). A scatter plot demonstrates this relationship (see figure 8.1); as the pre-operative goitre scores worsen (0 denotes best possible outcome and 100 denotes the worst possible outcome), the pre-operative FEV_1/PEF ratio increases (see figure 8.1). Interestingly, as the FEV_1/PEF ratio increases the likelihood of upper airway obstruction increases, with some definitions of upper airway obstruction being when the FEV_1/PEF ratio is 8 or above.

Goitre symptoms vs	Pearson's r	p value
PEF (l/min)	0.002	0.995
FEV_1	0.397	0.201
FEV_1/PEF	0.584	**0.045****

*Table 8.6. Pearson's correlation between pre-operative goitre symptoms and pre-operative lung function test parameters. ** denotes statistical significance when p<0.05*

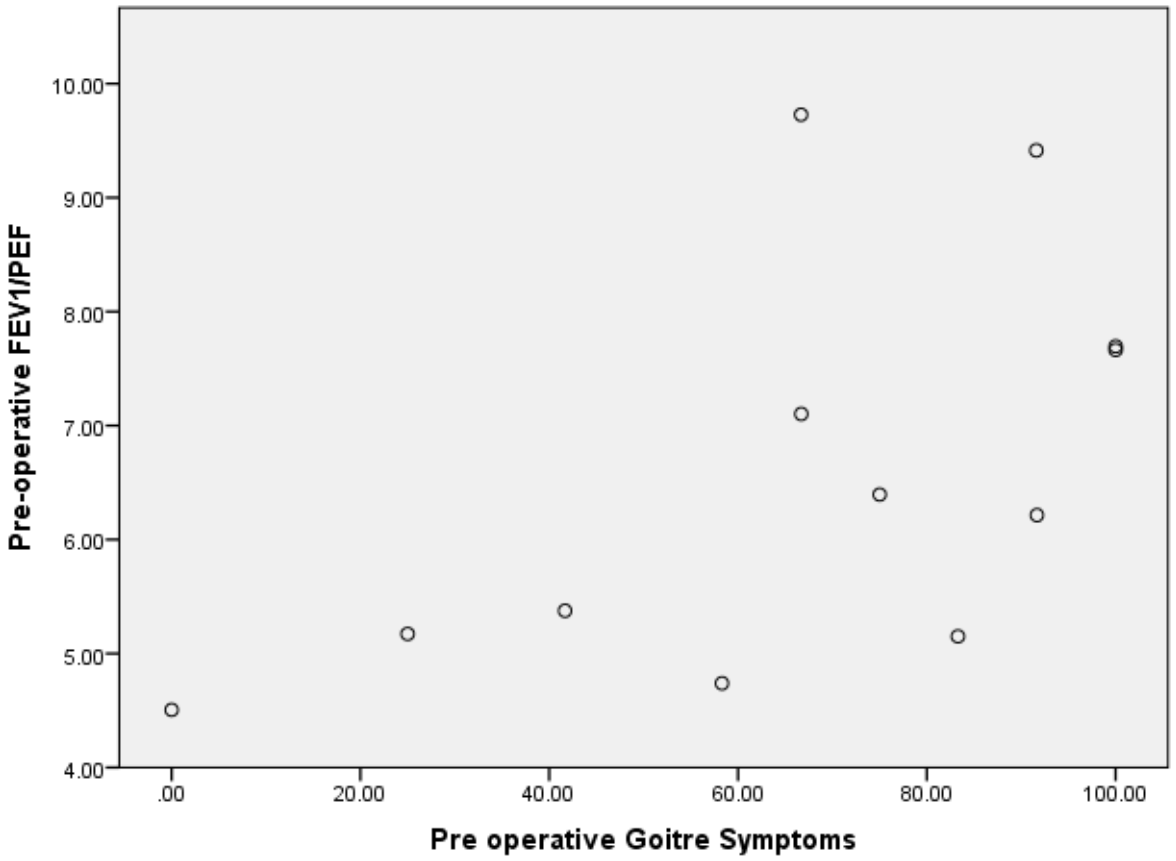


Figure 8.1. Pre-operative goitre symptoms vs pre-operative FEV1/PEF

Further analysis was performed to assess for a relationship between pre-operative goitre symptoms and: the weight of the excised thyroid gland, the pre-operative smallest cross-sectional area of the trachea and the pressure loss across the trachea as estimated using CFD at flow rates of 15L/min and 30L/min. No significant correlation was found between any of these variables (see table 8.7). This may be because of the small group size which may not have reached the size to detect a relationship.

Goitre symptoms vs	Pearson's r	Spearman's rho	p value
Weight of the excised thyroid (g)	-	0.289	0.286
Smallest cross-sectional area of the trachea (mm^2)	0.084	-	0.775
Pressure loss CFD 15L/min	-	-0.05	0.859
Pressure loss CFD 30L/min	-	-0.083	0.770

Table 8.7. Pearson's or Spearman's correlation between pre-operative goitre symptoms

8.4.2 MRC Dyspnoea Results

Twenty-one patients completed the pre- and post-operative MRC dyspnoea scoring. The median pre-operative MRC score was 3, this improved post operatively to a median MRC score of 1 (see table 8.8). Parametric and non-parametric testing was used to look at the relationship between the pre-operative MRC dyspnoea score and: the pre-operative lung function tests (PEF, FEV_1, FEV_1/PEF), the weight of the excised thyroid gland, the smallest cross-sectional area of the trachea, the pressure loss as estimated using CFD at a flow rate of 15L/min and 30L/min, and ThyPro pre-operative Goitre symptoms. There was no statistically significant correlation found between any of the variables apart from with the ThyPro pre-operative Goitre symptoms where there was a fair-moderate positive correlation (see table 8.9).

	Median (IQ range)
Pre-operative MRC dyspnoea scale score	3 (2)
Pre-operative MRC dyspnoea scale score	1 (1)

Table 8.8 Pre- and post-operative median scores (interquartile range) of the MRC dyspnoea scale score as reported by the subjects

Pre-operative MRC dyspnoea	Pearson's r	Spearman's rho	p value
PEF	0.004	-	0.894
FEV_1	-0.029	-	0.920
FEV_1/PEF	-0.026	-	0.929
Weight of the thyroid gland	-	0.141	0.566
Smallest cross-sectional area of the trachea	0.320	-	0.227
Pressure loss CFD 15L/min	-	-0.170	0.500
Pressure loss CFD 30L/min	-	-0.309	0.227
ThyPro pre-operative Goitre symptoms	**0.560****	**-**	**0.019**

*Table 8.9. Correlation co-efficient for pre-operative MRC score and: pre-operative lung function tests (PEF, FEV_1, FEV_1/PEF), weight of the excised thyroid gland, smallest cross-sectional area of the trachea, % reduction in the cross-sectional area of the trachea, pressure loss as calculated using CFD at a flow rate of 15L/min and 30L/min, and ThyPro pre-operative Goitre symptoms. **denotes statistical significance when $p<0.05$*

The limitation of using MRC dyspnoea scale is that it is only a 5-point scale and therefore if a patient has a slight improvement in their breathing post-operatively this may not be captured in this data. It also makes any correlations more difficult to identify.

MRC dyspnoea scale is a validated tool for assessing symptoms of breathlessness, however, it isn't a validated tool for specifically measuring breathlessness in patients with retrosternal goitres. There isn't a validated tool, readily available in the literature, for measuring symptoms of breathlessness in benign goitres. Nouraei et al (122) found that the pre-operative MRC dyspnoea score correlated strongly with the pre-operative degree of laryngotracheal stenosis and the pre-operative PEF and FEV_1 in a group of 40 patients known to have laryngotracheal stenosis.

The work of this thesis did not find a significant correlation between the pre-operative MRC dyspnoea score and the estimated, pre-operative estimated pressure loss across the compressed trachea, as calculated by CFD. The difference could be that laryngotracheal stenosis leads to a fixed compression of the airway which likely affects the patient's breathing in all positions. Whereas compressive goitres can vary in the degree of compression dependent on the position of the patient. Patients with compressive goitres commonly complain of positional dyspnoea when lying flat. (9) The MRC dyspnoea scale does not take into account

positional dyspnoea and therefore will not be particularly sensitive with regards to the type of breathlessness experienced by many patients with a symptomatic goitre.

8.5 Conclusions

There were two ThyPro scales which showed a significant improvement in scores following thyroidectomy: Goitre symptoms and Cosmetic complaints. All patients showed an improvement in their score for each of these two domains following thyroidectomy. The Cohen's D effect size was large for the improvement in Goitre symptoms following thyroidectomy and was moderate for the improvement in Cosmetic complaints.

There is a fair, positive correlation between pre-operative Goitre symptoms and the pre-operative FEV_1/PEF, and this was found to be statistically significant. This data set did not demonstrate any other statistically significant correlations between pre-operative Goitre symptoms and a number of other variables including PEF, FEV_1, the weight of the thyroid gland excised, the smallest cross-sectional area of the trachea, and the pre-operative pressure loss as estimated by CFD.

There was a fair-moderate positive correlation found between pre-operative MRC dyspnoea score and pre-operative ThyPro Goitre symptoms, and this was found to be statistically significant. No other statistically significant correlations were found with the pre-operative MRC dyspnoea score when looking at a range of other variables including pre-operative lung function tests, tracheal measurements, thyroid gland weight and estimated pressure loss. This may be accounted for by the fact that this was a small sample of patients, that the MRC dyspnoea score has a range of 1-5 points and thereby making it more difficult to identify relationships between this and other variables and also that the MRC breathlessness scale does not specifically ask about positional dyspnoea. Positional dyspnoea is the one of the most common types of breathing problem experienced by these patients with retrosternal goitres, the most common being exertional dyspnoea. (13) The perception of breathing involves complex neurological pathways, and it may be that patient's perceived symptoms do not match up with the objective measures we have used.

Overall, using the quality-of-life questionnaires helped patients describe their symptoms more accurately and was a useful tool in the outpatient clinic. Whilst in some post-operative clinic letters there was no mention of whether the patient's compressive symptoms had improved, both the ThyPro and the MRC scale helped to identify that there was an improvement following surgery. Health-related quality of life is an integral part of assessing a

patient. Using these tools both pre- and post-operatively will help identify which patients have benefitted from surgery.

Chapter 9 Conclusions and Further work

9.1 Geometric analysis of the airway
9.2 Validation of the tracheal volume mesh
9.3 Validation of the steady RANS model
9.4 Airflow through the tracheas of thyroid goitre study subjects
9.5 Use of CFD for surgical planning
9.6 Lung function tests
9.7 Quality of life questionnaires
9.8 Achievements and limitations
9.9 Future work
9.10 Concluding remarks

The aim of this thesis was to assess the use of computational fluid dynamics (CFD) to investigate the airflow through the tracheas of subjects with symptomatic, compressive, retrosternal thyroid goitres. In order to do this, 3D volume meshes were created to accurately represent patients' airways from individual CT scans. CFD was then used to assess airflow through the tracheas of study subjects undergoing thyroid surgery in a prospective, observational study. The CFD employed an SST (Menter) K-omega steady RANS turbulence model that was validated using an experimental model; this RANS-based model was then used to estimate pressure loss across the pathological tracheas. Twenty-one subjects were included in the study, and they underwent pre-and post-operative lung function tests and quality of life questionnaires. A geometric analysis was performed on the subjects' tracheas and the results were correlated with the pressure loss, as estimated by CFD. This chapter will highlight the key findings of the thesis.

There are a number of studies in the literature using CFD to assess airflow through the trachea, however these studies often include only one or two tracheal models. The tracheal models studied tend to be made from CT scans of healthy, anatomically normal tracheas which are then subsequently modified in a simplified way to represent a pathological stenotic segment. The work of this thesis is novel in the following respects: the study is of a series of twenty-one patients, the pathological (compressed) section of the trachea is real-life and not

digitally manipulated to represent a pathological trachea, and furthermore the study is a prospective study documenting both the pre- and post-operative quality of life of the patient. Furthermore, as many clinical scan protocols omit the glottis, whilst it may be momentarily closed in those scans which include it, a standardised glottis model has been digitally attached to each trachea, ensuring appropriate and comparable inspiratory inflow boundary conditions for each case. To our knowledge, this is the first study of its kind to validate a steady RANS k-omega turbulence model to study the airflow through the trachea of patients with compressive symptoms.

9.1 Geometric analysis of the airway

Accurate 3D representations of the main study subjects' tracheas were developed using thresholding to select the area of interest from the CT scans followed by a region growing technique. The surface meshes underwent geometric analysis. The mean cross-sectional area of the compressed part of the trachea (A_{min}) was 107.04 mm^2 (+/- 50.47). This is considerably smaller than the mean cross-sectional area of the tracheas in the study by Vock et al (37) which looked at the dimensions of healthy tracheas: men – 272 mm^2 (+/- 33) and women – 194 mm^2 (+/-35). Their study also concluded that if the tracheal cross-sectional area was less than 120mm^2 in women and less than 190mm^2 in men, this would suggest an abnormality. According to this rule of thumb, 90.5% of the main study subjects have a minimum cross-sectional area that would suggest an abnormality.

There are limitations to the geometric analysis study in the present work. The CT scans used to create surface meshes are static and although taken during 'quiet breathing' the airway may be captured at different parts of the breath cycle i.e., some subjects may be inspiring at the time of the CT scan, whilst others may be expiring. This is evident in the position of the vocal cords on the CT scans which included the glottis. The glottis can be seen in varying positions, suggesting the CT scan is taken in a different phase of the breath cycle. Although the changes to the diameter and cross-sectional area of the trachea will be minimal during quiet breathing, these changes do still exist. There are a number of studies which look at the changes in cross-sectional area of the trachea during different phases of the breath cycle, during maximum expiration the changes can be as great as 54.34% of the tracheal area.

The minimum tracheal diameter (D_{min}) was measured using the plane perpendicular to the centreline. Typically, in the clinical setting, the measurement of D_{min} would be obtained using CT scan imaging software e.g., PACS, in which it is more straightforward to measure

D_{min} in an axial plane, rather than a plane oriented perpendicular to the tracheal centreline. In the presence of goitre, the tracheal centreline is curved, so that D_{min} measured using the plane perpendicular to the centreline represents a more accurate representation of the true minimum diameter of the airway. A paired t-test was used to compare the measurements taken using the two methods. The result showed the difference to be significant, with the diameter measurements taken from PACS being significantly larger than those taken from planes perpendicular to the centreline. Using PACS measurements the mean % reduction in the diameter (D_{min}/diameter of the trachea 2cm above the carina) was 46.44 +/- 16.2, whilst using the measurements from the centreline showed a mean % reduction of 29.11 +/- 18.54. This suggests that the % reduction in tracheal diameter at the level of the maximum tracheal compression is likely to be overestimated when reviewing the CT scan in the clinical setting. The clinical implication of this is that more patients would be considered for surgery than if more accurate measurements were taken using the tracheal centreline. However, from a practical point of view, when assessing patients in clinic, there is currently insufficient time with existing software for 3D re-construction of tracheas from a CT scan or to measure the diameter or cross-sectional area of the trachea perpendicular to the centreline. If a single measurement i.e., the A_{min} was clinically validated as a measure of when to consider operating on patients with compressive goitres, this is a measurement that the radiologist could be asked to calculate on behalf of the clinical team. Future improvements in the capability, speed and ease of use of imaging software could thus improve the accuracy of geometrical assessment.

When creating a 3D representation of the airway, semi-automatic segmentation is the preferred choice due to the reduced amount of time it takes when compared to manual segmentation, and due to the improved accuracy when compared to full-automatic segmentation techniques. Semi-automatic segmentation requires an “expert” user to select a threshold. Weissheimer et al (125) demonstrated that using an interactive threshold rather than a fixed threshold produces more accurate 3D models. Therefore, for the work of this thesis, the 3D airway models were produced using an interactive threshold. Manual selection of a threshold was used for selecting the area of interest, the airway, on the CT scan of the study subjects by one ‘expert’ user. To check for intra-user variability a re-test threshold was performed >6 months since the original thresholds were selected by the same expert user. The mean difference in the original threshold and the re-test threshold was 18.18 HU (+/- 12.12). Once the tracheal surface meshes were created using the two different thresholds (original and re-test threshold) the mean difference in the A_{min} was only 1.48 mm^2 (+/-1.37). A paired t-test

showed that there was no significant difference between the A_{min} calculated from the surface geometry with the original threshold and the surface geometry with the re-test threshold. Previous studies have shown that inter-user variability in thresholding of the airway can be as high as 230 HU (56), which would have a significant impact on the A_{min} value. It is known that overall intra-user variability introduces less error than inter-user variability and therefore for a single study it is preferrable to have one 'expert' user to ensure the least amount of error is introduced. This work demonstrates that although there is still an element of intra-user variability for threshold selection, it is within an acceptable range. Going forwards it would be recommended that where possible one 'expert' user performs the task of threshold selection for creating accurate 3D surface mesh models of the tracheas in a study.

9.2 Validation of the tracheal volume mesh

A novel technique was used and validated to create the tracheal volume meshes. A number of modifications were employed in order to create tracheal models that could be made efficiently and to reduce the computational expense of running simulations to estimate pressure loss across the trachea. These modifications include the addition of a standardized glottis and the truncated airway – including the glottis but not the rest of the upper airway.

Lin et al (44) concluded that simulations of the airway through the trachea should include the larynx in order to accurately capture the flow effects of the upper airway. Choi et al (55) concluded that if the whole upper airway is not included, then a mass flow inlet should be used for the simulation. Ritchie 2019 (126) demonstrated the dramatic effect that glottic closure angle has on the pressure loss across the trachea. Due to the inter-subject variability of the glottic closure angle, in addition to the fact that some of the tracheal models did not have a glottis included, due to the limitations of the CT scan, a standardised glottis was used for all of the tracheal models. This is a novel technique that to our knowledge has not been used in the literature. The glottis was re-sized for each tracheal model and each of the models were checked to confirm they had the same glottic closure angle.

In order to validate the use of the truncated airway, two simulations were compared. A steady RANS CFD model was applied to estimate the pressure loss across a tracheal model which included a full upper airway. This value was then compared to the computed pressure loss across a model in which the geometry was identical up to just above the level of the glottis where it was then truncated. At a flow rate of 30L/min, there was a 0.8 Pa difference in the

computed pressure loss between an inlet plane above the glottis and an outlet plane above the level of the carina. This small difference is pressure loss between the two models is acceptable and is justified by the huge time and computational cost saving of using a truncated airway model.

9.3 Validation of the steady RANS model

Whilst large eddy simulation (LES) is considered to be more accurate than a RANS model of turbulence for simulating airflow through the human airway it is computationally expensive and time consuming. Running a steady RANS simulation of airflow through a tracheal model takes something in the region of a few hours, on a modest workstation, compared to LES which typically takes a number of days. A steady RANS model is computationally much cheaper than an LES model and could provide a relatively quick estimate of pressure loss across the trachea. For use as a clinical tool, ideally CFD simulations need to be computationally cheap, without compromising the accuracy. In order to validate an SST (Menter) k-omega steady RANS model of turbulence for the trachea, a study was carried out to compare the pressure loss across a tracheal model using an experimental model and the CFD simulation. Experimental work carried out by Ritchie 2019 (56), demonstrated the validity of CFD flow predictions through the trachea for a laminar flow model. This thesis used the same experimental model to validate CFD flow predictions using a steady RANS model. In the Ritchie study, a 3D surface mesh of a trachea and upper airway was printed using a 3D model with 37 pressure taps incorporated to allow for monitoring the pressure loss along the length of the model using a micromanometer and an alcohol manometer. The same 3D surface mesh was used to create a volume mesh for the CFD simulation. Measurements of static pressure were taken at the exact location as the pressure taps used in the experimental model.

An SST (Menter) k-omega steady RANS model of turbulence was used to simulate flow through the tracheal model at 30L/minute. The steady RANS model was found to provide a close fit to the experimental data, with all of the static pressure measurements along taps 1-37 being within +/- 3.5 Pa . Therefore, the steady RANS model was accepted as a method of simulating flow through the trachea for the purpose of this study.

In the main study of this thesis an SST (Menter) k-omega steady RANS model of turbulence was used to simulate flow through the trachea at flow rates 15L/min and 30L/min for twenty of the subjects. In the most constricted tracheal model (subject 21) a converged simulation was not achieved. Therefore, for this case instead, an unsteady LES model was

used. For future work in simulating flow through tracheal models, this work demonstrates that a steady RANS model is suitable for tracheas with an A_{min} of ≥ 25.7 mm^2. For highly compressed tracheas, the study indicates that an LES model may be required to obtain an accurate pressure loss estimate.

9.4 CFD assessment of the compressed airway

In comparing the pre-operative results of the RANS k-omega CFD analysis for the 21 subjects who underwent total thyroidectomy for compressive symptoms, with increasing compression, there was clearly an increased pressure loss across the trachea. The CFD computations show that static pressure exhibits the largest pressure drop at the level of the constriction in both the moderately and severely restricted tracheas. Partial recovery in pressure is observed to occur further down the trachea, when there is redistribution of the high velocity flow.

However, the CFD model provides much detail about the flow through the trachea of patients with compressive thyroid goitres, which is otherwise not available. Increased compression was observed to be associated with an increasing complexity of airflow within the trachea due to the increased strength of the 'jet' type flow induced by the constriction, breakdown of the jet, and separation of flow distal to the compressed area of the trachea. The breakdown of separated shear layers leads to the major source of fluctuations in airway flow and the areas of high vorticity in these areas. Highly accelerated flow rates and large-scale fluctuations would significantly affect the deposition patterns of inhaled therapeutic aerosols. Since aerosol deposition is known to be high in regions of high shear stress, such as the glottis, excessive deposition in the trachea could significantly compromise the ability of inhaled aerosols to reach the smaller airways. Factors other than pressure loss may thus be of significance in the assessment of compressed airways for certain patients. It is recommended that further studies on the consequences of compressed airways for aerosol deposition should be undertaken.

CFD modelling could also be a particularly useful tool when the decision to operate or not is complicated and further information is needed about the cause of the patient's breathlessness, e.g. in patients who have dual pathology of both the upper and lower airways. Given the lower Reynolds numbers of flow in the lower airways, changes in smaller airway calibre are more simply reflected in pressure loss, whereas the tracheal (and if captured by CT),

the additional bronchial pressure losses cannot be accurately estimated without CFD. The availability of CFD estimates for the large airway pressure losses overcomes this limitation, and thus the computational methodology employed here may be of more widespread clinical benefit.

Given the considerable efforts required for to set up and perform CFD simulations, part of this research also investigated the accuracy of simpler geometry-pressure loss correlations as an alternative. As stated above, the pressure loss across the trachea strongly correlates with the minimum cross-sectional area of the trachea (A_{min}). Using the A_{min} and an estimated loss coefficient could be a way of predicting pressure loss across the trachea. For this series of subjects, it was found that a loss co-efficient 1.43 and 1.3 for flow rates of 15L/min and 30L/min, respectively, accurately predicts the pressure loss (when compared with estimations of pressure loss calculated using CFD). A further study could be performed to correlate the pre-operative symptoms with predicted pre-operative pressure loss using A_{min} and a loss co-efficient, and to correlate post-operative improvement in symptoms with predicted pre-operative pressure loss. Using A_{min} and a loss co-efficient provides a very quick way of estimating the pressure loss across the trachea and would mean that a study involving a large number of subjects could take place. With a larger study, an inflexion point could be found, whereby at a certain pressure loss, the subject is likely to improve from surgery.

In young, fit and well patients with an enlarged thyroid goitre resulting in compressive symptoms, the decision to operate is more straight forward. In elderly patients with co-morbidities, when the risks of operating are much greater, surgeons and patients are presented with a more challenging decision. At present, the guidelines recommend considering surgery if there is more than a 35% constriction of the trachea. In this series of subjects, it has been found that the estimated pressure loss was only moderately correlated with the % constriction of the trachea measured using the minimum cross-sectional area of the trachea. Whereas the A_{min} and hydraulic diameter were found to be very strongly correlated with pressure loss. This would indicate that the A_{min} and the hydraulic diameter are better surrogate markers of the pressure loss across the constricted trachea. Further work could be carried out to see if there is a consistent inflexion point (of the A_{min}) where there is a sudden increase in the reported breathlessness. This inflexion point could be used as a guide to when to consider performing a thyroidectomy for high-risk patients.

One of the main limitations of this study is that it is inspiration focussed. Compressive thyroid goitres affect both inspiration and expiration. Unfortunately, it is difficult to simulate

expiration due to the difficulty in segmenting the lower airways and the lack of knowledge surrounding the expiratory flow from the lower airways. A further limitation is that a steady flow simulation was used. Breathing is cyclical and only 90% of inhalation is thought to be steady. Therefore, this work does not account for the initial and end part of inspiration where there is a changing flow rate. The flow was only simulated in truncated airway models which again further reduces the accuracy of modelling flow through the trachea.

9.5 Use of CFD for surgical planning

In addition to assessing the airway of patients with compressive goitres using CFD, simulation can also be used to assess the predicted post-operative changes. One of the subject's tracheal surface meshes was manipulated to represent the post-operative changes, with the compression removed. The trachea was severely compressed pre-operatively and the pressure loss was estimated to be 1057.3 Pa using an unsteady LES model at a flow rate of 30L/min. The predicted post-operative tracheal model had an estimated pressure loss of 18.70 Pa at 30L/min. This is a huge improvement in pressure loss across the trachea, if the trachea were to recover to its non-compressed state following thyroidectomy. Although the manipulated 'post-operative' trachea may not be an exact representation of the trachea following thyroidectomy, it is likely that the simulated post-operative trachea will provide an estimate of the expected improvements in pressure loss and other air flow parameters using CFD. Simulated post-operative changes in pressure loss could be correlated with post-operative quality of life changes in a large study of patients with compressive thyroid goitres. This could indicate at what "pressure loss improvement" leads to an improved post-operative quality of life.

There are some clinical scenarios whereby surgery can lead to a sudden expansion in the airway, which itself leads to flow disturbance. This was observed by Takeishi et al (90) in a paediatric patient who underwent surgery for tracheal stenosis. Following surgery to the stenotic segment there wasn't an improvement in the patient's symptoms. CFD demonstrated that the expansion led to flow disturbances in the airway and subsequently there wasn't an improvement in the pressure loss following corrective surgery. Predicting post operative changes is another area where using CFD can be helpful.

In order to explore the effects of a sudden expansion versus a more gradual expansion in the airway a tracheal model was modified to create two tracheal models; one with a stenotic segment followed by a sudden expansion and one with an identical stenotic segment followed

by a gradual expansion. Using an LES model of turbulence at 15L/min the pressure loss was 45.0 Pa and 43.0 Pa for the sudden and gradual expansion respectively. One might expect the pressure loss to be greater in the trachea with the more gradual expansion, due to the much longer length of constriction, however due to the greater flow disturbance in the trachea with the sudden expansion the pressure loss is roughly equivalent in both models. This highlights that simple measures such as minimum cross-sectional area or length of constriction do not tell the whole story, and airflow dynamics through the pathological trachea are complex and the detail provided by CFD simulations can be helpful.

Yang (2020) (96) carried out work in collaboration with this thesis project. The aim of the work was to assess if a simplified tracheal geometry could accurately reproduce the CFD results of the non-simplified tracheal geometry (the reference geometry), with an aim to reduce the computational cost of running simulations. Three subject's tracheal geometries were simplified using the centrelines of the reference geometries. A steady RANS computation was used to calculate the pressure loss across the simplified tracheal models and the results compared with the pressure loss across the reference tracheas. The simplified geometries fairly accurately reproduce the pressure loss across the trachea when compared to the reference geometries, with a roughly 2-3% relative difference for the moderately and severely constricted tracheas. The work stream involved in producing a simplified geometry from the reference geometry's centreline involves a lot of steps and is still quite time consuming. There is potential for this process to be simplified further. A few key parameters taken from the CT scan may be enough to recreate a much more simplified tracheal geometry. For example: the diameter taken at the first tracheal ring of the trachea, the diameter at the constriction, and the length of constriction. These measurements can be easily measured either by a clinician or by a radiologist. Future work could involve creating simplified tracheal geometries using some basic key measurements and assessing if the pressure loss across the trachea compares well with the pressure loss across the reference tracheal model.

9.6 Lung function tests

The main study subjects underwent pre- and post-operative lung function tests. When comparing the two sets of outcomes, overall, there was an improvement seen in the post-operative FEV_1, PEF and a reduction in the FEV_1/PEF ratio, although the results were not

statistically significant. 62% of the study group had a pre-operative flow volume loop with an appearance of upper airway obstruction, 92% of which had a normal flow volume loop post-operatively.

Four subjects underwent pre-operative upright and supine lung function testing. The lung function tests improved with the patient in the upright position indicating that in order to fully assess patients with compressive goitre the lung function testing could be carried out with the patient in the supine position. This small study indicates that if spirometry is going to be used as part of the pre-operative assessment of patients undergoing thyroidectomy for a compressive thyroid goitre, then the patient should undergo both upright and supine lung function tests in order to capture the effects of the compressive goitre. Future work could involve a prospective study looking at pre- and post-operative upright and supine spirometry in a larger cohort of patients.

9.7 Quality of life questionnaires

The main study subjects underwent pre- and post-surgery quality of life questionnaires: ThyPro and MRC dyspnoea scale. From the ThyPro questionnaires the goitre symptoms and cosmetic complaints showed a large and moderate improvement, respectively, following surgery. Multiple regression analysis demonstrated that pre-operative ThyPro scores do not predict the estimated pre-operative pressure loss across the compressed trachea. This is likely to be due to the fact that the ThyPro questionnaire covers a large range of complaints and isn't solely associated to the airway symptoms of the subjects.

There was a fair, positive correlation between pre-operative Goitre symptoms and the pre-operative FEV_1/PEF, and this was found to be statistically significant. This would indicate that as the size of the goitre increased the reported symptoms worsen and the lung function parameter FEV_1/PEF also worsens.

Overall, the ThyPro is a useful tool for assessing post-operative quality of life however this study has not shown that the pre-operative scores are useful in predicting the degree of pressure loss across the compressed trachea.

There was a fair-moderate positive correlation found between pre-operative MRC dyspnoea score and pre-operative ThyPro Goitre symptoms, and this was found to be statistically significant. There was also a fair-moderate positive correlation found between post-operative MRC dyspnoea score and post-operative ThyPro Goitre symptoms, and this was

found to be statistically significant. This is logical and indicates that as a subject's goitre increases in size, their symptoms as reported in the ThyPro goitre symptoms worsen and their score in the MRC breathlessness scale also worsens. No other statistically significant correlations were found in relation to the MRC dyspnoea scores however this is likely to be due to the small study size and the small range of scores in the scale (1-5). A further limitation of the MRC dyspnoea scale is that it does not ask specifically about positional dyspnoea which is one of the most common type of breathing problem experienced by patients with retrosternal goitres, the most common being exertional dyspnoea.

Due to the complexity of the perception of breathlessness, patients' symptoms do not always correlate well with quantitative measurements i.e., spirometry. Studies have shown that the dyspnoea severity as reported by the MRC dyspnoea scale is a more sensitive predictor of 5 year mortality in COPD patients than spirometry, thereby suggesting that the complex functioning of enteroceptors are far from the simplicity of spirometry. (124)

The symptom of breathlessness is one that is commonly perceived by patients with a compressive thyroid goitre. This is not normally measured using a scale or questionnaire in clinical practice and although it is unlikely to help predict which patients will benefit from surgery, it would be a useful additional tool to be used in clinic to measure the impact of the breathlessness on the patient's daily life. Importantly, it could be a helpful tool for those patients who are being managed conservatively and monitored on an annual basis, allowing clinicians to assess if the patient's perception of breathlessness is increasing over time.

9.8 Main achievements and limitations

A novel technique was used and validated to create the tracheal volume meshes. A number of modifications were employed in order to create tracheal models that could be made efficiently and to reduce the computational expense of running simulations to estimate pressure loss across the trachea. These modifications include the addition of a standardized glottis and the truncated airway – including the glottis but not the rest of the upper airway. This novel method can be used for future studies utilising CFD to estimate pressure loss across the trachea.

The work of this thesis has validated the use of an SST (Menter) k-omega steady RANS model of turbulence for the trachea in compressed tracheas with an A_{min} of ≥ 25.7 mm^2 USING

the results from a physical experiment. For highly compressed tracheas, the study indicates that an LES model may be required to obtain an accurate pressure loss estimate.

At present, the guidelines recommend considering surgery if there is more than a 35% constriction of the trachea. In this series of subjects, it has been found that the estimated pressure loss was only moderately correlated with the % constriction of the trachea measured using the minimum cross-sectional area of the trachea. Whereas the A_{min} and hydraulic diameter were found to be very strongly correlated with pressure loss. This would indicate that the A_{min} and the hydraulic diameter are better surrogate markers of the pressure loss across the constricted trachea.

The orifice loss equation and a loss co-efficient of 1.6 and 1.3 for flow rates of 15L/min and 30L/min respectively provided an accurate estimation of the pressure loss across the trachea in this cohort of patients.

A small sub-study of patients, within the work of this thesis, has demonstrated that in order to capture the effects of a compressive goitre on lung function testing then spirometry should be performed in both the upright and supine position. Future work could involve a prospective study looking at pre- and post-operative upright and supine spirometry in a larger cohort of patients.

One of the main limitations of this thesis is that the CFD studies are inspiration focussed. The 3D volumes meshes, used for employing CFD studies, have been made using a static CT image whilst the patient is inspiring. Compressive thyroid goitres affect both inspiration and expiration. Unfortunately, it is difficult to simulate expiration due to the difficulty in segmenting the lower airways and the lack of knowledge surrounding the expiratory flow from the lower airways. Therefore, the CFD studies have only been able to make an estimation of the pressure loss across the airway during inspiration. In addition to this breathing is an entirely dynamic process with much of the airway, including the trachea moving throughout the breath cycle, whilst the volumes meshes utilised in the work of this thesis are from a static CT image.

A further limitation is that a steady flow simulation was used. Breathing is cyclical and only 90% of inhalation is thought to be steady. Therefore, this work does not account for the initial

and end part of inspiration where there is a changing flow rate. The flow was only simulated in truncated airway models which again further reduces the accuracy of modelling flow through the trachea.

9.9 Future work

A_{min} was found to be very strongly correlated with estimated pressure loss across the trachea in this series of patients with compressive goitres. Further work into the geometric analysis of the airway could be carried out to see if there is a consistent inflexion point of the A_{min}, where there is a sudden increase in the reported breathlessness. This inflexion point could be used as a guide to when to consider performing a thyroidectomy for high-risk patients.

Given the reasonably accurate estimation of pressure loss across the trachea using the orifice loss equation and a loss co-efficient, a much larger prospective study of patients could be carried out to correlate surgical outcomes with the predicted pressure loss using the A_{min} of the patient's trachea and the orifice loss equation. The estimated pressure loss could be used as a predictor for surgical success and aid in surgical planning for high-risk patients when the decision to operate is not straight forward.

9.10 Concluding remarks

It is hoped that this work has provided a foundation for future work in the field of assessing the airflow through compressed tracheal models. For elderly, complex patients with dual airway pathology e.g., a compressive thyroid goitre and COPD, providing an estimate of the pressure loss across the trachea could be an extremely useful adjunct when considering whether to perform a thyroidectomy. Although there isn't a clear role for the use of CFD in assessing patients with compressive thyroid goitres in the clinical setting at present, further work using simplified techniques of estimating pressure loss may demonstrate that a simple measure e.g., A_{min}, or the hydraulic diameter may provide a clinically useful inflexion point at which patients are more likely to benefit from surgery.

Bibliography

1. Berghout A, Wiersinga WM, Smits NJ, Touber JL. Determinants of thyroid volume as measured by ultrasonography in healthy adults in a non-iodine deficient area. Clin Endocrinol (Oxf). 1987;26(3):273-80.
2. CFCF. Diagrammatic view of thyroid gland. p. https://commons.wikimedia.org/wiki/File:Anterior_thyroid.jpg.
3. Katlic MR, Grillo HC, Wang CA. Substernal goiter. Analysis of 80 patients from Massachusetts General Hospital. Am J Surg. 1985;149(2):283-7.
4. Kiriyak ND. The thoracic inlet. p. https://commons.wikimedia.org/wiki/File:Anatomy_of_the_thoracic_inlet.webp.
5. Carlson BM. The Human body Chapter 9 The Endocrine system: Academic press; 2019.
6. Vanderpump MP, Tunbridge WM, French JM, Appleton D, Bates D, Clark F, et al. The incidence of thyroid disorders in the community: a twenty-year follow-up of the Whickham Survey. Clin Endocrinol (Oxf). 1995;43(1):55-68.
7. Day TA, Chu A, Hoang KG. Multinodular goiter. Otolaryngol Clin North Am. 2003;36(1):35-54.
8. Lindskog BI, Malm A. Diagnostic and Surgical Considerations on Mediastinal (Intrathoracic) Goiter. Dis Chest. 1965;47:201-7.
9. Banks CA, Ayers CM, Hornig JD, Lentsch EJ, Day TA, Nguyen SA, et al. Thyroid disease and compressive symptoms. Laryngoscope. 2012;122(1):13-6.
10. White ML, Doherty GM, Gauger PG. Evidence-based surgical management of substernal goiter. World J Surg. 2008;32(7):1285-300.
11. Cirocchi R, Trastulli S, Randolph J, Guarino S, Di Rocco G, Arezzo A, et al. Total or near-total thyroidectomy versus subtotal thyroidectomy for multinodular non-toxic goitre in adults. Cochrane Database Syst Rev. 2015(8):CD010370.
12. Pieracci FM, Fahey TJ, 3rd. Substernal thyroidectomy is associated with increased morbidity and mortality as compared with conventional cervical thyroidectomy. J Am Coll Surg. 2007;205(1):1-7.
13. Stang MT, Armstrong MJ, Ogilvie JB, Yip L, McCoy KL, Faber CN, et al. Positional dyspnea and tracheal compression as indications for goiter resection. Arch Surg. 2012;147(7):621-6.
14. Bates AJ, Cetto R, Doorly DJ, Schroter RC, Tolley NS, Comerford A. The effects of curvature and constriction on airflow and energy loss in pathological tracheas. Respir Physiol Neurobiol. 2016;234:69-78.
15. unknown. Schematic of the upper and lower airways. p. https://commons.wikimedia.org/wiki/File:Poumons2.jpg.
16. Radiology of the trachea [Internet]. UptoDate. [cited 14.01.2021]. Available from: https://www.uptodate.com/contents/radiology-of-the-trachea.
17. , BruceBlaus. Trachea. p. https://commons.wikimedia.org/wiki/File:Blausen_0865_TracheaAnatomy.png.
18. Vihsadas. Lung Volumes. p. https://commons.wikimedia.org/wiki/File:LungVolume.jpg.
19. Physiology of dyspnoea [Internet]. UptoDate. 2020 [cited 14.01.2020]. Available from: https://www.uptodate.com/contents/physiology-of-dyspnea.
20. UptoDate. Efferent and afferent signals that contribute to the sensation of dyspnea. 5.0 ed. UptoDate.

21. Faizal WM, Ghazali NNN, Khor CY, Badruddin IA, Zainon MZ, Yazid AA, et al. Computational fluid dynamics modelling of human upper airway: A review. Comput Methods Programs Biomed. 2020;196:105627.
22. Mylavarapu G, Mihaescu M, Fuchs L, Papatziamos G, Gutmark E. Planning human upper airway surgery using computational fluid dynamics. J Biomech. 2013;46(12):1979-86.
23. Bates AJ, Comerford A, Cetto R, Doorly DJ, Schroter RC, Tolley NS. Computational fluid dynamics benchmark dataset of airflow in tracheas. Data Brief. 2017;10:101-7.
24. Ma B, Lutchen KR. CFD simulation of aerosol deposition in an anatomically based human large-medium airway model. Ann Biomed Eng. 2009;37(2):271-85.
25. Riazuddin VN, Zubair M, Abdullah MZ, Ismail R, Shuaib IL, Hamid SA, et al. Numerical Study of Inspiratory and Expiratory Flow in a Human Nasal Cavity. Journal of Medical and Biological Engineering. 2011;31(3):201-6.
26. Longest PW, Tian G, Khajeh-Hosseini-Dalasm N, Hindle M. Validating Whole-Airway CFD Predictions of DPI Aerosol Deposition at Multiple Flow Rates. J Aerosol Med Pulm Drug Deliv. 2016;29(6):461-81.
27. Stapleton KW, Finlay WH. On the paper "estimation of the size distribution of aerosols produced by jet nebulizers as a function of time". Journal of Aerosol Science. 1999;30(3):393-5.
28. Bates AJ, Comerford A, Cetto R, Schroter RC, Tolley NS, Doorly DJ. Power loss mechanisms in pathological tracheas. J Biomech. 2016;49(11):2187-92.
29. Xiao Q, Cetto R, Doorly DJ, Bates AJ, Rose JN, McIntyre C, et al. Assessing Changes in Airflow and Energy Loss in a Progressive Tracheal Compression Before and After Surgical Correction. Ann Biomed Eng. 2020;48(2):822-33.
30. De Backer JW, Vanderveken OM, Vos WG, Devolder A, Verhulst SL, Verbraecken JA, et al. Functional imaging using computational fluid dynamics to predict treatment success of mandibular advancement devices in sleep-disordered breathing. J Biomech. 2007;40(16):3708-14.
31. Zhao K, Malhotra P, Rosen D, Dalton P, Pribitkin EA. Computational fluid dynamics as surgical planning tool: a pilot study on middle turbinate resection. Anat Rec (Hoboken). 2014;297(11):2187-95.
32. Moore VC. Spiromtery: step by step. Breathe. 2012;8.
33. Jmarchn. Doing Spirometry. 2013. p. https://commons.wikimedia.org/wiki/File:DoingSpirometry.JPG.
34. Rugiu MG, Piemonte M. Surgical approach to retrosternal goitre: do we still need sternotomy? Acta Otorhinolaryngol Ital. 2009;29(6):331-8.
35. Chen AY, Bernet VJ, Carty SE, Davies TF, Ganly I, Inabnet WB, 3rd, et al. American Thyroid Association statement on optimal surgical management of goiter. Thyroid. 2014;24(2):181-9.
36. Shepard JO, Flores EJ, Abbott GF. Imaging of the trachea. Ann Cardiothorac Surg. 2018;7(2):197-209.
37. Vock P, Spiegel T, Fram EK, Effmann EL. CT assessment of the adult intrathoracic cross section of the trachea. J Comput Assist Tomogr. 1984;8(6):1076-82.
38. Ranu H, Wilde M, Madden B. Pulmonary function tests. Ulster Med J. 2011;80(2):84-90.
39. Stern EJ, Graham CM, Webb WR, Gamsu G. Normal trachea during forced expiration: dynamic CT measurements. Radiology. 1993;187(1):27-31.
40. Boiselle PM, O'Donnell CR, Bankier AA, Ernst A, Millet ME, Potemkin A, et al. Tracheal collapsibility in healthy volunteers during forced expiration: assessment with multidetector CT. Radiology. 2009;252(1):255-62.

41. Petersen J, Wille MM, Raket LL, Feragen A, Pedersen JH, Nielsen M, et al. Effect of inspiration on airway dimensions measured in maximal inspiration CT images of subjects without airflow limitation. Eur Radiol. 2014;24(9):2319-25.
42. Ederle JR, Heussel CP, Hast J, Fischer B, Van Beek EJ, Ley S, et al. Evaluation of changes in central airway dimensions, lung area and mean lung density at paired inspiratory/expiratory high-resolution computed tomography. Eur Radiol. 2003;13(11):2454-61.
43. Sorensen JR, Lauridsen JF, Dossing H, Nguyen N, Hegedus L, Bonnema SJ, et al. Thyroidectomy Improves Tracheal Anatomy and Airflow in Patients with Nodular Goiter: A Prospective Cohort Study. Eur Thyroid J. 2017;6(6):307-14.
44. Lin EL, Bock JM, Zdanski CJ, Kimbell JS, Garcia GJM. Relationship between degree of obstruction and airflow limitation in subglottic stenosis. Laryngoscope. 2018;128(7):1551-7.
45. Reynisson PJ, Scali M, Smistad E, Hofstad EF, Leira HO, Lindseth F, et al. Airway Segmentation and Centerline Extraction from Thoracic CT - Comparison of a New Method to State of the Art Commercialized Methods. PLoS One. 2015;10(12):e0144282.
46. Aykac D, Hoffman EA, McLennan G, Reinhardt JM. Segmentation and analysis of the human airway tree from three-dimensional X-ray CT images. IEEE Trans Med Imaging. 2003;22(8):940-50.
47. Lamba R, McGahan JP, Corwin MT, Li CS, Tran T, Seibert JA, et al. CT Hounsfield numbers of soft tissues on unenhanced abdominal CT scans: variability between two different manufacturers' MDCT scanners. AJR Am J Roentgenol. 2014;203(5):1013-20.
48. Tschirren J, Hoffman EA, McLennan G, Sonka M. Intrathoracic airway trees: segmentation and airway morphology analysis from low-dose CT scans. IEEE Trans Med Imaging. 2005;24(12):1529-39.
49. Conradi SH, Lutey BA, Atkinson JJ, Wang W, Senior RM, Gierada DS. Measuring small airways in transverse CT images correction for partial volume averaging and airway tilt. Acad Radiol. 2010;17(12):1525-34.
50. Nakano H, Mishima K, Ueda Y, Matsushita A, Suga H, Miyawaki Y, et al. A new method for determining the optimal CT threshold for extracting the upper airway. Dentomaxillofac Radiol. 2013;42(3):26397438.
51. Weissheimer A, de Menezes LM, Sameshima GT, Enciso R, Pham J, Grauer D. Imaging software accuracy for 3-dimensional analysis of the upper airway. American Journal of Orthodontics and Dentofacial Orthopedics. 2012;142(6):801-13.
52. Taubin G. LINEAR ANISOTROPIC MESH FILTERING. IBM T.J. Watson Research Center; 2001.
53. Piccinelli M, Veneziani A, Steinman DA, Remuzzi A, Antiga L. A framework for geometric analysis of vascular structures: application to cerebral aneurysms. IEEE Trans Med Imaging. 2009;28(8):1141-55.
54. Lin CL, Tawhai MH, McLennan G, Hoffman EA. Characteristics of the turbulent laryngeal jet and its effect on airflow in the human intra-thoracic airways. Respir Physiol Neurobiol. 2007;157(2-3):295-309.
55. Choi J, Tawhai MH, Hoffman EA, Lin CL. On intra- and intersubject variabilities of airflow in the human lungs. Phys Fluids (1994). 2009;21(10):101901.
56. Ritchie L. 'Application of computational methods as an adjunct to upper airway assessment': Imperial College, London; 2018.
57. Brouns M, Verbanck S, Lacor C. Influence of glottic aperture on the tracheal flow. J Biomech. 2007;40(1):165-72.
58. Brancatisano T, Collett PW, Engel LA. Respiratory movements of the vocal cords. J Appl Physiol Respir Environ Exerc Physiol. 1983;54(5):1269-76.

59. Dekker E. Transition between laminar and turbulent flow in human trachea. J Appl Physiol. 1961;16:1060-4.
60. Bates AJ, Doorly DJ, Cetto R, Calmet H, Gambaruto AM, Tolley NS, et al. Dynamics of airflow in a short inhalation. J R Soc Interface. 2015;12(102):20140880.
61. Bonnema SJ. Upper airway obstruction due to goiter: an overlooked problem! J Postgrad Med. 2008;54(2):82-3.
62. Brouns M, Jayaraju ST, Lacor C, De Mey J, Noppen M, Vincken W, et al. Tracheal stenosis: a flow dynamics study. J Appl Physiol (1985). 2007;102(3):1178-84.
63. Persak SC, Sin S, McDonough JM, Arens R, Wootton DM. Noninvasive estimation of pharyngeal airway resistance and compliance in children based on volume-gated dynamic MRI and computational fluid dynamics. J Appl Physiol (1985). 2011;111(6):1819-27.
64. Mylavarapu G, Murugappan S, Mihaescu M, Kalra M, Khosla S, Gutmark E. Validation of computational fluid dynamics methodology used for human upper airway flow simulations. J Biomech. 2009;42(10):1553-9.
65. Loring SH, Topulos GP, Hubmayr RD. Transpulmonary Pressure: The Importance of Precise Definitions and Limiting Assumptions. Am J Respir Crit Care Med. 2016;194(12):1452-7.
66. Powell T, Williams EM. Effect of resistive load on the inspiratory work and power of breathing during exertion. PLoS One. 2012;7(11):e49681.
67. Otis AB, Fenn WO, Rahn H. Mechanics of breathing in man. J Appl Physiol. 1950;2(11):592-607.
68. Frank NR, Mead J, Whittenberger JL. Comparative sensitivity of four methods for measuring changes in respiratory flow resistance in man. J Appl Physiol. 1971;31(6):934-8.
69. Chovancova M, Elcner J. The pressure gradient in the human respiratory tract. Epj Web Conf. 2014;67.
70. Olson DE, Dart GA, Filley GF. Pressure drop and fluid flow regime of air inspired into the human lung. J Appl Physiol. 1970;28(4):482-94.
71. Banner MJ. Respiratory muscle loading and the work of breathing. J Cardiothorac Vasc Anesth. 1995;9(2):192-204.
72. Bates AJ, Comerford A, Cetto R, Schroter RC, Tolley NS, Doorly DJ. Power loss mechanisms in pathological tracheas. J Biomech. 2016;49(11):2187-92.
73. Shih TC HH, Chen PY, Tu CY, Tseng TI, Ho YJ. Study of pre- and post-stent implantation in the trachea using computational fluid dynamics. J Med Biol Eng. 2014;34(2):150–156.
74. Wassermann K, Koch A, Warschkow A, Mathen F, Muller-Ehmsen J, Eckel HE. Measuring in situ central airway resistance in patients with laryngotracheal stenosis. Laryngoscope. 1999;109(9):1516-20.
75. Pedley TJ, Schroter RC, Sudlow MF. The prediction of pressure drop and variation of resistance within the human bronchial airways. Respir Physiol. 1970;9(3):387-405.
76. Markow M, Janecki D, Orecka B, Misiolek M, Warmuzinski K. Computational fluid dynamics in the assessment of patients' postoperative status after glottis-widening surgery. Adv Clin Exp Med. 2017;26(6):947-52.
77. Chen FL, Horng TL, Shih TC. Simulation analysis of airflow alteration in the trachea following the vascular ring surgery based on CT images using the computational fluid dynamics method. J Xray Sci Technol. 2014;22(2):213-25.
78. Verbanck S, de Keukeleire T, Schuermans D, Meysman M, Vincken W, Thompson B. Detecting upper airway obstruction in patients with tracheal stenosis. J Appl Physiol (1985). 2010;109(1):47-52.
79. Bates AJ. Mechanics of Airflow in Human Inhalation: Imperial College London; 2014.

80. Choi S, Miyawaki S, Lin CL. A Feasible Computational Fluid Dynamics Study for Relationships of Structural and Functional Alterations with Particle Depositions in Severe Asthmatic Lungs. Comput Math Methods Med. 2018;2018:6564854.
81. Martonen TB, Zhang Z, Yu G, Musante CJ. Three-dimensional computer modeling of the human upper respiratory tract. Cell Biochem Biophys. 2001;35(3):255-61.
82. Fulcher LP, Scherer RC, Anderson NV. Entrance loss coefficients and exit coefficients for a physical model of the glottis with convergent angles. J Acoust Soc Am. 2014;136(3):1312.
83. Anastasiadou S, Al Yaghchi C. Glottic Stenosis. StatPearls. Treasure Island (FL)2022.
84. Fukushi I, Pokorski M, Okada Y. Mechanisms underlying the sensation of dyspnea. Respir Investig. 2021;59(1):66-80.
85. Schwartzstein RM, Simon PM, Weiss JW, Fencl V, Weinberger SE. Breathlessness induced by dissociation between ventilation and chemical drive. Am Rev Respir Dis. 1989;139(5):1231-7.
86. Song B, Li Y, Sun J, Qi Y, Li P, Li Y, et al. Computational fluid dynamics simulation of changes in the morphology and airflow dynamics of the upper airways in OSAHS patients after treatment with oral appliances. PLoS One. 2019;14(11):e0219642.
87. Capelli C, Sauvage E, Giusti G, Bosi GM, Ntsinjana H, Carminati M, et al. Patient-specific simulations for planning treatment in congenital heart disease. Interface Focus. 2018;8(1):20170021.
88. Sundareswaran KS, de Zelicourt D, Sharma S, Kanter KR, Spray TL, Rossignac J, et al. Correction of pulmonary arteriovenous malformation using image-based surgical planning. JACC Cardiovasc Imaging. 2009;2(8):1024-30.
89. Findlay JM, Sadler GP, Bridge H, Mihai R. Post-thyroidectomy tracheomalacia: minimal risk despite significant tracheal compression. Br J Anaesth. 2011;106(6):903-6.
90. Takeishi N, Miki T, Otani T, Ii S, Morita K, Wada S. Fluid dynamic assessment of tracheal flow in infants with congenital tracheal stenosis before and after surgery. Medical & Biological Engineering & Computing. 2019;57(4):837-47.
91. Forrester J. Flow through a converging-diverging tube and its implications in occlusive vascular disease: Iowa state univeristy; 1968.
92. Cleynen O. Boundary Layer Separation. 2015.
93. S. Taherian HRR, J. Bonifacio, B. Z. Gomez, Thomas Waddington. Particulate Deposition in a Patient With Tracheal Stenosis. Journal of Engineering and Science in Medical Diagnostics and Therapy. 2018;Vol. 1.
94. Yu S, Wang J, Sun X, Liu Y. Numerical study of the effects of bronchial structural abnormalities on respiratory flow distribution. Biomed Eng Online. 2016;15(Suppl 2):164.
95. E.M. Sparrow JPA, *, W.J. Minkowycz Flow separation in a diverging conical duct: Effect of Reynolds number and divergence angle. International Journal of Heat and Mass Transfer. 2009;2 (2009) 3079–3083.
96. Yang W. Application of Computational Science to Diagnosis and Modelling of Flow in the Trachea: Imperial College London; 2020.
97. Insitute NHLaB. Spirometry NIH. 2013.
98. Miller MR, Hankinson J, Brusasco V, Burgos F, Casaburi R, Coates A, et al. Standardisation of spirometry. Eur Respir J. 2005;26(2):319-38.
99. SPhotographer J. Flow-volume-loop. 2012.
100. Pellegrino R, Viegi G, Brusasco V, Crapo RO, Burgos F, Casaburi R, et al. Interpretative strategies for lung function tests. Eur Respir J. 2005;26(5):948-68.
101. UK A. 2022.

102. Geraghty JG, Coveney EC, Kiernan M, O'Higgins NJ. Flow volume loops in patients with goiters. Ann Surg. 1992;215(1):83-6.
103. Albareda M, Viguera J, Santiveri C, Lozano P, Mestron A, Bengoa N, et al. Upper airway obstruction in patients with endothoracic goiter enlargement: no relationship between flow-volume loops and radiological tests. Eur J Endocrinol. 2010;163(4):665-9.
104. Miller MR, Pincock AC, Oates GD, Wilkinson R, Skene-Smith H. Upper airway obstruction due to goitre: detection, prevalence and results of surgical management. Q J Med. 1990;74(274):177-88.
105. Melissant CF, Smith SJ, Perlberger R, Verschakelen J, Lammers JW, Demedts M. Lung function, CT-scan and X-ray in upper airway obstruction due to thyroid goitre. Eur Respir J. 1994;7(10):1782-7.
106. Thusoo TK, Gupta U, Kochhar K, Hira HS. Upper airway obstruction in patients with goiter studies by flow volume loops and effect of thyroidectomy. World J Surg. 2000;24(12):1570-2.
107. Meysman M, Noppen M, Vincken W. Effect of posture on the flow-volume loop in two patients with euthyroid goiter. Chest. 1996;110(6):1615-8.
108. Loring SH, Garcia-Jacques M, Malhotra A. Pulmonary characteristics in COPD and mechanisms of increased work of breathing. J Appl Physiol (1985). 2009;107(1):309-14.
109. Qi S, Li Z, Yue Y, van Triest HJ, Kang Y. Computational fluid dynamics simulation of airflow in the trachea and main bronchi for the subjects with left pulmonary artery sling. Biomed Eng Online. 2014;13:85.
110. Sorensen JR, Hegedus L, Kruse-Andersen S, Godballe C, Bonnema SJ. The impact of goitre and its treatment on the trachea, airflow, oesophagus and swallowing function. A systematic review. Best Pract Res Clin Endocrinol Metab. 2014;28(4):481-94.
111. Officer TM, Pellegrino R, Brusasco V, Rodarte JR. Measurement of pulmonary resistance and dynamic compliance with airway obstruction. J Appl Physiol (1985). 1998;85(5):1982-8.
112. Mancebo J, Isabey D, Lorino H, Lofaso F, Lemaire F, Brochard L. Comparative effects of pressure support ventilation and intermittent positive pressure breathing (IPPB) in non-intubated healthy subjects. Eur Respir J. 1995;8(11):1901-9.
113. Fleury B, Murciano D, Talamo C, Aubier M, Pariente R, Milic-Emili J. Work of breathing in patients with chronic obstructive pulmonary disease in acute respiratory failure. Am Rev Respir Dis. 1985;131(6):822-7.
114. Cross TJ, Sabapathy S, Beck KC, Morris NR, Johnson BD. The resistive and elastic work of breathing during exercise in patients with chronic heart failure. Eur Respir J. 2012;39(6):1449-57.
115. Schmitz-Winnenthal FH, Schimmack S, Lawrence B, Maier U, Heidmann M, Buchler MW, et al. Quality of life is not influenced by the extent of surgery in patients with benign goiter. Langenbecks Arch Surg. 2011;396(8):1157-63.
116. Promberger R, Hermann M, Pallikunnel SJ, Seemann R, Meusel M, Ott J. Quality of life after thyroid surgery in women with benign euthyroid goiter: influencing factors including Hashimoto's thyroiditis. Am J Surg. 2014;207(6):974-9.
117. Cramon P, Bonnema SJ, Bjorner JB, Ekholm O, Feldt-Rasmussen U, Frendl DM, et al. Quality of life in patients with benign nontoxic goiter: impact of disease and treatment response, and comparison with the general population. Thyroid. 2015;25(3):284-91.
118. Watt T, Bjorner JB, Groenvold M, Rasmussen AK, Bonnema SJ, Hegedus L, et al. Establishing construct validity for the thyroid-specific patient reported outcome measure (ThyPRO): an initial examination. Qual Life Res. 2009;18(4):483-96.

119. Watt T, Cramon P, Hegedus L, Bjorner JB, Bonnema SJ, Rasmussen AK, et al. The thyroid-related quality of life measure ThyPRO has good responsiveness and ability to detect relevant treatment effects. J Clin Endocrinol Metab. 2014;99(10):3708-17.
120. Watt T, Hegedus L, Groenvold M, Bjorner JB, Rasmussen AK, Bonnema SJ, et al. Validity and reliability of the novel thyroid-specific quality of life questionnaire, ThyPRO. Eur J Endocrinol. 2010;162(1):161-7.
121. Wong CK, Lang BH, Lam CL. A systematic review of quality of thyroid-specific health-related quality-of-life instruments recommends ThyPRO for patients with benign thyroid diseases. J Clin Epidemiol. 2016;78:63-72.
122. Nouraei SA, Nouraei SM, Randhawa PS, Butler CR, Magill JC, Howard DJ, et al. Sensitivity and responsiveness of the Medical Research Council dyspnoea scale to the presence and treatment of adult laryngotracheal stenosis. Clin Otolaryngol. 2008;33(6):575-80.
123. Mullerova H, Lu C, Li H, Tabberer M. Prevalence and burden of breathlessness in patients with chronic obstructive pulmonary disease managed in primary care. PLoS One. 2014;9(1):e85540.
124. Banzett RB, O'Donnell CR. Should we measure dyspnoea in everyone? Eur Respir J. 2014;43(6):1547-50.
125. Weissheimer A, Menezes LM, Sameshima GT, Enciso R, Pham J, Grauer D. Imaging software accuracy for 3-dimensional analysis of the upper airway. Am J Orthod Dentofacial Orthop. 2012;142(6):801-13.
126. Ritchie L. Application of computational methods as an adjunct to upper airway assessment: Imperial College London; 2019.
127. McIntyre C, Jacques T, Palazzo F, Farnell K, Tolley N. Quality of life in differentiated thyroid cancer. Int J Surg. 2018;50:133-6.
128. McIntyre C, Tolley N. A critical review of thyroidectomy consent in the UK. International Journal of Surgery. 2019;66:84-8.
129. Calmet H, Bertomeu PF, McIntyre C, Rennie C, Gouder K, Houzeaux G, et al. Computational modelling of an aerosol extraction device for use in COVID-19 surgical tracheotomy. J Aerosol Sci. 2022;159:105848.
130. George MM, McIntyre CJ, Zhou J, Kugathasan R, Amos DC, Dillon IJ, et al. Viral Infectivity in Patients Undergoing Tracheotomy With COVID-19: A Preliminary Study. Otolaryngol Head Neck Surg. 2021;165(6):819-26.
131. DiMarco A, Chotalia R, Bloxham R, McIntyre C, Tolley N, Palazzo FF. Does fluoroscopy prevent inadvertent parathyroidectomy in thyroid surgery? Ann R Coll Surg Engl. 2019;101(7):508-13.
132. DiMarco A, Chotalia R, Bloxham R, McIntyre C, Tolley N, Palazzo FF. Autofluorescence in Parathyroidectomy: Signal Intensity Correlates with Serum Calcium and Parathyroid Hormone but Routine Clinical Use is Not Justified. World J Surg. 2019;43(6):1532-7.
133. <BAETS-Audit-National-Report-2017.pdf>.
134. Underbjerg L, Sikjaer T, Rejnmark L. Long-Term Complications in Patients With Hypoparathyroidism Evaluated by Biochemical Findings: A Case-Control Study. J Bone Miner Res. 2018;33(5):822-31.
135. David K, Moyson C, Vanderschueren D, Decallonne B. Long-term complications in patients with chronic hypoparathyroidism: a cross-sectional study. Eur J Endocrinol. 2018.
136. Vadiveloo T, Donnan PT, Leese CJ, Abraham KJ, Leese GP. Increased mortality and morbidity in patients with chronic hypoparathyroidism: A population-based study. Clin Endocrinol (Oxf). 2019;90(2):285-92.

137. Astor MC, Lovas K, Debowska A, Eriksen EF, Evang JA, Fossum C, et al. Epidemiology and Health-Related Quality of Life in Hypoparathyroidism in Norway. J Clin Endocrinol Metab. 2016;101(8):3045-53.
138. Underbjerg L, Sikjaer T, Rejnmark L. Health-related quality of life in patients with nonsurgical hypoparathyroidism and pseudohypoparathyroidism. Clin Endocrinol. 2018;88(6):838-47.
139. Underbjerg L, Sikjaer T, Mosekilde L, Rejnmark L. Postsurgical Hypoparathyroidism-Risk of Fractures, Psychiatric Diseases, Cancer, Cataract, and Infections. Journal of Bone and Mineral Research. 2014;29(11):2504-10.
140. Vokes TJ, Mannstadt M, Levine MA, Clarke BL, Lakatos P, Chen K, et al. Recombinant Human Parathyroid Hormone Effect on Health-Related Quality of Life in Adults With Chronic Hypoparathyroidism. J Clin Endocrinol Metab. 2018;103(2):722-31.
141. Bowling A, Bond M, Jenkinson C, Lamping DL. Short Form 36 (SF-36) Health Survey questionnaire: which normative data should be used? Comparisons between the norms provided by the Omnibus Survey in Britain, the Health Survey for England and the Oxford Healthy Life Survey. J Public Health Med. 1999;21(3):255-70.
142. Buttner M, Musholt TJ, Singer S. Quality of life in patients with hypoparathyroidism receiving standard treatment: a systematic review. Endocrine. 2017;58(1):14-20.
143. Meola A, Vignali E, Matrone A, Cetani F, Marcocci C. Efficacy and safety of long-term management of patients with chronic post-surgical hypoparathyroidism. J Endocrinol Invest. 2018;41(10):1221-6.
144. Lopes MP, Kliemann BS, Bini IB, Kulchetscki R, Borsani V, Savi L, et al. Hypoparathyroidism and pseudohypoparathyroidism: etiology, laboratory features and complications. Arch Endocrinol Metab. 2016;60(6):532-6.
145. Abate EG, Clarke BL. Review of Hypoparathyroidism. Front Endocrinol (Lausanne). 2016;7:172.
146. Harvey S, Hayer S. Parathyroid-Hormone Binding-Sites in the Brain. Peptides. 1993;14(6):1187-91.
147. Sikjaer T, Moser E, Rolighed L, Underbjerg L, Bislev LS, Mosekilde L, et al. Concurrent Hypoparathyroidism Is Associated With Impaired Physical Function and Quality of Life in Hypothyroidism. J Bone Miner Res. 2016;31(7):1440-8.
148. Sikjaer T, Amstrup AK, Rolighed L, Kjaer SG, Mosekilde L, Rejnmark L. PTH(1-84) replacement therapy in hypoparathyroidism: a randomized controlled trial on pharmacokinetic and dynamic effects after 6 months of treatment. J Bone Miner Res. 2013;28(10):2232-43.
149. Nussdorfer GG, Bahcelioglu M, Neri G, Malendowicz LK. Secretin, glucagon, gastric inhibitory polypeptide, parathyroid hormone, and related peptides in the regulation of the hypothalamus- pituitary-adrenal axis. Peptides. 2000;21(2):309-24.

List of Publications and Contributions

McIntyre C, Jacques T, Palazzo F, Farnell K, Tolley N. Quality of life in differentiated thyroid cancer. Int J Surg. 2018;50:133-6. (127)

McIntyre C, Tolley N. A critical review of thyroidectomy consent in the UK. International Journal of Surgery. 2019;66:84-8. (128)

Calmet H, Bertomeu PF, McIntyre C, Rennie C, Gouder K, Houzeaux G, et al. Computational modelling of an aerosol extraction device for use in COVID-19 surgical tracheotomy. J Aerosol Sci. 2022;159:105848 (129)

George MM, McIntyre CJ, Zhou J, Kugathasan R, Amos DC, Dillon IJ, et al. Viral Infectivity in Patients Undergoing Tracheotomy With COVID-19: A Preliminary Study. Otolaryngol Head Neck Surg. 2021;165(6):819-26. (130)

DiMarco A, Chotalia R, Bloxham R, McIntyre C, Tolley N, Palazzo FF. Does fluoroscopy prevent inadvertent parathyroidectomy in thyroid surgery? Ann R Coll Surg Engl. 2019;101(7):508-13.(131)

DiMarco A, Chotalia R, Bloxham R, McIntyre C, Tolley N, Palazzo FF. Autofluorescence in Parathyroidectomy: Signal Intensity Correlates with Serum Calcium and Parathyroid Hormone but Routine Clinical Use is Not Justified. World J Surg. 2019;43(6):1532-7.(132)

Xiao Q, Cetto R, Doorly DJ, Bates AJ, Rose JN, McIntyre C, et al. Assessing Changes in Airflow and Energy Loss in a Progressive Tracheal Compression Before and After Surgical Correction. Ann Biomed Eng. 2020;48(2):822-33. (29)

Oral Presentations

Quality of Life in Differentiated Thyroid Cancer, BAETS, Belfast, October 2017

Thyroidectomy Consent – A UK Study, BAETS, Belfast, October 2017

The Impact of Permanent Hypoparathyroidism on Quality of Life, BAETS, Belfast, October 2017

Computational fluid dynamics as a tool for assessing tracheal compression in patients with retrosternal goitres, Society for computational fluid dynamics for the nose and airway (SCONA), London, April 2018

Artificial intelligence Thyroid MDT, Imperial Women in Innovation, London, February 2018

A Critical Review of Thyroidectomy Consent in the UK, World Congress on Thyroid Cancer, Boston, July 2018

Quality of life in differentiated thyroid cancer, World Congress on Thyroid Cancer, Boston, July 2018

Artificial intelligence Thyroid MDT, BAETS, Glasgow, October 2018 – British Journal of Surgery Prize presentation

Appendices

Quality of Life in Patients with Post-Surgical Hypoparathyroidism

Charlotte McIntyre, Aimee Di-Marco, Professor Fausto Palazzo, and Professor Neil Tolley

Abstract

Introduction

Post-surgical hypoparathyroidism can be temporary or permanent. and seen most commonly following total thyroidectomy with a reported rate of late hypocalcaemia of 6.5% (5th BAETS National Audit). BAETS defines permanent hypoparathyroidism as the need for long term calcium +/- vitamin D supplements to maintain normocalcaemic 6 months post surgery.

Hypoparathyroidism confers a burden on patient lifestyle due to a need for regular blood tests, life long medication, clinic appointments and effects secondary to fluctuations in serum calcium. Few studies have looked at the Health-related quality of life (HRQOL) impact in this patient group.

Methods

To evaluate the HRQOL in patients with post-surgical hypoparathyroidism a validated Short Form 36-Item Health Survey version 2 (SF-36) tool was used. An anonymised survey was sent to members of Hypopara UK with post-surgical hypoparathyroidism who were more than 12 months post surgery. Hypopara UK is a patient organisation for those living with parathyroid disorders in the UK. The survey included questions on demographics, aetiology, current medications, associated renal problems and the SF-36. SF-36 covers 8 domains of HRQOL. Results were analysed using IBM SPSS. Mean values across the 8 domains were compared with those of a control population using a non-paired t-test.

Results

248 questionnaires were completed by participants with post-surgical hypoparathyroidism over the age of 18. The median age was 35 years (range 19-83) and male: female ratio was 1:10. The median number of years since surgery was 7 (range 1-52). Participants had surgery for: benign thyroid disease 43.5%, thyroid cancer 34.3%, parathyroid surgery 18%, other neck surgery e.g. laryngectomy 2.4%, renal hyperparathyroidism 1.6%. Participants reported their current medication to include: both calcium and active vitamin D 42%, active vitamin D only 28%, magnesium 14%, calcium only 6%. Across all domains of the SF-36 the study population has significantly lower quality of life (p value >0.001) than that of the control population. The lowest scoring domains were energy/fatigue, role limitations due to physical health and general health.

Conclusion

The study has found that the average quality of life in this group of patients is significantly lower than that of the UK population. A large number of patients suffer with fatigue, role limitations due to their physical health and an overall a low level of general health.

Introduction

Post-Surgical hypoparathyroidism is a characterised by hypocalcaemia, hyperphosphatemia and an inappropriately low PTH level. Surgical induced hypoparathyroidism is either temporary or permanent and can occur following any central neck surgery although total thyroidectomy is the main cause with a incidence of 6.5% (133). Permanent hypoparathyroidism is defined as a need for long-term calcium +/- vitamin D supplementation to maintain a normal serum calcium 6 months post surgery.

Despite treatment with regular supplements serum calcium can significantly fluctuate. Transient hypercalcaemia can lead to impaired renal function, and transient hypocalcaemia can lead to paraesthesiae and in extreme cases, seizures. One function of PTH is to increase the renal excretion of serum phosphate and therefore, low PTH can lead to high serum phosphate levels. High serum phosphate levels are associated with increased risk of cardiovascular disease. (134)

David et al performed a retrospective cross-sectional study of 148 patients with hypoparathyroidism (post-surgical 84%, non-surgical 9% and pseudo-hypoparathyroidism 7%) being managed in a tertiary centre over a 12 month period. They found that 15% of patients had renal stones, 16% of patients suffered cramping and paraesthesias with 5% of patients requiring hospitalisation. Of the 148 patients 47% had been screened for calciuria, and of those that had been screened 36% had calciuria outside of the normal reference range (135). Patients with hypoparathyroidism have an overall increased morbidity and mortality when compared with the normal population (136).

Hypoparathyroidism imposes a burden on patient lifestyle due to the need for regular blood tests, need for lifelong medication, clinic appointments and symptoms due to fluctuations in serum calcium. PTH receptors are present in the central nervous system and the adrenal cortex. Hypoparathyroidism may impact on health-related quality of life (HRQOL) through a secondary impaction on these organs. Few studies have looked at the HRQOL in this patient group.

A study in Norway identified patients with surgical and non-surgical hypoparathyroidism from electronic hospital databases. Of the 511 patients identified, 283 responded to a postal questionnaire. 70% were post-surgical, 25% were non-surgical and 6% were pseudo-hypoparathyroidism. The non-surgical group comprised: idiopathic (26%), Autoimmune Polyendocrine Syndrome-1 (15%), Autosomal Dominant Hypocalcaemia (18%), hypoparathyroidism sensorineural hearing deafness and renal problems (1%), DiGeorge (8%), other causes (2%). The patients completed Short Form-36 quality of life (SF-36 QOL) questionnaire and the authors found that patients with hypoparathyroidism had significantly lower QOL across all eight domains of the SF-36 than the normal population. In addition, they

found that patients with post-surgical hypoparathyroidism had worse scores than the non-surgical group. (137)

Underbjerg et al looked at the QOL in patients with post-surgical hypoparathyroidism (50 patients), non-surgical hypoparathyroidism (57 patients), and pseudo hypoparathyroidism (30 patient). Patients completed the SF-36 QOL questionnaire and they also found that across all 8 domains patients with post-surgical and non-surgical hypoparathyroidism had reported significantly lower scores compared with a control population. Patients with pseudo hypoparathyroidism scored significantly lower in 5/8 domains. Across most domains of the SF-36 they found that the non-surgical and post-surgical groups did not have significantly different scores (138).

Another study which identified 688 patients with hypoparathyroidism from the Danish national registry found that they had a significantly higher incidence of depression and psychiatric symptoms when compared with healthy controls. (139)

In order to assess if endocrine surgeons appreciated the impact of hypoparathyroidism on the patients HRQOL, a Harvard based study compared the SF-36 QOL scores for patients with post-surgical hypoparathyroidism with 102 experienced endocrine surgeons who were asked to fill out the questionnaire whilst imagining they had post-surgical hypoparathyroidism. They found the patients had significantly lower scores in the questionnaire, indicating that even experienced endocrine surgeons under-estimate the impact that post-surgical hypoparathyroidism has on the patients HRQOL. (140)

Our study examined in detail at the HRQOL in patients in the UK with post-surgical hypoparathyroidism and specifically the HRQOL in the different subgroups for post-surgical hypoparathyroidism in relation to the type of surgery they underwent.

Methods

To evaluate the HRQOL in patients with post-surgical hypoparathyroidism we used the Short Form 36-Item Health Survey version 2 (SF-36). An anonymised survey was sent to members of Hypopara UK with post-surgical hypoparathyroidism who were over 12months post surgery. Hypopara UK is a patient organisation for those living with parathyroid disorders in the UK. The anonymised survey included questions on demographics, aetiology, current medications, associated renal problems and the SF-36 QOL questionnaire. A patient focus group was consulted and was instrumental in designing the first part of the anonymised survey. Important issues surrounding the management and the associated complications of post-surgical hypoparathyroidism were highlighted and question content was checked to ensure that medical terms were understood.

SF-36 covers 8 domains of HRQOL including: general health, pain, social functioning, emotional well-being, energy and fatigue, role limitations due to emotional health, role limitations due to physical health and physical functioning. Results were analysed using IBM SPSS. Mean values across the 8 domains were compared with those of a control population using a non-paired t-test. The results for the control population were taken from a study of 2056 randomly selected patients from a UK population carried out in 1999. Due to most of our post-surgical hypoparathyroidism sample comprising a female population, we decided to compare the mean SF-36 scores of our group with the female normal population SF-36 scores (141).

Further evaluating the data, we present the mean SF-36 QOL scores across the different post-surgical groups including patients who had undergone surgery for: benign thyroid disease, thyroid cancer, primary hyperparathyroidism, renal parathyroid disease and other neck surgery.

Results

The questionnaire was sent to 417 members of Hypopara UK and there were 273 respondents, giving a 65% response rate. Patients were excluded if they were younger than 18 years or if they had undergone surgery within the last 12 months, leaving a total of 248 patients. The mean age of the group was 35 years (range 19-83) and the male to female ratio was 1:10. The median number of years since surgery was 7 (range 1-52). Patients were asked to report the indication for surgery. 43.5% of patients had surgery for benign thyroid disease, 34.3% had surgery for thyroid cancer, 18% had surgery for primary hyperparathyroidism, 2.4% had other neck surgery e.g. laryngectomy, and 1.6% of patients had surgery for renal parathyroid disease (see table one: patient demographics).

Table one: Patient demographics

Number of patients contacted	417
Number of completed questionnaires	273
Number included in the study	248
Mean age (years)	35 (range 19-83)
Median number of years since surgery	7 (range 1-52)
Male to female ratio	1:10
Surgery for benign thyroid disease	43.5%
Surgery for thyroid cancer	34.3%
Surgery for primary hyperparathyroidism	18%
Other neck surgery e.g. laryngectomy	2.4%
Renal parathyroid disease	1.6%

Patients were asked to record their current medication for the treatment of their post-surgical hypoparathyroidism. Most patients reported taking both calcium supplements and active vitamin D supplements (42%), 28% reported taking active vitamin D only, 6% reported taking calcium supplements only and 14% of patients reported taking magnesium supplements. (See table two: Patient reported medications)

Table two: Patient reported medications

Medication	% of patients reporting use
Calcium and active vitamin D	42
Active vitamin D only	28
Magnesium supplements	14
Calcium supplements only	6

Patients reported on their ease of access to having blood tests to check their serum calcium levels and any reported renal problems. 62.5% reported easy access to having a blood test whereas 37.5% reported difficult access. 21.3% of patients reported that they were known to

have high levels of calcium in their urine, 15.7% reported they have renal damage secondary to high calcium levels, 11.3% of patients report having high serum phosphate levels and 13.3% of patients report having known renal stones. (see table three: Patient reported associated renal problems)

Table three: Patient reported associated renal problems

Associated renal problem:	% of patients
High urinary calcium levels	21.3
Renal damage secondary to high calcium levels	15.7
Renal calculi	13.3
High serum phosphate levels	11.3

SF-36 results

The mean SF-36 scores across the eight domains for all 243 patients were calculated and compared with the normative data set using a non-paired two-tailed T-test (see table four and figure one). The mean SF-36 scores were significantly lower across all 8 domains. The lowest scores for the post-surgical hypoparathyroid group were for the energy and fatigue domain, role limitations due to physical health and the general health domain.

Figure one: Mean SF-36 scores for post- surgical hypoparathyroidism group and the normal population

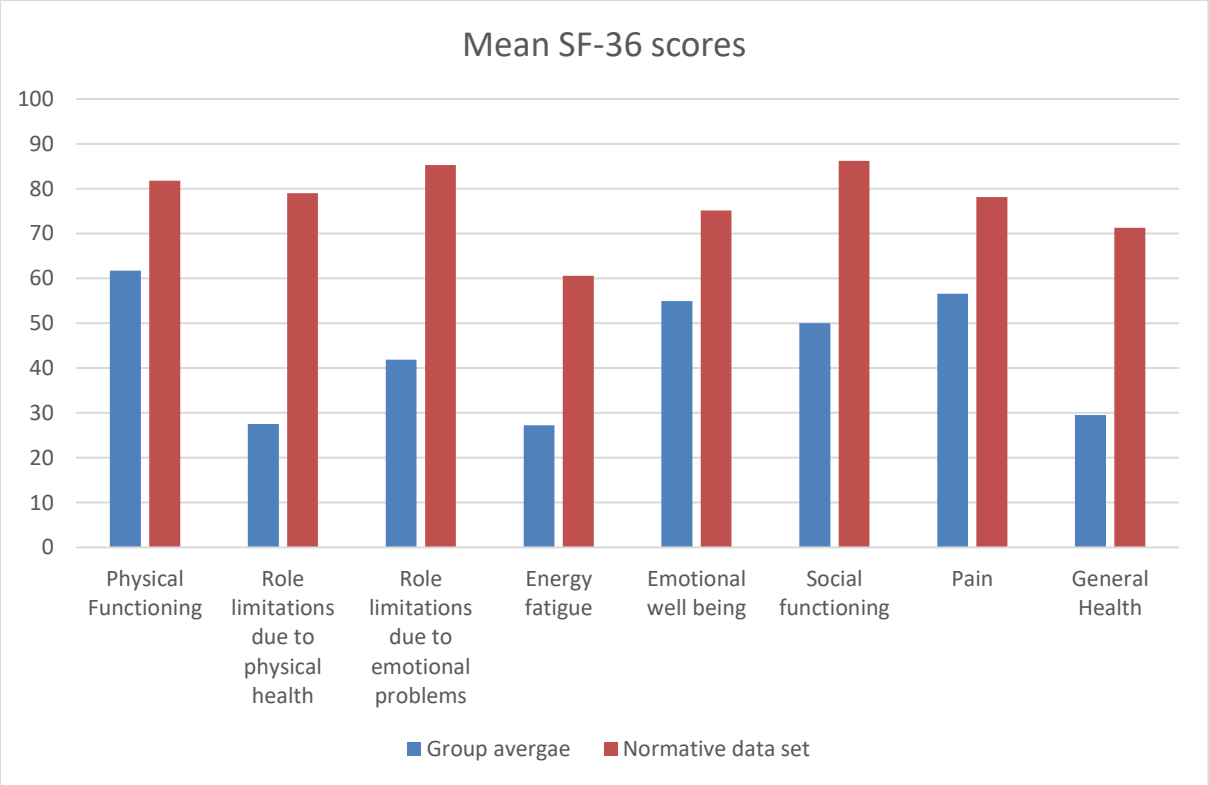


Table four: Mean SF-36 scores for post- surgical hypoparathyroidism group and the normal population

SF-36 Domain	Hypoparathyroid group Mean score (IQ range)	Normal population Mean score (IQ range)	Statistical significance using t-tailed t-test
Physical Functioning	61.7 (39.5)	81.8 (25.7)	>0.0001
Role limitations due to physical health	27.5 (44.7)	79.0 (36.5)	>0.0001
Role limitations due to emotional health	41.9 (49.4)	85.3 (32.0)	>0.0001
Energy fatigue	27.2 (26.4)	60.6 (21.6)	>0.0001
Emotional well being	54.9 (29.3)	75.1 (18.6)	>0.0001
Social Functioning	50 (29.4)	86.2 (23.4)	>0.0001
Pain	56.6 (28.8)	78.1 (26.8)	>0.0001
General health	29.5 (30.30)	71.3 (22.8)	>0.0001

The SF-36 scores were further subdivided into mean scores according to the primary reason for surgery (see table five and figure two). Overall the subgroup who had surgery for renal parathyroid disease scored lowest in most domains. These patients are likely to have other additional co-morbidities secondary to their renal disease which likely impacts negatively on their HRQOL. However, it is important to note that this is a very small group of patients (1.6% of the study).

Figure 2: Mean SF-36 scores for patients with hypoparathyroidism according to the primary reason for surgery

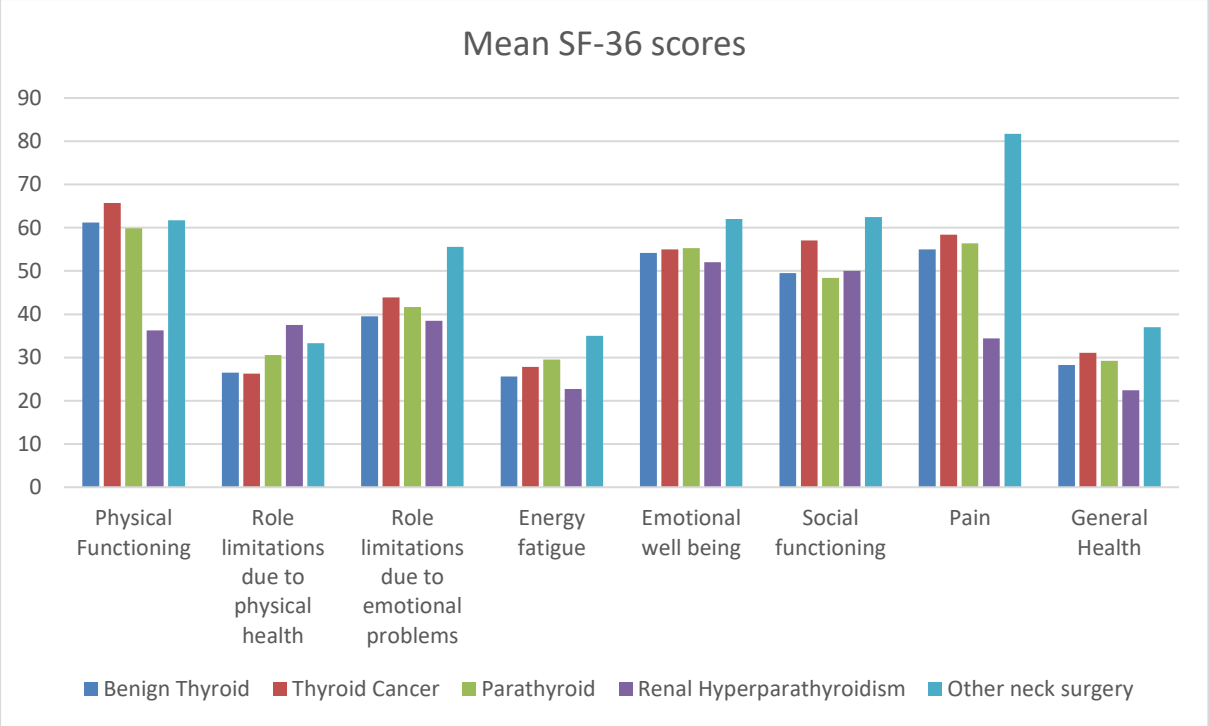


Table 5: Mean (inter-quartile range) SF-36 scores for patients with hypoparathyroidism according to the primary reason for surgery

SF 36 Domain	Benign Thyroid	Thyroid Cancer	Parathyroid	Renal parathyroid disease	Other neck surgery
Physical Functioning	61.2 (39.8)	65.7 (38.4)	59.9 (39.7)	36.3 (35.8)	61.7 (41.5)
Role limitations due to physical health	26.5 (44.2)	26.3 (44.1)	30.6 (46.2)	37.5 (50.0)	33.3 (48.2)
Role limitations due to emotional problems	39.5 (49.0)	43.9 (49.7)	41.7 (49.5)	38.5 (50.6)	55.6 (51.1)
Energy fatigue	25.6 (25.0)	27.8 (25.6)	29.5 (30.0)	22.7 (30.1)	35.0 (33.5)
Emotional well being	54.2 (28.8)	55.0 (29.5)	55.3 (29.3)	52.0 (36.5)	62.0 (30.8)
Social functioning	49.5 (31.4)	57.1 (31.6)	48.4 (32.0)	50.0 (42.3)	62.5 (37.7)
Pain	55.0 (26.5)	58.4 (30.4)	56.4 (29.1)	34.4 (29.3)	81.7 (26.7)
General Health	28.3 (28.7)	31.1 (31.0)	29.2 (31.9)	22.4 (28.7)	37.0 (30.0)

Discussion

The demographics of our UK based study to assess the HRQOL in patients with post-surgical hypoparathyroidism are similar to those reported in previous studies (137, 138, 142).

The most common reason for post-surgical hypoparathyroidism is surgery for benign thyroid problems e.g. benign thyroid goitre. 43.5% of our study group had surgery for benign thyroid disease.

Our study population is largely female which reflects the large female preponderance of thyroid disease. The gold standard for treating post-surgical hypoparathyroidism is with a combination of vitamin D and calcium supplements and this is reflected in the patient reported outcomes of their current medications. The majority of the study population taking both calcium and active vitamin D (40%). 37.5% of patients reported difficulty accessing blood tests. This assumes great importance to patients with hypoparathyroidism due to the unpredictable nature of transient changes in serum calcium.

21.3% of patients reported having high urinary calcium levels, this is lower than reported in other studies (143-145). 13.3% of patients report having renal stones which is again lower than reported in other studies (135, 144, 145). It is important to note that this is a patient reported questionnaire and patients' medical files have not been accessed. Therefore, this can only be interpreted as a guide to the number of patients with high urinary calcium levels.

The SF-36 scores show that the study group have a significantly lower HRQOL across all 8 domains compared with the normal population. This reflects other studies found in the literature where the QOL in patients with hypoparathyroidism is lower than normal. It is likely that factors such as regular blood tests, lifelong medication, clinic appointments have an impact on the HRQOL of these patients. A number of explanations and theories exist as to why patients with treated hypoparathyroidism have such poor HRQOL.

HRQOL is poor in patients with hypoparathyroidism despite treatment with calcium and vitamin D and despite well controlled serum calcium levels. This has led some clinicians to believe that it might be the lack of PTH that leads to some aspects of the reported low QOL (142). PTH receptors are found in the brain and other parts of the central nervous system (146). Reduced or undetectable serum PTH levels may lead to some of the mental and psychological disturbances seen in hypoparathyroidism.

PTH receptors are also found in skeletal muscle and it is thought that some of the low scores in QOL in the physical domains may be in part due to lack of PTH action within the skeletal muscle. Sikjaer et al found that patients with both hypothyroidism and hypoparathyroidism had impaired muscle function when compared with healthy controls (147). One study looked at the effect of PTH (1-84) therapy on muscle strength and QOL in patients with hypoparathyroidism. Sixty-two patients with chronic hypoparathryoidism were randomized to six months of treatment with PTH (1-84) 100 μg/d s.c. or to placebo treatment. They found that after six-months there was no improvement in QOL or muscle function in patients in the treatment group. However, treatment once daily with subcutaneous PTH injections does not mimic PTH release in a patient without hypoparathyroidism (148).

PTH receptors are found in the hypothalamus-pituitary-adrenal axis. PTH has been found to enhance the release of ACTH and stimulate the release of aldosterone and glucocorticoid secretion from the adrenal gland (149). The lack of PTH action in patients with hypoparathyroidism leads to a disturbance in this pathway and may have some involvement in the reduced QOL.

There are a number of limitations to our study, mainly that the majority of the patients in our group with post-surgical hypoparathyroidism have undergone thyroid surgery for either

benign disease or the treatment and investigation of thyroid cancer and therefore may also have a reduced quality of life secondary to hypothyroidism. We did not access patient medical records and therefore we cannot comment if patients who had undergone thyroid surgery are being adequately treated with thyroid hormone replacement therapy. Sikjaer et al carried out a study to compare the quality of life in patients with hypothyroidism with patients with both hypothyroidism and hypoparathyroidism and healthy matched controls using the SF-36. When compared with the control group the patients with hypothyroidism only had significantly lower scores in the following domains: role-physical, bodily pain, vitality and mental health. When compared with the control group the patients with both hypothyroidism and hypoparathyroidism had significantly lower scores in all domains apart from the role-emotional domain. The patients with both hypothyroidism and hypoparathyroidism had significantly lower scores than the patients with hypothyroidism only in the physical functioning and the role-physical domain (147).

There is also likely to be a selection bias in the patients who have completed the questionnaire. We have introduced a selection bias by contacting only patients who are members of Hypopara UK. We do not have a UK national database of all patients diagnosed with hypoparathyroidism. Patients who have sought membership in a national society may be more likely to be suffering from long term symptoms of their disorder.

Conclusion

The demographics of our UK based study to assess the HRQOL in patients with post-surgical hypoparathyroidism are similar to those reported in previous studies. The majority of the patients are taking both calcium and active vitamin D supplements. 37.5% of patients reported difficulty accessing blood tests, a factor that subsumes great importance to patients with hypoparathyroidism due to the unpredicatable nature of changes in serum calcium. The SF-36 scores show that the study group have a significantly lower HRQOL across all 8 domains compared with the normal population. A large number of patients suffer with fatigue, role limitations due to their physical health and overall a low level of general health. The lower HRQOL is likely to be contributed to by the need for regular blood tests, clinic appointments, and the need for lifelong medication. Fluctuations in serum calcium levels and low or undetectable PTH levels can lead to mood disturbances, psychiatric disorders, renal problems and muscle impairment, all of which will contribute to the overall lower HRQOL.